Universitat Autònoma de Barcelona

SIVA-1 Role in Neurons: a Novel FAIM-L Functional Antagonist

Elena Coccia

PhD Thesis

SIVA-1 Role in Neurons:

a Novel FAIM-L Functional Antagonist

Elena Coccia

Directors:

Joan X. Comella Carnicé

María José Pérez García

Doctorat en Neurociències

Institut de Neurociències

Universitat Autònoma de Barcelona

2020

Alla mia famiglia,

A(lla) mi(a) gente.

AKNOWLEDGEMENTS

I am writing this in my home in Barcelona during the days of lockdown for the CO-VID 2019 pandemic outbreak. I hope everything in the world will be less scary the day I get to be a Dr.. It feels kind of right, during these days of nothing but uncertainty, to be thinking about all the people I am missing right now, for whom I have been grateful during these last years.

So here it goes, the part that most people will read, and also the part that meant the most during all this 6 ½ (wow!!) years – my people.

En Barcelona he crecido, aprendido y definido (creo) cual quiero sea mi sitio en el mundo. Tengo mucho que agradecer a todos los que habéis compartido estos años conmigo. De aquí, no solo me llevo buenos recuerdos, sino que gente y amistades que seguirán acompañándome en el futuro, aunque sea lejos de aquí.

En primer lugar, Joan, gracias por la oportunidad que me diste hace unos años de entrar a ser parte de tu grupo. Gracias por haber sido a partir de ese momento un mentor en todos los sentidos y haberme ayudado en echar las bases y construir una visión de la ciencia y de la vida que siempre llevaré conmigo.

Gracias Mari por el apoyo de estos últimos años y por ayudarme a llevar a cabo mis objetivos.

Quim, gracias por el día a día en el lab y tu ayuda y vista critica en cada trabajo que he escrito los últimos años.

Y a los que también han ayudado en mis primeros pasos en el mundo de la ciencia, gracias a los que he "aprendido a pensar" como un científico: Miguel S., Victor Y., Cristina M. y Beatriz A.; gracias.

A los que han pasado por el lab en todas sus versiones, el #203, el #118, y el “de la UAB”, sobretodo a unos cuantos, que se han convertido en mucho, mucho mas que lab-mates. Gracias a vosotros ha habido ganas de llegar al lab también en los días mas negros.

Bruna y Laura, habéis sido mi guía en los años compartidos en el lab y os habéis mantenido una constante en los siguientes también. Gracias por haber estado para compartir la alegría de los buenos momentos y para los ánimos en los malos. Nunca hemos tenido suficientes horas para nuestras cenas, y aunque puede que haya menos aún, se que cada vez será como si no hubiera pasado ni un día.

Jorge y Koen. Los dos con la cabeza llena de información de todo tipo, con vosotros he aprendido de ciencia, de música, de series, de memes y de muchas tonterías, y me encanta este mix. Gracias por la buena energía constante, los años con vosotros han sido the loudest of them all, en los que aburrirse nunca ha sido una opción.

Isa, hemos vivido juntas mucho de esta etapa, han sido años de cambios, de momentos complicados y de momentos muy buenos, me ha encantado compartirlos contigo. Gracias por cuidar de todo lo que esta a tu alrededor cada día, y por la amistad que tenemos (mirar apartado Retis for more..).

Mireia, a ti gracias por tu visión nunca negativa y por haber compartido con nosotras todos los cambios de los últimos años, aunque no siempre en el mismo pasillo, nunca has estado lejos.

Anna y Raquel, bibis, a vosotras gracias por haber estado a mi lado y compartir de la manera mas cercana más de lo que recuerdo. Gracias por todo lo que ha llenado cada día. Podemos pasar horas hablando de todo y de nada, que, a ver, algún momento hemos tenido en plan “science”, y unos cuantos en plan “sirius”

también, pero gracias sobretodo por los muchos tan bonitos, y tan tontos también, de reír hasta casi llorar. Ha sido un tesoro teneros.

A Edu, Irene y las Mónicas, gracias por haber sido una extensión del lab en todo lo bueno, por habernos acogido a veces, y por dejaros acoger unas otras.

A los peces del lab gracias por enseñarnos que la vida puede cambiar en dos días y mejor aprovechar cada momento, y que no siempre hay que confiar en los vecinos, aunque parezcan friends.

A todas las gentes del VHIR: Tao, Rai, Marga, el equipo de coordinación, y las muchas caras y nombres que han pasado por los pasillos estos años. Por los buenos días, las charlas del café y los "hola que tal" a los que siguen ganas de escuchar una respuesta, las VHIRRAS, las cenas de becarios et al.. Gracias, ha sido una suerte estar en un ambiente como este.

A las chicas del CEHPE, no hemos tenido mucho tiempo y el virus nos lo ha puesto mas difícil aún, pero nuestros ratitos al sol han sido cada día el mejor momento para recargar pilas.

Y ya saliendo del lab, gracias a unas pocas personas más, con las que ha sido mucho mas fácil cada cambio y elegir Barcelona como casa. Gracias porque me llevo unas amistades de oro.

Isa y David por vuestra presencia constante, nuestros viajes, nuestras comidas-cenas-desayunos-meriendas, por los buenos consejos y siempre hacerme estar mejor.

Blanca, Ester, Laura, Isa, por haber estado siempre, para escuchar, desconectar, y compartir cada momento y cada estado de animo (que ha habido muchos). Entre las cinco hemos vivido en pocos años cambios para una vida entera, pero una constante ha sido esta amistad que ha ido haciéndose mas y mas fuerte.

Tengo ganas de seguir viviendo cambios con vosotras (y que sean todos a mejor eh, y sin confinament).

To the ones I hope to join soon, my NYC Lab. Thanks to Tim Ahfeldt, for giving me the opportunity to join the amazing group of people of your team, for guiding me the months that I have been there. I have learnt so much, I cannot wait to keep it going in the future.

And thanks to the rest of the team, Tanya, Gustavo Lily and Carlitos. The scientific part is definitely cool, but all the rest is great. I am excited to come back, create new songs about random stuff and add food, games, and karaoke plans to the list.

Gracias a todo Sunseteo, por acogerme desde el primer día, y por llenar los meses de mi "intercambio" de buenos recuerdos (y bueno, también de unos cuantos momentos que no recuerdo mucho..). Esperadme para mas eh, a ver si me dejan volver pronto.

Jaume, gracias por mucho mas de lo que voy a escribir, por haber llenado lo que llevamos de año de momentos tanto inesperados como bonitos, pero sobretodo por toda la ilusión de lo que será.

E infine grazie a tutti quelli che sono le mie radici, perché se sono come sono è grazie a voi, e alla vostra costante presenza.

A chi mi è stato vicino da Roma, da quella magnifica sezione E del Tuscé che ci ha unito, o addirittura da prima.

Grazie a Ersilia per essermi stata accanto a ogni passo e per essere letteralmente e figuratamente l'amica di una vita.

Grazie a Jacopo per essere stato l'appoggio più importante nella decada in cui sono cresciuta e ho imparato di più.

E grazie ai miei amici di sempre, a Cami e il resto della mia Compagnia Bella. Sono orgogliosa dell'amicizia che abbiamo e di quanto siamo cambiati insieme, rimanendo gli stessi. Sono così fortunata che servirebbe un paragrafo solo per elencarvi tutti, non vi nomino ma chiunque mi conosca un minimo sa chi siete. Grazie per tutti i momenti condivisi, le risate, i viaggi, le chiamate, i messaggi, le volte che siete venuti a trovarmi, le volte in cui mi avete accolto come se non fosse passato neanche un giorno. In realtà non mi abituerò mai a essere lontana da voi, ma spero di continuare a sentirvi vicino sempre, com'è stato finora.

Grazie alla mia famiglia, di cui sono fiera, in cui ognuno è stato capace di essere di esempio. Sparsa ma così insieme, è grazie a voi che so che il sentirsi uniti va ben oltre la distanza geografica.

Mamma e Papà, grazie per l'amore incondizionato, l'appoggio costante, l'incoraggiamento, e avermi sempre spinto a seguire la mia curiosità. Spero un giorno di arrivare alla metà di quello che siete voi, in tutti gli aspetti delle vostre vite.

Now that I read this altogether, it feels kind of bittersweet.. most of the people I am thankful for are/have been/will be far from me, different cities, other countries.

Wherever I will go, there will always be somebody I am missing. But I feel extremely lucky, cause in all these places where YOU are, it will feel like home.

A tutti, grazie, vi voglio bene.

A todos, gracias, os quiero.

ABSTRACT

ABSTRACT

Apoptosis is the main type of programmed cell death, essential for the correct development of nervous system. Even if in adult neurons apoptosis has been related to the pathology of neurodegenerative diseases, apoptotic machinery activation has been also described as necessary in non-lethal regulatory events, such as synaptic plasticity and axonal pruning. Apoptosis activation, which culminates with engagement of effector caspases, is modulated by hundreds of proteins. One of the regulators of apoptosis is the long isoform of Fas Apoptosis Inhibitory Molecule (FAIM-L), a neuronal specific death receptor antagonist shown capable to modulate neuronal caspase activation. FAIM-L carries out its anti-apoptotic activity by binding to X-linked Inhibitor of Apoptosis Protein (XIAP). XIAP is an inhibitor of caspases, and its levels are modulated by the ubiquitin-proteasome pathway. FAIM-L interaction with XIAP prevents its ubiquitination and degradation, allowing therefore its anti-apoptotic activity. This interaction also modulates non-apoptotic functions of caspases, such as the endocytosis of AMPA receptor (AMPAR), the main mechanism in long-term depression (LTD), and axonal pruning. To date consensus binding motifs of FAIM-L, which could shed light on its molecular mechanism of action, are unknown.

Our group performed a two-hybrid screening to discover novel FAIM-L-interacting proteins. We found a functional interaction of SIVA-1 with FAIM-L. SIVA-1 is a protein described as pro-apoptotic and able to interact with XIAP. In this work we show that SIVA-1 modulates FAIM-L function by disrupting the interaction of FAIM-L with XIAP, thereby promoting XIAP ubiquitination. By modulating the inhibitors of apoptosis XIAP and FAIM-L, SIVA-1 induces caspase-dependent neuronal cell death. Furthermore, we show SIVA-1 to be a novel modulator of synaptic plasticity. After induction of LTD in an *in vitro* neuronal model, SIVA-1 protein levels are rapidly increased, and SIVA-1 overexpression is sufficient to induce caspase-dependent internalization of AMPAR. SIVA-1

increase is also present during axonal pruning, and SIVA-1 overexpression accelerates the degeneration process.

In summary, our studies uncover a new functional partner of FAIM-L, SIVA-1. We propose SIVA-1 as a caspase modulator in neurons, and therefore to be a crucial regulator in neuronal cell death and plasticity.

RESUMEN

La apoptosis es el principal tipo de muerte celular programada, esencial para el correcto desarrollo del sistema nervioso. En el adulto, la apoptosis en neuronas se ha relacionado con enfermedades neurodegenerativas, pero una activación de la maquinaria apoptótica también se ha descrito como necesaria en eventos reguladores no letales, como la plasticidad sináptica y la degeneración axonal. La activación de la apoptosis, que culmina con la activación de las caspasas efectoras, está modulada por centenares de proteínas. Uno de los reguladores de la apoptosis es la isoforma larga del gen de FAIM (FAIM-L), un antagonista de receptores de muerte específico neuronal capaz de modular la activación de caspasas. FAIM-L lleva a cabo su actividad antiapoptótica uniéndose a XIAP, un inhibidor de las caspasas, cuyos niveles están modulados por la vía ubiquitina-proteasoma. La interacción de FAIM-L con XIAP previene su ubiquitinación y degradación, permitiendo así su actividad antiapoptótica. Esta interacción también modula las funciones no apoptóticas de las caspasas, como la endocitosis del receptor AMPA (AMPAR), el principal mecanismo en la depresión sináptica a largo plazo (LTD), y la degeneración axonal. Conocemos muy poco de las características estructurales de FAIM-L, que podrían aclarar su mecanismo de acción molecular.

Para completar nuestro estudio sobre FAIM-L, nuestro grupo realizó un ensayo *two hybrid* para detectar proteínas que interactúan con FAIM-L, y se encontró una interacción funcional de SIVA-1 con FAIM-L. SIVA-1 es una proteína descrita como proapoptótica y capaz de interactuar con XIAP. En este trabajo mostramos que SIVA-1 modula la función de FAIM-L al impedir la interacción de FAIM-L con XIAP, promoviendo así la ubiquitinación de XIAP. Al modular los inhibidores de la apoptosis XIAP y FAIM-L, SIVA-1 induce la muerte celular neuronal dependiente de caspasa. Además, mostramos que SIVA-1 es un modulador de plasticidad sináptica. Después de la inducción de LTD en un modelo neuronal *in*

vitro, los niveles de proteína SIVA-1 aumentan rápidamente y su sobreexpresión es suficiente para inducir la internalización dependiente de caspasa de AMPAR. El aumento de SIVA-1 también está presente durante la degeneración axonal, y su sobreexpresión acelera el proceso de degeneración.

En resumen, con nuestro estudio describimos la función de SIVA-1 en neuronas. Proponemos SIVA-1 como un modulador de caspasas y, por lo tanto, como un regulador crucial en la muerte celular y la plasticidad neuronal.

RESUM

L'apoptosi és el principal tipus de mort cel·lular programada, essencial per al correcte desenvolupament de sistema nerviós. En l'adult, l'apoptosi en neurones s'ha relacionat amb malalties neurodegeneratives, però una activació de la maquinària apoptòtica també s'ha descrit necessària en esdeveniments reguladors no letals, com la plasticitat sinàptica i la degeneració axonal. L'activació de l'apoptosi, que culmina amb l'activació de les caspases efectores, està modulada per centenars de proteïnes. Un dels reguladors de l'apoptosi és la isoforma llarga de el gen de FAIM (FAIM-L), un antagonista de receptors de mort específic neuronal capaç de modular l'activació de caspases. FAIM-L duu a terme la seva activitat antiapoptòtica unint-se a XIAP, un inhibidor de les caspases. Els nivells de XIAP estan modulats per la via ubiquitina-proteasoma. La interacció de FAIM-L amb XIAP prevé la seva ubiquitinación i degradació, permetent així la seva activitat antiapoptòtica. Aquesta interacció també modula les funcions no apoptòtiques de les caspases, com l'endocitosi de el receptor AMPA (AMPAR), el principal mecanisme en la depressió sinàptica a llarg termini (LTD), i la degeneració axonal. Coneixem molt poc de les característiques estructurals de FAIM-L, que podrien aclarir el seu mecanisme d'acció molecular.

Per completar el nostre estudi sobre FAIM-L, el nostre grup va realitzar un assaig *two hybrid* per detectar proteïnes que interactuen amb FAIM-L, i es va trobar una interacció funcional de SIVA-1 amb FAIM-L. SIVA-1 és una proteïna descrita com proapoptòtica i capaç d'interactuar amb XIAP. En aquest treball mostrem que SIVA-1 modula la funció FAIM-L a l'impedir la interacció de FAIM-L amb XIAP, promovent així la ubiquitinación de XIAP. A l'modular els inhibidors de l'apoptosi XIAP i FAIM-L, SIVA-1 indueix la mort cel·lular neuronal dependent de caspasa. A més, vam mostrar que SIVA-1 és un modulador de plasticitat sinàptica. Després de la inducció de LTD en un model neuronal in vitro, els nivells de proteïna SIVA-1 augmenten ràpidament i la seva sobreexpressió és suficient per

induir la internalització depenent de caspasa de AMPAR. L'augment de SIVA-1 també està present durant la degeneració axonal, i la seva sobreexpressió accelera el procés de degeneració.

En resum, amb el nostre estudi descrivim la funció de SIVA-1 en neurones. Proposem SIVA-1 com un modulador de caspases i, per tant, com un regulador crucial en la mort cel·lular i la plasticitat neuronal.

CONTENTS

CONTENTS

ABBREVIATIONS

ABBREVIATIONS

A

aa	Amino Acids
a.u.	arbitrary units
AD	Alzheimer's Disease
AIF	Apoptosis Inducing Factor
AMPA	a-amio-3hydroxy-5-methyl-4-isoxazole-propionic acid
AMPAR	AMPA Receptor
ANOVA	Analysis of Variance
Apaf-1	Apoptotic Protease Activating Factor-1
APP	Amyloid Precursor Protein
APS	Ammonium Persulfate
AS	Alternative Splicing
Aβ	β -amyloid

B

BAK	BCL-2 Antagonist or Kller (BAK)
BAX	BCL-2 Effector Proteins BCL-2-associated X protein
BCL-2	B-cell CLL/Lymphoma 2
BH	BCL-2 homology
BIR	Baculovirus IAP repeat
bp	Base Pairs
BRUCE	Survivin and BIR-containing Ubiquitin Conjugating Enzyme
BSA	Bovine Serum Albumin

C

C57BL/6	C57 black 6
Ca^{2+}	Calcium
CARD	Caspase Recruitment Domain
cDNA	Complementary DNA

CDS	Coding Sequence
chLTD	Chemical LTD
CHX	Cycloheximide
cIAP1	cellular IAP1
cIAP2	cellular IAP2
CO_2	Carbon Dioxyde

D

DD	Death Domain
DDHR	Death Domain Homology Region
DED	Death Effector Domain
DISC	Death-Inducing Signaling Complex
DIV	Days *in vitro*
DMEM	Dulbecco's Modified Medium
DMSO	Dimethyl Sulfoxide
DNA	Deoxyribonucleic Acid
DNase	Deoxyribonuclease
DRG	Dorsal Root Ganglia

E

ECL	Enhanced Chemiluminescence
EDTA	Ethylenediaminetetraacetic Acid
ER	Endoplasmic Reticulum
ERK	Extracellular Signal-Regulated Kinase

F

FADD	Fas-Associated Death Domain Protein
FAIM	Fas Apoptotic Inhibitory Molecule
FasL	Fas Ligand
FBS	Fetal Bovine Serum

G

GAPDH	Glyceraldehyde 3-Phosphate Dehydrogenase
GFP	Green Fluorescent Protein
GluA2	Glutamate ionotropic receptor AMPA type subunit 2
GSK3	Glycogen synthase kinase-3

H

h	hours
HEPES	4-(2-hydrixyethyl)-1-piperazineethanesulfonic acid
HIV	Human Immunodeficiency Virus
HRP	Horsearadish Peroxidase
HS	Horse Serum

I

IBM	IAP-binding motif
IkB	Inhibitors of KB
IKK	IkB kinase
ILP2	IAP-Like Protein 2
IMS	Intermembrane Space
IP	Immunoprecipitation

K

K	Lysine residue
Kbp	Kilobase pairs
kDA	Kilo Dalton
KO	Knock-out

L

LFG	Lifeguard
LTD	Long-term Depression
LTP	Long-term Potentiation

M

miRNA	Micro RNAs
min	minutes
ML-IAP	Melanoma Inhibitor of Apoptosis Protein
MOMPS	Mitochondrial Outer Membrane Permeabilization
MPT	Mitochondrial Permeability Transition Pore
mRNA	Messenger RNA

N

NB	Naphtol Blue Black Stain
NCCD	Nomenclature Committee on Cell Death
NF-66	Neurofilament-66
NF-κB	Nuclear Factor κB
NGF	Nerve Growth Factor
NIAP	Neuronal IAP
NIK	NF-κB-Inducing Kinase
NMDA	N-methyl-D-aspartate
nSR100	Neural specific serine/arginine Repetitive Splicing Factor

P

PBS	Phosphate Buffered Saline
PCD	Programmed Cell Death
PCR	Polymerase Chain Reaction

Q

qRT-PCR	Quantitative Reverse Transcription PCR
Q-VD	Quinoline-Val-Asp-CH_2-OPH

R

RHD	Rel Homology Domain
RING	Really Interesting New Gene Domain

ROS Reactive Oxygen Species

S

S.E.M. Standard Error of the Mean

SAH Putative Amphipathic Helix Domain

shRNA Short Hairpin RNA

SMAC Second Mitochondria-Derived Activator of Caspases

T

TMBIM transmembrane Bax inhibitor-1 motif–containing protein

TNF Tumor Necrosis Factor

TRADD TNF Receptor Associated Death Domain

TSS Translational Start Sites

U

UTR Untreanslated Region

V

v/v volume /volume

W

w/v weight/volume

Wt Wild Type

X

XIAP X-linked Inhibitor of Apoptosis

INTRODUCTION

1. INTRODUCTION

1.1 Programmed cell death

Preservation of tissue homeostasis during development and the entire life of an organism requires a crucial control of the balance between cell survival and cell removal.

Naturally occurring cell death was first described in 1842 by Carl Vogt[1] and it was assumed to be a passive phenomenon until mid-1960. Decades of findings have since then unveiled and characterized in great detail a set of genetically encoded mechanisms for targeted elimination of cells, giving rise to the term programmed cell death (PCD)[2–4].

PCD ensures the elimination of superfluous, irreversibly damaged, and/or potentially harmful cells. Defects in PCD signaling cascades are broadly studied as major therapeutic target, as they determine etiology of several diseases, on one hand diseases associated with the irreversible loss of post-mitotic tissues (such as in neurodegeneration[5–7]); or, on the other hand, defects in PCD efficiency that cause uncontrolled cell expansion or accumulation (such as autoimmune disorders[8] and cancer[9]).

1.1.1 Types of cell death

Exposition to unrecoverable perturbations of the intracellular or extracellular environment induces a series of signal transduction pathways that can activate multiple forms of PCD.

According to the current classification system of cell death updated by the Nomenclature Committee on Cell Death (NCCD), PCD can be classified into

multiple subtypes, based on their morphological features and molecular characteristics[10,11].

Main types of PCD and their hallmarks are reported in Table 1.1.

PCD type	Morphological features	Biochemical features	Elicitors
Apoptosis	Cell rounding, nuclear condensation, membrane blebbing, apoptotic body formation	Caspases activation, DNA fragmentation, mitochondrial potential dissipation, phosphatidylserine exposure	Death receptor activation, DNA damage, metabolic stress
Necroptosis	Cell swelling, plasma membrane rupture, moderate chromatin condensation	RIPK1, RIPK3 and MALK activation, formation of necrosome	Activation of death receptors, Toll like receptors, virus infection
Ferroptosis	Smaller mitochondria, reduced mitochondria crista, elevated mitochondrial membrane densities and ruptures	Iron accumulation, lipid peroxidation, mitochondrial potential dissipation, conversion of MAP1LC3B-I to -II, glutaminolysis	Iron accumulation-induced ROS production
Autophagy-dependent	Autophagic vacuolization	Conversion of MAP1LC3B-I to -II, increased autophagic flux and lysosomal activity	Starvation
Lysosome-dependent	Lysosome and plasma membrane rupture	Lysosomal membrane permeabilization, release of lysosomal enzymes, lysosomal iron-induced oxidative injury	ROS, lipid metabolites

Table 1.1. Hallmarks of major types of PCD. Reviewed in Galluzzi et al., 2018[12].

1.2 Apoptosis

Apoptosis is a crucial type of PCD. The expression 'apoptosis' (from Ancient Greek 'falling off') was first coined by Kerr *et al.* in 1972, who described specific morphological characteristics of the dying cells: cellular shrinkage and formation of apoptotic bodies[13].

As schematically reported in Figure 1.1, apoptosis is accompanied by several morphological changes: rounding-up of the cell, reduction of cellular volume (pyknosis), chromatin condensation, nuclear fragmentation, plasma membrane blebbing, and later separation of cell fragments into apoptotic bodies, which *in vivo* are later engulfed by phagocytic cells and degraded[12,14]. The whole process of apoptosis is carried out without associated inflammatory reaction[15].

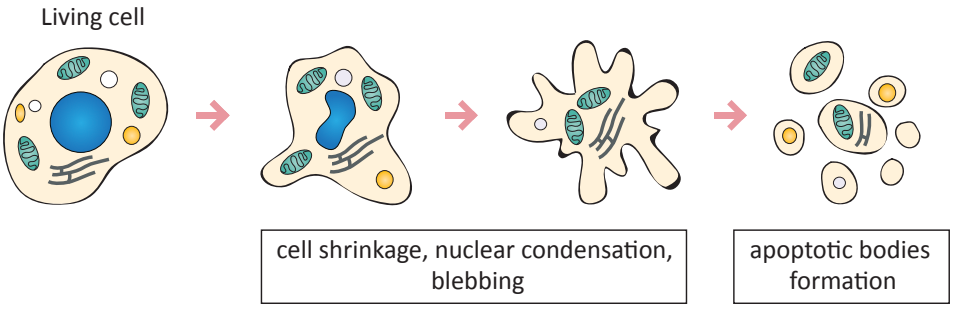

Figure 1.1: Hallmarks of apoptosis. Cells undergo several morphological changes during apoptosis: cell shrinkage, nuclear condensation and membrane blebbing. Organelles usually stay intact. The process culminates in the formation of apoptotic bodies.

All morphological changes observed during apoptosis are consequence of biochemical events that are initiated by an apoptotic stimulus, and that are tightly regulated by pro- and anti-apoptotic molecules.

Apoptotic initiation can occur through two main pathways which differ in the initial apoptotic stimuli: the intrinsic - or mitochondrial - pathway and the extrinsic - or dead receptor (DR) - pathway (Figure 1.2). Both pathways converge on the activation of the central executioner of apoptosis, effector caspase-3 and caspase-7[3,4,10].

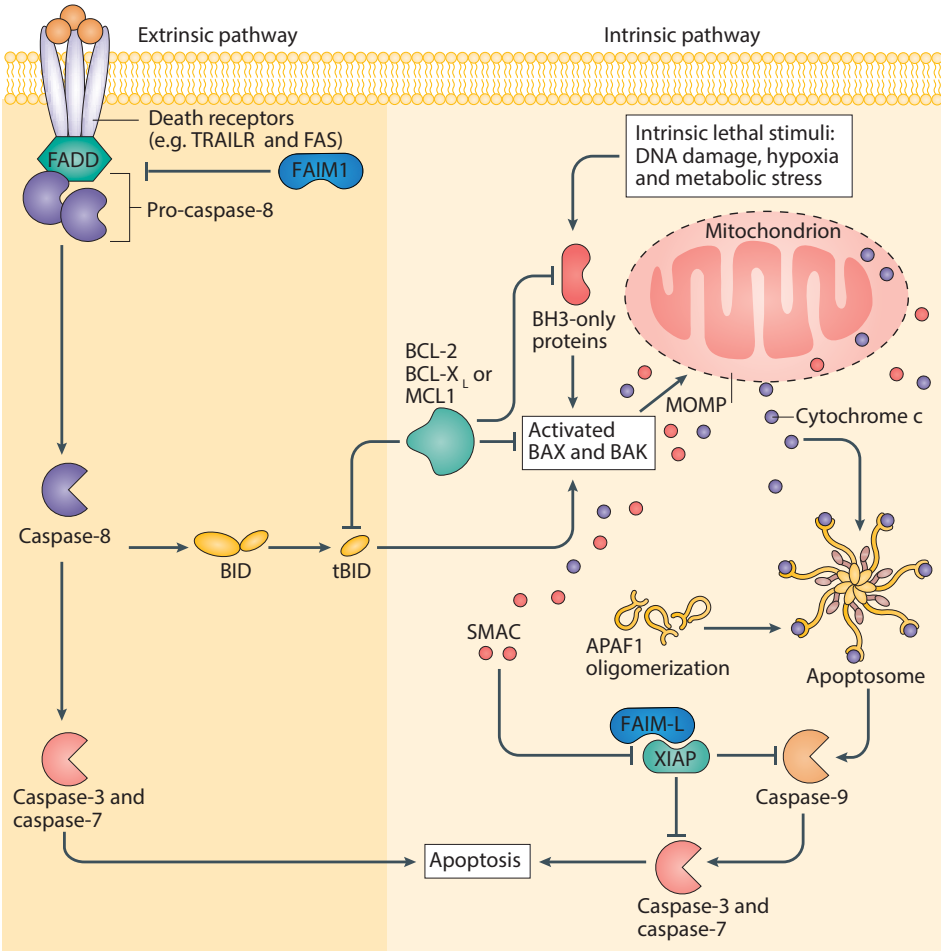

Figure 1.2: Extrinsic and intrinsic apoptotic signaling pathways. The extrinsic pathway is initiated via death receptors (DRs) at the cell membrane. Ligands engage DRs and induce the recruitment of caspase-8, that can either directly activate effector caspases or induce the mitochondrial pathway through cleavage of BID. The intrinsic pathway, on the other hand, is activated by intrinsic signals and is controlled by the BCL-2 protein family. The signals induce mitochondrial outer membrane permeabilization (MOMP) and release of pro-apoptotic factors which activate the caspase-9-dependent pathway through the formation of the apoptosome. Both pathways lead to the activation of caspases and, ultimately, to apoptosis. Figure adapted from Ichim and Tait, 2016[16].

Although each pathway involves its own initiators and adapters, many molecules are shared and can influence each other[17].

1.2.1 Intrinsic apoptotic pathway

Intrinsic apoptotic pathway is engaged by a wide array of intracellular stimuli, including hypoxia, DNA damage, reactive oxygen species (ROS) or growth factors withdrawal[18,19].

The critical step for intrinsic apoptosis is the widespread mitochondrial outer membrane permeabilization (MOMP), which is controlled by pro- and anti-apoptotic proteins, members of the BCL-2 (B-cell CLL/Lymphoma 2) protein family[20].

MOMP is generally engaged via BCL-2-associated X protein (BAX) and BCL-2 antagonist or killer (BAK), which form the mitochondrial permeability transition (MPT) pore. This process causes the loss of mitochondrial transmembrane potential and also allows the release of pro-apoptotic factors from the intermembrane space (IMS) into the cytosol[18,21,22]. These factors (listed in Table 1.2) facilitate apoptosis either by blocking caspase inhibitors as the X-linked Inhibitor of Apoptosis (XIAP)[23], or translocating to the nucleus and inducing chromatin condensation and fragmentation[21,24–27]. Cytochrome-c is released from IMS and once in the cytoplasm associates with apoptotic protease activating factor-1 (Apaf-1) and caspase-9, to form the apoptosome[28,29]. Apoptosome in turn activates caspase-9 through dimerization, inducing cleavage and activation of downstream effector caspases, such as caspase-3[30] (Figure 1.2).

Protein	Apoptotic activity
Cytochrome-c	Component of the electron transport in respiratory chain. Assembles with Apaf-1 and pro-caspase-9 to form the apoptosome.
Smac/DIABLO	IAP antagonist. Binds to and inhibits IAP proteins (cIAP1, cIAP2 and XIAP) promoting their degradation.
OMI/HtrA2	IAP antagonist. Binds to and inhibits IAP proteins (cIAP1, cIAP2 and XIAP) promoting their degradation. It also mediates cytoskeletal proteins degradation.
Apoptosis inducing factor (AIF)	Oxidoreductase. Translocates to the nucleus where it induces DNA degradation and chromatin condensation.
Endonuclease G	Nuclease. It translocates to the nucleus upon apoptotic stimuli where it mediates DNA fragmentation.

Table 1.2. Mitochondrial-released apoptotic proteins.

1.2.2 Extrinsic apoptotic pathway

The extrinsic apoptotic pathway originates at the plasma membrane when specific extracellular ligands bind to cell surface transmembrane death receptors (DRs)[31,32].

Up to now, eight receptors have been identified as members of DR subfamily. DRs are transmembrane proteins that contain a N-terminal domain composed by 2-4 cysteine-rich domain that mediates ligand binding, a transmembrane region, and a C-terminal intracellular tail known as death domain (DD)[32,33] (Figure 1.3).

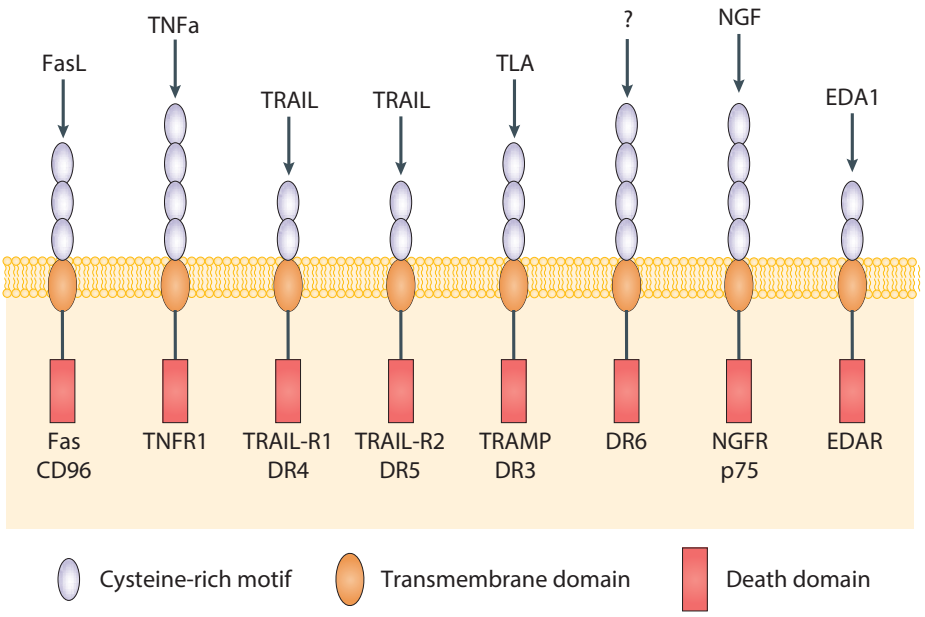

Figure 1.3: Death receptors and their ligands. Eight human death receptors and their ligands are represented. Domain composition is indicated in the legend.

Induction of cell death pathways requires ligand binding and oligomerization/trimerization of the receptor. Upon clustering, receptors recruit cytoplasmic adapter proteins through their DD to form de death-inducing signaling complex (DISC). DISC is composed by adaptor proteins such as Fas-associated death domain protein (FADD)/TNF receptor associated death domain (TRADD), and initiator pro-caspases (caspase-8/-10)[34,35].

Initiator caspases are then activated through dimerization and proceed with the apoptotic cascade. Two types of cells have been identified in accordance to the efficacy of DR signaling pathway[36,37]:

- Type I cells (such as liver cells): high levels of DISC formation and pro-caspase-8 concentration lead to direct cleavage and activation of downstream effector caspases (caspase-3/-7).

- Type II cells (such as neurons): lower levels of DISC formation and caspase-8 activation require an amplification loop of the apoptotic signal to drive effector caspases activation. The loop involves mitochondrial engagement through the cleavage of BID, a pro-apoptotic BCL-2 family member. Its cleavage generates truncated-BID (t-BID) which in turn activates BAX and BAK to form the MTP and induce the mitochondrial pathway.

Differences in receptor's DDs determine the recruitment of diverse adaptor proteins, that can lead to different outcomes for a cell[38,39]. FADD-recruiting DRs (Fas, DR4, DR5) have apoptosis as main signaling pathway[40], while TRADD-recruiting DRs (TNFR1, DR3) can also induce necroptosis - a form of caspase-independent PCD - or pro-survival, differentiation, or proliferation signaling through the activation of the NF-κB transcription factor[41] (Box 1).

Box 1. Nuclear Factor-κB (NF-κB)

NF-κB is a family of 'rapid-acting' transcription factors essential in regulating cellular responses. NF-κB is a mediator of pro-survival signaling but has been reported to have diverse functions depending on cellular context. All members of NF-κB family (p50, p52, p65 (RelA), RelB, and c-Rel) share a N-terminal Rel Homology domain (RHD) responsible for DNA binding and dimerization. p50 and p52 are synthesized as large precursors (p105 and p100) which undergo processing to generate active subunits. NF-κB members are present as inactive dimers in cytoplasm because are either in association with Inhibitors of κB (IκB) proteins (IκBα, IκBβ, IκBε), or, in case of p50 and p52, inhibited by their own IκB-like domain in the C-terminal of the precursor proteins. Activation pathways lead to inhibitor degradation, which leaves NF-κB complex free to enter nucleus and induce specific genes transcription. In the canonical activation pathway, the IκB kinase (IKK) is transiently activated and phosphorylates IκB proteins, which are in turn targeted for ubiquitination and proteasomal degradation (Box 2). In the non-canonical pathway, NIK activates IKKα, which mediates p100 phosphorylation (usually in a dimer with RelB) which results in its ubiquitination and proteolytic processing, which leads to the formation of p50[42–44].

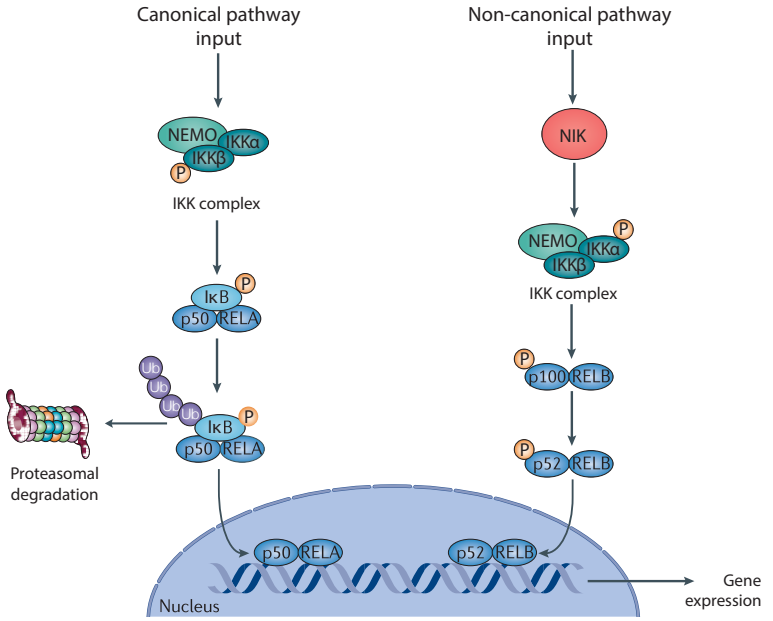

1.3 Mediators of apoptosis

1.3.1 Caspases

Caspases (cysteine aspartic acid-specific proteases) are a group of highly specific proteases that cleave their substrates by hydrolyzing peptide bonds after the aspartic acid residue preferentially in the X-X-X-Asp-Gly/Ser/Ala peptide motif[45]. Caspases are synthesized as inactive zymogens (pro-caspases) and require dimerization and often cleavage for activation[46,47]. All share a similar structure comprising a pro-peptide of variable length followed by a large and small subunit (Figure 1.4).

According to their functions human caspases can be grouped into pro-inflammatory caspases (caspase-1/-4/-5/-12), which are involved in the regulation of inflammatory cytokine processing (as IL1β and IL18)[48]; and apoptotic caspases.

Apoptotic caspases can be divided into two subcategories based on their mechanism of action in the signaling cascade[49]:

- Initiator caspases (caspase-2/-8/-9/-10) share a common structure that consist in protein-protein interaction domains, such as the caspase recruitment domain (CARD) or a tandem of two death effector domain (DED), which promote their interaction with initiator molecules. They exist as inactive monomers and are activated by homo-dimerization and autocatalytic cleavage, which results in stabilization of the dimer.

- Effector caspases (caspase-3/-6/-7) act downstream the initiator enzymes and generally have shorter pro-domains. They are produced as pro-caspase dimers that become active after cleavage mediated by an initiator caspase. Once activated, effector caspases act on multiple and specific cellular

substrates, allowing demolition of cytoarchitecture, degradation of organelles and overall, dismantle the cell. Caspases can additionally accelerate a feedback loop cleaving and activating other effector caspases[50].

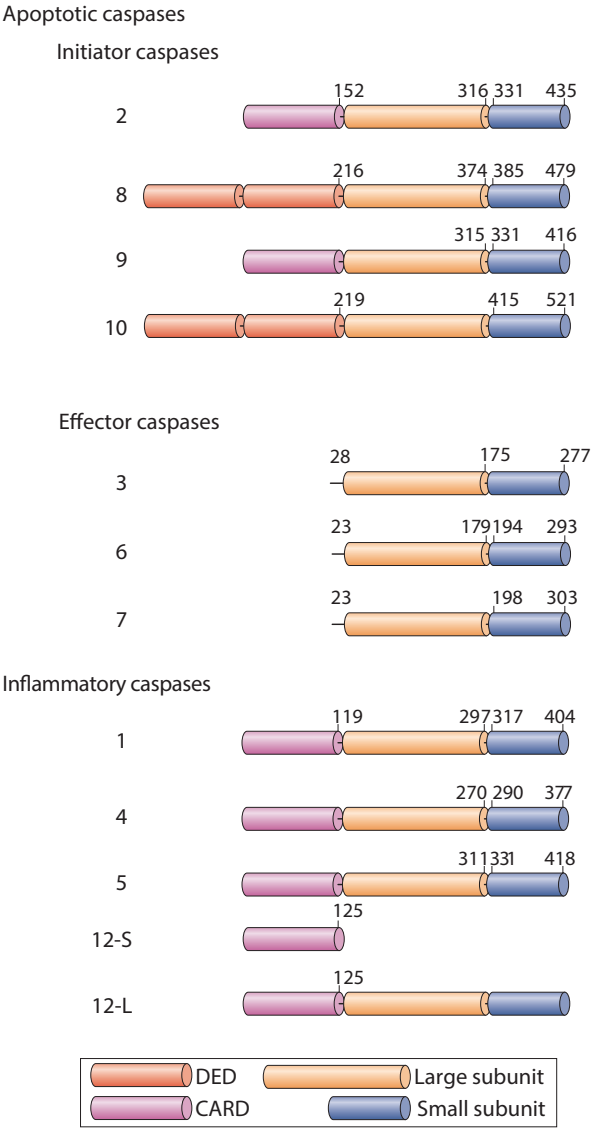

Figure 1.4: Schematic representation of caspase classification, domains and cleavage sites. Mammalian caspases can be divided into apoptotic and inflammatory caspases. Initiator apoptotic and inflammatory caspases contain pro-peptides composed by protein-protein interaction domains as CARD or DED. Cleavage at the marked aspartic acid residues results in pro-peptide removal and maturation of the caspases through structural rearrangements. Figure adapted from Taylor et al., 2008[47].

Given the critical role they play during apoptosis, and that they provoke irreversible changes within cell fate, caspase activity must be highly and specifically regulated. Several proteins have been described to directly regulate caspase-3 activation or modulate the steps that, from the apoptotic stimuli, lead to caspase-activation signaling.

1.3.2 BCL-2 protein family

Apoptotic mitochondrial events have a key role in dictating whether a cell commits to apoptosis or survival. The regulation of the pathway that culminates in mitochondrial permeabilization in apoptosis is highly regulated by members of the BCL-2 protein family and their complex network of interactions.

BCL-2 family members contain different BCL-2 homology (BH) conserved domains that confer protein functions and are used to classify them into three classes[47] (Figure 1.5):

- Anti-apoptotic members (such as BCL-2 or BCL-XL): contain four BH domains (BH-1, BH-2, BH-3 and BH-4). These proteins inhibit MOMP by either binding to BH3-only proteins – such as BAX and BAK, impeding MTP formation - or other modulators of cell death[51].
- Pro-apoptotic multidomain members (such as BAX, BAK, and BOK): contain three BH domains (BH-1, BH-2 and BH-3). These members can directly induce MOMP.
- BH-3 only members (such as PUMA, BID, and BIM): containing only the BH-3 domain. These members relay on apoptotic signal to inhibit anti-apoptotic members of BCL-2 family and therefore indirectly activate BAX and BAK at the mitochondrial membrane, where they trigger MOMP through MTP formation[52].

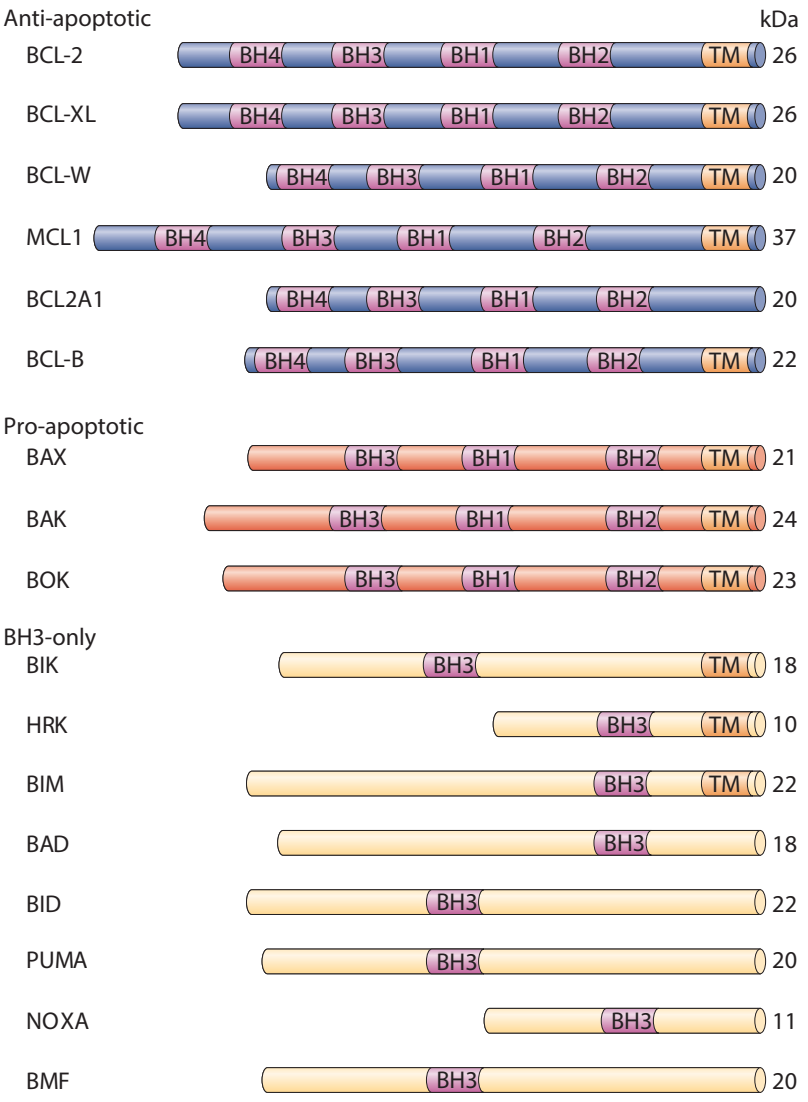

Figure 1.5: Schematic representation of BCL-2 family members' classification and domains. Members of the BCL-2 family. All members possess at least one of four conserved motifs known as BCL-2 Homology domains (BH1, BH2, BH3 and BH4). Most members also contain transmembrane domains (TM). Anti-apoptotic proteins possess all four BH domains and inhibit apoptosis by interacting with the pro-apoptotic members of the family. Pro-apoptotic members are grouped into two subfamilies: the multi-domain members, which promote MOMP, and the BH3-only proteins. Figure adapted from Taylor et al., 2008.

1.3.3 Inhibitor of Apoptosis Proteins

Inhibitor of apoptosis proteins (IAPs) are a conserved family of proteins that block cell death induced by a wide spectrum of apoptotic stimuli, including DRs, viral infection, growth factor withdrawal, radiation or chemotherapeutic agents[53]. Their action is carried out by direct binding and inhibition of caspases, or by promoting survival signaling[54].

IAPs are defined by the presence of at least one baculovirus IAP repeat (BIR) domain. The BIR domain is a 70-80 amino acid (aa) zinc-binding region that mediates protein-protein interaction and is essential for anti-apoptotic activity[55]. So far, 8 human proteins have been identified to belong to the IAP family: X-linked Inhibitor of Apoptosis Protein (XIAP), cellular IAP1 (cIAP1), cellular IAP2 (cIAP2), IAP-Like Protein 2 (ILP2), Melanoma Inhibitor of Apoptosis Protein (ML-IAP), Neuronal IAP (NIAP), Survivin, and BIR-containing Ubiquitin Conjugating Enzyme (BRUCE) (Figure 1.6).

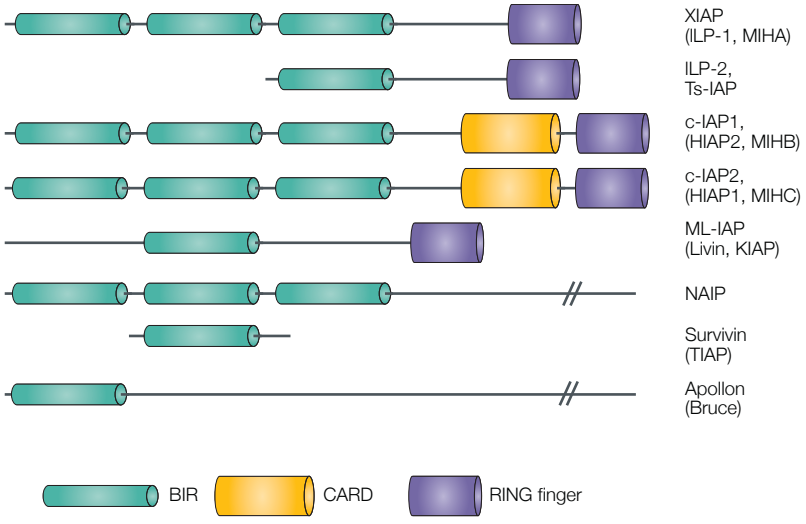

Figure 1.6: Schematic representation of inhibitors of apoptosis protein family and their domains: IAPs are composed by several domains. They have between one and three BIR domains that allow them to interact with other proteins, moreover they can include other functional domains as the CARDs that mediate protein-protein interaction and RING domain which confers them E3 ligase activity to IAPs.

Most of IAPs also harbor a C-terminal RING finger domain, which confers E3 ubiquitin ligase activity allowing IAPs to target proteins for proteasomal degradation (Box 2)[56,57].

After pro-apoptotic stimuli, IAPs levels and activation are regulated by pro-apoptotic proteins released by the mitochondria such as Smac/DIABLO and HtrA2/OMI, which bind to IAPs through their IAP-binding motif (IBM), displacing caspases from their inhibition and therefore enhancing cell death pathways[58].

1.3.3.1 cIAP1 and cIAP2

Cellular inhibitors of apoptosis 1 and 2 (cIAP1 and cIAP2) are cytosolic proteins that contain three N-terminal BIR domains, a caspase-recruitment domain (CARD), and a RING domain on their C-terminal[56] (Figure 1.6). cIAP1/2 have a weak caspase-inhibitor potential[59]. Nevertheless, both cIAP1 and cIAP2 have a vital role in inflammation. They inhibit DR-induced apoptosis and promote NF-κB signaling (Box 1), resulting as determinant modulators in the outcome of TNFR1-mediated signal transduction[60,61].

Box 2. Ubiquitination

Ubiquitination is a post-translational modification in which ubiquitin is covalently attached to target proteins. Depending on the number of ubiquitin units attached and the type of chains, ubiquitination effect may differ: it can either affect the protein localization, activity, interactions, or be a signal for protein degradation via the proteasome[62]. Mono-ubiquitination is the addition of just one molecule of ubiquitin and it induces the recruitment of the target proteins to downstream effectors[63]. Ubiquitin molecules can be added to the first, giving rise to poly-ubiquitination chains on a single lysine (K) residue on the substrate protein. Ubiquitin have seven lysine residues that can serve as point of ubiquitination. K63-linked poly-ubiquitin chains modulate protein through conformational, protein interaction or localization changes; K48-linked, is the best characterized polyubiquitination and targets the protein for degradation by the proteasome, a multi-compartment protease[64]. Ubiquitin is activated by enzyme-1 (E1) in an ATP-dependent manner, then is transferred to a ubiquitin conjugating enzyme (E2). Finally, a ubiquitin-protein ligase (E3) specifically attaches ubiquitin to the target through the amino group of a lysine residue. E2 and E3 then lengthen the ubiquitin chain so that the protein can be recognized and degraded by the 26S proteasome[65].

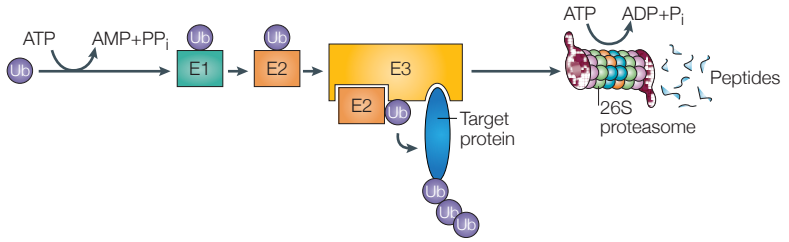

Adapted from Welchman et al., 2005

1.3.3.2 X-chromosome-linked inhibitor of apoptosis (XIAP)

The X-chromosome-linked inhibitor of apoptosis (XIAP) is a potent cytosolic inhibitor of caspases. It can directly bind and inhibit active caspase-3, -7, and -9[66,67]. XIAP contains three N-terminal BIR domains and a C-terminal RING domain with E3 ligase activity (Figure 1.6). The second BIR domain, together with the preceding linker, is responsible for caspase-3 and -7 binding and inhibition. The third BIR domain binds to and inhibits caspase-9[68,69].

Following apoptotic stimuli and MOMP, IAP antagonists such as Smac/DIABLO and Omi/HtrA2 bind to XIAP's BIR domains through their IBM, inhibiting XIAP-mediated inhibition of caspases. Interaction with IAP antagonists also reduces XIAP levels, as it induces auto-ubiquitination of XIAP through its RING domain, which targets the protein for proteasomal degradation[56,58].

As it will be explained in section 1.7 caspases are involved in mediating not only cell death, but also regulatory events required to refine mature neuronal circuits, such as long-term depression (LTD) and neurite pruning. XIAP has been shown to potently suppress caspase activation during their non-apoptotic function, and to be essential in restricting caspase activity to sub-lethal amounts, emerging as a plasticity modulator in both processes[70,71].

1.3.4 Death Receptor antagonists

Several types of molecules, such as IAPs and BCL-2 family members, regulate DR signaling by blocking the apoptotic cascade at different levels and conferring cells protection and survival[72,73]. Additionally, there are several proteins, known as death receptor antagonists, that are able to shut down DR signaling.

DR antagonists have a substantial role in neurons, during development and mature stages, and many of them present a specific neuronal expression pattern.

Developing neurons freely activate cell death pathway to regulate the number of neuronal networks forming. Once they become terminally differentiated, however, neurons have to remain alive and functional for the whole life of the organism[74]. Apoptotic machinery expression is maintained in neurons even once they are mature and have to promote survival at all costs, indicating that the proteins involved in apoptosis can be relevant in processes other than cell death induction.

Despite their name, death receptors are involved in several physiological processes such as cell differentiation, cell survival and neurite outgrowth[75–78]. DR signals and their modulation through DR antagonists, is therefore extremely important in neurons, to modulate physiological plasticity processes, as well as to grant additional protection to multiple stimuli that can affect neuronal integrity.

1.3.4.1 Cellular FLICE-like inhibitory protein (c-FLIP)

c-FLIP presents three protein variants: the short form (cFLIPS), the Raji isoform (c-FLIPR), and the long form (cFLIPL). All are structurally related to caspase-8, but lack proteolytic activity[79]. They contain two DED motifs that mediate their recruitment to death receptors, where they compete for DR binding with initiator caspases. c-FLIPL also harbors on its N-terminus a catalytically inactive pseudo-caspase domain, through which it can form a heterodimer with initiator caspase-8/-10 and inhibit them. cFLIPS/L have been reported to have multifunctional roles in different signaling pathways as well as activating or upregulating several cytoprotective and pro-survival signaling proteins such as

AKT[80,81], extracellular signal-regulated kinases (ERK)[76,82] and NF-κB[83,84]. In neurons, FLIPL acts as a modulator of neurite growth in developing neurons[82].

1.3.4.2 Fas Apoptotic Inhibitory Molecules (FAIMs)

Among the proteins reported to modulate DR signaling, Fas Apoptotic Inhibitory Molecules (FAIM) stand out. FAIM1, FAIM2 and FAIM3 all inhibit Fas-induced cell death, but they do not share structure nor functional mechanisms (Figure 1.7).

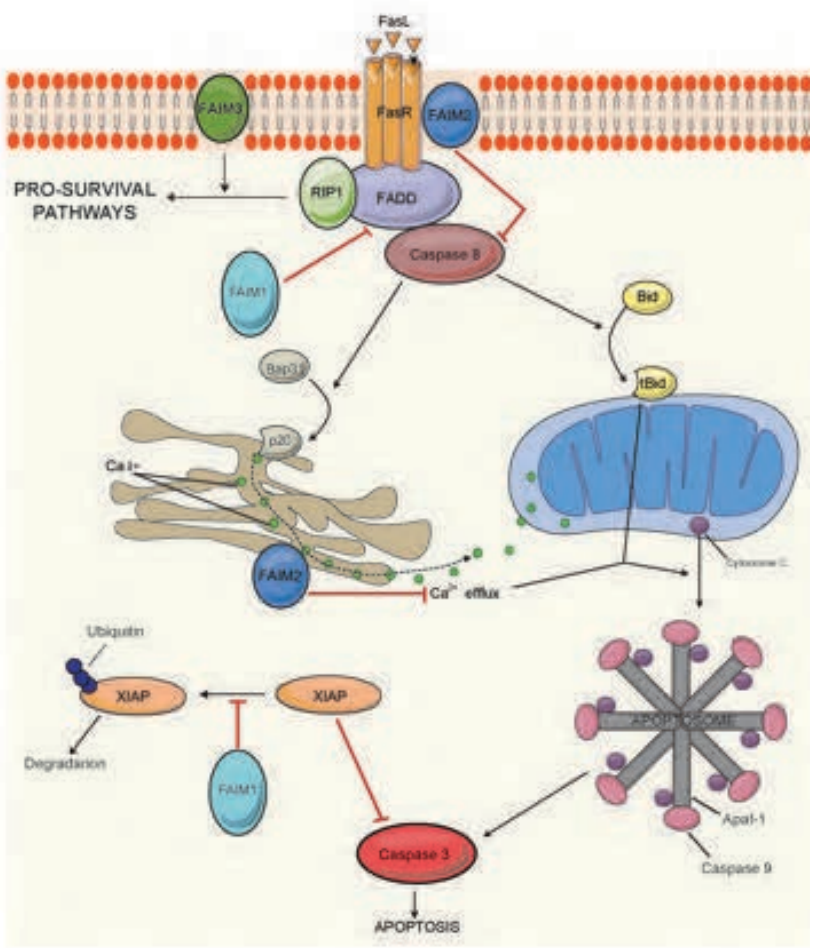

Figure 1.7 Schematic representation of FAIM family proteins in the apoptotic death receptor (DR) signaling cascade.

Figure 1.7 FAIM1 isoforms (FAIM-S and FAIM-L) prevent cell death by binding the Fas receptor and inhibiting caspase-8 cleavage. In addition, the neuron-specific isoform FAIM-L inhibits the autoubiquitination and subsequent degradation of XIAP. In plasma membrane, FAIM2 interacts with Fas receptor and inhibits caspase-8 cleavage. FAIM2 also interacts with BCL-XL at the endoplasmic reticulum where is able to inhibit calcium efflux from the ER, thereby impeding calcium-induced mitochondrial permeabilization. FAIM3 inhibits apoptosis through the disruption of DISC formation either through interaction with c-FLIP or FADD. A second mechanism of FAIM3-mediated protection is dependent on the ubiquitination of RIPK1. FAIM3 shifts DR signaling from cell death toward pro-survival through the activation of the MAPK/ERK and NF-κB pathways. Figure adapted from Planells-Ferrer et al., 2016[85].

FAIM1 has been extensively studied by our lab and will be described in section 1.4.

1.3.4.2.1 FAIM2 – Lifeguard (LFG)

FAIM2 - also known as Lifeguard (LFG) or TMBIM2 - was described as a transmembrane protein primarily expressed in neurons, able to protect from Fas-induced cell death – and not TNFR1-mediated signaling - by directly interacting with Fas, without displacing FADD binding[86,87].

LFG was described to be part of the family of transmembrane Bax inhibitor-1-motif-containing proteins (TMBIM) as TMBIM2. TMBIM proteins have anti-apoptotic activity and are involved in modulating calcium homeostasis at the endoplasmic reticulum (ER) and autophagy[88]. Calcium efflux from ER upon Fas stimulation has been shown to contribute to FasL-induced apoptosis[89]. Fas signaling relies on caspase-8 mediated cleavage of Bap31 and the formation of micropores between ER and mitochondria, which induce MOMP[90].

Our group has described that LFG protects against FasL-induced cell death by interacting with BCL-XL at ER, where it inhibits calcium efflux and the consequent calcium-induced mitochondrial permeabilization[91].

LFG confers neuronal protection in several pathological situations. Its neuroprotective functions have been reported in *in vivo* and *in vitro* models of transient cerebral ischemia[92], retinal detachment[93], pneumococcal meningitis[94] and Parkinson's disease[95].

In cancer, LFG has also been found associated with the biology of certain types of tumors. Its levels are up-regulated in some kinds of breast cancer, to which FAIM2 confers protection against Fas-induced cell death[96,97].

Our lab reported in 2014 that LFG levels correlated with neuroblastoma aggressiveness. Being LFG an anti-apoptotic protein, it was unexpected to find it down-regulated in the most aggressive types of neuroblastoma. Our lab showed that the downregulation of LFG modulates several genes involved in cell cycle and cell adhesion, resulting in reduced cell adhesion, increased migration and metastasis *in vivo*. Moreover, LFG transcription was repressed by MYCN, whose expression designates neuroblastoma cases with worst progniosis[98].

1.3.4.2.2 FAIM3 – TOSO

FAIM3 - or TOSO - is expressed especially in digestive and urinary tracts and cerebellum. FAIM3 is a transmembrane protein that belongs to the immunoglobulin family[99].

Overall, FAIM3 remains poorly characterized. It has been reported to be protective against DR-induced cell death mainly through two mechanisms: disruption of DISC formation[100] and promotion of pro-survival signaling through MAPK/ERK, NF-κB pathways [101,102]. FAIM3 has also been linked to immune system, as it is crucial for pro-inflammatory function of dendritic cells[103].

1.4 FAIM1

Human *FAIM1* gene contains six exons and three putative translational start sites (TSS) (Figure 1.8).

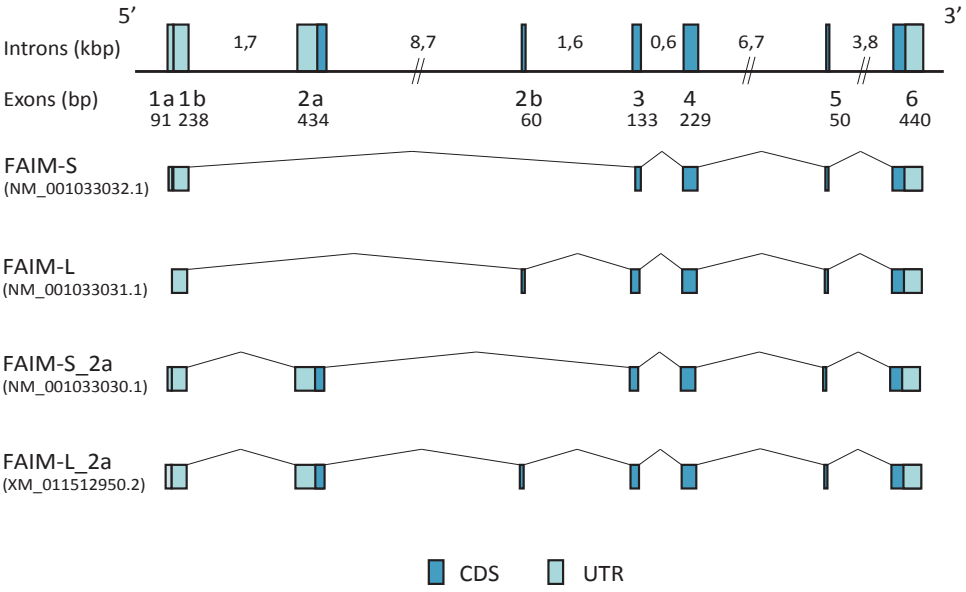

Figure 1.8: Genomic organization and splice variants of FAIM gene. The genomic structure of FAIM locus gives rise to four transcripts. Intron length is indicated above (kilobase pairs). Exon length is indicated below (base pairs). The following four transcripts are represented: FAIM-S (GenBank accession number NM_001033032.1), FAIM-L (GenBank accession number NM_001033031.1), FAIM-S_2a (GenBank accession number NM_001033030.1) and FAIM-L_2a (GenBank accession number XM_011512950.2). CDS: coding sequence; UTR: untranslated region. Adapted from Coccia et al., 2017[104]

FAIM-short (FAIM-S), and FAIM-long (FAIM-L) are the two main products of *FAIM1* gene. They differ by the inclusion of exon 2b at the 5'. We have recently characterized two additional isoforms, which correspond to FAIM-S and FAIM-L with the inclusion of exon 2a in their transcripts (Table 1.3, Figure 1.8).

In neurons, both new isoforms are able to promote neurite outgrowth when overexpressed.

Nevertheless, FAIM-S_2a and FAIM-L_2a endogenous expression is barely detectable at protein level. We could clearly detect them only blocking proteasome with an inhibitor (MG132). Interestingly, we described that, when overexpressed, most of 2a_isoforms mRNA is actually translated to the shorter corresponding isoforms, indicating that FAIM-S and FAIM-L TSS are preferentially targeted during translation for protein synthesis[104].

Isoform	Expression	Function in Neurons	Ref
FAIM-S	Ubiquitous	Neurite outgrowth promotion	105
FAIM-L	Neuronal	Anti-apoptotic activity, plasticity processes modulator	106,107
FAIM-S_2a	Ubiquitous	Neurite outgrowth promotion	104
FAIM-L_2a	Neuronal	Neurite outgrowth promotion	104

Table 1.3: Human *FAIM1* gene isoforms.

The two neuronal isoforms FAIM-L and FAIM-L_2a are generated by alternative splicing (AS) through the inclusion of exon 2b in their transcript. Based on a study by Raj and colleagues that screened for neuron specific splicing isoforms regulated by the 100-kDa Neural specific serine/arginine Repetitive Splicing Factor (nSR100), we showed that this factor is responsible for exon 2b inclusion in *FAIM1* isoforms[104,108]. nSR100 is an alternative splicing factor that regulates a network of brain-specific alternative exons, especially relevant during neurogenesis. nSR100 knock-out (KO) mice show impairment in the development of central and peripheral nervous system. nSR100 has been shown to have essential roles in correct neurite outgrowth, axon guidance and layering of cortical neurons[109–111].

FAIM1 expression is positively regulated by the ERK pathway activation in neuronal models. Recently we have exanimated, as other modulators of FAIM1 levels, micro-RNAs, small non-coding RNAs that can regulate expression at the post-transcriptional level targeting mRNA for degradation. As reported in Annex 8.1 we performed an *in silico* analysis to detect possible miRNA of interest and

corroborated in human neuroblastoma cell lines that miR-206, miR-1-3p and miR-133b are able to target and decrease FAIM isoforms expression.

Although FAIM1 gene is highly conserved evolutionarily, FAIM transcripts are structurally unrelated to other DR-induced apoptosis inhibitors[112] and structural analyses did not find any recognizable effector binding motif[113]. Interestingly, Kaku and colleagues recently suggested that FAIM-S and FAIM-L protein sequences show a significant underrepresentation of cysteine residues, which may be important to prevent unwanted crosslinking and denaturation and therefore grant these proteins a high resistance to stress conditions[114].

1.4.1 FAIM-S

FAIM-S was first isolated by Dr. Rothstein's group in B cells resistant to Fas-mediated cell death, where it provides protection against cell death and increases CD40-induced NF-κB activation[115]. FAIM-S is ubiquitously expressed and is capable to induce resistance to Fas-mediated cell death in several cell types[105,115,116]. Remarkably, in neurons, FAIM-S does not directly protect from DR-induced apoptosis, but it has a role in promoting NGF-dependent neuronal differentiation and branching through activation of ERK and NF-κB pathways[105].

Recently, the same group has shown that FAIM-S is able to protect against environmental insults that cause accumulation of cytotoxic and aggregated proteins, such as oxidative stress and heat shock. The protective mechanism in this case is reported to be caspase-independent and based on the ability to bind to protein aggregates and prevent their fibrillization/aggregation. Rothstein and colleagues proposed that FAIM-S structure can contribute to this novel function[114,117,118], as a relatively unstructured N-terminal region[113] could be important in binding aggregation-prone targets.

Dr. Lam's group reported FAIM-S regulation of insulin signaling[119] and first generated a FAIM1 null mouse in 2009. These mice present a spontaneous non-hyperphagic obesity, an increased fatty acid synthesis in liver, and reduced insulin receptor beta, supporting the involvement of FAIM-S in energy homeostasis and insulin signaling[120].

Some inconsistency is however found in the reports about FAIM1-KO mice phenotype. The phenotype described by Lam's group was not reproduced by our group on the same mice, and in our study some phenotypic characteristics changed based on the genetic background of the mice strain used. Moreover, Rothstein group also reported recently the generation of FAIM1-KO mice, in which they could not observe any obvious phenotypic changes[114]. Several factors can influence the appearance of phenotypes when analyzing mice models, such as genetic background of mice strain, flanking genes modifications during the generation of the mice, or environmental factors. The discrepancy on reports about FAIM1-KO mice makes therefore difficult for us to appoint any phenotype described to the lack of FAIM1.

1.4.2 FAIM-L

Following FAIM-S description, a longer isoform, FAIM-L, was identified in 2001 by Rothstein's group[121]. FAIM-L is expressed almost exclusively in neurons, and it is therefore included among neuronal-specific DR antagonists.

Compared to FAIM-S, it presents 22 additional aa at the N-term and is generated by alternative splicing, by the inclusion of exon 2b. nSR100 activates neural exon inclusion by binding to intronic UGC-containing motifs proximal to 3' splice sites. The same motifs serve to weaken 3' splice recognition and skip neuronal exons in non-neuronal cells[109,110]. A putative nSR100 binding site is present before the start of FAIM1 exon 2b (-41 GCUGC/GCUGCGU-13).

In our lab, we have been focused on describing FAIM-L and its mechanism of action and we have been able to describe part of its relevance in neurons over the years.

FAIM-L expression is especially high during neuronal differentiation *in vitro* and *in vivo*, where it reaches its maximal expression during embryonic and early postnatal stages. FAIM-L expression appears at early stages of neuronal differentiation, making it one of the earliest and most specific among neuronal markers[106].

Our group has reported that FAIM-L overexpression blocks Fas and TNFR1-induced cell death, and that knock down of FAIM-L by specific short hairpin RNA (shRNA) makes neurons susceptible to DR-induced cell death[106]. We showed that FAIM-L is able to protect neurons through two mechanisms: direct binding to non-stimulated Fas receptor, therefore impairing caspase-8 recruitment to the DISC[122], and acting on the regulation of XIAP. FAIM-L can directly bind to XIAP's BIR2 domain and impair its auto-ubiquitination and consequent degradation by the proteasome. Therefore, FAIM-L maintains XIAP levels, enabling it to inhibit effector caspases, and to promote survival[123] (Figure 1.9). Moreover, we have shown that, through its stabilization of XIAP, FAIM-L is also able to inhibit caspase-dependent non-apoptotic functions, such as long-term synaptic depression and neurite pruning[107], emerging as a regulator in neuronal cell death and in essential processes for neuronal physiology.

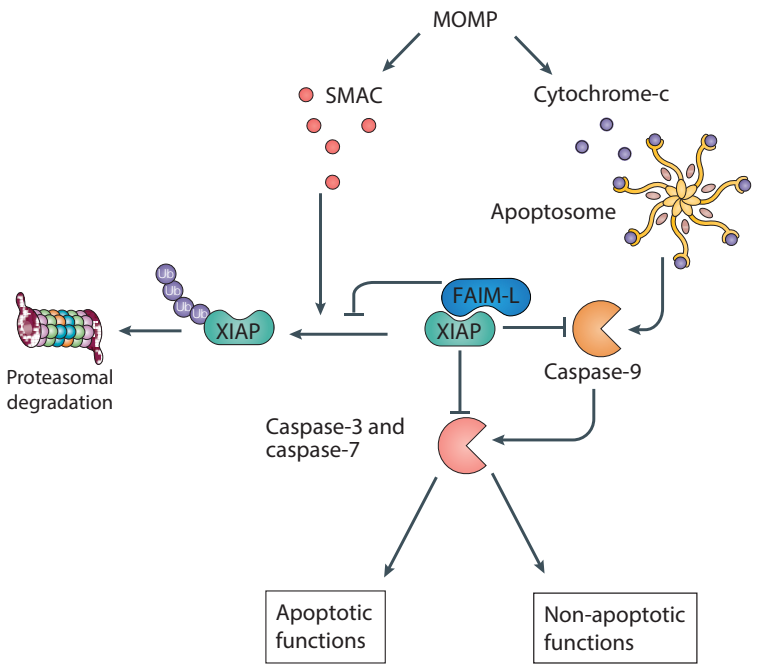

Figure 1.9 FAIM-L mechanism of action. Once MOMP is engaged by death signals or neuronal plasticity signals, molecules released by mitochondria induce XIAP auto-ubiquitination and degradation by the proteasome, leading to loss of caspase inhibition and therefore caspase activation. However, in the presence of FAIM-L, XIAP auto-ubiquitination is inhibited, leading to protection from caspase-apoptotic and non-apoptotic functions.

In 2015 we reported FAIM-L implication in pathological neurodegeneration in the main neurodegenerative disease, Alzheimer's Disease (AD) (Box 3). FAIM-L expression levels are progressively reduced in hippocampus of patients of AD and transgenic mouse models of the disease present a reduction in entorhinal and hippocampal cortex levels of FAIM-L before the onset of degeneration. *In vitro* experiments have shown that Amyloidβ (Aβ) is responsible for the decrease observed in FAIM-L levels.

We showed that FAIM-L levels are key in determining the inflammatory response of neurons, specifically to TNFα. In physiological conditions, FAIM-L allows TNFα to be protective against Aβ toxicity. However, Aβ accumulation

induces a decrease in FAIM-L levels, which in turn determines loss of TNFα protection. FAIM-L decrease appears therefore crucial for contributing to neurodegeneration. Restoration of FAIM-L in an *in vitro* model of Aβ toxicity allows to recover the protective function of TNFα[124,125].

Box 3. Alzheimer's disease (AD)

AD is the most common neurodegenerative disease that progressively impairs memory and cognitive skills. Defining pathological hallmarks of the disease at the anatomical level are brain atrophy associated with loss of synapses and neurons. At the microscopic level, deposition of extracellular accumulation of Aβ plaques, intracellular microtubule-associated protein tau aggregates, and neuroinflammation[126]. Neurons affected in AD follow a dying-back process where abnormalities in synaptic function and axonal integrity long precede somatic cell death[127]. Many factors involved in apoptosis have been also involved in the pathology of AD, and caspase dysregulation has been implicated in several stages of the disease[128–132]. The hallmarks of the pathology have been directly related to breaking the balance among pro- and anti-apoptotic factors and induce caspase activation, with consequences in neurite selective degeneration[133], synapses loss[131], and finally induction of apoptotic cell death[134].

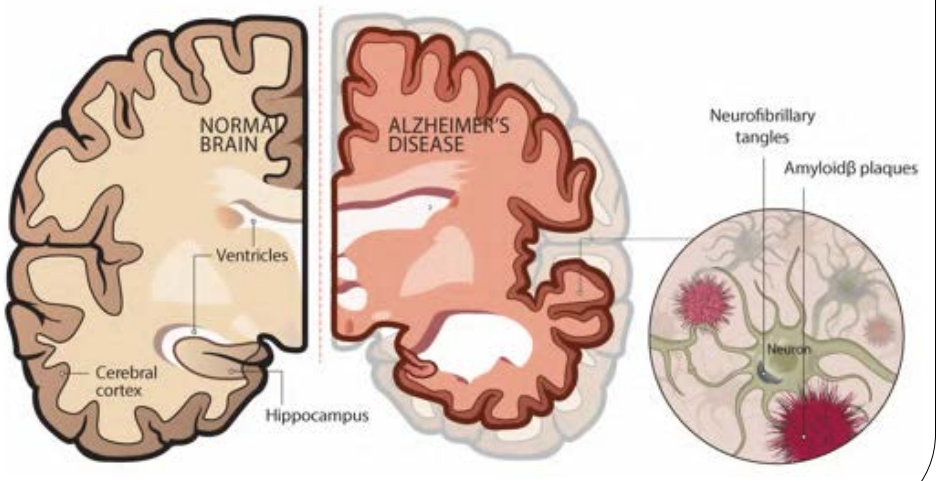

Adapted from illustration by Stacy Jannis/Alzheimer's association.

Interestingly, Kaku and colleagues have documented the capacity of both FAIM-S and FAIM-L to bind to and suppress spontaneous fibrillization/aggregation of accumulated proteins, including $A\beta^{114}$. FAIM isoforms impair accumulation in a direct manner, since this effect is measured with recombinant proteins in *in vitro* assays, in absence of other cellular components.

FAIM-L appears therefore to be a modulator of essential processes for correct neuronal development, plasticity, and resistance to degeneration. To further deepen our characterization, we were interested in detecting FAIM-L-interacting proteins, as none was reported other than XIAP. To this end, our lab performed a two-hybrid screening approach, a molecular biology technique that allows the fast screening of protein-protein potential interactions (Box 4).

Our lab used as bait both full-length and the specific N-terminal aa sequence of FAIM-L (MASGDDSPIFEDDESPPYSLEK). Six proteins were detected to be potential partners of FAIM-L (reported in Table 1.4). The hit we found more interesting was the N-terminal sequence of SIVA-1, a pro-apoptotic protein.

Two-hybrid hit	Sequence
SIVA-1 (ΔSIVA-1)	MPKRSCPFADAAPLQLKVHVGLKELSHGVFAERYSREV
FERM RhoGEF	HELKKDLIGIDNLVTPGREFIRLGSLSKLSGKGLQQRMFFLFNDVLLYTSRGLTASNQFKVH GQLPLYGMTIEESEEEWGVPHCLTLRGQRQSIIVAASSRSEMEKWMEDIQMAIDLAEKSN GPTPELLASSPPDNKSPDEA
GAPDH	YSNRMVDLMAYMASKE
COMMD1	EGGKSLSGLLSGLAQNAFHGHSGVTEELLHSQLYPEVPPEEFRPFLAKMRGLLKSIASADM DFNQLEAFLTAQTKKQGGITSEQAAVISKFWKSHKIKIRESLMKQSRWDNGLRGLSWRVD GKSQSRHSTQIHSPVAIIELEFGKNGQESEFLCLEFDEVKVKQILKKLSEVEESINRLMQAA
Calcyclin	DKFVKIYITLTGVHQVPTENVQVHFTERSFDLLVKNLNGKNYSMIVNNLLKPISVESSSKKV KTDTVIILCRKKAENTRWDYLTQVEKECKEKE
AP2m1	PKRACQFNRTQLGDCSGIGDPTHYGYSTGQPCVFIKMNRVINFYAGANQSMNVTCVGKR DEDAENLGHFVMFPANGSIDLMYFPYYGKKFHVNYTQPLVAVKFLNVTPNVEVNVECRI NAANIATDDERDKFAGRVAFKLRINKT

Table 1.4: Yeast two-hybrid analysis results.

Box 4. Yeast two-hybrid technique

The yeast double hybrid technique provides a sensitive method to detect protein interactions, also those relatively weak and transient[135]. This technology can be used to identify new interactions between proteins, confirm suspected interactions and define domains of interaction. The system exploits the modular nature of transcription factors, which can be split into a DNA-binding domain and an activating domain. The protein of interest is expressed fused to the DNA binding domain of a reporter gene (bait), while another protein - or a full library of cDNAs - are expressed in fusion to the activation domain (pray). In case of a positive interaction between bait and pray, the transcription factor is activated and result in the expression of a reporter gene. In case of a negative interaction the transcription factors domains do not associate, and no reporter gene is expressed. Reported genes show a phenotype that allows for selection and retrieval of protein-encoding sequences inserted.

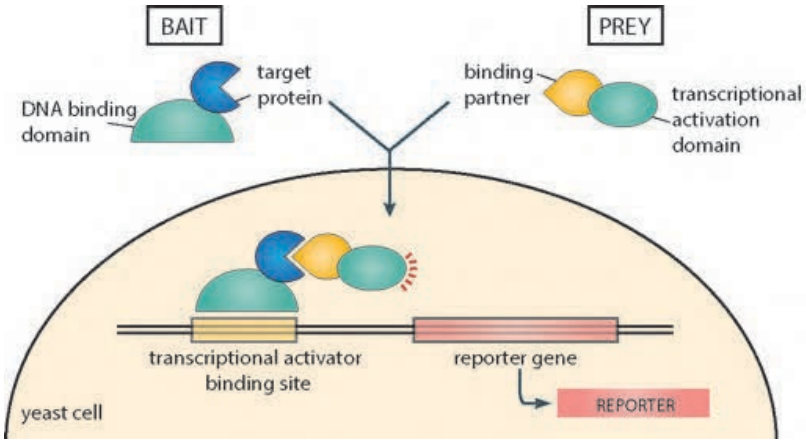

1.5 SIVA-1

SIVA-1 was first described in 1997 in immune cells, as an adaptor protein that binds to the cytoplasmic tail of CD27 receptor[108], and has been later found to interact and modulate signal transduction of also other TNFR family receptors, including GITR, CD40 and OX40[109]. It exists as two alternative splice isoforms, SIVA-1 and SIVA-2.

SIVA-1 is a 175 aa length protein and contains in its structure two regions that are essential for its promotion of apoptosis: a death domain homology region (DDHR) and a putative amphipathic helix domain (SAH) (Figure 1.10). Its C-terminal contains two cysteine-rich regions. SIVA-2 isoform lacks exon 2 that contains the DDHR, and presents a greatly reduced apoptotic activity[138].

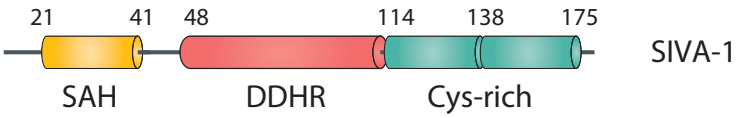

Figure 1.10: Schematic representation of SIVA-1 domains: SIVA-1 contains an amphipathic helical region (SAH) in the N-terminal region, a death domain homology region (DDHR) in the central part, and two cysteine (Cys)-rich regions at its C-terminal region.

SIVA-1 has been described to play a critical role in apoptosis in a wide variety of cell types[136–139] and to be capable of inducing extensive apoptosis through multiple mechanisms in response to various triggers[140–142].

Ectopic expression of SIVA-1 triggers apoptosis. Several typical markers have been reported, such as BAK/BAX translocation to mitochondrial membrane, cytochrome-c release and caspase-3 activation[139,143–145]. Moreover, SIVA-1 can inhibit anti-apoptotic members of BCL-2 family by direct binding through its SAH domain[145,146].

Some studies have revealed a key role for SIVA-1 in T cell receptor activation-mediated cell death[147,148]. These same studies propose SIVA-1 induction of cell death to be mediated by inhibition of the NF-κB pathway. SIVA-1 loss results, in fact, in enhanced NF-κB-dependent expression of anti-apoptotic proteins, such as BCL-XL and c-FLIP. Resch et al. also proposed an NF-κB-inhibition in SIVA-1-induced cell death, through interaction and inhibition of XIAP[149].

SIVA-1 has been reported to be a transcriptional target of both p53 and E2F1[144]. SIVA-1 is specifically upregulated during p53 tumor suppression protein-induced apoptosis, and results crucial for apoptosis during DNA damage and neuronal and kidney ischemia in *in vitro* an *in vivo* models[143,144,150].

Beyond its role in apoptosis, SIVA-1 also regulates other cellular processes, such as cellular migration[151,152], autophagy[153], and proliferation[151,154]. In cancer studies SIVA-1 has been found to have a role as pro- or anti-malignant factor, depending on cellular context[155].

Studies carried out in ovarian and cervical cancer cells show that SIVA-1 suppresses migration and invasion of cancer cells, and overall prevents metastasis through phosphorylation of stathmin, a microtubule destabilizer[151,154].

In other cases, instead, SIVA-1 has been reported to have the opposite role. Pro-oncogenic role of SIVA-1 has been linked to a negative feedback loop regulation that can induce degradation of p53[156], and to its involvement in mitochondrial respiratory capacity and energy production. Van Nostrad and colleagues showed in non-small cell lung cancer that SIVA-1 knockdown reduces energy production and results in autophagy, suggesting that SIVA-1 is necessary to facilitate tumorogenesis[153].

In line with the findings of SIVA-1 as a protein of relevance in several cellular processes, Jacobs and colleagues reported an essential role of SIVA-1 during embryonic development, during which a tight regulation of cellular proliferation and differentiation mechanisms is essential. They generated a *Siva-1* KO mice and reported that *Siva-1* deficiency results in mid-gestational embryonic lethality, associated with several developmental abnormalities, developmental delay and defects in neural tube closure[157].

1.6 Apoptotic role of caspases in neurons

1.6.1 Apoptosis in the nervous system development

During nervous system development, physiological neuronal loss contributes to sculpting neuronal network. After exiting cell cycle, neurons start axonal elongation to innervate their targets. It is during this phase that approximately 30-70% of newly generated neurons in the adult nervous system undergo programmed cell death, assuring therefore only the appropriate connections to remain. Several mechanisms have been described to take place during this stage in development, such as competition of neurons for limiting amounts of pro-survival factors produced by targets and glia, or induction of PCD signaling in those neurons migrating to ectopic positions or innervating inappropriate targets[158–161].

Experimental manipulations have shown that in peripheral nervous system, target excision leads to cell death of innervating neurons[162,163]. This led to the hypothesis, and later the molecular confirmation, of a neurotrophic theory, which relies on the concept that neuronal targets regulate fate of innervating neurons. Like for all cells, neuronal survival requires trophic support. Immature neurons depend on the availability of these factors, released by their targets, to induce survival pathways. Survival of only those neurons that innervate their targets allows to match the size of developing neuronal populations to the extent of their post-synaptic targets[158].

In central nervous system, neuronal activity and neurotransmitter input seem to play an essential role in survival, since blocking synaptic transmission through brain development increases neuronal death[158,164]. Neuronal activity can in fact promote survival of those neurons that are correctly integrated in the circuit by

directly modulating the expression of anti-apoptotic proteins and by inducing the expression of secreted trophic factors such as BDNF[165,166] and GDNF[167].

Changes in expression and activity of apoptotic machinery components allow for modulation and temporal restriction of cell death. Several pro- and anti-apoptotic proteins are highly expressed in the nervous system during development. Many regulators expression peaks in embryonic day 12 to 15, which corresponds to early neurogenesis, and then are downregulated after birth. Mice models have been extremely useful in determining which of these proteins are essential for a correct development. A clear role of intrinsic apoptotic components was confirmed by the studies carried out in transgenic mice. Table 1.5 reports some genes with a high expression in central nervous system during development and whose genetic editing induces neuronal phenotypes.

Gene modification	Transgenic mice neuronal phenotype	Ref.
Bcl-2 overexpression	Larger brain, more neurons.	168,169
Bcl-x overexpression	Lethal around E13. Extensive apoptotic cell death in post-mitotic differentiating neurons.	170
Bax knock out	Widespread apoptosis of neuronal precursors.	171
Caspase-3 knock out	Phenotype and lethality strongly dependent on genetic background. Inappropriate amplification of specific populations of neural progenitors, neural overgrowth.	172
Caspase-9 knock out	Lethal perinatally. Severe defects in brain morphogenesis.	172,173
Apaf1 knock out	Severe defects in brain morphogenesis.	174

Table 1.5: Neuronal phenotype of transgenic mice models of intrinsic apoptotic genes.

1.7 Non-apoptotic role of caspases in neurons

Accumulating evidence in the last two decades supports a non-apoptotic and non-inflammatory function of caspases in the nervous system[71,131,175,176]. Studies have in fact shown that restricted and localized caspase activation within neurons allows for essential processes in neuronal development and functions, such as synaptic physiology and neurite rearrangement. Inhibitors of caspases have been shown to impair neuronal remodeling and memory formation[177–180].

Localized activation of caspases in living neurons is achieved by several regulatory mechanisms that limit the proteases activity in order to prevent a widespread activation and consequent neuronal loss, such as a limited engagement of mitochondria in the activation, strict regulation by anti-apoptotic proteins and quick change in protein status and activity through transcription, degradation or post-transcriptional modifications[181].

The two main plasticity processes regulated by caspase non-apoptotic activity are hippocampal long-term depression and dendrite pruning.

1.7.1 Long-Term Depression (LTD)

Many forms of learning and memory require experience-dependent synaptic adjustments in the hippocampus[182].

Glutamate is the most abundant excitatory neurotransmitter. It binds to N-methyl-aspartate (NMDA) receptors (NMDAR), amino-3-hydroxy-5-methylisoxazole-4-propionic acid (AMPA) receptors (AMPAR), and metabotropic glutamate receptors (mGluR). Once bound, it triggers an increase in calcium levels in the stimulated spine[183].

In NMDAR-dependent synaptic modifications, the outcome of calcium entry is either a gain in AMPAR expression in synapses experiencing an increase in their strength (long–term potentiation, LTP) or a decrease in the number of surface AMPAR in weakening synapses (long-term depression, LTD)[184]. During these changes, spines can also undergo size remodeling, shrinkage, or be lost[183,185].

AMPAR are heterotetrameric complexes that are composed of different combinations of subunits (GluR1-4). In the adult hippocampus two major subtypes of AMPAR exist that contain either GluR1/GluR2 or GluR2/GluR3 subunits. In LTD, both GluR1- and GluR2-containing receptors can undergo inducible internalization, after which receptors can either be recycled back on the surface or be targeted for elimination in lysosomes[186].

Studies have shown a great conservation between apoptotic and LTD induction pathways. Caspase-3 is found to be the essential effector of LTD, which, in fact, is abolished in the hippocampus of caspase-3 deficient mice[70]. LTD requires essential players of the apoptotic pathway, mitochondrial engagement and cytochrome-c release. Mitochondria distribution and motility are regulated by synaptic activity, they can be found in dendrites, and sometimes in individual spines, allowing for a spatial control of the pathway activation[187].

As schematically reported in Figure 1.11, NMDAR stimulation increases calcium levels in the synapses. In turn, calcineurin dephosphorylates AMPAR and BAD. BAD dephosphorylation promotes its activation and relocation to mitochondria[188], and therefore induces mitochondrial disruption, cytochrome-c release, apoptosome activation and ultimately caspase-3 activation[189]. Caspase-3 precise mechanism is yet to be elucidated, but it has been shown that caspase-

dependent cleavage of the protein kinase AKT removes inhibition on glycogen synthase kinase-3 (GSK-3) activity, which is required for AMPAR endocytosis[190].

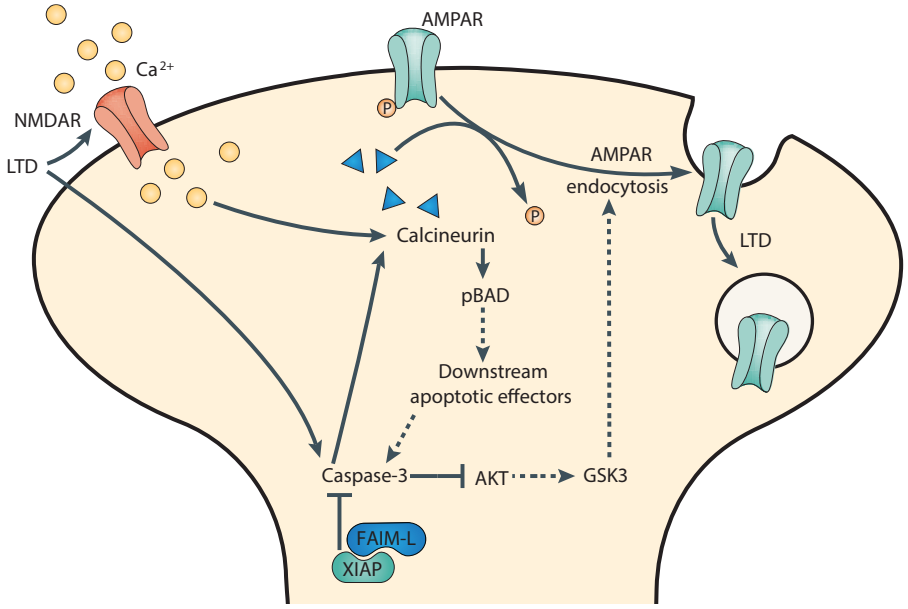

Figure 1.11: Long Term Depression schematic representation. Calcium entrance following NMDA stimulation activates calcineurin which de-phosphorylates AMPAR and pBAD, which leads to downstream effect such as mitochondrial disruption, apoptosome activation and ultimately caspase-3 activation. Caspase-3 cleaves AKT and in turn allows GSK-3 to induce AMPAR internalization. Anti-apoptotic proteins such as XIAP, and FAIM-L inhibit caspase activation in this process.

There are several mechanisms to fine-tune the activation intensity of caspase-3, thereby favoring a transient activity in LTD, instead of a persistent activation that would commit cells to induce apoptosis. The *in vitro* model of chemical LTD (chLTD) shows that NMDA treatment induces a rapid and transient increase in active caspase-3 and cytosolic cytochrome-c, which peaks within 30min of NMDA treatment before decreasing to baseline. Interestingly, BAX and BAD have been shown to be sufficient and necessary for mitochondrial factor release during LTD. However, as opposed to apoptotic induction, in this situation BAX does not form pores in mitochondrial membrane, therefore resulting in only a

mild engagement of mitochondria that could explain the transient activation of the apoptotic cascade[70,188].

Anti-apoptotic proteins have also a role in restricting the physiological activation of caspases to local sites and to suppress it so that it does not spread to the whole cell. LTD has been shown to be abolished by anti-apoptotic proteins present in post-synaptic terminals such as XIAP, FAIM-L – which acts through its role in XIAP levels stabilization - and BCL-2[70,107,182].

During plasticity processes it is essential to have a local and rapid turnover of components of the synaptic proteome, composed by ion channels, neurotransmitter receptors, regulators of synaptic function, and adhesion and scaffolding molecules. Synapses are equipped to have the rapid and dynamic changes in protein levels necessary for plasticity. Both translation machinery and proteasomal system are found in synapses, so that protein new synthesis and degradation occurs rapidly and independently of the cell soma - that can be located up to hundreds of microns away[191–193].

Synthesis of new proteins encoded by pre-existing messenger RNAs (mRNAs) in the synapses, has been demonstrated to occur in response to stimulation, and even if it is not necessary for initiation of AMPAR endocytosis in hippocampal LTD, it is required for AMPAR trafficking for its maintenance[194–196].

1.7.2 Dendritic pruning

Pruning of axon and dendrites is a crucial process that sculpts neuronal connections, as it removes excessive or inaccurate projections without resulting in the death of the cell. The mechanism can involve small-scale pruning of axon terminals, or large-scale removal of branches[197].

Pruning is characterized by cytoskeletal destabilization, microtubular disassemble, neurofilament fragmentation and degradation of axonal components. The portion of the axon destined for removal is finally engulfed and digested by surrounding glia[198].

During development of peripheral nervous system the deprivation of NGF from only the distal axons of neurons promotes axon pruning and remodeling, without causing neuronal death[133,199]. The *in vitro* culture of peripheral sensory neurons is a convenient system to study the process, and has been widely used as a model for developmental disease[200].

Experimental results show that in response to local NGF withdrawal, a pathway that converges with apoptotic initiation is activated (Figure 1.12).

BAX engagement is required to induce cytochrome-c release from mitochondria[133], and a caspase-9 to caspase-3 cascade is activated and found to be crucial for the degeneration[160,197]. Caspase-3 is the main effector, activating caspase-6, which plays a significant but subsidiary downstream role[177]. Caspases finally orchestrate cytoskeleton fragmentation and organelle degradation.

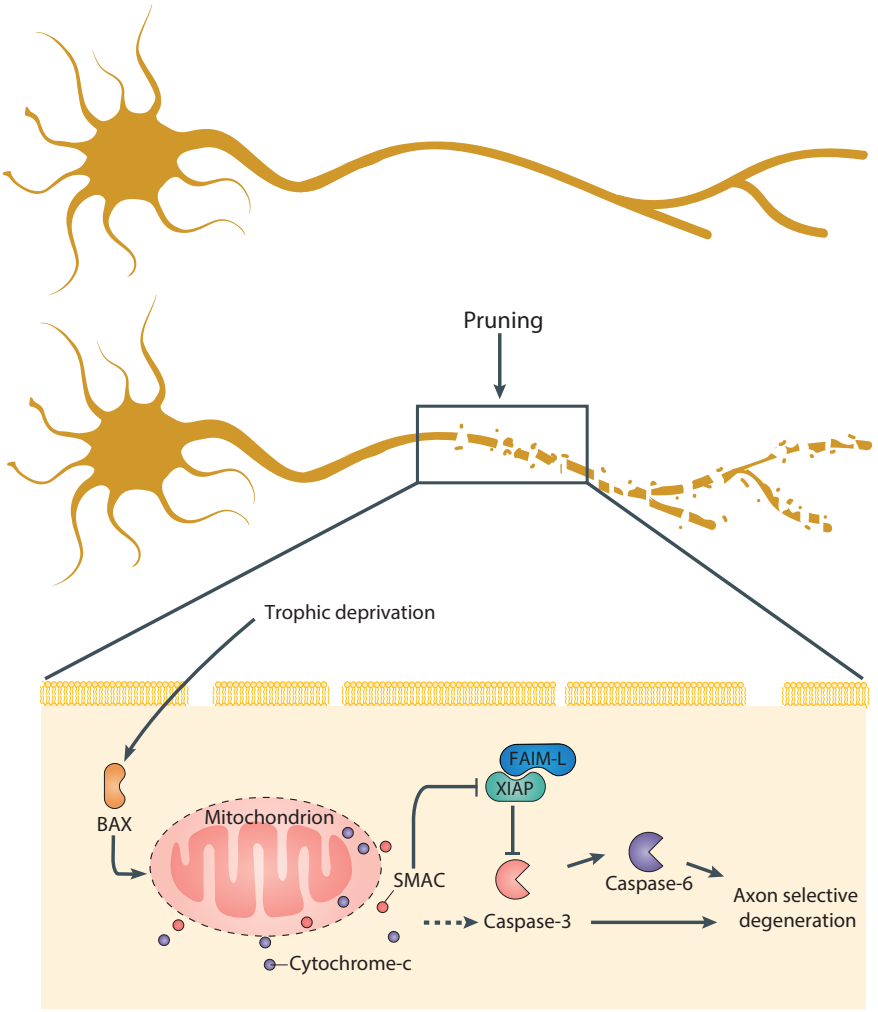

Figure 1.12: Schematic representation of axonal pruning. Trophic factor deprivation induces activation of BCL-2 family member BAX. Mitochondrial engagement is required to activate caspase-9 to caspase-3 cascade. Caspase-3 activates caspase-6 and induces structural changes and axon selective degeneration.

As in LTD, caspases are activated locally, only in those neuronal processes or branches destined to be eliminated.

Caspase-3 activity restriction results crucial for survival of the neuron. A mechanism for temporal and spatial restriction appears to be the engagement of the apoptotic pathway not in its full potential. Even though cytochrome-c release and caspase-9 activation are detected, the adaptor Apaf-1 is dispensable

for axon pruning, raising the possibility that caspase activation occurs independently of the apoptosome and can therefore be limited[199]. Studies have also found that IAPs can bind to caspases in a sort of IAP-based “clutch system”, in which active caspases are stalled, ready for quick release upon stimuli, bypassing the need for Apaf-1 and apoptosome formation.

XIAP has been described as essential in spatial restriction of caspase activity during pruning. Together, low Apaf1 engagement and high FAIM-L levels grant a strict control of XIAP post-cytochrome-c inhibition of caspases and therefore can stop the wave of caspase activation before it can reach cell soma[107,201].

HYPOTHESIS AND OBJECTIVES

2. HYPHOTHESIS AND OBJECTIVES

Pathological and physiological activation of caspases in the adult brain share the same molecular mechanism in their effector phase. New insights in the regulation of caspase activation contribute to better understand not only physiological plasticity functions, but also pathophysiological mechanisms of neurodegenerative disorders.

In our lab, we have described FAIM-L, a neuronal anti-apoptotic protein, and its role in protecting XIAP levels, essential for caspase inhibition. We have involved this mechanism in apoptosis and neuronal-specific plasticity changes. Since balance between the activity of pro- and anti-apoptotic proteins is essential for the physiology of neurons, we were intrigued by the finding that SIVA-1, a pro-apoptotic protein, was a possible FAIM-L functional partner. Moreover, SIVA-1 was already described as a XIAP functional partner.

Overall, the general goal of this work was to describe SIVA-1 role in caspase-activation in neurons, a context in which both the anti-apoptotic proteins FAIM-L and XIAP exert decisive roles. We hypothesized SIVA-1 to be a functional antagonist of both XIAP and FAIM-L in caspase activation in neurons, and therefore have an opposite effect in caspase-dependent outcomes - cell death and plastic neural changes.

Accordingly, we proposed the following objectives:

1. Corroborate and functionally characterize SIVA-1 interaction with XIAP and FAIM-L.
2. Study SIVA-1 expression and localization in neurons.
3. Investigate the implication of SIVA-1 in apoptosis in neurons.
4. Investigate the implication of SIVA-1 in physiological non-apoptotic function of caspases in neurons.

MATERIAL and METHODS

3. MATERIAL AND METHODS

3.1 Cell culture

The following reagents were used in cell culture.

Reagent	Description	Supplier
Cell media		
DMEM	Dulbecco's Modified Eagle Medium	TFS
Neurobasal	Basal media designed for neuronal cell maintenance	TFS
Opti-MEM	Modification of Minimal Essential Medium	TFS
PBS	Phosphate saline solution buffer	TFS
L15	Leibovitz media	Sigma-Aldrich
Cell media supplements		
AraC	Cytosine β-D-arabinofuranoside	Sigma-Aldrich
B27	Optimized supplement for neurons	TFS
DMSO	Dimethylsulfoxide	TFS
FBS	Heat-inactivated Fetal Bovine Serum	TFS
Glutamax	L-glutamine alternative	TFS
HEPES	4-(2-hydeoxyethil)-1-Piperazineethanesulfonic acid	TFS
HS	Heat-inactivated Horse Serum	TFS
L-glutamine	Amino acid	TFS
N2	Serum-free supplement	TFS
NGF	Nerve Growth Factor	Alomone Labs
Pen/Strep	Penicillin/Streptomycin (antibiotics)	TFS
Coating		
Laminin	Extracellular matrix protein	Sigma-Aldrich
Poly-D-lysine	Poly-amino acid	Sigma-Aldrich
Poly-L-ornithine	Poly-amino acid	Sigma-Aldrich
Type I collagen	Extracellular matrix protein	BD Biosciences
Enzymes		
DNaseI	Nuclease	Roche
Trypsin-EDTA	Serine protease	TFS

Supplier	Headquarters
Alomone Labs	Ein Kerem, Israel
BD Bioscience	Franklin Lakes, NJ USA
Roche	Basel, Switzerland
Sigma-Aldrich	St.Louis, MO, USA
TFS: Thermo Fisher Scientific	Waltham, MA, USA

3.1.1 Cell lines

All cell lines were obtained from cell bank (ATCC – American Type Culture Collection, Manassas, VA, USA). Cells were amplified and stored in liquid nitrogen to maintain a continuous stock. Early passage number of cell lines are preferably kept cryopreserved, as they conserve the characteristics of the original population and do not present selections or modifications of cellular genotype that could appear during prolonged manipulation. Upon thawing, cells were maintained in culture under controlled conditions.

Cells were grown at 37°C in 5% CO_2 atmosphere in a humidified incubator. For pelleting, centrifugations were carried out at 200*x*g for 5 minutes (min). Cell media components differ for cell types and are specified in the corresponding paragraph.

3.1.1.1 Subculture, cryopreservation, and thawing of cell lines

To subculture cells, medium was removed, and dissociation was performed using a 1:5 (v/v) dilution of 0.25% trypsin-EDTA in PBS. Cells were then incubated at 37°C until detachment, and trypsin was inhibited with fresh culture media. Cells were harvested, centrifugated and seeded in culture dishes with fresh media.

In order to cryopreserve cell lines, cells were harvested and pelleted. Pelleted cells were resuspended in cryopreservation medium (10% DMSO in FBS). DMSO is used to prevent formation of ice crystals, which could damage and disrupt cell membranes during the freezing procedure. Cells were aliquoted in cryovials and stored at -80°C in a Mr. Frosty™ Freezing Container (Thermo Scientific), which is designed to achieve the optimal rate of cooling close to a -1°C/min. On the next day, cells were transferred to a liquid nitrogen tank for long-term storage.

For thawing, cells were withdrawn from liquid nitrogen and thawed in a water bath at 37°C. In order to ensure the highest viability possible, cells were rapidly processed to quickly remove DMSO and therefore avoid DMSO-mediated toxicity. Cell suspension was diluted in cell culture media at 37°C. After centrifugation, cells were resuspended in complete culture media and seeded into 100mm culture dishes.

3.1.1.2 HEK293T

Human embryonic kidney 293 cells (HEK293) is a cell line derived from human embryonic kidney grown in tissue culture. HEK293T are a variant of the HEK293, which contains the SV40 Large T-antigen that allows replication of transfected plasmids containing the SV40 origin of replication[202]. HEK293T can be efficiently transfected and support high levels of viral protein expression and have therefore been widely used in research for retroviral and lentiviral production, gene overexpression, and protein production. In this work, HEK293T cells were used for lentiviral production and transient protein overexpression for biochemical analysis.

H293T culture medium	
Medium	
DMEM	
Supplements	
FBS	10%
Pen/Strep	20U/mL;20µg/mL

3.1.1.3 PC12

PC12 cell line is derived from a pheochromocytoma of rat adrenal medulla. The neural crest embryonic origin of these cells gives them neuronal characteristics, they express some neuron-specific protein and can respond to nerve growth factor (NGF) treatment with neurite outgrowth[203]. PC12 cells were plated in

culture dishes precoated with collagen. For coating, a solution of 66,4µg/ml type I collagen in sterile Milli-Q water was added to complete coverage of the plate and allowed to polymerize for at least 30min at room temperature.

PC12 culture medium	
Medium	
DMEM	
Supplements	
FBS	6%
HEPES	10mM
HS	6%
Pen/Strep	20U/mL;20µg/mL

3.1.2 Primary murine neuron cultures

To obtain murine embryos for neurons or tissue isolation, mice C57BL/6 mice were manipulated and euthanatized following the experimental procedures conformed to the EU directive 2010/63EU and were approved by the Research Commission on Ethics of the Hospital Vall d'Hebron.

3.1.2.1 Cortical and hippocampal neurons

Neurons were cultured from embryonic day 15-16 C57BL/6 wild type mouse embryo forebrains. Cerebral cortex and hippocampi were dissected in PBS and pelleted with a rapid centrifugation 15'' at 800*x*g. Cells were enzymatically dissociated with a solution containing 0,05% trypsin in PBS and incubated for 5-10min in a 37°C bath. Enzymatic digestion was stopped by adding primary neurons seeding medium. Then, DNaseI (around 200K units/ml) was added to minimize the presence of free-floating DNA fragments and cells clumps. Cells were pelleted with a 5min centrifugation at 800*x*g and resuspended in seeding medium. Cells were then filtered through a 40µm nylon mesh and counted. A density of $8,6x10^4$ cells/cm^2 for biochemical analysis, or $4,3x10^4$ cells/cm^2 for immunocytochemistry was then plated on plates and coverslips precoated

overnight with a solution of 10µg/mL poly-D-lysine. Three hours (h) after seeding, medium was replaced with complete primary neurons culture medium. Half of medium volume was changed every 3-4 days.

Primary neurons seeding medium	
Medium	
DMEM	
Supplements	
FBS	5%
HS	5%
Pen/Strep	20U/mL;20µg/mL

Primary neurons culture medium	
Medium	
Neurobasal	
Supplements	
B27	2%
Glutamax	1%
Pen/Strep	20U/mL;20µg/mL

3.1.2.2 Dorsal Root Ganglia (DRG)

Dorsal root ganglia (DRG) are satellite collections of sensory neuron cell somas found along the dorsal spinal roots of spinal nerves. Culture of DRG explants *in vitro* provides a versatile model extensively used to study mechanisms of axonal outgrowth and axonal degeneration and pruning after axotomy or trophic factor deprivation[204,205].

DRGs were extracted from E11 C57BL/6 wild type mouse embryos. Dissection was carried out in L15 dissection medium. Each ganglion was harvested and plated in wells precoated with a double coating. For coating, plates or coverslips were covered by a 0.01% poly-L-ornithine solution and maintained at 37°C overnight. On the next day poly-L-ornithine coating was removed, and laminin was added diluted at a final concentration of 20µg/mL into DRG basal medium. Laminin was maintained at 37°C for at least 4h. Once explants were harvested, they were directly plated on the laminin mixture and DRG growth media supplemented with 20µg/mL NGF was added. DRG growth medium is supplemented with Cytosine β-D-arabinofuranoside (AraC), a DNA synthesis inhibitor used to remove proliferating cells and therefore obtain a pure (>90%) neuronal culture.

DRG basal medium	
Medium	
DMEM	
Supplements	
Glutamine	2mM
Glucose	250µM
Na_2CO_3	400µM
Pen/Strep	20U/mL;20µg/mL

DRG growth medium	
Medium	
DRG basal medium	
Supplements	
B27	2%
N2	1%
AraC	0.2µl/mL

At day *in vitro* (DIV) 2, NGF deprivation was achieved by washing and replacing the media with fresh DRG growth media. Deprivation was carried out for 8 or 24h, then explants were processed.

3.1.3 Cell treatments

All reagents used for cell treatment were dissolved to stock solution following the manufacturer's recommendation. For treatment, reagents were diluted into culture media to reach the desired working concentration. Reagents and concentration are listed in the table below.

Reagent	Description	Working concentration	Provider
Q-VD	Pan-caspase inhibitor	10 µM	Merk Millipore
MG132	Proteasome inhibitor	10 µM	Sigma-Aldrich
NMDA	NMDAR agonist	50 µM	Sigma-Aldrich
BAPTA-AM	Calcium chelator	50µM	Sigma-Aldrich
Cycloheximide	Translation inhibitor	1µg/ml	Sigma-Aldrich
Supplier		Headquarters	
Merk Millipore		Billerica, MA, USA	

3.1.3.1 Q-VD

(Q-VD) is a compound specifically designed to be a pan-caspase inhibitor. Q-VD irreversibly binds to active caspases and blocks apoptosis. It has proven to be highly effective, to have cell permeability and minimal toxicity[206].

In this work, Q-VD was added to neurons after lentiviral transfection and maintained in culture until final time point.

3.1.3.2 MG132

MG132 is a synthetic peptide designed to be a cell permeable proteasome inhibitor. It binds to and blocks the 26S proteasome, the ATP-dependent protease complex that degrades ubiquitin-conjugated proteins[207]. In this work MG132 was used to inhibit proteasome and therefore detect accumulation of proteins otherwise degraded.

3.1.3.3 NMDA

N-Methyl-D-aspartic acid (NMDA) is a specific agonist of the glutamate ionotropic receptor NMDAR. In this work NDMA was diluted in culture media and used to induce chemical long term depression (chLTD), an *in vitro* model of LTD, a NMDAR-dependent synaptic modification[70].

3.1.3.4 BAPTA-AM

BAPTA-AM is a membrane permeable calcium (Ca^{2+}) chelator. In this work it has been used to evaluate intracellular Ca^{2+} signaling. BAPTA-AM was diluted in culture media 30min before NMDA stimulation and maintained during it.

3.1.3.5 Cycloheximide

Cycloheximide (CHX) is an inhibitor of protein synthesis. It interferes with the translocation step in protein synthesis thus blocking it. In this work CHX was diluted in culture media 60min before NMDA stimulation and maintained during it.

3.2. Cell transfection

Transfection enables the introduction of purified molecules of nucleic acid into cells. Several protocols can be used to efficiently delivery plasmid DNA into the cell's nucleus. In this work we used:

- Formation of DNA-containing soluble aggregates with Calcium Phosphate method.
- Lipid-mediated DNA transfection with liposome-based vectors (Lipofectamine2000).
- Virus-mediated DNA delivery (lentiviral infection).

3.2.1 Plasmids

DNA plasmids are circular molecules of double-stranded DNA with variable length. DNA plasmids were produced in bacteria, where they can be replicated and inherited independently of host genome.

Bacteria were grown in LB broth medium (10g/l tryptone, 5g/l yeast extract, 5g/l NaCl) at 37°C with proper antibiotic (Ampicillin), since plasmids include selection genes that aid bacteria selection. Plasmids were then extracted and purified using commercially available kits (Qiaprep Spin Miniprep Kit (QIAGEN; Hilden, Germany) and the Nucleobond Xtra Maxi kit (Macheley-Nage, Düren, Germany)).

For this study the following plasmids were used:

Vector	Backbone
Expression plasmids	
3xFLAG-FAIM-L	pcDNA3
3xFLAG-SIVA-1	pcDNA3
3xHA-FAIM-L	pcDNA3
3xHA-SIVA-1	pcDNA3
3xHA-ΔSIVA-1	pcDNA3
6xMyc-XIAP	pcDNA3
Empty vector	pcDNA3
6x His-human-Ubiquitin	pCl
YFP	pcDNA3
Lentiviral expression plasmids	
3xHA-SIVA-1	pEIGW
Empty vector	pEIGW
FAIM-L	pEIGW
shScr	pLVTHM
shSIVA-1	pLVTHM
siControl	PL-SIN
siSIVA-1	PL-SIN

6x-His-human-Ubiquitin vector was kindly provided by Dr. Dirk Bohmann (University of Rochester Medical Center, New York, USA). siRNA targeting human SIVA-1 and the control siRNA in the Pl-SIN vector were kindly gifted by Dr. Ulrike Resch (Medical University of Vienna, Vienna, Austria). All other constructs were generated in the lab.

3.2.2 Calcium Phosphate method

Calcium phosphate transfection is a simple, time-efficient and non-expensive method suitable for transfection of adherent, stable cell lines. It is based on the formation of calcium phosphate and DNA precipitate, which can adhere to cell surface and be brought into cells by endocytosis. In this work this method was used to transfect HEK293T cells for transient protein overexpression.

Procedure details for 100mm culture vessel	
Vector of interest	12-24µg
Transfection H_2O	up to 450µl
$CaCl_2$ (25mM)	50µl
HeBS 2x	500µl

The day before transfection, cells were seeded at 80% confluence in culture medium. Next day, DNA of interest is diluted in transfection water (Milli-Q water buffered with 2,5mM Hepes, pH7.3), and $CaCl_2$ is added to a final concentration of 250mM. Same volume of HeBS 2x (280mM NaCl, 50mM Hepes, 0,5mM Na_2HPO_4) was added to the mixture in a drop-wise manner while vortexing. The mixture was incubated 20min at room temperature to allow the formation of fine calcium phosphate-DNA precipitate. The suspension was then added to the cell culture, and the precipitates were taken up by the cells. Six hours after transfection, media is replaced with fresh culture medium.

The day post transfection high efficiency of overexpression is usually achieved. A YFP vector condition was always added to monitor the amount of transfection efficiency by fluorescence microscopy.

3.2.3 Lipofectamine method

This method is based on the use of the catationic liposoluble reagent Lipofectamine 2000 (Invitrogen). In presence of DNA in an aqueous environment, Lipofectamine 2000 forms liposomes that entrap the nucleic acid. The DNA-containing liposomes are added to media and fuse with plasma membrane allowing molecules to enter the cells.

The transfection protocol was adapted from the manufacturer's recommendations. Cells were seeded at high density (80-90% confluence). On

the day of transfection, Lipofectamine 2000 and DNA molecules were diluted separately in OptiMem Reduced Serum Medium. After 5min of incubation, DNA mix and Lipofectamine 2000 mix were combined and incubated for 20min to allow lipid complex formation. Complexes were then added dropwise to the cell culture. Culture medium was changed 4-6h after transfection to avoid toxicity of the reagent.

Procedure details for 100mm culture vessel	
DNA of interest	12-24µg
Lipofectamine 2000	30µl
OptiMEM	2x 500µl

This transfection method was used in this work to transfect HEK293T cells in order to produce high-titer lentiviral particles, and PC12 cells and primary neurons for transient protein overexpression.

In case of primary neurons transfection, Glutamax supplement in cell media was substitute by 0.5mM L-glutamine starting the day before transfection, recommended to decrease possible toxicity of medium[208].

3.3. Lentiviral production

Lentiviral vectors allow efficient gene transfer in cells, including terminally differentiated cells such as neurons. Up to date three generation of vectors derived from the HIV-1 lentivirus have been developed for lentiviral production. In this work, we used a second-generation system designed by Prof. Didier Trono (Laboratory of Virology and Genetics, École Polytechnique Fédérale de Lausanne, Lausanne, Switzerland, http://tronolab.epfl.ch/)[209,210].

For this system, three plasmids are co-expressed in HEK293T cells in a specific ratio:

1. pEIGW/pLVTHM – expression vector, which carries the gene of interest or short hairpin (sh) RNA. The transgene is flanked by various elements necessary for encapsidation, reverse transcription and integration in the host genome. It also contains GFP under EIF1α promoter, which allows assessing transfection efficiency of host cells.
2. psPAX2 – packaging vector, which contains, under the control of the highly robust CAG promoter, genes necessary for efficient lentiviral packaging and activity, including TAT protein, DNA polymerase and reverse transcriptase.
3. pMD2.G – envelope vector, which encodes for the vesicular stomatitis virus VSV-G protein, necessary for viral penetration in host cell's plasma membrane.

Prior to seeding, culture dishes were coated with poly-D-lysine 10µg/ml. Coating was allowed to polymerize at 37°C for 30min and it was later rinsed with sterile Milli-Q water. Four to five million HEK293T cells were seeded per 100mm dish. Next day, the three plasmids were co-transfected in the indicated amounts using Lipofectamine 2000 reagent.

Procedure details for 100mm culture vessel	
pEIGW/pLVTHM	12µg
psPAX2	8µg
pMD2.G	4µg

Forty-eight hours post-transfection, the medium was removed and centrifuged at 1000*xg* for 5 min to eliminate cells or particles in suspension. The supernatant was filtered through a 0.45µm filter (GE Healthcare Lifescience, Chichago, IL, USA) and concentrated by ultracentrifugation using a TH-641 rotor (Thermo Scientific) at 107,000*xg* for 1.5h at 4°C. Once centrifuged, viruses were resuspended in a solution of PBS containing 2% BSA (w/v), a carrier protein that

ensures preservation of the virus. Viral particles can be stored at –80°C for long periods without apparent loss of efficiency.

For infection, lentiviral particles were added to the medium. Transduction efficiency was assessed by direct counting of GFP-positive cells.

3.4 Analysis of mRNA expression levels by qPCR

In this work we assessed changes in expression of gene of interest by the analysis of mRNA levels by qRT-PCR.

3.4.1 RNA extraction

Tissue and cell samples were harvested in ice-cold PBS and pelleted by centrifugation at 500*x*g, 3min at 4°C. Total mRNA was extracted from cells using the RNeasy Mini Kit (QIAGEN, Hilden, Germany) according to the manufacturer's instructions. Briefly, cells were lysed and homogenized under denaturing conditions in a guanidine-isothiocyanate-based buffer supplemented with β-mercaptoethanol. Then, ethanol was added to promote selective binding of RNA to the silica membrane used for purification and sample was applied to the spin column. After washing steps to remove sample contaminant, high quality RNA was eluted using ddH_2O free of RNases and DNases and RNA concentration was quantified with a Nanodrop (Thermo Fisher Scientific).

3.4.2 Conversion of RNA to cDNA

RNA samples were converted to cDNA through reverse transcription using the High Capacity RNA-to-cDNA Kit (Thermo Fisher Scientific) according to the manufacturer's instructions. Briefly, 1µg of RNA was mixed with retro-transcriptase enzyme and buffer and was loaded into a thermal cycler to undergo protocol steps:

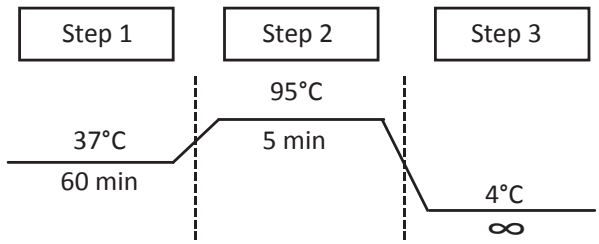

1. Primer annealinng and reverse transcription
2. Enzyme and RNA denaturation/inactivation/degradation
3. Short-term storage

3.4.2 Quantitative PCR (qPCR)

For the analysis of mRNA expression levels, cDNA samples were submitted to quantitative PCR using SYBR Green PCR Master Mix (Applied Biosystems) as a reporter. SYBR Green dye is a double strand DNA-binding dye. During PCR, DNA polymerase amplifies the target sequence and as more qPCR product is created, SYBR dye fluorescence intensity increases proportionally.

Primers against target genes were designed using the NCBI primer designing tool (www.ncbi.nlm.nih.gov/tools/primer-blast/), considering an optimal Tm of 60°C, a product ranging 80-150 nucleotides. Primer sequences are listed in the following table:

Gene	Primer Sequence (5'-3')
SIVA-1	Forward: GATCACATATCGAGCGAAGA
	Reverse: GCCTTCCCATCCACAGATCT
L27	Forward: AGCTGTCATCGTGAAGAA
	Reverse: CTTGGCGATCTTCTTCTTGCC

cDNA was diluted 1:10 in nuclease-free water and mixed with 0.4µM of primers and SYBR Green PCR Master Mix. qPCR reaction was performed in 384-well plates (Thermo Fisher Scientific) and all reactions were run in triplicates.

Samples were subjected to a PCR amplification protocol using a 7900HT Real-Time PCR System (Thermo Fisher Scientific). Specificity of the reaction was verified by melting curve analysis.

Once PCR was completed, data were analyzed using the SDS 2.3 software (Thermo Fisher Scientific). mRNA expression levels were quantified using Ct values, which indicate at which cycle probe-induced fluorescent signal reached a predetermined threshold.

Lower Ct values correlate with fluorescent signal detection at earlier PCR cycles, which indicates the presence of higher cDNA copy numbers and higher mRNA expression levels.

Data were normalized for cDNA copy numbers of the house-keeping gene (L27, ribosomal RNA), by subtracting the Ct value of the housekeeping gene from the Ct values of the gene of interest

$$Ct_{(\text{gene of interest})} - Ct_{(\text{housekeeping gene})} = \Delta Ct$$

These ΔCt values can be used directly for absolute quantification, indicating the cycle at which the gene of interest was detected, or can be used for relative quantification to compare the expression levels to control conditions, as measured in relative fold change. Relative fold-change in expression was determined by the comparative $2^{-\Delta\Delta Ct}$ method[211], where

$$\Delta\Delta Ct = Ct_{(\text{sample})} - Ct_{(\text{control sample})}.$$

3.5. Protein detection by Western Blot

Western blot is an analytical technique used to detect specific proteins in samples. It requires an efficient protein extraction from samples to ensure an accurate reflection of their levels and physiological state.

3.5.1 Protein extraction

Different protein extraction methods have been used in this work, according to the purpose of extraction. In some cases, a non-denaturation extraction was required to preserve protein structure to assess activity or interaction. If no following biochemical analysis was required, cells were harvested in ice-cold PBS pH7.2 and lysed in SET lysis buffer (10 mM Tris-HCl pH7.4, 150mM NaCl, 1mM EDTA and 1% sodium dodecyl sulfate (SDS)). SDS ensures a high extraction efficiency and release of proteins from macromolecular structures, it allows the interaction between proteins to be quickly broken, and completely denaturalizes and inactivates all enzymes in the sample, including proteases and phosphatases. SET buffer was added keeping a proportion of 1:50 (v/v) between cell pellet and lysis buffer. In order to ensure fragmentation of genomic DNA released during lysis, and consequently reduce viscosity, samples were sonicated.

3.5.2 Protein quantification

To ensure comparison between samples, protein concentrations were quantified by a modified Lowry assay (DC protein assay, Bio-Rad). This method relies on using a reagent which exhibits a color change proportional to protein concentration, and then measuring it using colorimetric techniques.

3.5.3 Sample preparation

Once quantified, samples were prepared for further analysis in SDS-Polyacrylamide gel electrophoresis (SDS-PAGE) and protein immunodetection. Between 20 and 30µg of protein were mixed with Laemmli's loading buffer (60mM Tris-HCl pH6.8, 4mM EDTA, 10% Glycerol, 2% SDS, 100mM dithiothreitol (DTT) and traces of Bromophenol blue) and denatured by incubation at 95°C for 5min. DTT reduces disulphide bonds and SDS is a powerful ionic detergent, which has an hydrophobic end and a negatively charged part. The hydrophobic dodecyl part interacts with hydrophobic amino acids in proteins, breaking 3D structures and transforming proteins into linear molecules coated with negatively charged SDS groups. These charges give every protein the same charge-to-mass ratio, assuring a separation dependent only on their molecular weight once they are loaded on an SDS-PAGE.

3.5.4 SDS-PAGE

SDS-polyacrylamide gel electrophoresis (PAGE) is a widely used method to separate proteins by size through electrophoresis, formulated by Ulrich K. Laemmli in 1970[212]. Gels are formed by the polymerization of acrylamide, through the action of the cross-linking factor bis-acrylamide, an initiator, and a catalyzer, all in the presence of 0.1 (w/v) SDS. Acrylamide and bis-acrylamide are used in a final proportion of 37.5:1. The final percentage of acrylamide/bis-acrylamide determines the separation range of the gel. Gels are composed by a stacking and a resolving part. Stacking gel (pH6.8) is the part of the gel where proteins are loaded and stacked together, whereas the resolving gel (pH8.8) is where proteins are separated by size. Components are specified in the table.

Reagent	Description	Stacking gel concentration	Resolving gel concentration
Acrylamide solution	Cross linking polymer	4% (w/v)	8-12% (w/v)
Tris-HCl pH6.8	Buffer	280mM	-
Tris-HCl pH8.8	Buffer	-	375mM
SDS	Denaturizing agent	0.1% (w/v)	0.1% (w/v)
APS	Initiator of polymerization, source of free radicals	0.05% (w/v)	0.05% (w/v)
TEMED	Catalyst for free radical formation from APS	0.1% (v/v)	0.05% (v/v)

The two parts of the gel mainly differ by pH and acrylamide concentration. Protein migration is achieved by running a current through the gel in presence of running buffer (Tris 25mM, glycine 192mM, SDS 0,1%, pH8.3). In the stacking gel, the low pH allows the presence of a small zone where proteins concentrate, between two fronts composed by protonated glycine (slowly migrating) and Cl^- (quickly migrating). Once it reaches the resolving gel, the change in pH converts glycine to a negatively charged state. Glycine then migrates more quickly than the proteins, leaving them to be separated according to size. The increased polyacrylamide concentration of resolving gel slows down the migration of the proteins according to size, since low molecular weight proteins move faster through the polyacrylamide pores than high molecular weight proteins.

Electrophoresis was performed in a Mini-PROTEAN cuvette (Bio-Rad), at constant amperage (25mA/gel).

3.5.5 Protein immunodetection

After migration, proteins were transferred from the gel to the surface of polyvinyl difluoride (PVDF) membranes (Merk Millipore) using the wet transfer system (Bio-Rad). Previous to transfer, PVDF membrane was activated in methanol and hydrated in ddH_2O. PVDF membrane and polyacrylamide resolving gel were kept in close contact by a cassette and submerged in ice-cold

transfer buffer (25 mM Tris-HCl, 192 mM glycine, 20% methanol), a conducting solution. Transfer was carried out at 100 V for 90 min.

Following transfer, membranes were blocked to prevent non-specific binding of antibodies to membrane surface in TBS-T (20 mM Tris–HCl, 150 mM NaCl pH8 and 0.1% Tween 20) containing 5% non-fat dry milk, for 1h at room temperature. Once blocked, membranes were sequentially probed for antibody staining and detection. Membranes were probed with the antibodies and dilutions detailed in the following table.

Antibody	Working dilution	Media	Source	Ref	Supplier
Primary antibodies					
anti-actin-HRP	1:2000	TBS-T	Rabbit	sc-1616HRP	SCBT
anti-α-tubulin	1:10000	TBS-T	Mouse	T5168-.2ML	Sigma-Aldrich
anti-calnexin	1:1000	5% BSA	Mouse	ab31290	Abcam
anti-caspase-3	1:1000	5% BSA	Rabbit	05-668	CST
anti-cytochrome c	1:1000	5% BSA	Mouse	556433	BD Bioscience
anti-FAIM-L	1:2000	5% BSA	Rabbit	-	In house
anti-FLAG	1:10000	5% BSA	Mouse	F3165	Sigma-Aldrich
anti-GAPDH	1:5000	5% BSA	Rabbit	Ab9485	Abcam
anti-GluA2	1:1000	5% BSA	Mouse	MAB397	Merk Millipore
anti-HA	1:2000	5% BSA	Rat	11867423001	Roche
anti-Histone3	1:1000	5% BSA	Rabbit	9715	CST
anti-Myc	1:1000	TBS-T	Mouse	sc-40	SCBT
anti-NF-66	1:1000	TBS-T	Rabbit	PRB572C	Covance Research
anti-pan ERK	1:5000	TBS-T	Mouse	610123	BD Bioscience
anti-PDS95	1:2000	5% BSA	Rabbit	3450	CST
anti-SIVA-1	1:1000	5% BSA	Chicken	SAB3500697	Sigma-Aldrich
anti-Synapsin II	1:1000	5% BSA	Rabbit	ADI-VAS-SV061-E	Enzo Life Science
anti-XIAP	1:1000	TBS-T	Mouse	610762	BD Bioscience

Supplier	Headquarters
Covance Research	Princeton, NJ, USA
CST: Cell Signaling Technology	Danvers, MA, USA
SCB: Santa Cruz Biothechnology	Santa Cruz, CA, USA
Enzo Life Science	Farmingdale, NY, USA

Antibody	Working dilution	Media	Source	Ref	Supplier
Secondary antibodies					
anti-Chicken IgY-HRP	1:10000	5% milk	Goat	SAB3700226	Sigma-Aldrich
anti-Mouse IgG-HRP	1:10000	5% milk	Goat	A9044	Sigma-Aldrich
anti-Rabbit IgG-HRP	1:10000	5% milk	Goat	A0545	Sigma-Aldrich
anti-Rat IgG-HRP	1:10000	5% milk	Goat	A9037	Sigma-Aldrich

Primary antibodies were incubated overnight at 4°C. Membranes were washed in TBS-T for 5min three times to eliminate excess of primary antibody and then incubated 1h at room temperature with proper secondary antibody diluted in blocking solution. After incubation, membranes were washed three times for 10min in TBS-T. Secondary antibodies are coupled with horseradish peroxidase enzyme (HRP), which enables detection by enhanced chemiluminescence using the EZ-ECL Chemiluminescence detection kit (Biological Industries). HRP catalyzes the oxidation of cyclic diacyl hydrazides, such as luminol, in presence of H_2O_2. This reaction produces chemiluminescence, which can be detected using SuperRX Fuji Medical X-RAY Films (Fujifilm Corporation).

In some cases, after blotting, Naphtol Blue Black stain (NB) was used as a loading control. NB rapidly stains protein bands on western blot membranes and it can therefore be useful to ensure equally loading when housekeeping protein levels are altered. Membranes were stained in a solution containing 10% methanol, 2% acetic acid and 0.1% NB for 5-10min. Then, membranes were washed twice in a de-coloration solution (50% methanol, 7% acetic acid) and let dry.

3.6 Subcellular fractionation

Subcellular fractionation is a method employed to separate cellular compartments and therefore determine intracellular-specific characteristic of proteins.

In this work we used sequential centrifugations at increasingly higher speeds. The different sedimentation rates of various cellular components make it possible to pellet them by centrifugation and use the supernatant at higher speeds for lighter compartments isolation.

Whole brains were dissected from C57BL/6 adult mice and were homogenized in sub-fractionation buffer (10mMHEPES pH7.4, 2mM EDTA, 0.32M sucrose, EDTA free 1X protease inhibitor cocktail). Every step was carried out at 4°C to best preserve all intracellular components. As represented in Figure 3.1 cell homogenates were centrifuged sequentially at 600*x*g for 10min to remove nuclei and unbroken cells, 3000*x*g for 10min to pellet the plasma membrane sheets and heavy mitochondria (heavy membranes, HM), 1500*x*g for 15min to yield light mitochondrial and membrane fraction (LM), and finally 1h at 100,000*x*g to yield microsomal (pellet, Mi) and cytosolic fractions (supernatant, C). Nuclear fraction (N) was extracted from the 600*x*g pellet with centrifugations at 500*x*g for 15min. The supernatants were centrifuged twice at each speed, and pellets were washed twice by resuspension in sub-fractionation buffer and re-centrifugation. Pellets were lysed in SET buffer. Samples were heat-denatured in Laemmli buffer and subjected to SDS-PAGE.

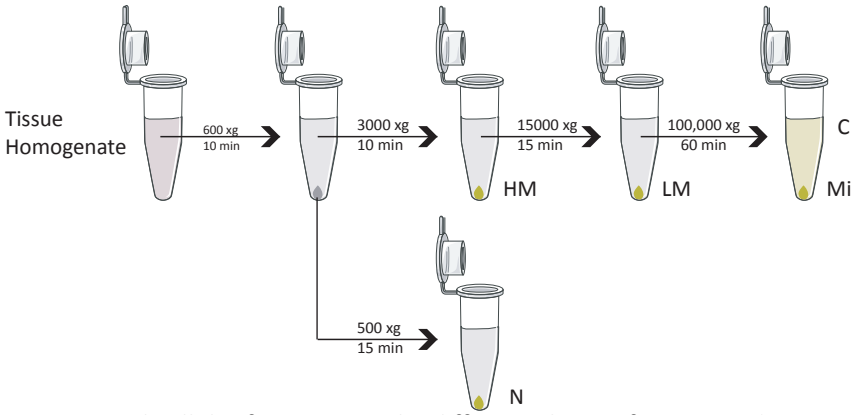

Figure 3.1: Subcellular fractionation by differential centrifugation. Schematic representation of general steps for cell compartments isolation. HM: heavy membrane fraction, LM: light membrane fraction, C: cytosolic fraction, Mi Microsomal fraction, N: Nucleus.

3.7 Preparation of Crude Synaptosomal Fractions from Mouse Brains

To analyze content of synaptic terminals we used a bio-protocol published in 2017 (https://doi.org/10.21769/BioProtoc.2423) that, on the same basis as the subcellular fractionation previously described, allows to rapidly isolate crude synaptosomal fractions through few centrifugations. Mice brains were homogenized in ice-cold Synaptosome Lysis Buffer (5mMHEPES pH7.5, 0.32M sucrose, EDTA free 1X protease inhibitor cocktail) in a 1:10 ratio (w/v). After 30 min incubation on ice, nuclei were pelleted with a centrifugation of 1000*x*g, 10min at 4°C. Supernatant was furtherly processed with a 12,000*x*g centrifugation of 10min at 4°C to separate crude synaptosomal fraction (pellet) and soluble enzymes and microsomal fraction (supernatant). Supernatants were centrifuged twice at each speed, and pellets were washed twice by resuspension in buffer and re-centrifugation. The pellet yielding crude synaptosomal fraction was lysed in SET buffer. Samples were heat-denatured in Laemmli buffer and subjected to SDS-PAGE.

3.8 Immunoprecipitation

Immunoprecipitation (IP) is used to isolate a specific protein out of a solution and relies on the use of a specific antibody that can be precipitated using a sedimental matrix.

This method can be employed to study intact protein complexes and analyze interactions between proteins utilizing a whole cell extract where proteins are present in their native state. Cells have to be lysed in non-denaturing conditions in order to maintain any interactions that may occur.

In this work, some IP experiments were performed on endogenous proteins, and others were performed on lysates of cells transfected to overexpress tagged proteins. Specifically, we used FLAG-, and Myc- tagged proteins as bait. After 24-48h of transient transfection for ectopic expression, or after 24 h in culture in case of endogenous IP, HEK293T and PC12 cells were rinsed in PBS 1x and lysed in IP lysis buffer (20 mM Tris/HCl, pH7.4, 150 mM NaCl, 2 mM EDTA, 10% Glycerol, 1% Triton X-100, and supplemented with a EDTA free 1X protease inhibitor cocktail). Samples were lysed for 30min on ice and centrifuged at 12,000 x*g* at 4°C. One mg of total protein was used for IP. Forty µl of specific FLAG M2 Affinity monoclonal agarose beads (Sigma-Aldrich) or anti-ubiquitin-conjugated agarose beads (Santa Cruz Biothechnologies) were used for IP:FLAG and IP:ubiquitin respectively. Samples were incubated overnight on an orbital shaker at 4°C. For IP:Myc, lysates were precleared by 30 min of incubation with 20 µl conjugated protein G suspension and 0.25 µg/µl control mouse IgG. Afterwards, 1 µg Myc antibody was added to each sample and incubated for 4h at 4°C on an orbital shaker. Finally, 20µl conjugated protein G suspension was added and incubated overnight on an orbital shaker. After overnight incubation, agarose beads were washed five times with IP lysis buffer and eluted. Insulin

syringes were used during washes to remove all the buffer. Finally, the protein complexes were eluted from beads using one of two methods:

- Competitor peptide elution - for IP:FLAG and IP:Myc: beads were resuspended in a solution containing epitope following the manufacturer's protocol. Peptides have high specificity and affinity for the antibody, they compete with the protein complex displacing the antibody interaction, and complexes are released in solution[213].
- Laemmli buffer elution – for IP:ubiquitin: a more harsh elution in which the complex were eluted by adding Laemmli buffer without DTT and boiling samples at 95°C for 5min. Denaturant SDS in the buffer allows for complex release from the beads. DTT is removed for elution to avoid release IgG from beads, which would result in immunoglobulins in western blot[214].

Whole cell lysate and immunoprecipitated proteins were finally analyzed by western blot.

3.9 Ubiquitin assay

Ubiquitination is a protein modification that can alter the property of its targets in a variety of ways, from localization, activity, to their degradation. In this work we were interested in detecting changes on ubiquitination levels of specific proteins when these were co-overexpressed with some other interacting-proteins. Several strategies can be used to detect ubiquitination levels, in this work we used the 6xHis-ubiquitin assay developed by the Tansey laboratory (www.tanseylab.com). For this protocol, a plasmid coding for human ubiquitin tagged with a 6xHis affinity tag is expressed in cells. 6xHis-ubiquitin is then incorporated into ubiquitinated proteins, that can be purified by affinity. The purified pool of ubiquitinated proteins can be analyzed for the presence of the proteins of interest by western blot.

HEK293T cells were transfected with an overexpression plasmid mix of the proteins of interest, along with a plasmid which encodes 6xHis-tagged human ubiquitin. After 24h, a 6h MG132 treatment was performed and then, cells were rinsed and collected in ice-cold PBS. Part of the sample was collected and lysed in SET buffer to load as total lysate. The rest of the sample was lysed in buffer A (6 M guanidine-HCl, 0.1 M Na2HPO4/NaH2PO4, 10mM imidazole, pH8.0) and sonicated. His-tagged proteins were purified adding 50µl of ProBond™Ni-NTA-agarose resin (Thermo Fisher Scientific) and incubating samples on rotation using an orbital shaker for 3h at room temperature. Samples were spun and washed twice with buffer A, twice in buffer A/TI (1 volume of buffer A for 3 volumes of buffer TI), and once more in buffer TI (25 mM Tris-HCl, 20 mM imidazole, pH6.8). Insulin syringes were used during washes to remove all the buffer. Finally, proteins were eluted by resuspension in 80µl of Laemmli buffer 2x supplemented with 250mM imidazole and boiled for 10min at 95°C. Samples were then separated from agarose by using an insulin syringe and analyzed by western blot.

3.10 Cell surface biotinylation

Biotinylation of cell surface proteins is one of the most well-known techniques to assess surface levels and trafficking of a protein of interest. In this work, we used the Pierce Cell Surface Protein Isolation Kit (Thermo Fisher Scientific), with an adapted protocol. The reagent used is Sulfo-NHS-SS-Biotin, which binds amine groups of proteins on cell surface through a covalent interaction. Due to its negative charge it is unable to penetrate cell membrane, ensuring a specific labeling of cell surface proteins. After cell lysis, cell surface proteins can be isolated by immunoprecipitation using NeutrAvidin Agarose beads, with which biotin groups form disulfide groups and have high affinity. To release proteins from NeutrAvidin agarose beads, reducing agents can be used (such as DTT). Proteins can finally be analyzed by western blot.

Cultured neurons were transferred to ice-cold PBS and washed twice. Sulfo-NHS-SS-Biotin was diluted in ice-cold PBS and added to cells at a final concentration of 0.25µg/µl (412µM). Plates were incubated for 30min at 4°C with slow agitation. Free biotin was inactivated by three washes in cold quenching solution (50mM glycine in PBS). Cell cultures were immediately harvested by scraping in cold TBS. After pelleting, cells were lysed for 30min at 4°C in Triton lysis buffer (50mM Tris-HCl pH7.4, 150mM NaCl, 1mM EDTA, 1% Triton X-100, EDTA free 1X protease inhibitor cocktail). Homogenates from cultures were centrifuged at 10,000*x*g for 20min to pellet insoluble fraction. Protein concentration was adjusted obtain equal concentration in all the samples. Twenty µg of protein homogenates were stored as total lysates. Biotinylated surface proteins in the remaining supernatant were incubated with 40µl of 50% avidin-agarose beads ((v/v) in lysis buffer), 2h at 4°C on an orbital shaker. Labeled proteins were then isolated by sequential centrifugation and beads resuspension. Insulin syringes were used during washes to remove all the buffer. Finally, proteins were eluted by resuspension in 60µl of Laemmli buffer 2x and incubated 30 minutes at room temperature while vigorously shaking every 10 minutes. Sample was separated from beads by using an insulin syringe, and then analyzed by western blot.

3.11. Cell death assay

Cell death can be evaluated with various types of assays, which assess cell death or viability hallmarks[12,215]. There are indeed some characteristics and specific changes in cells undergoing apoptosis, such as changes in cellular morphology, DNA condensation and fragmentation, protein activation, protein cleavage. In this thesis cell death was assessed by chromatin staining with Hoechst dye and by caspase-3/7 activity assay.

3.11.1 Hoechst staining

Hoechst dyes are fluorescent stains that bind to the minor groove in double stranded DNA. Once bound, Hoechst dyes can be excited by ultraviolet light (UV) (350nm) and emit in the blue spectrum (maximal emission 461nm), allowing nuclear detection, and the assessment of nuclear condensation and/or fragmentation (Figure 3.2).

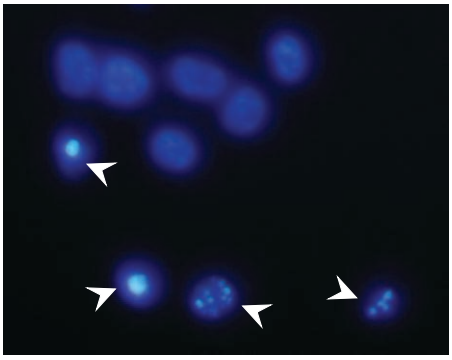

Figure 3.2: Nuclear morphology. Hoechst staining of SKNAS cells. Staining of nuclear chromatin allows the detection of nuclear morphologies, such as healthy nuclei, condensed and fragmented nuclei (arrows).

In this work, we used Hoechst 33342, which is cell-permeable and can thus penetrate cell membranes and bind to DNA in fixed and live cells without compromising cell viability.

Cells were stained with 0.05µg/ml of Hoechst 33342 in PBS and incubated for 30min protected by light. Images were taken with fluorescent microscopy using a UV light at 20x magnification. Cell death was finally assessed analyzing the images. Using cell counter Plugin of ImageJ software[216], we counted both cells with fragmented nuclei and intact cells, and then calculated the percentage of apoptotic cells.

3.11.2 Caspase activity

Caspases are the major effectors of apoptosis, and their activation can be used as a biochemical hallmark of cell viability status. Ac-DEVD-AMC is a synthetic tetrapeptide fluorogenic compound that has been developed to be substrate for caspase-3/7 and become fluorescent after cleavage by caspases. The amount of fluorescent signal therefore indicates the relative amount of caspase activation.

Cells were harvested in ice-cold PBS and then lysed 30min in ice with caspase assay buffer (20mM Hepes/NaOH pH7.2, 10% sucrose, 150mM NaCl, 5mM EDTA, 0.1% CHAPS, 1% Igepal CA-630, EDTA free 1X protease inhibitor cocktail). Lysates were cleared by centrifugation at 16,000*x*g for 5min and the protein concentration was quantified using the Lowry-based DC protein assay. The assay was performed in black 96-well plates in triplicate. Twenty µg of lysate were diluted in a total volume of 50µl of buffer. Additional 50µl of complete caspase activity buffer were then added to the well (caspase activity 2x completed with 10mM of Ac-DEVD-Afc substrate and 25µM DTT). After an incubation of 4h at 37°C caspase activity was assessed in a fluorimeter using 405nm excitation and 535nm emission filters.

3.12 Immunofluorescence analysis

Immunofluorescence uses the specificity of antibodies to their antigen to target fluorescent dyes to specific biomolecule targets within a cell, and therefore allows visualization of the distribution of the target molecule through the sample. Cells are fixed and permeabilized to allow antibodies to cross the plasma membrane. Samples are sequentially incubated with primary antibody, against the target molecule, and then secondary antibody, which recognizes the primary antibody and carries the fluorophore. After labeling samples are ready to be

visualized in a fluorescent microscope. In this work, images were acquired with a confocal laser scanning microscope (spectral FV1000; Olympus).

Antibody	Working dilution	Source	Ref	Supplier
Primary				
anti-βIII tubulin	1:1000	Rabbit	PRB-435P	Covance Research
anti-calnexin	1:500	Rabbit	2433	CST
anti-GFP	1:2000	Rabbit	ab6556	Abcam
anti-GluA2	1:1000	Mouse	MAB397	Merk Millipore
anti-HA	1:500	Rat	11867423001	Roche
anti-PSD95	1:200	Mouse	MAB1598	Sigma-Aldrich
anti-Rab5	1:500	Rabbit	2143	CST
anti-SIVA-1	1:100	Rabbit	sc-48768	SCBT
anti-SIVA-1	1:100	Mouse	SAB3500697	Sigma-Aldrich
anti-SIVA-1	1:100	Chicken	SAB3500697	Sigma-Aldrich
anti-Synapsin II	1:200	Rabbit	ADI-VAS-SV061-E	Enzo Life Science
anti-TrkA	1:1000	Mouse	-	In house
anti-XIAP	1:1000	Mouse	610762	BD Bioscience
Secondary				
anti-Chicken IgY (H+l)-Alexa Fluor® 594	1:500	Goat	A11045	Thermo Fisher Scientific
anti-Mouse IgG (H+l)-Alexa Fluor® 594	1:500	Goat	A11005	Thermo Fisher Scientific
anti-Mouse IgG (H+L)-Alexa Fluor 488	1:500	Goat	A11001	Thermo Fisher Scientific
anti-Mouse IgG- Alexa Fluor® 568	1:500	Goat	A11004	Thermo Fisher Scientific
anti-Mouse IgG- Alexa Fluor® 647	1:500	Goat	Ab150115	Abcam
anti-Mouse IgG- Alexa Fluor® 647	1:133.3	Goat	Ab150115	Abcam
anti-Rabbit IgG (H+l)-Alexa Fluor® 594	1:500	Goat	A11012	Thermo Fisher Scientific
anti-Rabbit IgG-Alexa Fluor® 488	1:500	Goat	A11012	Thermo Fisher Scientific
anti-Rabbit IgG-Alexa Fluor® 488	1:500	Goat	A11012	Thermo Fisher Scientific
Supplier		Headquarters		
Abcam		Cambridge, UK		

3.12.1 Immunocytochemistry

In this work, we performed immunofluorescence of cortical and hippocampal neurons and DRG explants. Cells were rinsed with PBS at room temperature and fixed in 4% paraformaldehyde/PBS for 30min at room temperature. They were washed twice with PBS and subsequently permeabilized and blocked 60min at room temperature with Permeabilization buffer (PB), containing 5% FBS, 5% BSA, and 0.1% Triton X-100 in PBS. Then, cells were incubated overnight with the primary antibodies diluted in PB as listed in the table. Cells were rinsed three times with PBS and incubated with corresponding Alexa-secondary antibodies diluted in PB for 1h at room temperature protected from light. If nuclear staining was required, it was performed during secondary antibody incubation with 0.05µg/ml of Hoechst 33342 in PBS. MitoTracker staining (Invitrogen) was used following manufacturer's instructions to stain mitochondria. Coverslips were mounted on slides with prolong diamond mounting medium (Thermo Fisher).

3.12.2 Colocalization analysis

Fluorescence microscopy is widely used to asses to what extent two biomolecules or structures in a cell are associated with each other. Colocalization analysis refers to several approaches that attempt to characterize association from two or more different fluorescent labels, each having a separate emission wavelength.

Protein colocalization in the dual-color confocal images was measured quantitatively using the JACoP Plug-in of FIJI software[217] (http://fiji.sc/wiki/index.php/Colocalization_Analysis). Colocalization was determined by Mander's (M1 and M2) and Pearson's (R) colocalization coefficients[218].

Mander's coefficients are useful for assessing to what extent a structure or molecule can be found in a particular location or organelle (co-occurrence of two signals). M1 and M2 coefficients values express for each fluorophore the numbers of co-occurring pixels as a fraction of the total number. They range from 0 (uncorrelated distributions of two probes with one another) to 1 (perfect spatial overlap of two signals). In this work we used M1 to assess to what proportion of SIVA-1 (signal in channel 1) was present within a particular compartment or organelle (signal in channel 2).

Pearson's coefficient values describe, on the other hand, the relationship between two image signals calculated by linear regression (correlation among two signals). The assumption is that if two imaging targets are functionally related, their abundances will also be predictably related to each other wherever they locate in the same region. This assumption is therefore fundamental when probing two molecules that are thought to bind to (or repulse each other). Values can range from 1 to -1, with 1 standing for complete positive correlation and -1 for complete negative correlation. In this work we used R to assess SIVA-1 relationship to other functional targets (FAIM-L and XIAP).

At least 15 cells were considered for quantification.

3.12.3 GluA2 internalization assay

Assessment of cell surface/internalized levels of GluA2 receptor was performed through antibody-feeding assay. As represented in the diagram of Figure 3.3 this method permits to track surface receptors trafficking by labeling them with specific antibodies. An incubation with the receptor antibody was performed, and after chemical LTD induction, cells are fixed, and two different secondary

antibodies are used to label respectively internalized and endocytosed primary antibody[219].

Experiments were performed in hippocampal neurons at 12-14 DIV, time points in which cells have been shown to present mature and functional synapses[220].

Cells were incubated with antibodies against the N-terminus of GluA2 (2µg/ml) for 60min at 18-20°C. Neurons were then either stimulated with medium containing NMDA (50 µM) for 15min at 37°C or left unstimulated. Subsequently, they were fixed for 5 min at room temperature in paraformaldehyde:sucrose (4% v/v) in PBS, which does not permeabilize cells. Surface-remaining antibody-labeled receptors were visualized by means of a1 h incubation with saturated AlexaFluor-647 secondary antibody (15µg/ml). Neurons were then permeabilized for 2min with cold methanol (−20°C), and internalized antibody-labeled GluA2 was detected by a 1 h incubation with Alexa 568-conjugated secondary antibody (1µg/ml). Simultaneously, infected GFP-positive or HA-positive neurons were stained with antibodies against GFP or HA. Thus, the GFP fluorescence of infected neurons was enhanced by a 30min incubation with Alexa 488-conjugated secondary antibody. After three washes in PBS 1x, the coverslips were mounted on slides with Prolong diamond mounting medium (Thermo Fisher). For GluA2 internalization and surface staining, a z-stack of images was obtained through various filter channels (Alexa-488, Alexa-568 and Alexa-674).

Typically, 25 serial 2D images were recorded at 45nm intervals. Image acquisition settings were identical in each experiment. FIJI software was used to make 2D projections from the z-stack of images. We measured the total integrated intensity of internalized GluA2 and surface-remaining GluA2 in the same region of infected (GFP/HA-positive) neurons.

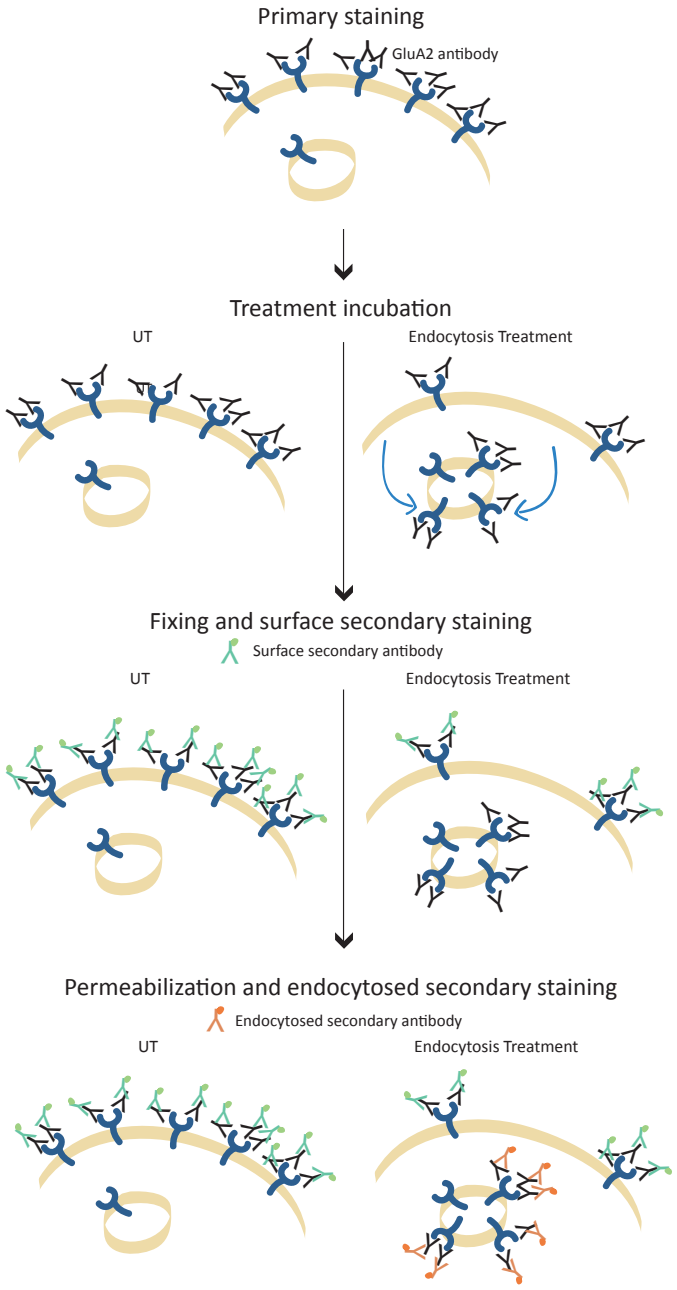

Figure 3.3: GluA2 antibody feeding protocol. Surface receptors are labeled with GluA2 antibody before treatment. After treatment induction cells are fixed in absence of a permeabilization agent, and surface receptor is saturated with secondary antibody (green). Subsequently cells are permeabilized and internalized antibody is labelled with a different secondary antibody (red). Left part represents untreated (UT) condition, right side represents treatment condition.

3.13 Experimental design and statistical analysis

All results were confirmed in at least three independent experiments. Representative images and western blots are shown in figures, while measurements of all repeated experiments are considered in the graphs. Data sets were plotted and analyzed using GraphPad Prism v5 (GraphPad Software; La Jolla, CA, USA). Values were excluded using the analysis to identify outliers included in the software. Values are expressed as mean ± SEM. Statistical significance was set at $p<0.05$ and was determined by two tailed unpaired t-test for comparisons between two groups, or by two-way ANOVA for multiple groups. Each specific test is indicated in the figure legends.

RESULTS

4. RESULTS

4.1 SIVA-1 interacts with both FAIM-L and XIAP

SIVA-1 was chosen as the protein of interest for this study, based on the results obtained deepening our characterization of FAIM-L. To identify potential functional partners of FAIM-L we performed a yeast-two-hybrid screening using as bait the full-length sequence of FAIM-L or the 22 N-terminal amino acids (MASGDDSPIFEDDESPPYSLEK), specific for the neuronal isoform[221].

As presented in Figure 4.1, the N-terminal fragment of SIVA-1 (ΔSIVA-1) was identified as one of the hits.

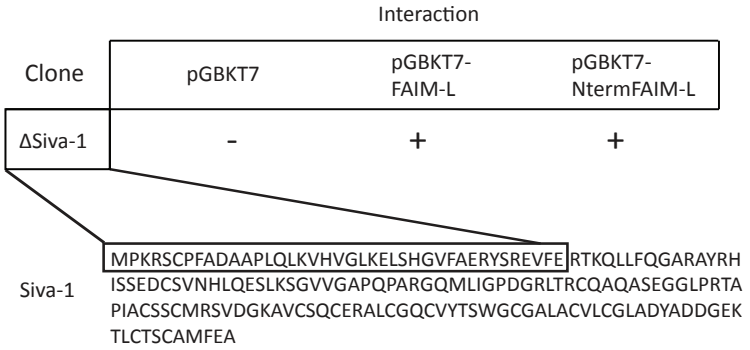

Figure 4.1: N-terminal of SIVA-1 (ΔSIVA-1) is detected in a two-hybrid screening using FAIM-L as bait. Schematic representation of the two-hybrid technique results. The N-terminal of SIVA-1 (ΔSIVA-1) interacted with both baits, namely full-length FAIM-L and FAIM-L-specific N-terminal 22 amino acids.

To confirm the findings of the two-hybrid technique we validated the interaction among FAIM-L and SIVA-1 in HEK 293T cells with co-immunoprecipitation experiments of overexpressed tagged proteins. We pulled down full-length FLAG-tagged FAIM-L and confirmed the interactions with both forms of SIVA-1 (HA-tagged-SIVA-1 and HA-tagged ΔSIVA-1) (Figure 4.2, lane 3 and 6). The truncated form of SIVA-1 and its interaction with FAIM-L was detected only in the presence of the proteasome inhibitor MG132 (Figure 4.2, lane 6), otherwise it was not stable and was consequently degraded. Overall, we corroborated that

FAIM-L interacts through its 22 amino acids N-terminal domain with the N-terminal domain of SIVA-1.

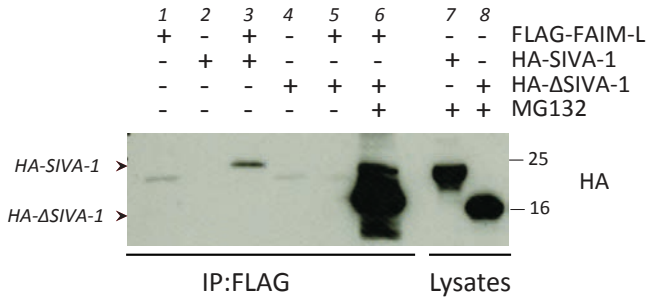

Figure 4.2: SIVA-1 interacts with FAIM-L through its N-terminal domain. Immunoprecipitation in HEK 293T cells of FLAG-FAIM-L using M2 Affinity FLAG. FAIM-L was immunoprecipitated and membrane was blotted with anti-HA to detect full-length SIVA-1 and ΔSIVA-1. Ten µM of MG132 was used to impair the degradation of ΔSIVA-1.

Our lab has previously reported XIAP as a FAIM-L-interacting partner[123]. XIAP is a potent inhibitor of caspases whose endogenous levels are crucial for FAIM-L protection against caspase activation and consequent apoptotic or non-apoptotic functions. In 2009 Resch and colleagues described an interaction between SIVA-1 and XIAP[149]. To corroborate the interaction in our system, we performed co-immunoprecipitation experiments of tagged proteins and corroborated that XIAP does indeed interact with both FAIM-L and SIVA-1 (Figure 4.3).

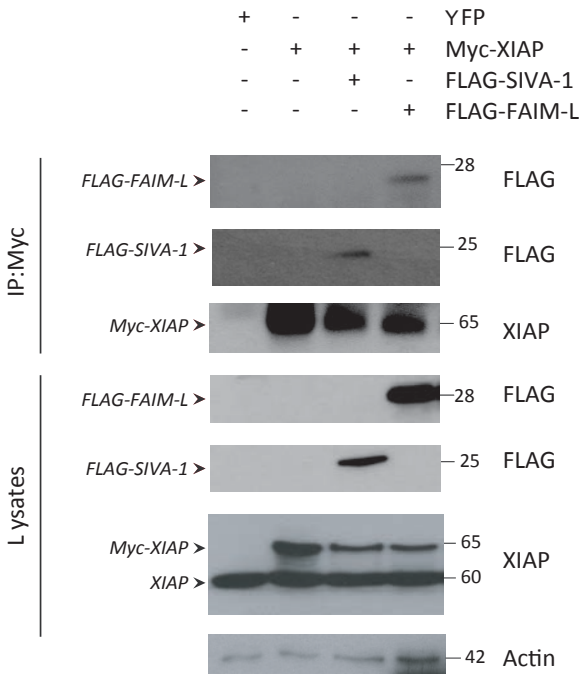

Figure 4.3: XIAP interacts with both FAIM-L and SIVA-1. Myc-XIAP immunoprecipitation using anti-Myc antibody. Cells were transiently transfected with Myc-XIAP, FLAG-FAIM-L and FLAG-SIVA-1. The membrane was blotted with anti-FLAG to detect both FAIM-L and SIVA-1. XIAP was used as a control of the immunoprecipitation and actin as loading control.

We then proceeded to show the interactions in a semi endogenous condition and locate them in the neuronal cells. We were limited in our study by the lack of a good antibody to detect endogenous FAIM-L by immunocytochemistry. We therefore decided to transfect primary cortical neurons with HA-FAIM-L and performed immunocytochemistry against HA, endogenous SIVA-1 and XIAP (Figure 4.4). Colocalization analysis revealed partial correlation of signals of SIVA-1 with both XIAP (Pearson's correlation value R=0.412±0.115) and HA-FAIM-L (R=0.607±0.060). We could also observe that the interactions between SIVA-1, XIAP and tagged FAIM-L take place in neuronal cytoplasm.

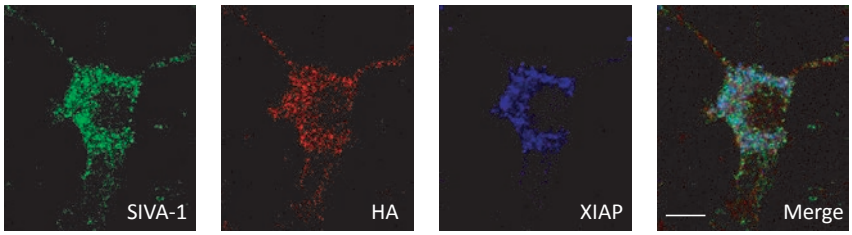

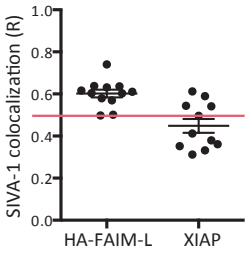

Figure 4.4: SIVA-1, FAIM-L and XIAP colocalize in neuronal cytoplasm. Representative confocal images of immunocytochemistry in cortical neurons. Neurons were transfected with HA-tagged FAIM-L at 4 DIV. Forty-eight h after transfection, immunofluorescence was performed staining with anti-SIVA-1 (green), anti-HA (to detect HA-FAIM-L, red), and anti-XIAP (blue). Scale bar 10 µm. Graph in the lower panel reports Pearson's correlation coefficients obtained in colocalization analysis.

Overall, we were able to show that the pro-apoptotic protein SIVA-1 interacts with two proteins described to be essential for neuronal protection against cell death and modulation of neuronal plasticity, FAIM-L and XIAP. SIVA-1 interacts with FAIM-L through its specific N-terminal, encoded by the neuronal exon of the gene, suggesting SIVA-1 modulation of neuronal-specific processes.

4.2 SIVA-1 is ubiquitously expressed and has a diffuse cytosolic localization in neurons

Since SIVA-1 was chosen as a protein of interest for our study, we started with a general characterization of the protein. First, we wanted to assess expression levels in murine tissues, and whether the protein is expressed in basal conditions.

Murine tissues from E15 and adult stages were processed to analyze mRNA and protein levels. As shown in Figure 4.5 SIVA-1 expression is found in all considered tissues at both age stages at mRNA (fold change relative to CX-E15 value, Figure 4.5A), and protein levels. SIVA-1 is ubiquitously expressed and presents highest levels in peripheral tissues. Embryonic stage expression in tissues results higher than adult stages.

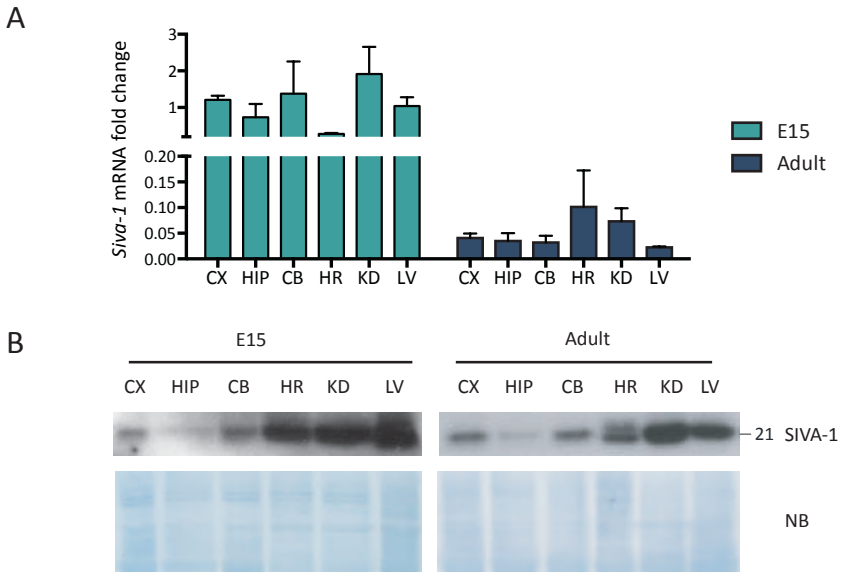

Figure 4.5: SIVA-1 is ubiquitously expressed in murine tissues. Embryonic stage E15 and adult murine tissue were processed. **A,** SIVA-1 mRNA levels were analyzed with qPCR. **B,** SIVA-1 protein levels. Membrane was blotted against SIVA-1, Naphtol Blue (NB) was used as a loading control. CX: cortex; HIP: hippocampus; CB: cerebellum; HR: heart; KD: kidney; LV: liver.

FAIM-L expression is found exclusively in neurons. We reported the interaction of SIVA-1 with FAIM-L, which opens up the possibility of study neuronal-specific function of this protein. The expression analysis indicates that neuronal tissues present indeed SIVA-1 expression, so we next determined its subcellular localization in primary murine neurons.

We performed immunocytochemistry in primary cultures of hippocampal and cortical neurons, and we analyzed SIVA-1 distribution in the cell body, carrying out colocalization analysis with several organelle markers (Figure 4.6). Selected markers are reported on Table 4.1.

Organelle	Immunocytochemistry	Subcellular fractionation
Cytoskeleton	βIII-tubulin	-
Cytosol	-	GAPDH
Endocytic vesicles	Rab5	Rab5
Endoplasmic Reticulum	Calnexin	Calnexin
Mitochondria	Mitotracker	Cytochrome c
Nucleus	Hoechst	Histone H3
Plasma membrane	Trk A	GluA2

Table 4.1: Table reporting organelle and specific markers used in immunocytochemistry and subcellular fractionation studies to label cellular components.

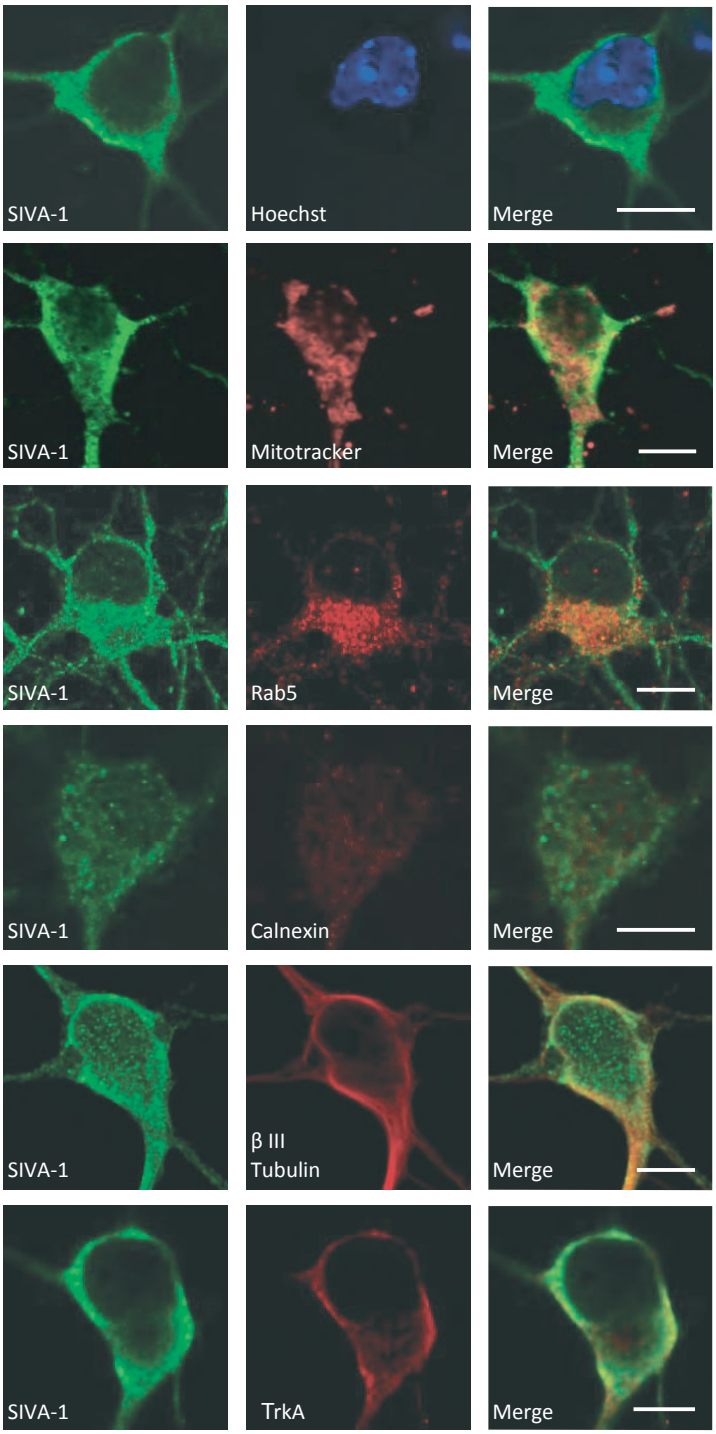

Figure 4.6: SIVA-1 has a mainly cytosolic distribution in neurons.

Figure 4.6: SIVA-1 has a mainly cytosolic distribution in neurons. Representative confocal images of hippocampal neurons. At 7 DIV, immunofluorescence was performed by staining with anti-SIVA-1 (green), Hoechst (nucleus marker, blue). MitoTracker (mitochondria marker), anti-Rab5 (early endosome marker), anti-calnexin (ER marker), anti-β III Tubulin (cytoskeleton marker) and anti-TrkA (cytosolic membrane marker) were stained in red. Scale bar 10 µm.

Mander's colocalization coefficients were obtained to assess co-occurrence of SIVA-1 with each marker (displayed in Figure 4.7). Only values higher than 0.5 were considered to indicate colocalization (red line Figure 4.7). SIVA-1 showed a mainly cytosolic distribution and colocalized with markers of the plasma membrane (TrkA; M1=0.68±0.02), endocytic vesicles (Rab5; M1=0.66±0.15) and cytoskeleton (βIII-tubulin; M1 0.71±0.14). SIVA-1 did not localize with mitochondria (MitoTracker; M1=0.41±0.04) or with the endoplasmic reticulum (Calnexin; M1=0.22±0.15). SIVA-1 expression was clearly excluded from the nucleus (Hoechst staining; M1=0.06±0.03).

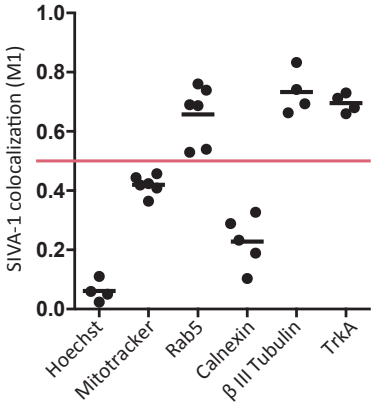

Figure 4.7: SIVA-1 has a mainly cytosolic distribution in neurons. Graph represents Mander's coefficients M1 corresponding to the channel 1 (SIVA-1) signal that co-located with the channel 2 (cellular markers) signal. Only values higher than 0.5 (red line) were considered to indicate colocalization.

We further examined SIVA-1 localization by performing a subcellular protein fractionation assay in whole murine brain. The subcellular fractionation allows, through a series of centrifugations, to separate subcellular compartments and analyze for differential protein level expression.

We detected SIVA-1 mainly in cytosolic and microsomal fractions, confirming the general cytosolic distribution of the protein. As expected, FAIM-L was found mainly in the same fractions (Figure 4.8).

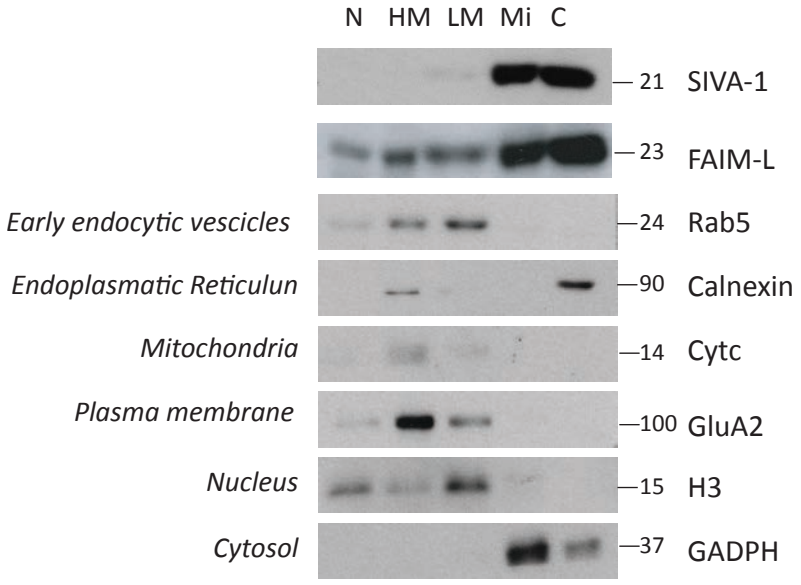

Figure 4.8: SIVA-1 has a mainly cytosolic distribution in neurons. Subcellular protein fractionation assay of adult mouse brain. Anti-histone 3 (H3) antibody was used as a nuclear marker, anti-GluA2 as a plasma membrane marker, anti-calnexin as reticular membrane protein, anti-cytochrome c (Cytc) as a mitochondrial protein, and anti-GAPDH as a cytosolic protein. N: nuclear fraction; HM: heavy membrane fraction; LM: light membrane fraction; Mi: microsomal fraction; C: cytosolic fraction.

Finally, to complete our study of neuronal expression, we considered SIVA-1 expression at synapses. As shown in Figure 4.9, we examined colocalization with synaptic markers in the neurites of 14 DIV hippocampal neurons. We found that SIVA-1 can locate in pre- and post- synaptic terminals as indicated by a positive correlation of immunostaining signal with both synapsinII (pre-synaptic marker; M1=0.50±0.05; arrows) and PSD95 (post-synaptic marker; M1=0.48±0.06; asterisks).

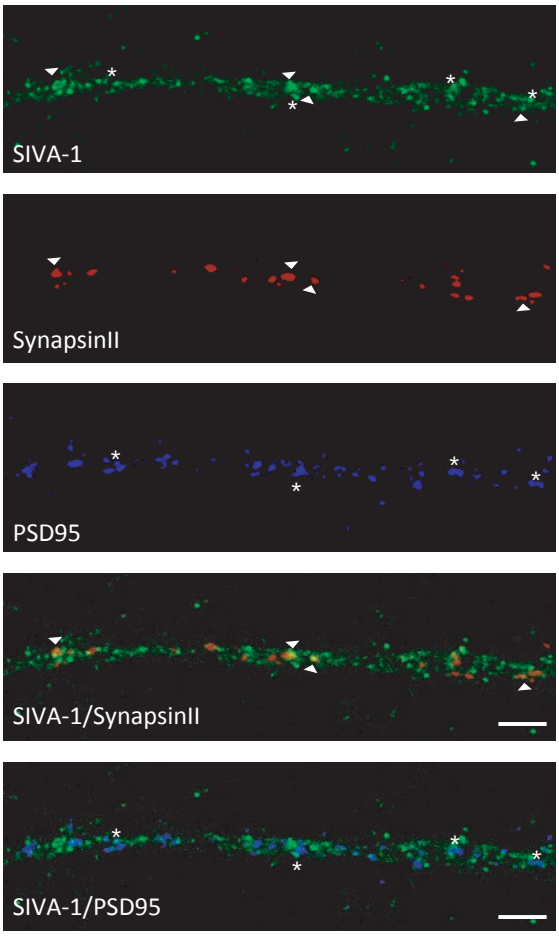

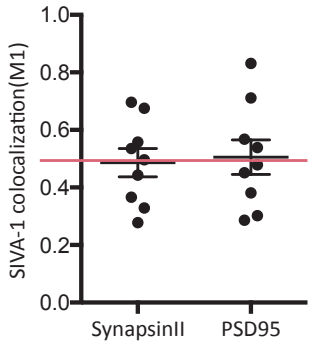

Figure 4.9: SIVA-1 locates at synapses terminals. Representative confocal images of hippocampal neurites. At 14 DIV, immunofluorescence was performed by staining with anti-SIVA-1 (green), pre-synaptic markers synapsinII (red) post-synaptic marker PSD95 (blue). The graph represents Mander's coefficient corresponding to colocalization between SIVA-1 and the synaptic markers. SIVA-1 was found to locate in some of the synapses (arrows and asterisks). Scale bar 2 µm.

Crude synaptosome isolation (Figure 4.10) confirmed that even if SIVA-1 is mainly present in microsomal and soluble fraction, it can be also found in synaptosomes. FAIM-L presents the same distribution.

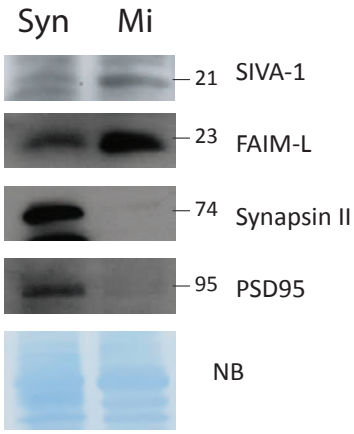

Figure 4.10: SIVA-1 locates at synapses terminals. Crude synaptosome isolation of murine adult brain. SIVA-1 and FAIM-L partially locate in synaptosomes. SynapsinII was used as a pre-synaptic marker, PSD95 as a post-synaptic marker. Syn: crude synaptosome; Mi: microsomal and soluble fraction.

Taken together, our data indicate that SIVA-1 is expressed in the cytoplasm of neurons during development and adult stages, and that can also locate at synaptic terminals. SIVA-1 is found in tissues and primary neurons in basal condition, in absence of any pro-apoptotic stimuli.

4.3 SIVA-1 impairs FAIM-L/XIAP interaction and promotes XIAP ubiquitination

XIAP is a potent inhibitor of effector caspases, as it can directly bind and inhibit their activation. XIAP ubiquitination and degradation by the proteasome are crucial for caspase activation and induction of apoptosis[54]. As shown by our lab, FAIM-L is a XIAP-interacting protein that executes its anti-apoptotic function by inhibiting XIAP ubiquitination, hence stabilizing its levels and inhibiting caspases[123].

Having reported SIVA-1 interaction with both proteins we proceeded to address whether SIVA-1 interferes with the FAIM-L/XIAP interaction and XIAP ubiquitination.

To this end, we analyzed FAIM-L/XIAP interaction in presence of increasing amounts of overexpressed SIVA-1 in PC12 cells.

We performed an immunoprecipitation of Myc-XIAP and found the amount of co-immunoprecipitated FLAG-FAIM-L to be inversely correlated to SIVA-1 overexpression. The elution fraction of the IP:Myc presents decreasing levels of FLAG-FAIM-L, in accordance with the increasing amount of SIVA-1 (Figure 4.11, lanes 4-6). Quantification of XIAP/FAIM-L interaction in the graph is normalized to immunoprecipitated XIAP levels in the elution. Comparable levels of Myc-XIAP are immunoprecipitated in the three condition of differential expression of HA-SIVA. In the elution we can observe a distinct decrease in FLAG-FAIM-L in correspondence with SIVA-1 overexpression.

Overall, our results suggest that SIVA-1 impairs the interaction of FAIM-L with XIAP.

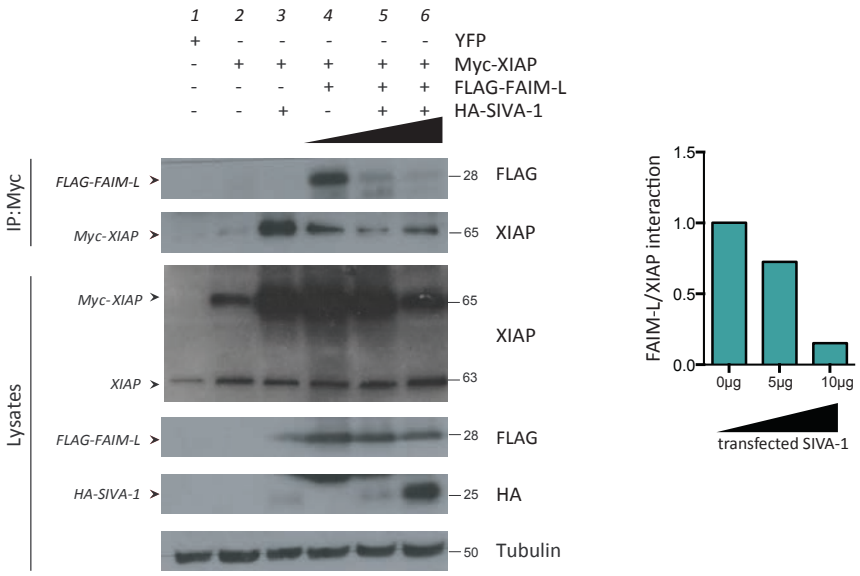

Figure 4.11: SIVA-1 impairs FAIM-L/XIAP interaction. PC12 cells were transiently transfected with Myc-XIAP, FLAG-FAIM-L and two concentrations of HA-SIVA-1. Myc-XIAP was immunoprecipitated using anti-Myc antibody. The membrane was blotted with anti-FLAG to detect FAIM-L and HA to detect SIVA-1. The antibody against XIAP was used as a control of the immunoprecipitation and anti-tubulin as loading control. Graph shows the amount of immunoprecipitated FAIM-L relative to immunoprecipitated XIAP.

Following the interaction impairment observation, we considered SIVA-1 modulation on XIAP ubiquitination. We performed a ubiquitin pull-down assay in lysates of HEK 293T cells transfected with His-tagged ubiquitin and overexpression plasmids of tagged XIAP, SIVA-1, and FAIM-L.

His-tagged ubiquitin was pulled down and eluted proteins were analyzed by SDS-PAGE.

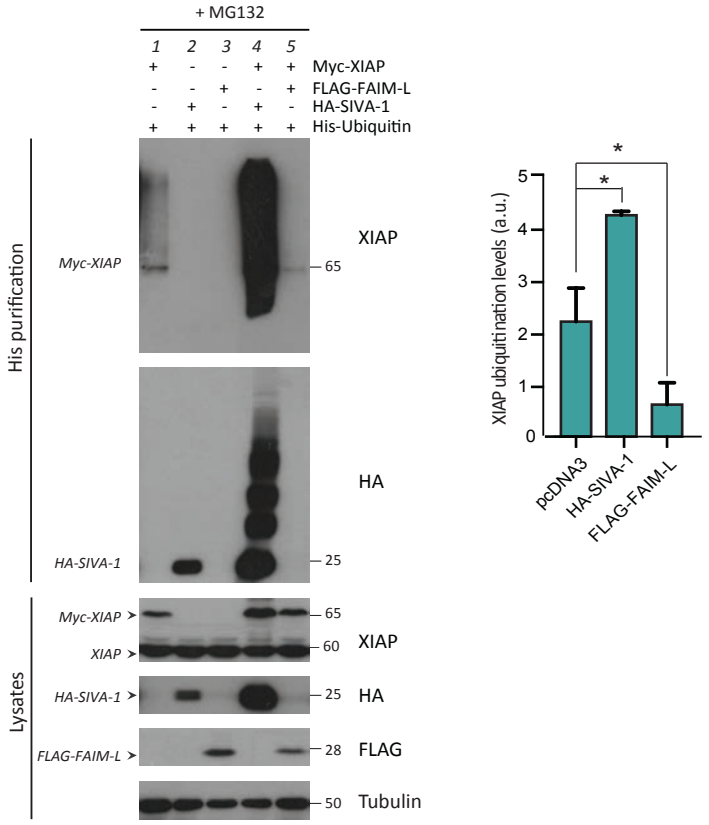

Figure 4.12: SIVA-1 and XIAP mutually promote their ubiquitination. HEK293T cells were transfected with Siva-1, XIAP and FAIM-L overexpression plasmids and treated with 10μM MG132. Successful transfection was confirmed by immunoblot of the lysates membrane with XIAP, HA and FLAG. Tubulin was used as loading control. Ubiquitin pull-down membrane was immunoblotted with HA and XIAP, an evident ubiquitination of both proteins is detectable. Graph shows XIAP ubiquitination levels quantification, normalized to total XIAP levels (a.u.). One-way ANOVA, *p≤ 0.05.

We analyzed ubiquitin levels of Myc-XIAP and HA-SIVA-1 in the pull-down elution. Both proteins are found to be ubiquitinated in presence of MG132 (Myc-XIAP lane 1, HA-SIVA-1 lane 2 Figure 4.12). What stands out, however, is that both proteins present a strong increase in ubiquitination levels when co-expressed (Figure 4.12, lane 4 and graph), suggesting a mutual regulation of the proteins. As expected, FAIM-L decreases XIAP ubiquitination (Figure 4.12, lane 5 and graph).

What we found especially interesting in the ubiquitin pull-down results was the opposite role on XIAP ubiquitination of SIVA-1 compared to FAIM-L. The ubiquitin pull-down was performed in HEK 293T, which do not express endogenous FAIM-L. Our evidence therefore suggests that the sole overexpression of SIVA-1 induces XIAP ubiquitination, regardless of FAIM-L presence. We can assume that the impairment of XIAP/FAIM-L interaction we report in Figure 4.11 is a mechanism through which SIVA-1 can additionally increase XIAP ubiquitination.

In a further analysis we considered the endogenous levels of XIAP ubiquitination. We immunoprecipitated endogenous ubiquitin with an anti-ubiquitin antibody conjugated with agarose in HEK 293T cells overexpressing HA-tagged SIVA-1, FAIM-L, or a combination of both proteins. As shown by high molecular bands in XIAP blot in Figure 4.13, XIAP presented basal endogenous ubiquitination. When SIVA-1 was overexpressed, ubiquitination pattern of XIAP was clearly enhanced. FAIM-L overexpression on the other hand reduced XIAP ubiquitination levels, thereby confirming our previous findings. Overexpression of FAIM-L partially restored SIVA-1-induced XIAP ubiquitination.

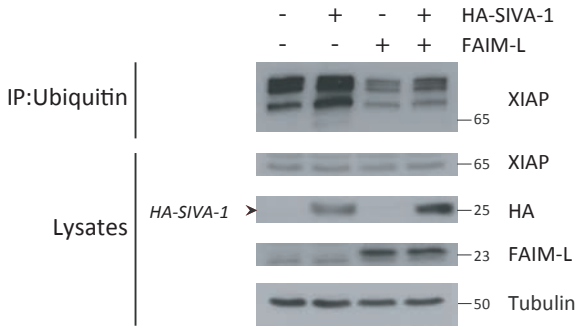

Figure 4.13: SIVA-1 and FAIM-L have opposite effects on XIAP ubiquitination. Cells were transfected with FAIM-L and SIVA-1 (HA-SIVA-1), and endogenous ubiquitin was immunoprecipitated using anti-ubiquitin antibody. The membrane was blotted with antibodies against FAIM-L, XIAP and HA to detect SIVA-1, and anti-tubulin was used as a loading control.

Finally, we wanted to consider how the lack of SIVA-1 could be affecting endogenous levels of XIAP ubiquitination. We knocked down SIVA-1 levels in HEK 293T using a siRNA designed against the human sequence of SIVA-1 and already validated by Resch and colleagues[149], and performed an endogenous ubiquitin pull-down. As shown in Figure 4.14, XIAP basal ubiquitination levels appeared to be unaffected by SIVA-1 knock down.

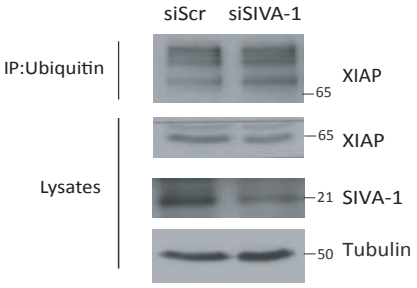

Figure 4.14: SIVA-1 knock down has no effect on XIAP ubiquitination. Cells were transfected with siScr or siSIVA-1 and endogenous ubiquitin was immunoprecipitated using anti-ubiquitin antibody. The membrane was blotted with antibodies against XIAP and SIVA-1, and anti-tubulin was used as a loading control.

Overall, comparing our results, it can be deduced that SIVA-1 and FAIM-L exert opposite effects on XIAP ubiquitination, respectively promoting and inhibiting it. SIVA-1 promotes XIAP ubiquitination by displacing FAIM-L interaction and also by a direct, FAIM-L independent, manner.

4.4 SIVA-1 induces apoptotic cell death through caspase-3 activation

SIVA-1 has been extensively described as a pro-apoptotic protein in different cell types[137,143,144]. As part of our characterization, we wanted to explore SIVA-1 apoptotic function in our *in vitro* model of hippocampal primary neurons.

First, we produced lentiviral particles expressing HA-SIVA-1 to explore the effects of its ectopic expression. As shown in Figure 4.15 SIVA-1 overexpression was confirmed by western blot analysis of HA-SIVA-1 and by immunocytochemistry, by counting GFP-positive cells.

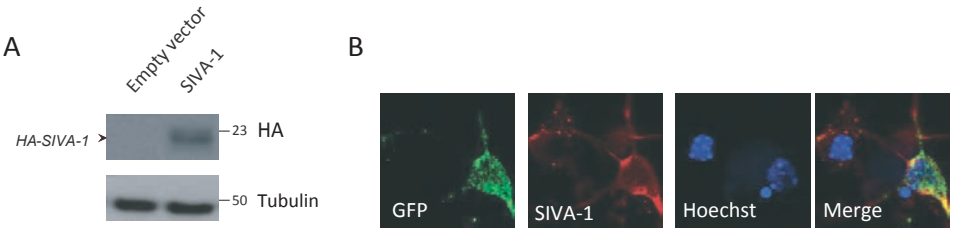

Figure 4.15: SIVA-1 overexpression in primary neurons. Primary neurons were infected with lentiviral particles carrying HA-SIVA-1 plasmid for 72h. **A,** SIVA-1 expression verified by western blot. HA was used to detect SIVA-1 and tubulin as a loading control. **B,** Immunocytochemistry of SIVA-1 and GFP to confirm lentiviral transfection and overexpression. Hoechst staining was used as a nuclear marker. Scale bar 10µm.

SIVA-1 was overexpressed in hippocampal neurons, and we assessed cell death by counting the condensation and/or fragmentation of chromatin, a typical hallmark of apoptosis. As seen in Figure 4.16, SIVA-1 was sufficient to induce an increase in the percentage of apoptotic nuclei. Treatment of cells with the pan-caspase inhibitor Q-VD consistently abrogated SIVA-1-induced apoptosis, indicating that SIVA-1 is promoting cell death through caspase activation.

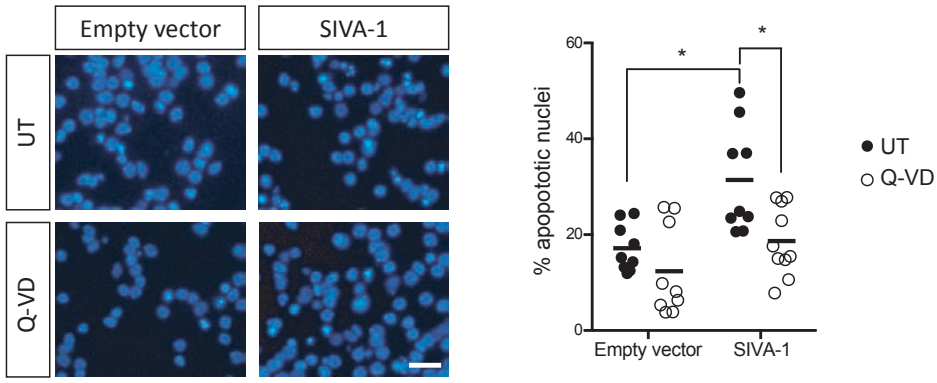

Figure 4.16: SIVA-1 induces apoptotic cell death. Representative images of Hoechst staining in control and overexpressing cells in absence or presence of Q-VD. Right graph represents quantification of the percentage of nuclei with apoptotic morphology. SIVA-1 induces apoptotic cell death, and Q-VD treatment rescues neurons from SIVA-1 induced cell death. Two-way ANOVA *p≤ 0.05. Scale bar 20µm.

The main executioners of apoptosis are effector caspases, such as caspase-3. Caspases are synthesized as inactive zymogens (pro-caspases) that are then activated through cleavage into a smaller subunit. We further confirmed caspases involvement in SIVA-1 induced cell death, by exploring caspase-3 cleavage and activity.

As shown by the western blot in Figure 4.17A, SIVA-1 overexpression is sufficient to cause an increase of cleaved caspase-3. The cleavage is accompanied by an increase of caspase-3 activity (measured as substrate cleavage quantification in caspase activity assay, Figure 4.17B). Treatment with Q-VD was successful: Q-VD completely abrogates both caspase-3 cleavage (Figure 4.17A) and activation (Figure 4.17B). Taken together our results indicate that SIVA-1 induces neuronal death through activation of caspase-3.

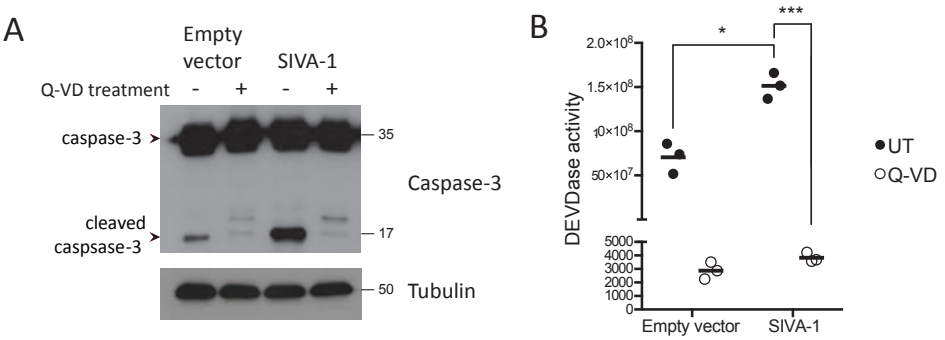

Figure 4.17: SIVA-1 induces caspase-3 cleavage and activation. A, SIVA-1 induces caspase-3 cleavage. Treatment with 10μM of pan-caspase inhibitor Q-VD abrogates it. Membrane was immunoblotted with anti-caspase-3 and tubulin as a loading control. **B,** DEVDase activity was measured in cells overexpressing SIVA-1 or control empty vector. SIVA-1 induces an activation of caspase-3. Q-VD treatment abrogates caspase-3 activity. UT: untreated; Q-VD: quinolyl-Val-Asp-OPh. Two-way ANOVA *p≤ 0.05; ***p≤ 0.001.

We also determined that SIVA-1 has no role in the basal death found in primary neurons. We knocked down SIVA-1 levels using a short hairpin RNA (shRNA) designed against the murine sequence of SIVA-1, and quantified apoptotic nuclei percentage. No change in cell death was found compared to the scrambled (shScr) condition, indicating that basal levels of cell death are SIVA-1-independent (Figure 4.18).

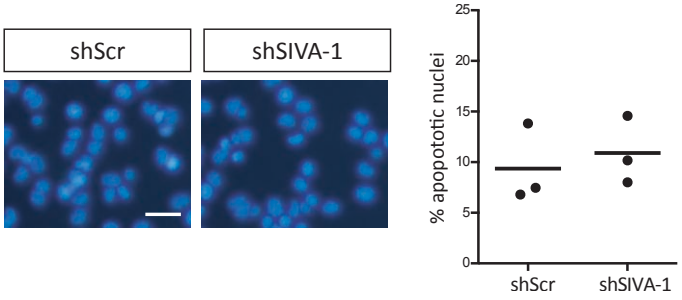

Figure 4.18: Basal cell death is SIVA-1-independent. Hippocampal neurons were infected with scrambled or short hairpin RNA of SIVA-1. Neurons were stained with Hoechst and neuronal cell death was quantified by counting the percentage of condensed of fragmented nuclei.

We established that SIVA-1 overexpression increases the percentage of apoptotic cell death in neurons. As reported in previous results in this work FAIM-L is an anti-apoptotic protein that acts as a functional antagonist of SIVA-1 in XIAP ubiquitination. Therefore, we decided to consider whether FAIM-L overexpression affects SIVA-1-induced cell death.

We infected neurons with overexpressing vector of both proteins, and quantified apoptotic nuclei. We report in Figure 4.19 that in cells overexpressing FAIM-L there is a clear protection against SIVA-1 induced cell death.

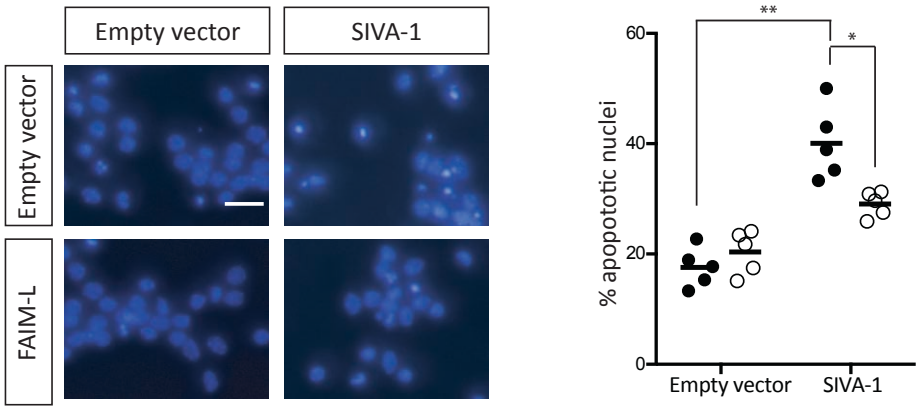

Figure 4.19: FAIM-L overexpression partially reduces SIVA-1 induced cell death. Hippocampal neurons were infected with SIVA-1, FAIM-L or a combination of both vectors. Neurons were stained with Hoechst and neuronal cell death was quantified by counting the percentage of condensed of fragmented nuclei. Two-way ANOVA, *≤ 0.05; **p≤ 0.01. Scale bar 20µm.

Here, we confirm SIVA-1 role as a pro-apoptotic protein in neurons, as its overexpression is sufficient to induce apoptotic cell death. We also find that FAIM-L is able to rescue neurons from SIVA-1 apoptotic cell death, supporting an antagonist effect of these two proteins on the same process, and overall extending our knowledge on FAIM-L functions.

4.5 SIVA-1 modulates GluA2 receptor trafficking

Synaptic plasticity is a crucial process that modifies synapses in response to neuronal activity. Neurons undergo long-lasting changes, essential for normal development and homeostasis, among these we found LTD in synapses. LTD is an NMDAR-dependent process that involves the removal and internalization of AMPAR in post-synaptic membranes. Li and colleagues described caspases to be necessary to mediate such regulatory events in the mature nervous system[70]. Thus, although global activation of caspases leads to cell death, restricted and localized activation controls normal physiology in living neurons. Some regulatory proteins of the intrinsic apoptotic pathway have been reported to modulate caspases activation in synaptic depression. Among these, anti-apoptotic XIAP and FAIM-L have been shown to be inhibitors of the process[70,107].

As shown in previous results, we found that SIVA-1 interacts with both XIAP and FAIM-L and is an activator of caspases. We therefore proceeded to analyze whether SIVA-1 also regulates caspase-dependent plasticity processes.

We considered LTD, whose main mechanism is the internalization of GluA2 subunit containing AMPAR. As an *in vitro* model, we adopted chemical-LTD (chLTD), a protocol previously described by Li *et al*., in which primary neurons undergo LTD changes with a 15min treatment of NMDA in media[70].

We corroborated caspase-3 activation induction when adopting this protocol. As showed in Figure 4.20 caspase-3 is transiently activated with 15min NMDA treatment. Since we wanted to later assess GluA2 internalization we also verified to have no change in the receptor level expression due to treatment.

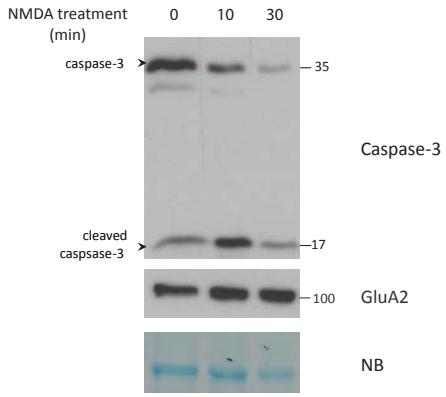

Figure 4.20: chLTD induces transient caspase-3 activation. Primary cortical neurons were treated with 50µM NMDA. Membrane was blotted against caspase-3 and GluA2. Naphtol Blue was used as loading control. Caspase-3 is transiently activated, with NMDA treatment, while GluA2 does not change expression levels.

In Figure 4.21 we corroborated that caspase-3 activation induced by NMDA treatment was transient and not functional for inducing apoptosis. We examined the possible toxicity of NMDA treatment and made sure that the protocol we used was not toxic to cells. The concentration we used (50µM) was found non-toxic until 12h of treatment.

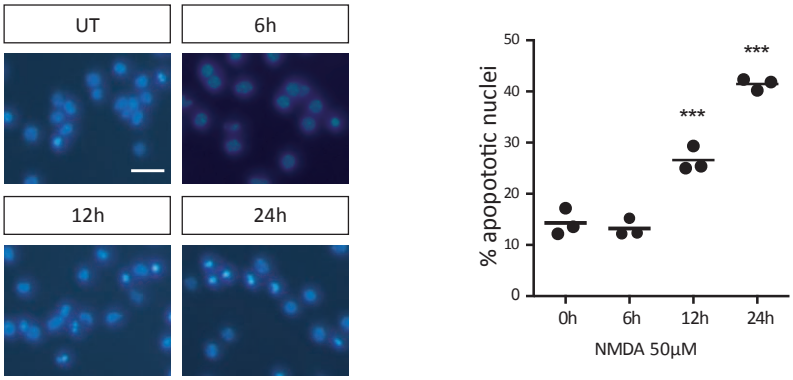

Figure 4.21: NMDA treatment used in chLTD is non-toxic. Hippocampal neurons were treated with 50µM NMDA at different time points. Neurons were stained with Hoechst and neuronal cell death was quantified by counting the percentage of condensed or fragmented nuclei. One-way ANOVA ***p≤ 0.001. Scale bar 20µm.

To determine SIVA-1 role in GluA2 internalization, AMPAR endocytosis was measured by means of an antibody feeding internalization assay, which allows to quantify surface and internalized receptor. Hippocampal primary neurons

were infected with HA-SIVA-1, FAIM-L and a combination of both lentiviral vectors (Figure 4.23A).

At 14 DIV cultures were treated with 50µM NMDA for 15min at 37°C to stimulate chLTD. All lentiviral vectors used were GFP-tagged, so that we were able to label and consider for analysis only transfected neurons. Given a lower transfection efficiency of SIVA-1 overexpression lentiviral particles, compared to FAIM-L, HA was selected to detect transfected neurons in the double infection condition.

As shown by representative images in Figure 4.22, and quantified in Figure 4.23B, we found that although no change was detected in SIVA-1-overexpressing neurons once NMDA treatment had been applied to induce chLTD, the sole ectopic expression of SIVA-1 was sufficient to induce an increase in the internalization levels of the endogenous AMPAR subunit. SIVA-1-induced internalization was blocked by the overexpression of FAIM-L (Figure 4.22B), thereby confirming a functional interaction between these two proteins. In agreement with the observations by Martinez-Mármol *et al.*, FAIM-L overexpression abrogated GluA2 internalization induced by chLTD.

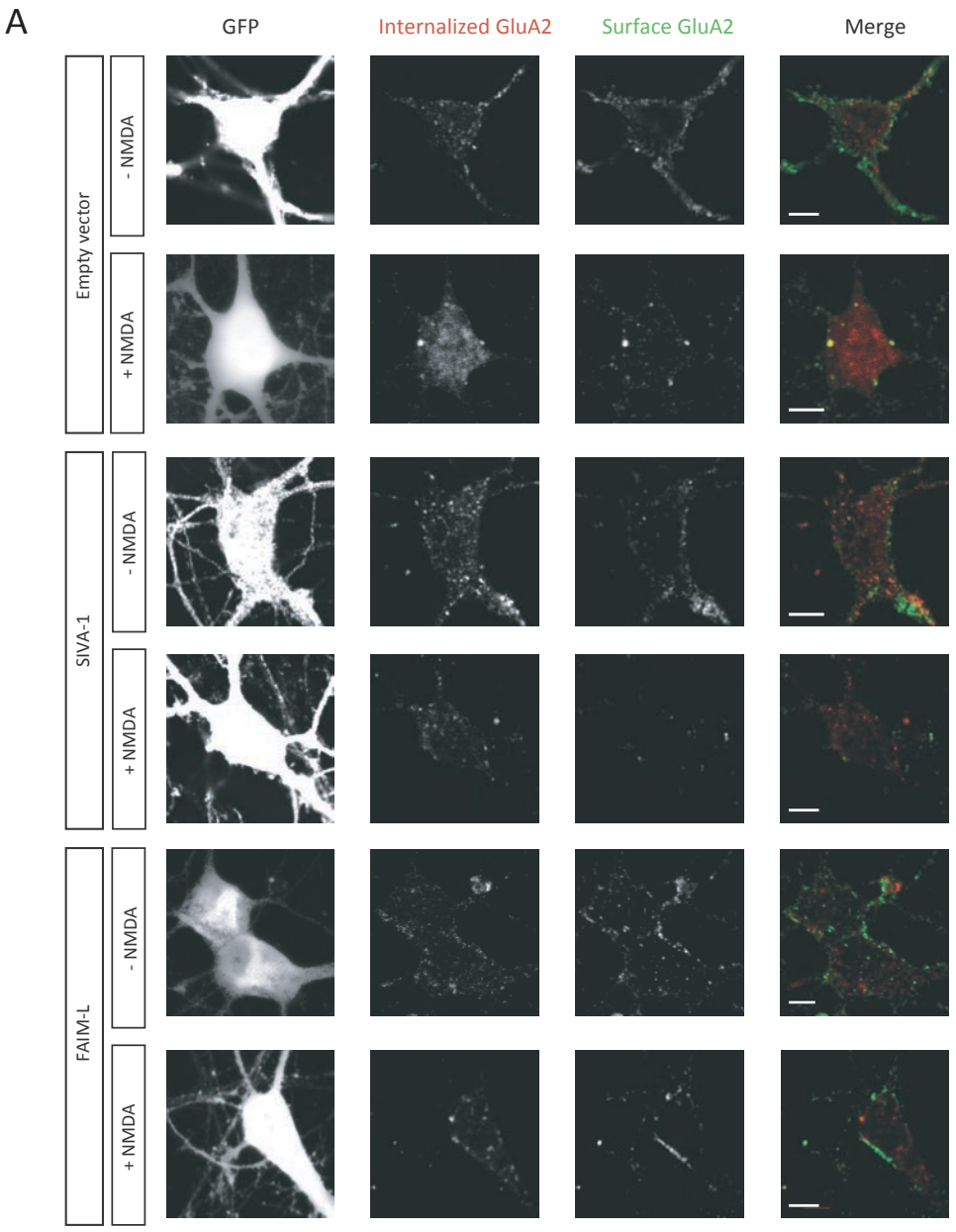

Figure 4.22: SIVA-1 promotes GluA2 internalization in basal conditions. A, Representative confocal images of neurons transfected with SIVA-1, FAIM-L or empty vector. **B,(next page)** Representative confocal images of neurons co-transfected with SIVA-1 and FAIM-L GluA2 internalization assay was performed in neurons treated with NMDA to stimulate LTD and in untreated neurons. Only GFP- or HA-positive cells (first column) were considered for quantification. Internalized GluA2 (second column, red in merge) and surface GluA2 (third column, green in merge) were measured**.** Scale bar 10 µm.

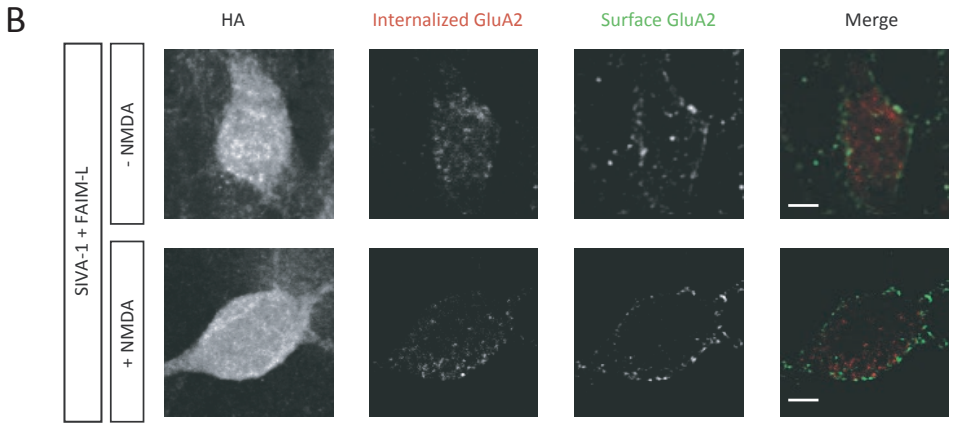

Figure 4.22 B

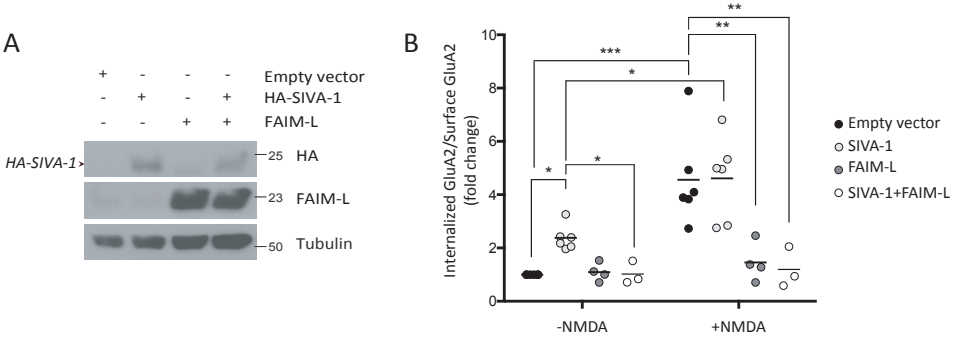

Figure 4.23: SIVA-1 promotes GluA2 internalization in basal conditions. A, Hippocampal neurons were infected with lentiviral particles carrying overexpression vectors of HA-SIVA-1, FAIM-L and a combination of both. Membrane was blotted against HA and FAIM-L, tubulin was used a loading control. **B,** Results were normalized to empty vector, untreated cells. Induction of chemical LTD induced GluA2 internalization in empty vector condition and SIVA-1 transfected cells. Non-stimulated cells overexpressing SIVA-1 showed an increase in GluA2 internalization. FAIM-L overexpression blocked LTD induction, and its overexpression with SIVA-1 in untreated cells restored basal levels of receptor internalization. Each point represents an independent experimental repeat in which 15-20 cells were analyzed. UT: untreated, NMDA: N-methyl-D-aspartate. Two-way ANOVA, *p≤ 0.05; ** p≤ 0.01; *** p≤ 0.001.

We further confirmed that SIVA-1 is sufficient to induce internalization of AMPAR, by assessing the amount of surface receptor through a biotinylation assay, which allows to isolate surface membrane proteins. We overexpressed

SIVA-1 in cortical neurons in absence of any other stimulus and performed the assay, confirming that SIVA-1 overexpression decreases surface receptor levels (Figure 4.24), while it does not change GluA2 total levels.

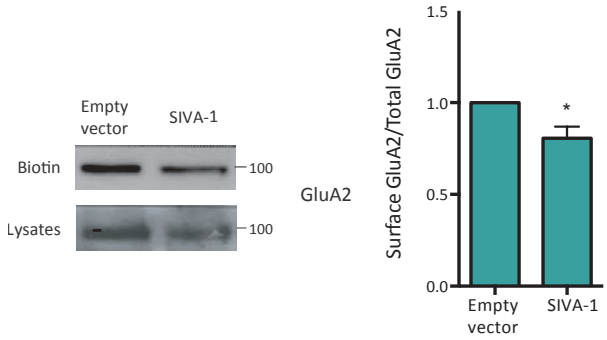

Figure 4.24: SIVA-1 overexpression reduces AMPAR surface levels. GluA2 surface receptor was isolated with the biotin surface assay in hippocampal cells transfected with SIVA-1 or empty vector as a control. Right panel shows quantification of GluA2 surface receptor. t-test *p ≤ 0.05.

Given that caspases are essential for GluA2 internalization during LTD, we addressed whether the decrease in GluA2 basal surface level in SIVA-1-overexpressing neurons was caspase-dependent. The presence of the pan-caspase inhibitor Q-VD totally abrogated SIVA-1-induced internalization of GluA2 (Figure 4.25 and quantification in Figure 4.26), restoring it to control condition (empty vector) levels. SIVA-1 effect is therefore caspase-dependent.

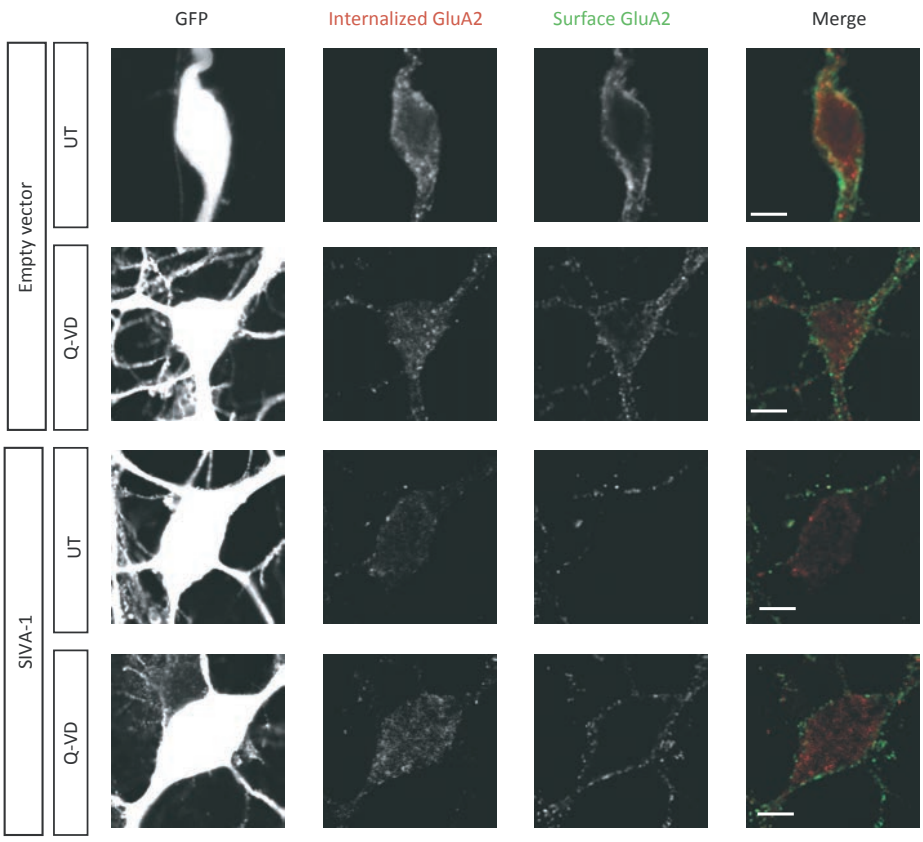

Figure 4.25: SIVA-1 induces GluA2 internalization in a caspase-dependent manner. Representative confocal images of neurons transfected with SIVA-1 or empty vector and treated with 10μM of Q-VD (caspase inhibitor). Only GFP-positive cells (first column) were considered for quantification (left panel). Scale bar 10 μm.

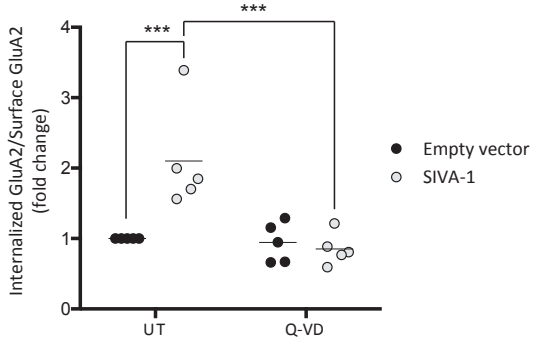

Figure 4.26: SIVA-1 induces GluA2 internalization in a caspase-dependent manner.

Figure 4.26: The results of the quantification of internalized GluA2 *vs.* surface GluA2 were normalized to empty vector, untreated cells (right panel). Each point represents an independent experimental repeat in which 15-20 cells were analyzed. SIVA-1-transfected cells showed greater internalization of GluA2 receptor, Q-VD treatment restored internalization to basal levels. Two-way ANOVA ***$p \leq 0.001$.

To further examine the role of SIVA-1 in the regulation of synaptic receptor internalization, we knocked down SIVA-1 levels and analyzed GluA2 internalization. A decrease in SIVA-1 levels was observed when a shRNA was used (Figure 4.28). No change was observed in untreated cells, but we did detect a decrease in GluA2 internalization in shSIVA-1-infected neurons after the induction of chLTD. GluA2-induced internalization was marked in shSIVA-1 neurons, but significantly decreased compared to control infected neurons (Figure 4.27 and Figure 4.28).

Taken altogether, in our work we conclude that SIVA-1 role as an activator of caspases is not exclusive to cell death but is also involved in receptor trafficking. We therefore add SIVA-1 to the list of modulators of apoptosis that can also modulate synaptic plasticity.

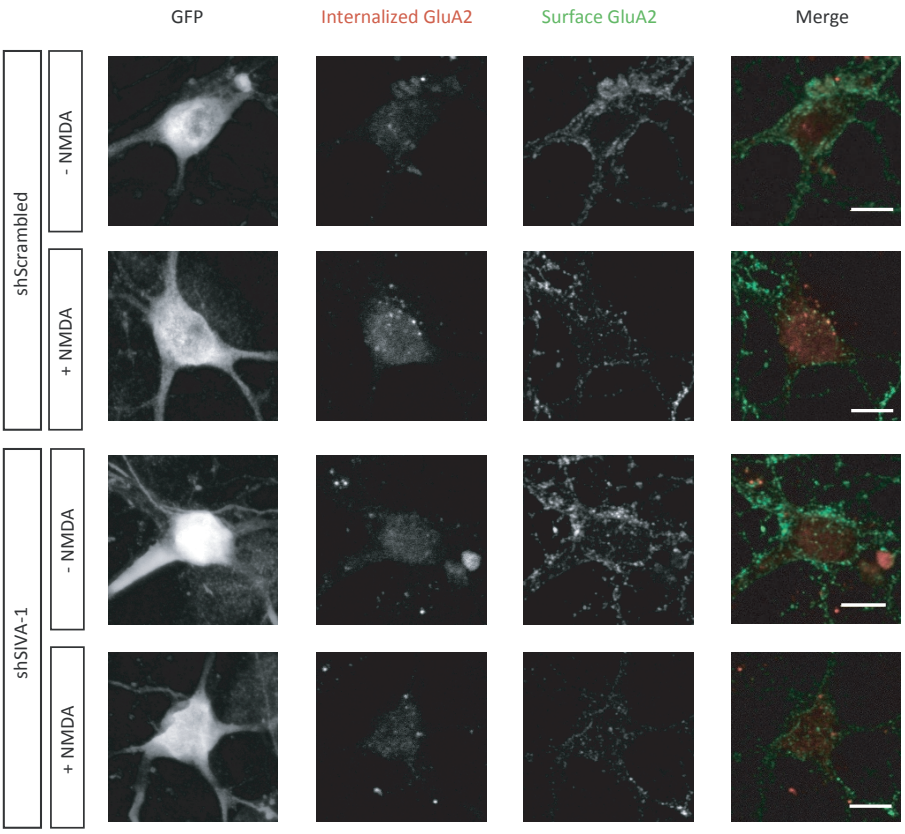

Figure 4.27: shSIVA-1 partially impairs GluA2 internalization in chLTD. Representative confocal images of neurons transfected with vectors carrying shSIVA-1 or shScramble as control. The GluA2 internalization assay was performed in neurons treated with NMDA to stimulate LTD and in untreated neurons. Only GFP-positive cells (first column) were considered for quantification. Internalized GluA2 (second column, red in merge) and surface GluA2 (third column, green in merge) were measured. Scale bar 10 µm.

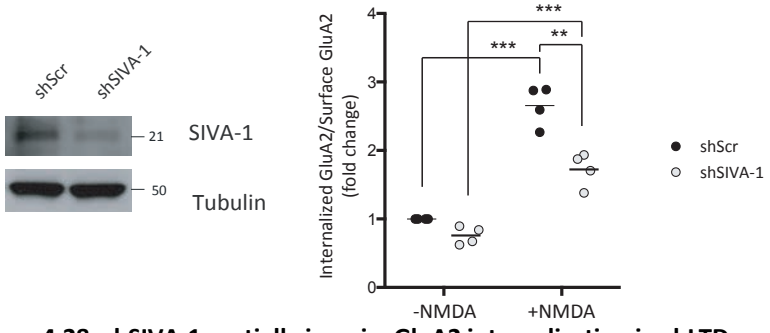

Figure 4.28: shSIVA-1 partially impairs GluA2 internalization in chLTD.

Figure 4.28: The results of the quantification of internalized GluA2 *vs.* surface GluA2 were normalized to shScr, untreated cells. Each point represents an independent experimental repeat in which 15-20 cells were analyzed. NMDA treatment induced GluA2 internalization in both shScr and shSIVA-1 cells. However, shSIVA-1 cells treated with NMDA showed a significant decrease in receptor internalization. Two-way ANOVA *p ≤ 0.05; ***p ≤ 0.001.

4.6 SIVA-1 levels are increased in chemical LTD

Our findings suggest a role of SIVA-1 in caspase-dependent GluA2 internalization. Since the expression of several modulators of synaptic plasticity is required for the correct induction and maintenance of plasticity changes, we analyzed SIVA-1 protein levels during chLTD induction. We were surprised to find a consistent increase in SIVA-1 expression just after 5min of NMDA treatment (Figure 4.29).

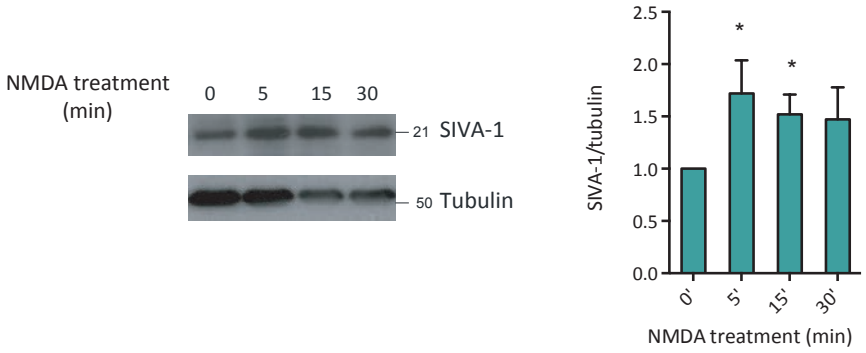

Figure 4.29: SIVA-1 protein levels are rapidly increased during chLTD. Primary neuronal cells were treated with 50 µM of NMDA at different time points (0-30min) and protein expression of SIVA-1 was analyzed by SDS-PAGE. Anti-tubulin was used as a loading control. Right panel shows quantification of 5 different experiments. SIVA-1 expression increased with 5 and 15 min treatment of NMDA. t-test * p ≤ 0.05.

The protein increase appeared to be transient, and to happen just after NMDA stimulation. We found that the rapid increase in protein was independent on SIVA-1 mRNA levels, which remained unaltered during chLTD induction (Figure 4.30).

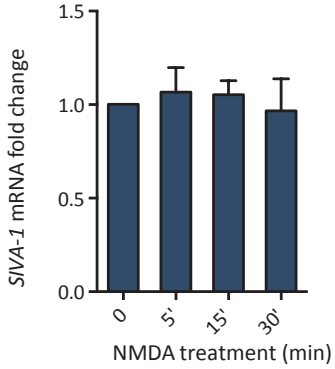

Figure 4.30: SIVA-1 mRNA levels are unaltered during chLTD. Primary cortical neurons were treated with 50µM of NMDA at different time points (0–30 min) and mRNA levels were analyzed by qPCR, which revealed no change in SIVA-1 mRNA expression after treatment.

Induction of chLTD by NMDA stimulation leads to an increase in Ca^{2+} inflow in neurons, followed by calcineurin and caspase-3 activation, and the internalization of AMPAR. Calcium entry via NMDAR activation represents the most important element for the initiation of NMDAR signaling cascade, including NMDAR influence on translation. When we pre-treated primary cortical neurons with BAPTA-AM, a calcium chelator, and stimulated chLTD, we found no increase in SIVA-1 protein levels. We obtained the same result with the translation inhibitor CHX (Figure 4.31).

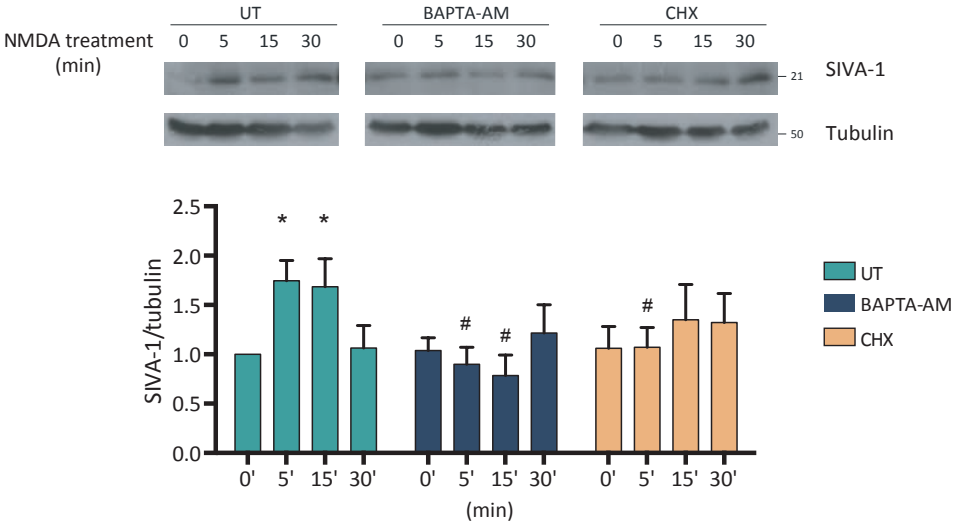

Figure 4.31: Calcium signal induces SIVA-1 translation in chLTD.

Figure 4.31: The increase in SIVA-1 levels was blocked by pretreatments with 50 µM of BAPTA-AM for 30 min or 1 µg/ml of cycloheximide (CHX) for 1h. Two-way ANOVA* $p \leq 0.05$ for comparison between time points in the same treatment, # $p \leq 0.05$ for comparison between treatments. UT: untreated.

With these results it stands clear that following the treatment with NMDA, activation of NMDAR signaling pathway through Ca^{2+} induces a rapid translation of modulator proteins, among them SIVA-1, which can then be involved in caspase activation and AMPAR internalization.

4.6 SIVA-1 role in neurite pruning

Axonal degeneration is an important process during development involved in the correct structure formation of nervous system.

An extensively used model to study axon pruning *in vitro* is NGF-dependent dorsal root sensory neurons[204,205]. Dorsal root ganglia (DRG) explants are plated in media supplemented with NGF and allowed to establish axons. They are thereafter subjected to NGF withdrawal and undergo caspase-dependent axonal degeneration.

Unsain and colleagues demonstrated that XIAP inhibits caspase activity in degenerating axons, and we demonstrated that FAIM-L, through stabilization of XIAP, also inhibit this process[71,107].

Figure 4.32 shows how we were able to detect axonal integrity changes in DRG explants subjected to NGF withdrawal. We allowed DRG to expand axons, and then deprived NGF from media for 8 or 24 hours.

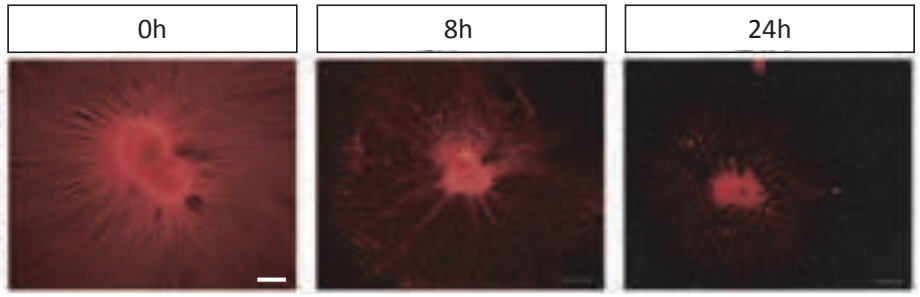

Figure 4.32: NGF deprivation causes neurite pruning in DRG explants. Representative images of DRG explants. At DIV 2 after plating in NGF-supplemented media, DRG explants were subjected to NGF withdrawal, and axonal integrity was assessed at 0, 8 and 24h after deprivation by immunocytochemistry against β III-tubulin. Scale bar 200µm. These data were included in a publication (Martinez-Mármol *et al*. 2016)

Considering our findings of SIVA-1 as a FAIM-L functional antagonist and regulator of caspase-dependent processes such as cell death and AMPAR trafficking, we wanted to assess SIVA-1 role in axonal pruning.

We started by analyzing protein levels in our model. As reported in Figure 4.33, DRG explants undergoing NGF deprivation present an activation of effector caspase-3 cleavage. Consistent with the activation of caspase-3, we detected also an increase in fragmented forms of NF-66 cleavage, indicating cytoskeleton disassembling.

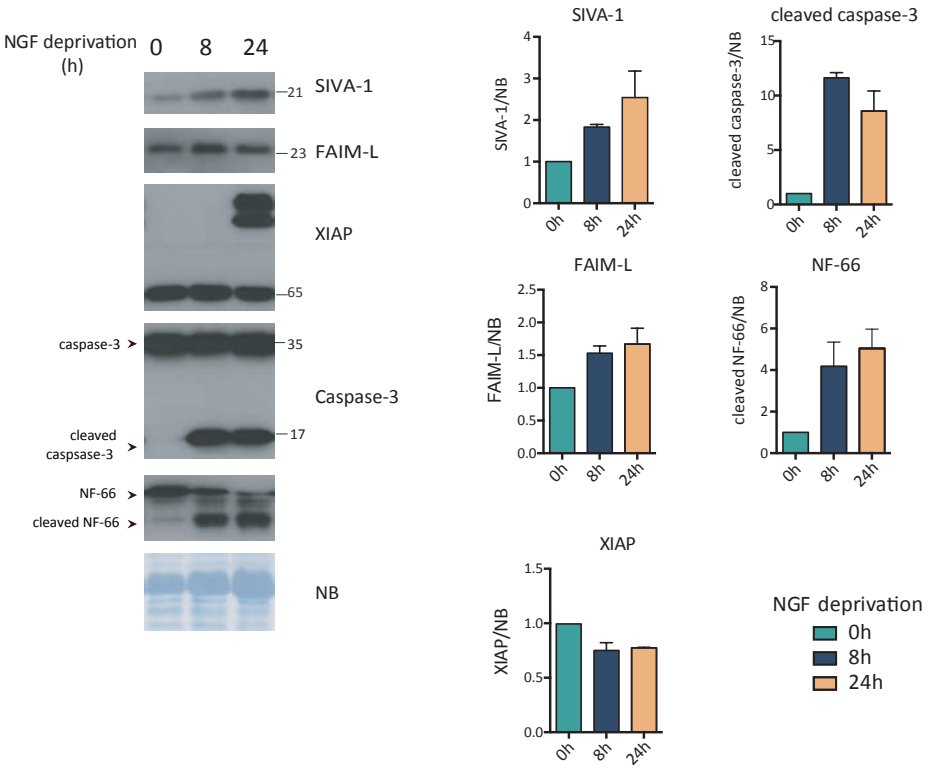

Figure 4.33: SIVA-1 levels increase during NGF deprivation. At DIV 2 after plating in NGF-supplemented media, DRG explants were subjected to NGF withdrawal. At 0, 8 and 24h after deprivation explants were lysed and analyzed by western blot. Membranes were blotted with anti-SIVA-1, XIAP, FAIM-L, caspase-3 and NF-66. Naphtol blue (NB) was used as a loading control. Graphs on the right represent the analysis of 3 separate experiments.

When considering SIVA-1 levels, we were able to show an increase in SIVA-1 protein levels all along the degeneration process. Also, two higher-molecular weight bands appeared in XIAP blot in the 24h deprivation condition, indicating some kind of post-translational modification of the protein.

After detecting SIVA-1 increase during deprivation, we proceeded to collect some preliminary results on SIVA-1 modulation in DRG explants. Lentiviral particles carrying SIVA-1, FAIM-L or empty vectors were added to the media at seeding. Following the protocol at DIV 2, explants were subjected to trophic factor deprivation.

What we found in our preliminary analysis is that SIVA-1-overexpressing DRG seem to present an accelerated degeneration. When we examined axon integrity through β III-tubulin immunocytochemistry, we could observe an accelerated disorganization of neurites in SIVA-1 overexpressing explants. FAIM-L on the other hand, protected explants from undergoing degeneration (Figure 4.34).

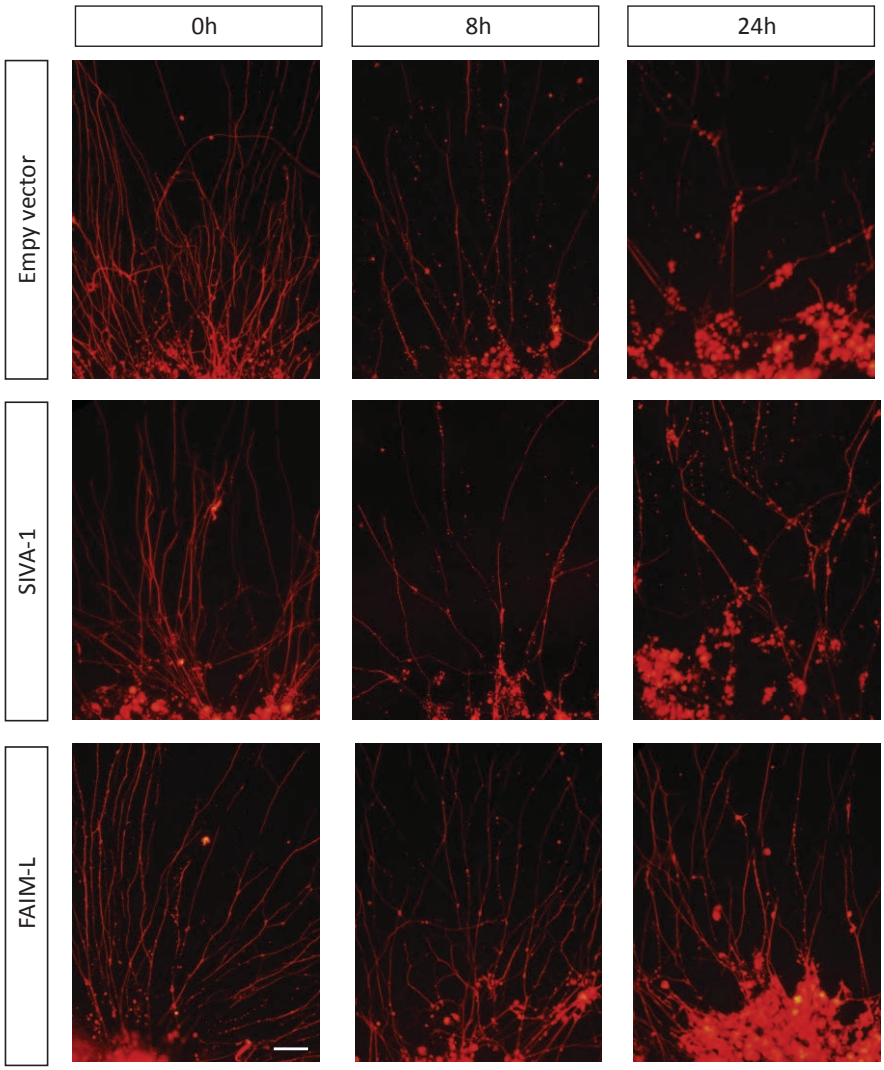

Figure 4.34: SIVA-1 accelerates neurite degeneration during NGF deprivation. DRG were plated and infected with SIVA-1, FAIM-L or empty vector viruses. At DIV 2 after plating in NGF-supplemented media, DRG explants were subjected to NGF withdrawal, and axonal integrity was assessed at 0, 8 and 24h after deprivation by immunocytochemistry against β III-tubulin. Scale bar 20µm.

Consistent with the accelerated degeneration observed, we found an increase in caspase-3 cleavage and fragmented NF-66 in SIVA-1 overexpressing DRG compared to empty vector condition. As expected, FAIM-L overexpression

partially protects from caspase-3 cleavage and NF-66 fragmentation (Figure 4.35).

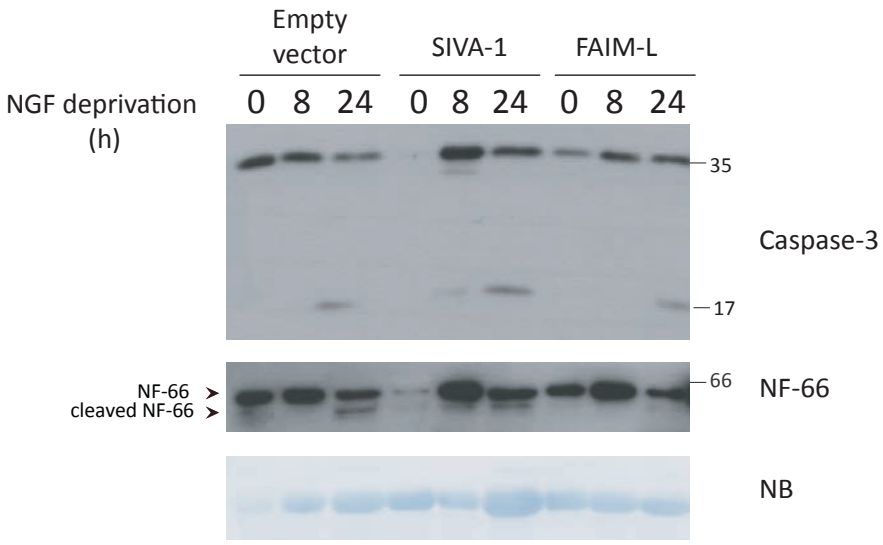

Figure 4.35: SIVA-1 levels increase during NGF deprivation. DRG were plated and infected with SIVA-1, FAIM-L or empty vector viruses. At DIV 2 after plating in NGF-supplemented media, DRG explants were subjected to NGF withdrawal, 0, 8 and 24h after deprivation explants were lysed and analyzed with western blot. Membranes were blotted with caspase-3 and NF-66. Naphtol blue was used as a loading control.

Overall, we show SIVA-1 is a functional antagonist of FAIM-L, as the two proteins carry on opposite functions on XIAP ubiquitination, caspase activation and consequently on cell death and plasticity processes, as LTD and pruning. With these results we include SIVA-1 in caspase modulation of essential neuron-specific mechanisms.

DISCUSSION

5. DISCUSSION

5.1 SIVA-1 emerges as a FAIM-L functional partner

Our group's goal has been to gain better understanding of FAIM1 isoforms function in neurons. In the last years the group has reported FAIM-S involvement in inducing neurite outgrowth[105] and FAIM-L mechanism in the protection against DR induced cell death[122,123], the involvement in plasticity process[107], and the correlation with AD patopathology[124].

Overall, we consider FAIM1 isoforms to be an extremely interesting topic of study, any description of their function may shed light on specific neuronal signaling pathways of development, differentiation, plasticity and resistance to toxic insults and degeneration.

Even though other FAIM genes have been reported (FAIM2 – or LFG – and FAIM3 – or TOSO), their nomenclature is based on the shared function of antagonizing DR induced cell death[222]. FAIM1 isoforms, in fact, are not part of any protein family, they do not share known consensus effector motif and lack even partial structure or sequence homology with other proteins.

FAIM-S and FAIM-L are the two main isoforms of *FAIM1* gene. Except the additional N-term sequence in FAIM-L, they share same sequence and structure. FAIM-L is the longer isoform, expressed only in neurons[122,221]. It presents 22 additional amino acids (aa) at the N-term, which contain the IBM motif necessary for its interaction with BIR2 domain of XIAP, and therefore its anti-apoptotic function[123].

Even though both FAIM isoforms were first described as modulators of DR signaling, they have been shown to have non-apoptotic functions, which extend also to caspase-independent processes[222,223].

In silico analyses indicate that *faim* genes are highly conserved among species and suggest an early appearance during evolution, as they are in fact present in premetazoan unicellular organisms genomes, such as *Miaenia brevicollis* and *Salpingoeca rosetta*[224,225]. *Faim* would have therefore appeared in evolution even before the death domain genes involved in animal apoptosis[226,227], implying functions beyond apoptosis and caspase regulation. In line with this observation, FAIM1 isoforms have been recently found to oppose stress-induced accumulation of protein aggregates and to reverse aggregation in *in vitro* and *in vivo* models[114,117,118]. The specific mechanism behind this function has yet to be clarified, but proteostasis regulation by FAIM-S is independent of any other cellular component, and it presents an independent pathway to deal with aggregates, as proteasomal and autophagic systems do not compensate for FAIM-S loss.

On the other hand, the 22aa codified by the specific neuronal exon that give rise to FAIM-L are conserved only in superior vertebrates. Remarkably, of all the genes involved in apoptotic machineries, DRs were the last to appear in evolutionary terms, as they are also found only in vertebrates[228]. FAIM-L would have therefore appeared, as result of alternative splicing, as a specific protein to counteract DR function in neurons, and therefore to equip them with an additional protection against cell death. Preliminary data show that the longer isoform maintains the ability to oppose aggregation, as both FAIM-S and FAIM-L are able to inhibit Aβ and α-synuclein A53T mutant aggregation[114].

Even though no developmental deficit has been reported in FAIM-KO mice, FAIM-L does increase during neuronal differentiation *in vitro* and *in vivo*, while FAIM-S levels remain constant[122]. FAIM-L is an early specific marker of developing neurons, its levels appear during the first stages of neuronal fate determination, suggesting a specific role of the protein during these stages.

FAIM-L is generated in neurons by alternative splicing, and we have shown, based on Raj and colleagues work[106], that nSR100 is able to induce the inclusion of the neuronal exon and therefore to give rise to FAIM-L transcript[229]. nSR100 is a neuronal specific splicing factor, essential for neuron differentiation. In accordance with the specific increase in FAIM-L levels – and not of FAIM-S -, nSR100 is also highly expressed during development. nSR100 knock out mice present development deficit, widespread changes in AS that primarily results in shift to non-neuronal patterns for cells[104].

FAIM-L mechanism of action and its regulation are far from being fully characterized, good tools of research are now being developed and novel important functions have been just recently reported or are currently under study. Anyway, our data suggest that this protein can be relevant during neuronal differentiation, as it modulates several pathways that can reflect on differentiation process. FAIM-L known functions depend on its interaction with, or modulation of, other proteins. Although these proteins are well established as mediators of cell death, they have been implied in a number of cellular processes important for differentiation of emerging neurons. (Table 5.1).

Protein	Processes regulated	Ref.
Fas-FasL	functional neurite regeneration, outgrowth and neuronal branching	111
XIAP	neurotrophin-mediated neurite outgrowth	75,78
SIVA-1	cytoskeleton reassembling	230
caspases	branching processes, axonal projections, synapses formation	151

Table 5.1: FAIM-L-related proteins and regulated processes relevant for differentiation.

In previous work, we have correlated FAIM-L levels with the progression of Alzheimer's Disease (AD). FAIM-L decreases in patients and mouse models of AD, and we showed in *in vitro* experiments that this decrease is directly caused by Aβ oligomers. FAIM-L levels are key determinant in the outcome of

neurodegeneration, as the decrease of its levels provoke the loss of TNFα protective effect against Aβ induced toxicty[124,125].

Overall, FAIM-L presents potential as a pharmacological target and diagnostic tool in neurodegeneration. Given also its features as a neuronal-specific protein, and modulator of neuronal-specific pathways of survival and plasticity, our lab was interested in shedding light on its mechanism of action. We were interested in mapping how the 22-specific aa of FAIM-L incorporate the neuronal specific functions of the protein.

To start the characterization, the lab performed a two-hybrid assay using full-length and N-specific terminal of FAIM-L to map neuronal-specific interactions. Among the hits arising (listed in Table 1.3), SIVA-1 was considered the best candidate for our study, mainly for two reasons:

- SIVA-1 was already reported as a pro-apoptotic protein. Its induction of cell death has been shown to be due to caspase-3 activation[143,145,150] or inhibition of NF-κB survival pathway[149,231].
- SIVA-1 was reported as a XIAP interacting protein. Resch and colleagues found SIVA-1 in a two-hybrid assay using XIAP as bait. They reported the interaction and found that it leads to mutual interference of their action[149].

We were therefore amused by the possibility of considering the interactions reported in a neuronal context, in which both XIAP and FAIM-L have key roles as modulators of specific plasticity and cell fate processes. In fact, although SIVA-1 function has been described in several models, its function has not been well documented in neurons. SIVA-1 pro-apoptotic role is reported in neurons only in response to p53-dependent signaling[143], but the mechanism of action has not been described in detail.

5.2 SIVA-1 is ubiquitously expressed, especially during embryonic development, and locates in neuronal cytoplasm

Our analysis of SIVA-1 expression and distribution in mice peripheral and nervous tissues at embryonic and adult stages shows that it has a ubiquitous expression in both developing and adult tissues.

Given that the focus of the study was on the neuronal functions of SIVA-1, we were especially interested in its levels in neuronal tissues. We observed SIVA-1 expression as especially high in the peripheral tissues analyzed. Even if comparatively low in nervous system, SIVA-1 levels were still detectable. We confirmed SIVA-1 expression in *in vitro* primary hippocampal and cortical culture before moving forward with the study.

Analysis of mRNA expression (Figure 4.5) reveals that in all considered tissues, SIVA-1 has a higher expression during embryonic stages compared to adult samples. Since physiological programmed cell death is an essential component of animal development, it is not uncommon for modulators of apoptosis to be highly expressed during this stage, to orchestrate a precise regulation of the signalling[4].

Many apoptotic proteins have been found to be crucial for a correct embryonic development. Among these, SIVA-1 appears to play an essential role, as its deletion results in embryonic lethality in mice[157]. However, is it unclear whether the phenotype observed in SIVA-1 KO mice is due to loss of its capacity as a pro-apoptotic protein. KO mice of key pro-apoptotic proteins in fact - such as Apaf1, caspase-3 and caspase-9 – do not present early midgestational embryonic lethality as observed in loss of SIVA-1[174,232,233]. It is therefore possible that the lethality observed in SIVA-1 KO is due to loss of its non-apoptotic, rather than caspase-3 related functions.

Our findings report that SIVA-1 is a functional antagonist of FAIM-L, which, as described in the previous section, is important during neuronal differentiation stages. Their interaction and the modulation of this interaction could be relevant also during neuronal development.

When we analyzed SIVA-1 localization we found that its protein levels are detectable in hippocampal and cortical neurons *in vitro* under basal conditions, lacking any kind of pro-apoptotic stimulus, suggesting that its function is not required only in cells undergoing apoptosis or differentiation processes.

We examined the subcellular distribution of endogenous SIVA-1 in primary hippocampal neurons (Figure 4.6, 4.7, 4.8). Previous studies carried out in various cell types reported controversial findings on the subcellular localization of this protein. By labeling endogenous SIVA-1 in immunocytochemistry we clearly detected a cytoplasmatic distribution, that excludes the nucleus, while some authors have described, in ectopic expression experiments, that SIVA-1 can accumulate in the nucleus[234–236]. We also confirmed our finding with a sub-fractionation assay. Although part of the nuclear fraction was found also in other cell components (see the nuclear marker – histone3 – signal in Figure 4.8), we detected a clear presence of SIVA-1 only in microsomal and cytosolic fractions, which appeared to be in optimal conditions, according to their specific markers. Several apoptotic proteins, such as BCL-2 family members regulate activation of apoptosis by locating in organelles, such as mitochondria or endoplasmic reticulum. Our data obtained with subcellular fractionation and immunocytochemistry in hippocampal neurons, show that SIVA-1 has diffuse cytosolic distribution, and it does not locate at any organelle. Mander's colocalization coefficient was used to determine colocalization with cellular compartments markers and we found a positive signal for plasmatic and vesicle membranes. SIVA-1 has been reported to have a membrane localization in response to DNA damage[150,237]. Anyway, our fractionation results suggest that

SIVA-1 does not locate in membranes, as we do not detect protein presence in the corresponding fractions (Figure 4.8). Positive colocalization in plasma membrane can therefore be due to just an interaction with receptors, which have previously been described for SIVA-1[143].

5.3 SIVA-1 and FAIM-L have opposite roles on XIAP modulation

Yeast two-hybrid, a sensitive standardized technique used to map interactions among proteins, revealed SIVA-1 to be an interaction partner of FAIM-L. We validated the interaction both by immunoprecipitation experiments of overexpressed tagged proteins and by immunocytochemistry (Figure 4.2, 4.3, 4.4).

Unfortunately, we were unable to detect the interaction of endogenous proteins through immunoprecipitation. We performed co-immunoprecipitation assays from adult mouse brain lysates, but the commercially available antibodies for SIVA-1 were not capable of immunoprecipitating the endogenous protein.

Instead, we decided to perform colocalization analysis of the proteins in primary murine neurons, which allowed also to locate the interaction inside the cell. In case of FAIM-L, lack of a working antibody for immunocytochemistry detection, prompted us to transfect a tagged protein and detect FAIM-L through label of the tag. Interactions were detected in cytosol, as the three proteins were found to have a cytosolic distribution (Figure 4.4).

Pearson's coefficient (R) was used to assess the interaction, as the value describes the spatial correlation of two signals by linear regression and is commonly used to determine protein interaction in immunocytochemistry. Values can range from 1 to -1, with 1 standing for complete positive correlation and -1 for complete negative correlation. In our study R was 0.6 for SIVA-1 and FAIM-L, and 0.4 for SIVA-1 and XIAP. A positive colocalization is defined for

values of at least 0.5. We have to consider here that we assessed colocalization in cells maintained in their basal state. We hypothesize that in case of any kind of stimulus increasing SIVA-1 levels or that would require SIVA-1 pro-apoptotic action, the interactions, and therefore colocalization values, would increase.

During the last years, our lab has shown that FAIM-L binds through its N-terminal to XIAP and protects it from ubiquitination, stabilizing its levels[123]. Once defined that SIVA-1 interacts with both proteins, we analyzed the possible functions of SIVA-1 in relation to the previously described FAIM-L function on XIAP modulation.

Our data show that SIVA-1 overexpression displaces the FAIM-L/XIAP interaction (Figure 4.11). Overexpression of SIVA-1 reduced the interaction detected by immunoprecipitation between FAIM-L and XIAP.

XIAP binds to SIVA-1 through its RING domain and to FAIM-L through its BIR2 domain[123,149]. Pro-apoptotic factors released by mitochondria such as Smac/DIABLO bind to XIAP in its BIR domains[21]. SIVA-1 therefore is not impairing other pro-apoptotic factors binding, and through the RING domain interaction could actually be directly stimulating XIAP ubiquitination in a synergistic effect with them.

Both XIAP and SIVA-1 present a neuronal-specific partner, as both interact with FAIM-L in the specific sequence of the isoform at the N-terminal domain. Even if we cannot exclude that the proteins can be present in a three-protein complex, the fact that both proteins interact with the same 22aa-sequence, and the reported impairment in XIAP/FAIM-L interaction when SIVA-1 is overexpressed, suggest that SIVA-1 is competing with XIAP for FAIM-L interaction.

Loss of interaction with FAIM-L can be sufficient to promote XIAP instability, thereby inducing ubiquitination-mediated proteasomal degradation. We reveal moreover that SIVA-1 overexpression has also a direct effect on promoting XIAP ubiquitination. Indeed, we found a striking increase in XIAP ubiquitination when SIVA-1 was co-expressed in HEK293T (Figure 4.12), which, not being of neuronal origin, do not express FAIM-L.

We have not characterized in depth how this increase in ubiquitination may happen. XIAP is usually considered to be the main catalyzer of its ubiquitination. It was described to be able to increase its ubiquitination in a recombinant, cell-free system[56] and moreover IBM-containing protein such as Smac trigger XIAP degradation in a RING-dependent manner[58]. Since the RING of XIAP can also serve for interactions, it could also indicate that another E3 ligase can bind to RING domain to catalyze ubiquitin ligation. Therefore, on one hand SIVA-1 interaction with XIAP RING domain might confer structural changes to XIAP that would permit auto-ubiquitination. On the other hand, SIVA-1 may serve as a ubiquitin ligase on XIAP. In fact, SIVA-1 has been described to have E3 ubiquitin ligase activity, and to direct E3 ubiquitin ligases to promote the ubiquitination of other targets and consequent changes in their function or stability[136–138].

We also report XIAP promotion in SIVA-1 ubiquitination, revealing a mutual regulation. XIAP has been shown to induce ubiquitination in interacting proteins involved in apoptosis, such as Smac[238], AIF[239]. In a complex process such as apoptosis, which involves hundreds of molecules, the cross-regulation between pro- and anti-apoptotic proteins is common and can often be mediated by ubiquitination[147,156,240].

Figure 4.13 shows clearly in an endogenous ubiquitin immunoprecipitation, that FAIM-L and SIVA-1 have opposite effects in XIAP ubiquitination levels. SIVA-1 increases ubiquitination, while FAIM-L decreases it. When the two proteins are

co-expressed, we detect an intermediate effect. The balance between FAIM-L and SIVA-1 would therefore regulate XIAP stability. In case in which SIVA-1 levels are low, FAIM-L is protecting XIAP not only directly by binding and inhibiting auto-ubiquitination, but also impeding that ubiquitination promotion factors such as SIVA-1 can interact with it. In the same way, when SIVA-1 increases, it would be improving XIAP ubiquitination by direct interaction and by sequestering FAIM-L, removing its protective effect.

When we tested the effect of SIVA-1 knock down on XIAP ubiquitination we did not detect any change, indicating that in basal conditions, XIAP ubiquitination levels are SIVA-1-independent (Figure 4.14).

5.4 SIVA-1 promotes apoptosis in neurons

We report the pro-apoptotic activity of SIVA-1 in primary cultures of hippocampal neurons. In line with previous findings, SIVA-1 overexpression is sufficient to induce apoptosis through effector caspase activation. Our findings are broadly supported as SIVA-1 pro-apoptotic role has already been addressed and reported in several cell types, such as immune system[58,241,242], ischemic kidneys[136,142] and cerebellar granular neurons[150].

It has to be taken into account that in cell death assessment, we are using a pool of cells, in which around 80% are infected with SIVA-1 lentiviral particles (assessed by GFP positive cell counting). We can therefore assume that in a population in which all cells would be transfected, we would observe even more significant changes.

Several mechanisms of actions have been described in SIVA-1-induced cell death. Caspase-3-dependent cell death has been reported through mitochondrial pathway activation[143], abrogation of BCL-2/BCL-XL anti-apoptotic

function through interaction[139,144], and inhibition of NF-κB pro-survival pathway[146].

Here we provide evidence that SIVA-1 participates in XIAP modulation and apoptosis antagonizing FAIM-L function. We propose therefore that neuronal cell death promotion induced by SIVA-1 overexpression occurs through XIAP destabilization and consequent inhibition of XIAP action on effector caspases.

Figure 4.20 shows that the same balance we observe in XIAP ubiquitination is maintained in cell death. FAIM-L is able to partially protect form SIVA-1 induced cell death. The two proteins are acting on the same cellular process with opposite effects and therefore, when overexpressed together, an intermediate phenotype is observed. As previously discussed, these findings might be of higher significance in a system in which the sample is composed only by 100% co-transfected cells, and not by a pool of them, composed by transfected and non-transfected cells.

5.5 SIVA-1 is involved in AMPAR internalization

Caspases can be activated without causing cell death in neurons, and their activation is actually necessary to mediate regulatory events in the mature nervous system, such as synaptic plasticity and axon pruning. Thus, although full activation of caspases leads to cell death, a restricted and localized activation controls normal physiology in living neurons[234,243,244]. Both outcomes of caspase activation require similar molecular pathway, and a strict modulation.

In neurons, caspases locate in dendrites, axons, and in pre- and post-synaptic terminals. At these sites, they can be locally activated[147,149]. Proteins that participate in apoptotic modulation are found in dendrites and synaptic terminals, which are also equipped with the tools for a rapid and strictly

regulated protein turnover, such as proteasome for degradation, translation machinery, and local mRNA[245].

Mitochondria are essential for activating the pathway that leads to caspase engagement in non-apoptotic activities. These organelles can be found in dendrites, and sometimes in individual spines. Moreover, their distribution and motility are regulated by synaptic activity, allowing for a spatial control of the pathway activation[246].

Activity-dependent changes in synaptic strength are recognized as mechanisms associated with spatial learning and memory in the hippocampus. LTP and LTD of excitatory synapses in response to glutamate are the best characterized forms of long-term plasticity. LTD is caspase-dependent and we have already shown that FAIM-L overexpression impairs it[107]. The main mechanism of LTD is the internalization of GluA2-containing AMPAR[247].

We used as a model for our study the extensively described chLTD[187], in which NMDA is added to cell media for a short treatment (15min). With NMDA stimulation, chLTD is induced. A rapid increase in calcium levels is triggered by NMDA receptor activation, followed by calcineurin activation. Calcineurin dephosphorylates AMPAR and pBAD, which in turn leads to activation of apoptotic-machinery components and finally caspase-3. The activation culminates in AMPAR internalization and therefore synaptic weakening[70,107,188,219,248].

Even if caspase-3 activation is transient and locally restricted in plasticity changes[249], changes are observed in the whole cell with chLTD. The whole cell undergoes activation of LTD and therefore receptor internalization is massive. For this reason, we decided to assess GluA2 internalization assay where it was easier to evaluate. In our quantification we took into account cell soma and part of dendrites (within a region of about 20µm from cell bodies). We considered

only transfected cells (GFP positive), in order to have specific data, not diluted by quantification of non-transfected cells.

Many apoptotic regulatory proteins have been reported to modulate caspase activation in synaptic transmission. Among these, pro-apoptotic BAD and BAX are essential activators of LTD[71,188], while anti-apoptotic XIAP and FAIM-L – in a XIAP dependent manner - block the process by caspase-3 inhibition[107].

When measuring surface GluA2-containing AMPAR levels in our primary cultures, we observed that SIVA-1 overexpression was sufficient to have a decrease in surface GluA2 levels, while total levels of the receptor were not affected (Figure 4.24, 4.25). GluA2 surface levels decrease caused by SIVA-1 is caspase-dependent, as we show that inhibition of caspase with Q-VD is able to abrogate this effect (Figure 4.26, 4.27). No change was observed in SIVA-1 overexpressing neurons once chLTD was applied. It is possible that the NMDA treatment used is already saturating the activation of the pathway, and therefore no further increase can be induced.

FAIM-L overexpression totally abrogates GluA2 internalization following chLTD and also restores SIVA-1 induction of GluA2 internalization in hippocampal neurons, indicating that both proteins act on the same pathway.

On the other hand, SIVA-1 knock-down significantly decreases receptor internalization following chLTD (Figure 4.28, 4.29), indicating that SIVA-1 is not essential for the internalization to occur, but it has a role promoting it.

Overall, with our results, SIVA-1 emerges as another regulator of apoptosis that is also involved in functions not related to cell death. Non-apoptotic roles have already been reported for SIVA-1. SIVA-1 participates in microtubule stability[70,107] or interleukin-2 expression[152] in other cell types. Ours is the first study to show a neuronal-specific role for SIVA-1. We show that SIVA-1 is

expressed under basal condition in hippocampal neurons and it also locates at synaptic terminals, interacts with neuronal-specific proteins, and is involved in neural plasticity processes.

When applying chLTD, we found a transient increase in SIVA-1 protein levels in primary cultures after just few minutes of NMDA treatment. The increase does not affect SIVA-1 mRNA levels and is blocked by cycloheximide, thereby indicating specific translational regulation.

The increase in SIVA-1 is directly associated with NMDA receptor stimulation after treatment, since a calcium chelating agent, BAPTA-AM, blocks this increase. BAPTA-AM pretreatment has been reported to block LTD induction, thus eliminating available calcium ions to start a stimulation response after NMDA or electrical application[250].

Protein composition at synapses is modulated in response to neuronal activity, through new synthesis and protein removal[251,252]. In LTD, internalization occurs rapidly after NMDAR is activated. Protein synthesis is required for LTD to be sustained, and inhibitors of translation cause a recovery of synaptic transmission in a few hours[246]. Enhanced SIVA-1 expression in chLTD supports the relevance of this protein in the modulation of synaptic plasticity induction. SIVA-1 mRNA would therefore be among those present at synapses. Upon synaptic activation, translation in individual synapses would induce SIVA-1 transient expression, possibly required for short-term impairment of XIAP inhibition of caspases, and therefore allow for them to activate.

5.6 SIVA-1 is involved in neurite degeneration

During development, neurons extend their axons to innervate target regions often resulting in superfluous connections. The outgrowth phase is followed by a regressive phase in which only suitable connections are maintained. Excessive axons, dendrites and synapses are selectively eliminated without resulting in the death of neurons.

Dorsal Root Ganglia explants rapidly grow their axons *in vitro* in presence of NGF. Once NGF is removed from media, they undergo axonal degeneration in a caspase-3 dependent manner[253]. We analyzed two timepoints, 8 and 24h after deprivation.

The main limitation of the experimental approach is the time of collection, 2DIV after infection, which can be not enough to have a substantial overexpression or knock down of the protein of interest.

We observed an increase in SIVA-1 levels in DRG explants undergoing axonal degeneration, and an accelerated degeneration in SIVA-1 overexpressing cells. Overall our data indicate that SIVA-1 could be involved in dendrite pruning and therefore suggest for it to be a player in an essential process for refinement of neuronal network and establishment of mature connections. The treatment of sensory neurons with the inhibitor of transcription actinomycin-D in soma, preserves axons from degeneration, demonstrating that caspase activation during pruning is thought to be regulated by gene transcription[254].

IAP modulation can be highly relevant to assure a local, restricted caspase-activation during pruning. IAPs are stabilized in soma, where caspase function needs to be repressed, and conversely inactivated in dendrites in which limited caspase activity is required[177,205]. SIVA-1 could be therefore required in axonal compartment to de-stabilize XIAP function and induce caspase activation. In

Figure 4.34 we observe two bands of high molecular weight appear after 24h deprivation, that could correspond to higher molecular weight forms of the protein, generated by post-translational modification, such as ubiquitination. XIAP ubiquitination has been reported in murine DRGs undergoing NGF deprivation[255] and pruning in *Drosophila melanogaster* requires DIAP1 (the XIAP homologue) degradation by the proteasome to occur[71].

5.7 Significance of our results in the physiological and pathological context

This study extends our knowledge on FAIM-L and its functions. SIVA-1 and FAIM-L carry out opposite effects on the same mechanisms, and this antagonist modulation could be relevant in neuronal development, in normal physiology, and also in pathological situations.

Our group has correlated FAIM-L levels with AD progression. Loss of FAIM-L, induced by Aβ oligomers, implies a higher susceptibility to stress insults for neurons, and overall a deregulation of the pathways that leads to caspase activation[124]. Moreover, based on the last findings of Dr. Rothstein lab, FAIM-L decrease could also be pathogenically linked to a more rapid, aggressive Aβ aggregation[114].

Extensive research has shown that the same cascade involved in delicate processes such as synapse plasticity or selective cell death, can trigger widespread cell damage and degeneration when deregulated. FAIM-L and SIVA-1 modulate caspase activation with opposite effect, so in case of a deregulation in the balance among these two proteins, caspases can be over-activated and therefore exacerbate the hallmarks of AD.

Hundreds of studies can be found on the correlation among caspase activation and AD pathological markers, such as increase in production of Aβ[107,256],

microtubule associated protein tau phosphorylation and aggregation[257], and as consequence, to deficits in cell survival, and plasticity pathways[5,129,130,258].

Mouse models of the disease, which overexpress human amyloid precursor protein (APP), have been extremely useful to detect which pathways are deregulated in the disease. Thank to these models, it was described that memory loss, beginning early in AD, can be attributed to processes previous to cell death. Aβ oligomers induce a deregulation of LTD, which causes disruption of synaptic plasticity, micro-pruning and spine loss[131,183,185,259–261].

Both FAIM-L and SIVA-1 levels are involved in these pathways. Any form of deregulation of their levels and functional imbalance can be important factors to consider for assessing progression or potential treatment of the disease.

Overall, we describe that SIVA-1 is a functional antagonist of FAIM-L. SIVA-1 impairs FAIM-L interaction with XIAP and promotes its ubiquitination. We propose this as one of the mechanisms through which SIVA-1 is able to induce caspase activation. SIVA-1-dependent caspase induction is functional for both its apoptotic and non-apoptotic activity (Figure 5.1). The balance among FAIM-L and SIVA-1 appears to be worth of consideration in both physiological and pathological situations.

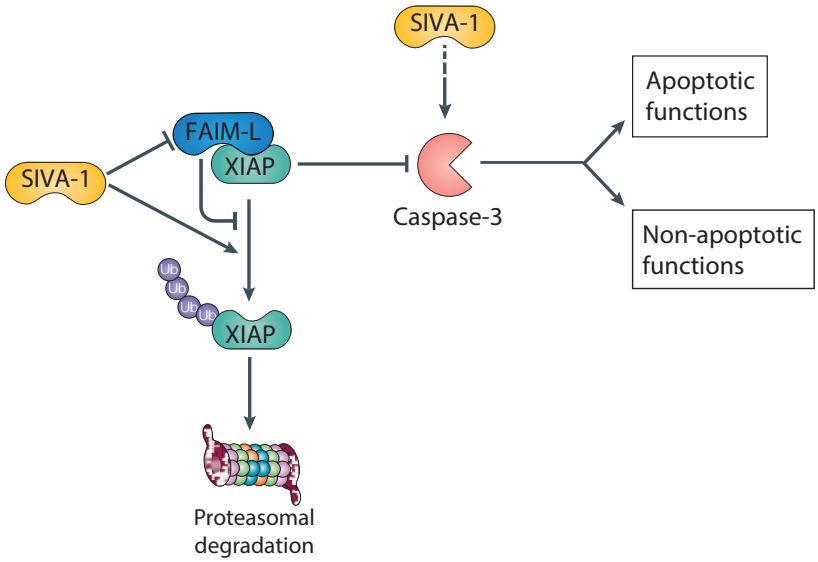

Figure 5.1 SIVA-1 is a FAIM-L functional antagonist. XIAP, the endogenous inhibitor of caspases, is degraded through a process of ubiquitination and proteasomal degradation. In neurons, XIAP is protected against degradation by FAIM-L. Both proteins inhibit caspase-dependent apoptotic and non-apoptotic processes. SIVA-1 has an opposite effect compared to FAIM-L, as it induces XIAP ubiquitination and caspase activation.

CONCLUSIONS

6. CONCLUSIONS

This work reveals novel key roles of SIVA-1 in neurons. We show that SIVA-1 interacts with both FAIM-L and XIAP, and that it is also a caspase activator. We associate SIVA-1-induced caspase activation with neuronal apoptosis, which is consistent with its previously described functions. Moreover, we involve SIVA-1 in non-apoptotic function of caspases. We demonstrate a novel function of SIVA-1 as regulator of synaptic function and propose its involvement in axonal pruning.

First: SIVA-1 interacts with both FAIM-L and XIAP in neuronal cytoplasm.

Second: SIVA-1 presents a cytoplasmic distribution in neuronal bodies and can locate to synapses.

Third SIVA-1 promotes XIAP ubiquitination and displaces FAIM-L/XIAP interaction.

Fourth: SIVA-1 induces caspase-3-dependent cell death.

Fifth: SIVA-1 promotes GluR2 internalization in a caspase-dependent manner.

Sixth: SIVA-1 protein levels are rapidly increased during chLTD.

Seventh: SIVA-1 is increased and induces an early caspase-3 activation during neuronal pruning.

REFERENCES

7. REFERENCES

1. Vogt, C. Untersuchungen über die Entwicklungsgeschichte der Geburtshelerkroete (Alytes obstetricians). *Solothurn Jent und Gassman* (1842).

2. Jacobson, M., Weil, M. & Raff, M. Programmed cell death in animal development. *Cell* **88**, 347–354 (1997).

3. Fuchs, Y. & Steller, H. Live to die another way: Modes of programmed cell death and the signals emanating from dying cells. *Nature Reviews Molecular Cell Biology* (2015). doi:10.1038/nrm3999

4. Fuchs, Y. & Steller, H. Programmed cell death in animal development and disease. *Cell* (2011). doi:10.1016/j.cell.2011.10.033

5. Castro, R. E. *et al.* Cell Death Targets and Potential Modulators in Alzheimer ' s Disease. *Current* 2851–2864 (2010). doi:BSP/CPD/E-Pub/198 [pii]

6. Loo, D. T. *et al.* Apoptosis is induced by beta-amyloid in cultured central nervous system neurons. *Proc. Natl. Acad. Sci. U. S. A.* **90**, 7951–5 (1993).

7. Galluzzi, L., Blomgren, K. & Kroemer, G. Mitochondrial membrane permeabilization in neuronal injury. *Nature Reviews Neuroscience* (2009). doi:10.1038/nrn2665

8. Strasser, A., Harris, A. W., Jacks, T. & Cory, S. DNA damage can induce apoptosis in proliferating lymphoid cells via p53-independent mechanisms inhibitable by Bcl-2. *Cell* (1994). doi:10.1016/0092-8674(94)90201-1

9. Dillon, C. P. & Green, D. R. Molecular cell biology of apoptosis and necroptosis in cancer. in *Advances in Experimental Medicine and Biology* (2016). doi:10.1007/978-3-319-39406-0_1

10. Galluzzi, L. *et al.* Molecular mechanisms of cell death: Recommendations of the Nomenclature Committee on Cell Death 2018. *Cell Death Differ.* **25**, 486–541 (2018).

11. Tang, D., Kang, R., Berghe, T. Vanden, Vandenabeele, P. & Kroemer, G. The molecular machinery of regulated cell death. *Cell Research* (2019). doi:10.1038/s41422-019-0164-5

12. Galluzzi, L. *et al.* Molecular mechanisms of cell death: Recommendations of the Nomenclature Committee on Cell Death 2018. *Cell Death and Differentiation* (2018). doi:10.1038/s41418-017-0012-4

13. Kerr, J. F. R., Wyllie, A. H. & Currie, A. R. Apoptosis: A basic biological phenomenon with wide-ranging implications in tissue kinetics. *Br. J. Cancer* (1972). doi:10.1038/bjc.1972.33

14. Galluzzi, L., Bravo-San Pedro, J. M., Kepp, O. & Kroemer, G. Regulated cell death and adaptive stress responses. *Cell. Mol. Life Sci.* **73**, 2405–2410 (2016).

15. Savill, J. & Fadok, V. Corpse clearance defines the meaning of cell death. *Nature* (2000). doi:10.1038/35037722

16. Ichim, G. & Tait, S. W. G. A fate worse than death: Apoptosis as an oncogenic process. *Nature Reviews Cancer* (2016). doi:10.1038/nrc.2016.58

17. Igney, F. H. & Krammer, P. H. Death and anti-death: Tumour resistance to apoptosis. *Nature Reviews Cancer* (2002). doi:10.1038/nrc776

18. Tait, S. W. G. & Green, D. R. Mitochondria and cell death: Outer membrane permeabilization and beyond. *Nature Reviews Molecular Cell Biology* (2010). doi:10.1038/nrm2952

19. Wu, C. C. & Bratton, S. B. Regulation of the intrinsic apoptosis pathway by

reactive oxygen species. *Antioxidants and Redox Signaling* (2013). doi:10.1089/ars.2012.4905

20. Kalkavan, H. & Green, D. R. MOMP, cell suicide as a BCL-2 family business. *Cell Death Differ.* (2018). doi:10.1038/cdd.2017.179

21. Saelens, X. *et al.* Toxic proteins released from mitochondria in cell death. *Oncogene* (2004). doi:10.1038/sj.onc.1207523

22. Muñoz-Pinedo, C. *et al.* Different mitochondrial intermembrane space proteins are released during apoptosis in a manner that is coordinately initiated but can vary in duration. *Proc. Natl. Acad. Sci. U. S. A.* (2006). doi:10.1073/pnas.0603007103

23. Van Loo, G. *et al.* The role of mitochondrial factors in apoptosis: A Russian roulette with more than one bullet. *Cell Death and Differentiation* (2002). doi:10.1038/sj.cdd.4401088

24. Arnoult, D. *et al.* Mitochondrial release of AIF and EndoG requires caspase activation downstream of Bax/Bak-mediated permeabilization. *EMBO J.* (2003). doi:10.1093/emboj/cdg423

25. Vande Walle, L., Lamkanfi, M. & Vandenabeele, P. The mitochondrial serine protease HtrA2/Omi: An overview. *Cell Death and Differentiation* (2008). doi:10.1038/sj.cdd.4402291

26. Norberg, E., Orrenius, S. & Zhivotovsky, B. Mitochondrial regulation of cell death: Processing of apoptosis-inducing factor (AIF). *Biochem. Biophys. Res. Commun.* (2010). doi:10.1016/j.bbrc.2010.02.163

27. Li, L. Y., Luo, X. & Wang, X. Endonuclease G is an apoptotic DNase when released from mitochondria. *Nature* (2001). doi:10.1038/35083620

28. Cecconi, F. Apaf1 and the apoptotic machinery. *Cell Death and Differentiation* (1999). doi:10.1038/sj.cdd.4400602

29. Babbitt, S. E., Sutherland, M. C., Francisco, B. S., Mendez, D. L. & Kranz, R. G. Mitochondrial cytochrome c biogenesis: No longer an enigma. *Trends in Biochemical Sciences* (2015). doi:10.1016/j.tibs.2015.05.006

30. Green, D. R. & Llambi, F. Cell death signaling. *Cold Spring Harb. Perspect. Biol.* (2015). doi:10.1101/cshperspect.a006080

31. Kumar, R., Herbert, P. E. & Warrens, A. N. An introduction to death receptors in apoptosis. *International Journal of Surgery* (2005). doi:10.1016/j.ijsu.2005.05.002

32. Guicciardi, M. E. & Gores, G. J. Life and death by death receptors. *FASEB Journal* (2009). doi:10.1096/fj.08-111005

33. Lavrik, I., Golks, A. & Krammer, P. H. Death receptor signaling. *J. Cell Sci.* (2005). doi:10.1242/jcs.01610

34. Wallach, D. *et al.* TUMOR NECROSIS FACTOR RECEPTOR AND Fas SIGNALING MECHANISMS. *Annu. Rev. Immunol.* (1999). doi:10.1146/annurev.immunol.17.1.331

35. Boldin, M. P. *et al.* Self-association of the 'death domains' of the p55 tumor necrosis factor (TNF) receptor and Fas/APO1 prompts signaling for TNF and Fas/APO1 effects. *J. Biol. Chem.* (1995). doi:10.1074/jbc.270.1.387

36. Scaffidi, G. *et al.* Differential modulation of apoptosis sensitivity in CD95 type I and type II cells. *J. Biol. Chem.* (1999). doi:10.1074/jbc.274.32.22532

37. Özören, N. & El-Deiry, W. S. Defining characteristics of types I and II apoptotic cells in response to TRAIL. *Neoplasia* (2002). doi:10.1038/sj.neo.7900270

38. Locksley, R. M., Killeen, N. & Lenardo, M. J. The TNF and TNF receptor superfamilies: Integrating mammalian biology. *Cell* (2001). doi:10.1016/S0092-8674(01)00237-9

39. Wilson, N. S., Dixit, V. & Ashkenazi, A. Death receptor signal transducers: nodes of coordination in immune signaling networks. *Nat. Immunol.* **10**, 348–355 (2009).

40. Peter, M. E. & Krammer, P. H. The CD95(APO-1/Fas) DISC and beyond. *Cell Death and Differentiation* (2003). doi:10.1038/sj.cdd.4401186

41. Siegmund, D., Lang, I. & Wajant, H. Cell death-independent activities of the death receptors CD95, TRAILR1, and TRAILR2. *FEBS Journal* (2017). doi:10.1111/febs.13968

42. Staudt, L. M. *et al.* Signaling to NF- κ B : Regulation by Ubiquitination Signaling to NF- k B : Regulation by Ubiquitination. 1–19 (2010). doi:10.1101/cshperspect.a003350

43. Vucic, D., Dixit, V. M. & Wertz, I. E. Ubiquitylation in apoptosis: A post-translational modification at the edge of life and death. *Nature Reviews Molecular Cell Biology* (2011). doi:10.1038/nrm3143

44. Hoesel, B. & Schmid, J. A. The complexity of NF-κB signaling in inflammation and cancer. *Molecular Cancer* (2013). doi:10.1186/1476-4598-12-86

45. Pop, C. & Salvesen, G. S. Human caspases: Activation, specificity, and regulation. *Journal of Biological Chemistry* (2009). doi:10.1074/jbc.R800084200

46. Mcilwain, D. R., Berger, T. & Mak, T. W. Caspase Functions in Cell Death and Disease. (2015). doi:10.1101/cshperspect.a008656

47. Taylor, R. C., Cullen, S. P. & Martin, S. J. Apoptosis: controlled demolition at the

cellular level. *Nat. Rev. Mol. Cell Biol.* **9**, 231–241 (2008).

48. Martinon, F. & Tschopp, J. Inflammatory caspases and inflammasomes: Master switches of inflammation. *Cell Death and Differentiation* (2007). doi:10.1038/sj.cdd.4402038

49. Cohen, G. M. Caspases: The executioners of apoptosis. *Biochemical Journal* (1997). doi:10.1042/bj3260001

50. Timmer, J. C. & Salvesen, G. S. Caspase substrates. *Cell Death and Differentiation* (2007). doi:10.1038/sj.cdd.4402059

51. Llambi, F. *et al.* A Unified Model of Mammalian BCL-2 Protein Family Interactions at the Mitochondria. *Mol. Cell* (2011). doi:10.1016/j.molcel.2011.10.001

52. Czabotar, P. E., Lessene, G., Strasser, A. & Adams, J. M. Control of apoptosis by the BCL-2 protein family: implications for physiology and therapy. *Nat. Rev. Mol. Cell Biol.* **15**, 49–63 (2014).

53. Salvesen, G. S., Duckett, C. S., Torrey, N., Road, P. & Arbor, A. Iap Proteins : Blocking the Road To Death ' S Door. *Nat. Rev. Mol. Cell Biol.* **3**, 1–10 (2002).

54. Silke, J. & Vucic, D. IAP family of cell death and signaling regulators. in *Methods in Enzymology* (2014). doi:10.1016/B978-0-12-801430-1.00002-0

55. Darding, M. & Meier, P. IAPs: Guardians of RIPK1. *Cell Death and Differentiation* (2012). doi:10.1038/cdd.2011.163

56. Yang, Y., Fang, S., Jensen, J. P., Weissman, A. M. & Ashwell, J. D. Ubiquitin protein ligase activity of IAPs and their degradation in proteasomes in response to apoptotic stimuli. *Science (80-.).* (2000). doi:10.1126/science.288.5467.874

57. Vaux, D. L. & Silke, J. IAPs, RINGs and ubiquitylation. *Nature Reviews Molecular*

Cell Biology (2005). doi:10.1038/nrm1621

58. Galbán, S. & Duckett, C. S. XIAP as a ubiquitin ligase in cellular signaling. *Cell Death Differ.* **17**, 54–60 (2010).

59. Eckelman, B. P. & Salvesen, G. S. The human anti-apoptotic proteins cIAP1 and cIAP2 bind but do not inhibit caspases. *J. Biol. Chem.* (2006). doi:10.1074/jbc.M510863200

60. Mahoney, D. J. *et al.* Both cIAP1 and cIAP2 regulate TNFα-mediated NF-κB activation. *Proc. Natl. Acad. Sci. U. S. A.* (2008). doi:10.1073/pnas.0711122105

61. Zhang, J. *et al.* Ubiquitin Ligases cIAP1 and cIAP2 Limit Cell Death to Prevent Inflammation. *Cell Rep.* (2019). doi:10.1016/j.celrep.2019.04.111

62. Komander, D. & Rape, M. The Ubiquitin Code. *Annu. Rev. Biochem.* **81**, 203–229 (2012).

63. Komander, D. The emerging complexity of protein ubiquitination. *Biochemical Society Transactions* (2009). doi:10.1042/BST0370937

64. Glickman, M. H. & Ciechanover, A. The ubiquitin-proteasome proteolytic pathway: Destruction for the sake of construction. *Physiological Reviews* (2002). doi:10.1152/physrev.00027.2001

65. Welchman, R. L., Gordon, C. & Mayer, R. J. Ubiquitin and ubiquitin-like proteins as multifunctional signals. *Nature Reviews Molecular Cell Biology* (2005). doi:10.1038/nrm1700

66. Nakamura, T. *et al.* Transnitrosylation of XIAP regulates caspase-dependent neuronal cell death. *Mol. Cell* **39**, 184–195 (2010).

67. Deveraux, Q. L. *et al.* IAPs block apoptotic events induced by caspase-8 and

cytochrome c by direct inhibition of distinct caspases. *EMBO J.* (1998). doi:10.1093/emboj/17.8.2215

68. Riedl, S. J. *et al.* Structural basis for the inhibition of caspase-3 by XIAP. *Cell* **104**, 791–800 (2001).

69. Suzuki, Y., Nakabayashi, Y., Nakata, K., Reed, J. C. & Takahashi, R. X-linked Inhibitor of Apoptosis Protein (XIAP) Inhibits Caspase-3 and -7 in Distinct Modes. *J. Biol. Chem.* **276**, 27058–27063 (2001).

70. Li, Z. *et al.* Caspase-3 activation via mitochondria is required for long-term depression and AMPA receptor internalization. *Cell* **141**, 859–871 (2010).

71. Unsain, N., Higgins, J. M., Parker, K. N., Johnstone, A. D. & Barker, P. A. XIAP regulates caspase activity in degenerating axons. *Cell Rep.* **4**, 751–763 (2013).

72. Keppler, O. T. *et al.* Differential sialylation of cell surface glycoconjugates in a human B lymphoma cell line regulates susceptibility for CD95 (APO-1/Fas)-mediated apoptosis and for infection by a lymphotropic virus. *Glycobiology* (1999). doi:10.1093/glycob/9.6.557

73. French, L. E. & Tschopp, J. Protein-based therapeutic approaches targeting death receptors. *Cell Death and Differentiation* (2003). doi:10.1038/sj.cdd.4401185

74. Roth, K. A. & D'Sa, C. Apoptosis and brain development. *Mental Retardation and Developmental Disabilities Research Reviews* (2001). doi:10.1002/mrdd.1036

75. Desbarats, J. *et al.* Fas engagement induces neurite growth through ERK activation and p35 upregulation. *Nature Cell Biology* (2003). doi:10.1038/ncb916

76. Marques-Fernandez, F. *et al.* TNFα induces survival through the FLIP-L-dependent activation of the MAPK/ERK pathway. *Cell Death Dis.* **4**, e493 (2013).

77. Wheeler, M. A. *et al.* TNF-α/TNFR1 Signaling Is Required for the Development and Function of Primary Nociceptors. *Neuron* (2014). doi:10.1016/j.neuron.2014.04.009

78. Zuliani, C. *et al.* Control of neuronal branching by the death receptor CD95 (Fas/Apo-1). *Cell Death Differ.* (2006). doi:10.1038/sj.cdd.4401720

79. Yu, J. W. & Shi, Y. FLIP and the death effector domain family. *Oncogene* (2008). doi:10.1038/onc.2008.299

80. Iyer, A. K. V. *et al.* Antioxidant c-FLIP Inhibits Fas Ligand-Induced NF-κB Activation in a Phosphatidylinositol 3-Kinase/Akt-Dependent Manner. *J. Immunol.* (2011). doi:10.4049/jimmunol.1002915

81. Quintavalle, C. *et al.* C-FLIPL enhances anti-apoptotic Akt functions by modulation of Gsk3B activity. *Cell Death and Differentiation* (2010). doi:10.1038/cdd.2010.65

82. Moubarak, R. S. *et al.* The death receptor antagonist FLIP-L interacts with Trk and is necessary for neurite outgrowth induced by neurotrophins. *J. Neurosci.* **30**, 6094–6105 (2010).

83. Fang, L. W., Tai, T. S., Yu, W. N., Liao, F. & Lai, M. Z. Phosphatidylinositide 3-Kinase Priming Couples c-FLIP to T Cell Activation. *J. Biol. Chem.* (2004). doi:10.1074/jbc.M303860200

84. Dohrman, A. *et al.* Cellular FLIP (Long Form) Regulates CD8 + T Cell Activation through Caspase-8-Dependent NF-κB Activation . *J. Immunol.* (2005). doi:10.4049/jimmunol.174.9.5270

85. Planells-Ferrer, L. *et al.* FAIMs: more than death-receptor antagonists in the nervous system. *J. Neurochem.* 11–21 (2016). doi:10.1111/jnc.13729

86. Somia, N. V. *et al.* LFG: An anti-apoptotic gene that provides protection from Fas-mediated cell death. *Proc. Natl. Acad. Sci. U. S. A.* (1999). doi:10.1073/pnas.96.22.12667

87. Fernández, M. *et al.* Lifeguard/neuronal membrane protein 35 regulates Fas ligand-mediated apoptosis in neurons via microdomain recruitment. *J. Neurochem.* (2007). doi:10.1111/j.1471-4159.2007.04767.x

88. Rojas-Rivera, D. & Hetz, C. TMBIM protein family: Ancestral regulators of cell death. *Oncogene* (2015). doi:10.1038/onc.2014.6

89. Wozniak, A. L. *et al.* Requirement of biphasic calcium release from the endoplasmic reticulum for Fas-mediated apoptosis. *J. Cell Biol.* (2006). doi:10.1083/jcb.200608035

90. Breckenridge, D. G., Stojanovic, M., Marcellus, R. C. & Shore, G. C. Caspase cleavage product of BAP31 induces mitochondrial fission through endoplasmic reticulum calcium signals, enhancing cytochrome c release to the cytosol. *J. Cell Biol.* (2003). doi:10.1083/jcb.200212059

91. Urresti, J. *et al.* Lifeguard Inhibits Fas Ligand-mediated Endoplasmic Reticulum-Calcium Release Mandatory for Apoptosis in Type II Apoptotic Cells. *J. Biol. Chem.* **291**, 1221–1234 (2016).

92. Komnig, D. *et al.* Faim2 contributes to neuroprotection by erythropoietin in transient brain ischemia. *J. Neurochem.* (2018). doi:10.1111/jnc.14296

93. Pawar, M. *et al.* FAS apoptotic inhibitory molecule 2 is a stress-induced intrinsic neuroprotective factor in the retina. *Cell Death Differ.* (2017). doi:10.1038/cdd.2017.109

94. C, T. S. *et al.* Modulation of hippocampal neuroplasticity by Fas/CD95 regulatory protein 2 (Faim2) in the course of bacterial meningitis. *J. Neuropathol. Exp.*

Neurol. (2014).

95. Komnig, D., Schulz, J. B., Reich, A. & Falkenburger, B. H. Mice lacking Faim2 show increased cell death in the MPTP mouse model of Parkinson disease. *J. Neurochem.* (2016). doi:10.1111/jnc.13847

96. Bucan, V. *et al.* Transactivation of lifeguard (LFG) by Akt-/LEF-1 pathway in MCF-7 and MDA-MB 231 human breast cancer cells. *Apoptosis* (2010). doi:10.1007/s10495-010-0493-9

97. Mï¿½ller, J., Maurer, V., Reimers, K., Vogt, P. & Bucan, V. TRIM21, a negative modulator of LFG in breast carcinoma MDA-MB-231 cells in vitro. *Int. J. Oncol.* 1634–1646 (2015). doi:10.3892/ijo.2015.3169

98. Planells-Ferrer, L. *et al.* MYCN repression of Lifeguard/FAIM2 enhances neuroblastoma aggressiveness. *Cell Death Dis.* **5**, e1401 (2014).

99. Murakami, Y. *et al.* Toso, a Functional IgM Receptor, Is Regulated by IL-2 in T and NK Cells. *J. Immunol.* (2012). doi:10.4049/jimmunol.1200840

100. Song, Y. & Jacob, C. O. The mouse cell surface protein TOSO regulates Fas/Fas ligand-induced apoptosis through its binding to Fas-associated death domain. *J. Biol. Chem.* (2005). doi:10.1074/jbc.M413609200

101. Nguyen, X. H. *et al.* Toso regulates the balance between apoptotic and nonapoptotic death receptor signaling by facilitating RIP1 ubiquitination. *Blood* (2011). doi:10.1182/blood-2010-10-313643

102. Hitoshi, Y. *et al.* Toso, a cell surface, specific regulator of Fas-induced apoptosis in T cells. *Immunity* (1998). doi:10.1016/S1074-7613(00)80551-8

103. Brenner, D. *et al.* Toso controls encephalitogenic immune responses by dendritic cells and regulatory T cells. *Proc. Natl. Acad. Sci. U. S. A.* (2014).

doi:10.1073/pnas.1323166111

104. Coccia, E. *et al.* Identification and characterization of new isoforms of human fas apoptotic inhibitory molecule (FAIM). *PLoS One* **12**, e0185327 (2017).

105. Sole, C. *et al.* The death receptor antagonist FAIM promotes neurite outgrowth by a mechanism that depends on ERK and NF-kapp B signaling. *J. Cell Biol.* **167**, 479–92 (2004).

106. Segura, M. F. *et al.* The Long Form of Fas Apoptotic Inhibitory Molecule Is Expressed Specifically in Neurons and Protects Them against Death Receptor-Triggered Apoptosis. *J. Neurosci.* **27**, 11228–11241 (2007).

107. Martínez-Mármol, R. *et al.* FAIM-L regulation of XIAP degradation modulates Synaptic Long-Term Depression and Axon Degeneration. *Sci. Rep.* **6**, 35775 (2016).

108. Raj, B. *et al.* A global regulatory mechanism for activating an exon network required for neurogenesis. *Mol. Cell* **56**, 90–103 (2014).

109. Raj, B. *et al.* A Global Regulatory Mechanism for Activating an Exon Network Required for Neurogenesis. *Mol. Cell* **56**, 90–103 (2014).

110. Calarco, J. A. *et al.* Regulation of vertebrate nervous system alternative splicing and development by an SR-related protein. *Cell* **138**, 898–910 (2009).

111. Quesnel-Vallières, M., Irimia, M., Cordes, S. P. & Blencowe, B. J. Essential roles for the splicing regulator nSR100/SRRM4 during nervous system development. *Genes Dev.* (2015). doi:10.1101/gad.256115.114

112. Planells-Ferrer, L. *et al.* Fas apoptosis inhibitory molecules: more than death-receptor antagonists in the nervous system. *J. Neurochem.* **139**, 11–21 (2016).

113. Li, G. *et al.* Structure determination of human Fas apoptosis inhibitory molecule and identification of the critical residues linking the interdomain interaction to the anti-apoptotic activity. *Acta Crystallogr. Sect. D Biol. Crystallogr.* **70**, 1812–1822 (2014).

114. Kaku, H. & Rothstein, T. L. FAIM opposes stress-induced loss of viability and blocks the formation of protein aggregates. *bioRxiv* 569988 (2019). doi:10.1101/569988

115. Schneider, T. J., Fischer, G. M., Donohoe, T. J., Colarusso, T. P. & Rothstein, T. L. A novel gene coding for a Fas apoptosis inhibitory molecule (FAIM) isolated from inducibly Fas-resistant B lymphocytes. *J. Exp. Med.* **189**, 949–56 (1999).

116. Kaku, H. & Rothstein, T. L. Correction: Fas Apoptosis Inhibitory Molecule Enhances CD40 Signaling in B Cells and Augments the Plasma Cell Compartment. *J. Immunol.* **185**, 771–771 (2010).

117. Kaku, H., Ludlow, A. V, Gutknecht, M. F. & Rothstein, T. L. FAIM Opposes Aggregation of Mutant SOD1 That Typifies Some Forms of Familial Amyotrophic Lateral Sclerosis. **14**, 1–8 (2020).

118. Kaku, H. & Rothstein, T. L. FAIM Is a Non-redundant Defender of Cellular Viability in the Face of Heat and Oxidative Stress and Interferes With Accumulation of Stress-Induced Protein Aggregates. **7**, 1–10 (2020).

119. Huo, J., Xu, S., Guo, K., Zeng, Q. & Lam, K.-P. Genetic deletion of faim reveals its role in modulating c-FLIP expression during CD95-mediated apoptosis of lymphocytes and hepatocytes. *Cell Death Differ.* **16**, 1062–70 (2009).

120. Huo, J. *et al.* Loss of Fas apoptosis inhibitory molecule leads to spontaneous obesity and hepatosteatosis. *Cell Death Dis.* **7**, e2091 (2016).

121. Zhong, X., Schneider, T. J., Cabral, D. S., Donohoe, T. J. & Rothstein, T. L. An

alternatively spliced long form of Fas apoptosis inhibitory molecule (FAIM) with tissue-specific expression in the brain. *Mol. Immunol.* **38**, 65–72 (2001).

122. Segura, M. F. *et al.* The long form of Fas apoptotic inhibitory molecule is expressed specifically in neurons and protects them against death receptor-triggered apoptosis. *J. Neurosci.* **27**, 11228–41 (2007).

123. Moubarak, R. S. *et al.* FAIM-L is an IAP-binding protein that inhibits XIAP ubiquitinylation and protects from Fas-induced apoptosis. *J. Neurosci.* **33**, 19262–75 (2013).

124. Carriba, P. *et al.* Amyloid-β reduces the expression of neuronal FAIM-L, thereby shifting the inflammatory response mediated by TNFα from neuronal protection to death. *Cell Death Dis.* **6**, e1639 (2015).

125. Carriba, P. & Comella, J. X. Neurodegeneration and neuroinflammation: Two processes, one target. *Neural Regen. Res.* **10**, 1581–1583 (2015).

126. 2018 Alzheimer's disease facts and figures. *Alzheimer's Dement.* (2018). doi:10.1016/j.jalz.2018.02.001

127. Scheff, S. W., Price, D. A., Schmitt, F. A., Dekosky, S. T. & Mufson, E. J. Synaptic alterations in CA1 in mild Alzheimer disease and mild cognitive impairment. *Neurology* (2007). doi:10.1212/01.wnl.0000260698.46517.8f

128. Nijhawan, D., Honarpour, N. & Wang, X. Apoptosis in neural development and disease. *Annu. Rev. Neurosci.* **23**, 73–87 (2000).

129. Boland, B. & Campbell, V. Aβ-mediated activation of the apoptotic cascade in cultured cortical neurones: A role for cathepsin-L. *Neurobiol. Aging* **25**, 83–91 (2004).

130. Deleglise, B. *et al.* B-Amyloid Induces a Dying-Back Process and Remote Trans-

Synaptic Alterations in a Microfluidic-Based Reconstructed Neuronal Network. *Acta Neuropathol. Commun.* **2**, 145 (2014).

131. D'Amelio, M. *et al.* Caspase-3 triggers early synaptic dysfunction in a mouse model of Alzheimer's disease. *Nat. Neurosci.* **14**, 69–79 (2011).

132. Obulesu, M. & Lakshmi, M. J. Apoptosis in Alzheimer's Disease: An Understanding of the Physiology, Pathology and Therapeutic Avenues. *Neurochemical Research* (2014). doi:10.1007/s11064-014-1454-4

133. Nikolaev, A., McLaughlin, T., O'Leary, D. D. M. & Tessier-Lavigne, M. APP binds DR6 to trigger axon pruning and neuron death via distinct caspases. *Nature* (2009). doi:10.1038/nature07767

134. Cotman, C. W., Poon, W. W., Rissman, R. A. & Blurton-Jones, M. The role of caspase cleavage of tau in Alzheimer disease neuropathology. *Journal of Neuropathology and Experimental Neurology* (2005). doi:10.1093/jnen/64.2.104

135. Young, K. H. Yeast Two-hybrid: So Many Interactions, (in) So Little Time…. *Biol. Reprod.* (1998). doi:10.1095/biolreprod58.2.302

136. Prasad, K. V *et al.* CD27, a member of the tumor necrosis factor receptor family, induces apoptosis and binds to Siva, a proapoptotic protein. *Proc. Natl. Acad. Sci. U. S. A.* **94**, 6346–6351 (1997).

137. Spinicelli, S. *et al.* GITR interacts with the pro-apoptotic protein Siva and induces apoptosis. *Cell Death Differ.* **9**, 1382–4 (2002).

138. Yoon, Y., Ao, Z., Cheng, Y., Schlossman, S. F. & Prasad, K. V. Murine Siva-1 and Siva-2, alternate splice forms of the mouse Siva gene, both bind to CD27 but differentially transduce apoptosis. *Oncogene* **18**, 7174–7179 (1999).

139. Py, B., Slomianny, C., Auberger, P., Petit, P. X. & Benichou, S. Siva-1 and an alternative splice form lacking the death domain, Siva-2, similarly induce apoptosis in T lymphocytes via a caspase-dependent mitochondrial pathway. *J. Immunol.* **172**, 4008–4017 (2004).

140. Zins, K. *et al.* Egr-1 upregulates siva-1 expression and induces cardiac fibroblast apoptosis. *Int. J. Mol. Sci.* **15**, 1538–1553 (2014).

141. Cao, C. *et al.* The ARG Tyrosine Kinase Interacts with Siva-1 in the Apoptotic Response to Oxidative Stress. *J. Biol. Chem.* **276**, 11465–11468 (2001).

142. Py, B. *et al.* The Siva protein is a novel intracellular ligand of the CD4 receptor that promotes HIV-1 envelope-induced apoptosis in T-lymphoid cells. *Apoptosis* **12**, 1879–1892 (2007).

143. Jacobs, S. B. R., Basak, S., Murray, J. I., Pathak, N. & Attardi, L. D. Siva is an apoptosis-selective p53 target gene important for neuronal cell death. *Cell Death Differ.* **14**, 1374–85 (2007).

144. Fortin, A. *et al.* The proapoptotic gene SIVA is a direct transcriptional target for the tumor suppressors p53 and E2F1. *J. Biol. Chem.* **279**, 28706–28714 (2004).

145. Chu, F. *et al.* Expression of Siva-1 protein or its putative amphipathic helical region enhances cisplatin-induced apoptosis in breast cancer cells: Effect of elevated levels of BCL-2. *Cancer Res.* **65**, 5301–5309 (2005).

146. Xue, L. *et al.* Siva-1 binds to and inhibits BCL-X(L)-mediated protection against UV radiation-induced apoptosis. *Proc. Natl. Acad. Sci. U. S. A.* **99**, 6925–30 (2002).

147. Gudi, R., Barkinge, J., Hawkins, S., Prabhakar, B. & Kanteti, P. Siva-1 promotes K-48 polyubiquitination of TRAF2 and inhibits TCR-mediated activation of NF-kappaB. *J. Environ. Pathol. Toxicol. Oncol.* **28**, 25–38 (2009).

148. Gudi, R. *et al.* Siva-1 negatively regulates NF-kappaB activity: effect on T-cell receptor-mediated activation-induced cell death (AICD). *Oncogene* **25**, 3458–62 (2006).

149. Resch, U. *et al.* Siva1 is a XIAP-interacting protein that balances NFkappaB and JNK signalling to promote apoptosis. *J. Cell Sci.* **122**, 2651–61 (2009).

150. Singaravelu, K. & Padanilam, B. J. p53 target Siva regulates apoptosis in ischemic kidneys. *Am. J. Physiol. Renal Physiol.* **300**, F1130–F1141 (2011).

151. Ma, Y. *et al.* Siva 1 inhibits proliferation, migration and invasion by phosphorylating Stathmin in ovarian cancer cells. *Oncol. Lett.* 1–7 (2017). doi:10.3892/ol.2017.6307

152. Li, N. *et al.* Siva1 suppresses epithelial-mesenchymal transition and metastasis of tumor cells by inhibiting stathmin and stabilizing microtubules. *Proc. Natl. Acad. Sci. U. S. A.* **108**, 12851–6 (2011).

153. Van Nostrand, J. L. *et al.* The p53 Target Gene SIVA Enables Non-Small Cell Lung Cancer Development. *Cancer Discov.* **5**, 622–635 (2015).

154. Liu, T., Ma, Y., Wang, Z., Zhang, W. & Yang, X. Siva 1 inhibits cervical cancer progression and its clinical prognosis significance. *Cancer Manag. Res.* **12**, 303–311 (2020).

155. Vachtenheim, J., Lischke, R. & Vachtenheim, J. Siva-1 emerges as a tissue-specific oncogene beyond its classic role of a proapoptotic gene. *OncoTargets and Therapy* (2018). doi:10.2147/OTT.S173001

156. Wang, X. *et al.* Siva1 inhibits p53 function by acting as an ARF E3 ubiquitin ligase. *Nat. Commun.* **4**, 1551 (2013).

157. Jacobs, S. B. R., Van Nostrand, J. L., Bowen, M. E., Baker, J. C. & Attardi, L. D. Siva

plays a critical role in mouse embryonic development. *Cell Death Differ.* (2019). doi:10.1038/s41418-019-0358-x

158. Dekkers, M. P. J., Nikoletopoulou, V. & Barde, Y. A. Death of developing neurons: New insights and implications for connectivity. *Journal of Cell Biology* (2013). doi:10.1083/jcb.201306136

159. Kristiansen, M. & Ham, J. Programmed cell death during neuronal development: The sympathetic neuron model. *Cell Death and Differentiation* (2014). doi:10.1038/cdd.2014.47

160. Buss, R. R. *et al.* Neuromuscular development in the absence of programmed cell death: Phenotypic alteration of motoneurons and muscle. *J. Neurosci.* (2006). doi:10.1523/JNEUROSCI.3528-06.2006

161. Yamaguchi, Y. & Miura, M. Programmed cell death in neurodevelopment. *Developmental Cell* (2015). doi:10.1016/j.devcel.2015.01.019

162. Bennett, M. R., Gibson, W. G. & Lemon, G. Neuronal cell death, nerve growth factor and neurotrophic models: 50 years on. *Autonomic Neuroscience: Basic and Clinical* (2002). doi:10.1016/S1566-0702(01)00358-7

163. Levi-Montalcini, R. & Hamburger, V. Selective growth stimulating effects of mouse sarcoma on the sensory and sympathetic nervous system of the chick embryo. *J. Exp. Zool.* (1951). doi:10.1002/jez.1401160206

164. Fiske, B. K. & Brunjes, P. C. NMDA receptor regulation of cell death in the rat olfactory bulb. *J. Neurobiol.* (2001). doi:10.1002/neu.1029

165. Hansen, H. H. *et al.* Mechanisms leading to disseminated apoptosis following NMDA receptor blockade in the developing rat brain. *Neurobiol. Dis.* (2004). doi:10.1016/j.nbd.2004.03.013

166. Hardingham, G. E., Fukunaga, Y. & Bading, H. Extrasynaptic NMDARs oppose synaptic NMDARs by triggering CREB shut-off and cell death pathways. *Nat. Neurosci.* (2002). doi:10.1038/nn835

167. Léveillé, F. *et al.* Suppression of the intrinsic apoptosis pathway by synaptic activity. *J. Neurosci.* (2010). doi:10.1523/JNEUROSCI.5115-09.2010

168. Veis, D. J., Sorenson, C. M., Shutter, J. R. & Korsmeyer, S. J. Bcl-2-deficient mice demonstrate fulminant lymphoid apoptosis, polycystic kidneys, and hypopigmented hair. *Cell* (1993). doi:10.1016/0092-8674(93)80065-M

169. Merry, D. E. & Korsmeyer, S. J. BCL-2 GENE FAMILY IN THE NERVOUS SYSTEM. *Annu. Rev. Neurosci.* (1997). doi:10.1146/annurev.neuro.20.1.245

170. González-García, M. *et al.* bcl-x is expressed in embryonic and postnatal neural tissues and functions to prevent neuronal cell death. *Proc. Natl. Acad. Sci. U. S. A.* (1995). doi:10.1073/pnas.92.10.4304

171. Deckwerth, T. L. *et al.* BAX is required for neuronal death after trophic factor deprivation and during development. *Neuron* (1996). doi:10.1016/S0896-6273(00)80173-7

172. Pompeiano, M., Blaschke, A. J., Flavell, R. A., Srinivasan, A. & Chun, J. Decreased apoptosis in proliferative and postmitotic regions of the caspase 3-deficient embryonic central nervous system. *J. Comp. Neurol.* (2000). doi:10.1002/1096-9861(20000717)423:1<1::AID-CNE1>3.0.CO;2-S

173. Hakem, R. *et al.* Differential requirement for Caspase 9 in apoptotic pathways in vivo. *Cell* (1998). doi:10.1016/S0092-8674(00)81477-4

174. Cecconi, F., Alvarez-Bolado, G., Meyer, B. I., Roth, K. A. & Gruss, P. Apaf1 (CED-4 homolog) regulates programmed cell death in mammalian development. *Cell* (1998). doi:10.1016/S0092-8674(00)81732-8

175. Hyman, B. T. Caspase activation without apoptosis: insight into Aβ initiation of neurodegeneration. *Nat. Neurosci.* **14**, 5–6 (2011).

176. Mukherjee, A. & Williams, D. W. More alive than dead : non-apoptotic roles for caspases in neuronal development , plasticity and disease. *Nat. Publ. Gr.* **44**, 1–11 (2017).

177. Simon, D. J. *et al.* A Caspase Cascade Regulating Developmental Axon Degeneration. *J. Neurosci.* **32**, 17540–17553 (2012).

178. Yang, J. *et al.* Regulation of axon degeneration after injury and in development by the endogenous calpain inhibitor calpastatin. *Neuron* **80**, 1175–1189 (2013).

179. Williams, D. W., Kondo, S., Krzyzanowska, A., Hiromi, Y. & Truman, J. W. Local caspase activity directs engulfment of dendrites during pruning. *Nat. Neurosci.* (2006). doi:10.1038/nn1774

180. Huesmann, G. R. & Clayton, D. F. Dynamic Role of Postsynaptic Caspase-3 and BIRC4 in Zebra Finch Song-Response Habituation. *Neuron* (2006). doi:10.1016/j.neuron.2006.10.033

181. Ertürk, A., Wang, Y. & Sheng, M. Local pruning of dendrites and spines by caspase-3-dependent and proteasome-limited mechanisms. *J. Neurosci.* **34**, 1672–1688 (2014).

182. Bateup, H. S. & Sabatini, B. L. For synapses, it's depression not death. *Cell* (2010). doi:10.1016/j.cell.2010.05.013

183. Oh, W. C., Hill, T. C. & Zito, K. Synapse-specific and size-dependent mechanisms of spine structural plasticity accompanying synaptic weakening. *Proc. Natl. Acad. Sci. U. S. A.* (2013). doi:10.1073/pnas.1214705110

184. Beattie, E. C. *et al.* Regulation of AMPA receptor endocytosis by a signaling

mechanism shared with LTD. *Nat. Neurosci.* (2000). doi:10.1038/81823

185. Zhou, Q., Homma, K. J. & Poo, M. M. Shrinkage of dendritic spines associated with long-term depression of hippocampal synapses. *Neuron* (2004). doi:10.1016/j.neuron.2004.11.011

186. Lee, S. H., Simonetta, A. & Sheng, M. Subunit rules governing the sorting of internalized AMPA receptors in hippocampal neurons. *Neuron* (2004). doi:10.1016/j.neuron.2004.06.015

187. Li, Z., Okamoto, K. I., Hayashi, Y. & Sheng, M. The importance of dendritic mitochondria in the morphogenesis and plasticity of spines and synapses. *Cell* (2004). doi:10.1016/j.cell.2004.11.003

188. Jiao, S. & Li, Z. Nonapoptotic Function of BAD and BAX in Long-Term Depression of Synaptic Transmission. *Neuron* (2011). doi:10.1016/j.neuron.2011.04.004

189. Pacher, P. & Hajnóczky, G. Propagation of the apoptotic signal by mitochondrial waves. *EMBO J.* (2001). doi:10.1093/emboj/20.15.4107

190. Hernández, F., Gómez de Barreda, E., Fuster-Matanzo, A., Lucas, J. J. & Avila, J. GSK3: A possible link between beta amyloid peptide and tau protein. *Experimental Neurology* (2010). doi:10.1016/j.expneurol.2009.09.011

191. Schuman, E. M., Dynes, J. L. & Steward, O. Synaptic Regulation of Translation of Dendritic mRNAs. *J. Neurosci.* **26**, 7143–7146 (2006).

192. tom Dieck, S., Hanus, C. & Schuman, E. M. SnapShot: Local Protein Translation in Dendrites. *Neuron* **81**, 958-958.e1 (2014).

193. Richter, J. & Klann, E. Translational control of synaptic plasticity and learning and memory. *Transl. Control Biol. Med.* **61**, 485–506 (2007).

194. Hoeffer, C. A. & Klann, E. NMDA receptors and translational control. in *Biology of the NMDA Receptor* (2008). doi:10.1201/9781420044157.ch6

195. Di Prisco, G. V. *et al.* Translational control of mGluR-dependent long-term depression and object-place learning by eIF2α *Nat. Neurosci.* **17**, 1–13 (2014).

196. Huang, F., Chotiner, J. K. & Steward, O. The mRNA for elongation factor 1α is localized in dendrites and translated in response to treatments that induce long-term depression. *J. Neurosci.* (2005). doi:10.1523/JNEUROSCI.1779-05.2005

197. Luo, L. & O'Leary, D. D. M. AXON RETRACTION AND DEGENERATION IN DEVELOPMENT AND DISEASE. *Annu. Rev. Neurosci.* (2005). doi:10.1146/annurev.neuro.28.061604.135632

198. Saxena, S. & Caroni, P. Mechanisms of axon degeneration: From development to disease. *Progress in Neurobiology* (2007). doi:10.1016/j.pneurobio.2007.07.007

199. Cusack, C. L., Swahari, V., Hampton Henley, W., Michael Ramsey, J. & Deshmukh, M. Distinct pathways mediate axon degeneration during apoptosis and axon-specific pruning. *Nat. Commun.* **4**, 1876 (2013).

200. Campenot, R. B. Local control of neurite development by nerve growth factor. *Proc. Natl. Acad. Sci. U. S. A.* (1977). doi:10.1073/pnas.74.10.4516

201. Potts, P. R., Singh, S., Knezek, M., Thompson, C. B. & Deshmukh, M. Critical function of endogenous XIAP in regulating caspase activation during sympathetic neuronal apoptosis. *J. Cell Biol.* (2003). doi:10.1083/jcb.200307130

202. DuBridge, R. B. *et al.* Analysis of mutation in human cells by using an Epstein-Barr virus shuttle system. *Mol. Cell. Biol.* (1987). doi:10.1128/mcb.7.1.379

203. Greene, L. A. & Tischler, A. S. Establishment of a noradrenergic clonal line of rat adrenal pheochromocytoma cells which respond to nerve growth factor. *Proc. Natl. Acad. Sci. U. S. A.* (1976). doi:10.1073/pnas.73.7.2424

204. Yang, J. *et al.* Regulation of axon degeneration after injury and in development by the endogenous calpain inhibitor calpastatin. *Neuron* **80**, 1175–1189 (2013).

205. Simon, D. J. *et al.* Axon Degeneration Gated by Retrograde Activation of Somatic Pro-apoptotic Signaling. *Cell* **164**, 1031–1045 (2016).

206. Caserta, T. M., Smith, A. N., Gultice, A. D., Reedy, M. A. & Brown, T. L. Q-VD-OPh, a broad spectrum caspase inhibitor with potent antiapoptotic properties. *Apoptosis* (2003). doi:10.1023/A:1024116916932

207. Goldberg, A. L. Development of proteasome inhibitors as research tools and cancer drugs. *J. Cell Biol.* (2012). doi:10.1083/jcb.201210077

208. Dalby, B. *et al.* Advanced transfection with Lipofectamine 2000 reagent: Primary neurons, siRNA, and high-throughput applications. *Methods* (2004). doi:10.1016/j.ymeth.2003.11.023

209. Naldini, L. *et al.* In vivo gene delivery and stable transduction of nondividing cells by a lentiviral vector. *Science (80-.).* (1996). doi:10.1126/science.272.5259.263

210. Naldini, L., Blomer, U., Gage, F. H., Trono, D. & Verma, I. M. Efficient transfer, integration, and sustained long-term expression of the transgene in adult rat brains injected with a lentiviral vector. *Proc. Natl. Acad. Sci.* (1996). doi:10.1073/pnas.93.21.11382

211. Livak, K. J. & Schmittgen, T. D. Analysis of relative gene expression data using real-time quantitative PCR and the 2-ΔΔCT method. *Methods* (2001). doi:10.1006/meth.2001.1262

212. Laemmli, U. K. Cleavage of structural proteins during the assembly of the head of bacteriophage T4. *Nature* (1970). doi:10.1038/227680a0

213. Tomomori-Sato, C., Sato, S., Conaway, R. C. & Conaway, J. W. Immunoaffinity purification of protein complexes from mammalian cells. *Methods Mol. Biol.* (2013). doi:10.1007/978-1-62703-284-1_22

214. Lal, A., Haynes, S. R. & Gorospe, M. Clean western blot signals from immunoprecipitated samples. *Mol. Cell. Probes* (2005). doi:10.1016/j.mcp.2005.06.007

215. Kroemer, G. *et al.* Classification of cell death: recommendations of the Nomenclature Committee on Cell Death 2009. *Cell Death Differ.* **16**, 3–11 (2009).

216. Schneider, C. A., Rasband, W. S. & Eliceiri, K. W. NIH Image to ImageJ: 25 years of image analysis. *Nat. Methods* **9**, 671–675 (2012).

217. Schindelin, J. *et al.* Fiji: An open-source platform for biological-image analysis. *Nature Methods* (2012). doi:10.1038/nmeth.2019

218. Dunn, K. W., Kamocka, M. M. & McDonald, J. H. A practical guide to evaluating colocalization in biological microscopy. *AJP Cell Physiol.* **300**, C723–C742 (2011).

219. Lee, S. H., Liu, L., Wang, Y. T. & Sheng, M. Clathrin adaptor AP2 and NSF interact with overlapping sites of GluR2 and play distinct roles in AMPA receptor trafficking and hippocampal LTD. *Neuron* **36**, 661–674 (2002).

220. Grabrucker, A., Vaida, B., Bockmann, J. & Boeckers, T. M. Synaptogenesis of hippocampal neurons in primary cell culture. *Cell Tissue Res.* (2009). doi:10.1007/s00441-009-0881-z

221. Zhong, X., Schneider, T. J., Cabral, D. S., Donohoe, T. J. & Rothstein, T. L. An alternatively spliced long form of Fas apoptosis inhibitory molecule (FAIM) with

tissue-specific expression in the brain. *Mol. Immunol.* **38**, 65–72 (2001).

222. Planells-Ferrer, L. *et al.* Fas apoptosis inhibitory molecules: more than death-receptor antagonists in the nervous system. *J. Neurochem.* **139**, 11–21 (2016).

223. Huo, J., Xu, S. & Lam, K. FAIM: An Antagonist of Fas-Killing and Beyond. 1–12 (2019).

224. King, N. *et al.* The genome of the choanoflagellate Monosiga brevicollis and the origin of metazoans. *Nature* (2008). doi:10.1038/nature06617

225. Fairclough, S. R. *et al.* Premetazoan genome evolution and the regulation of cell differentiation in the choanoflagellate Salpingoeca rosetta. *Genome Biol.* (2013). doi:10.1186/gb-2013-14-2-r15

226. Zmasek, C. M. & Godzik, A. Evolution of the animal apoptosis network. *Cold Spring Harb. Perspect. Biol.* (2013). doi:10.1101/cshperspect.a008649

227. Quistad, S. D. & Traylor-Knowles, N. Precambrian origins of the TNFR superfamily. *Cell Death Discovery* (2016). doi:10.1038/cddiscovery.2016.58

228. Gordeeva, A. V., Labas, Y. A. & Zvyagilskaya, R. A. Apoptosis in unicellular organisms: Mechanisms and evolution. *Biochemistry (Moscow)* (2004). doi:10.1023/B:BIRY.0000046879.54211.ab

229. Raj, B. *et al.* A global regulatory mechanism for activating an exon network required for neurogenesis. *Mol. Cell* **56**, 90–103 (2014).

230. Fadó, R. *et al.* X-linked inhibitor of apoptosis protein negatively regulates neuronal differentiation through interaction with cRAF and Trk. *Sci. Rep.* **3**, 2397 (2013).

231. Hench, V. K. & Su, L. Regulation of IL-2 gene expression by Siva and FOXP3 in

human T cells. *BMC Immunol.* **12**, 54 (2011).

232. Kuida, K. *et al.* Reduced apoptosis and cytochrome C-mediated caspase activation in mice lacking Caspase 9. *Cell* (1998). doi:10.1016/S0092-8674(00)81476-2

233. Woo, M. *et al.* Essential contribution of caspase 3/CPPp32 to apoptosis and its associated nuclear changes. *Genes and Development* (1998). doi:10.1101/gad.12.6.806

234. Hollville, E. & Deshmukh, M. Physiological functions of non-apoptotic caspase activity in the nervous system. *Semin. Cell Dev. Biol.* **82**, 127–136 (2018).

235. Verma, P. Axonal Protein Synthesis and Degradation Are Necessary for Efficient Growth Cone Regeneration. *J. Neurosci.* **25**, 331–342 (2005).

236. Ohsawa, S. *et al.* Maturation of the olfactory sensory neurons by Apaf-1/caspase-9-mediated caspase activity. *Proc. Natl. Acad. Sci. U. S. A.* (2010). doi:10.1073/pnas.0910488107

237. Chen, J. Y., Yang, L. X. & Huang, Z. F. The N-terminal 33 amino acid domain of Siva-1 is sufficient for nuclear localization. **46**, 1021–1027 (2013).

238. MacFarlane, M., Merrison, W., Bratton, S. B. & Cohen, G. M. Proteasome-mediated degradation of Smac during apoptosis: XIAP promotes Smac ubiquitination in vitro. *J. Biol. Chem.* (2002). doi:10.1074/jbc.M200317200

239. Wilkinson, J. C., Wilkinson, A. S., Galban, S., Csomos, R. A. & Duckett, C. S. Apoptosis-Inducing Factor Is a Target for Ubiquitination through Interaction with XIAP. *Mol. Cell. Biol.* (2008). doi:10.1128/mcb.01065-07

240. Han, J. *et al.* SIVA1 directs the E3 ubiquitin ligase RAD18 for PCNA monoubiquitination. *J. Cell Biol.* **205**, 811–827 (2014).

241. Iwai, K., Fujita, H. & Sasaki, Y. Linear ubiquitin chains: NF-κB signalling, cell death and beyond. *Nat. Rev. Mol. Cell Biol.* **15**, 503–8 (2014).

242. Lee, J. C. & Peter, M. E. Regulation of apoptosis by ubiquitination. *Immunol. Rev.* **193**, 39–47 (2003).

243. Hyman, B. T. & Yuan, J. Apoptotic and non-apoptotic roles of caspases in neuronal physiology and pathophysiology. *Nat. Rev. Neurosci.* **13**, 395–406 (2012).

244. Nakajima, Y. & Kuranaga, E. Caspase-dependent non-apoptotic processes in development. *Cell Death Differ.* 1–9 (2017). doi:10.1038/cdd.2017.36

245. Gilman, C. P. & Mattson, M. P. Do apoptotic mechanisms regulate synaptic plasticity and growth-cone motility? *Neuromolecular Med.* **2**, 197–214 (2002).

246. Alvarez-Castelao, B. & Schuman, E. M. The regulation of synaptic protein turnover. *Journal of Biological Chemistry* (2015). doi:10.1074/jbc.R115.657130

247. Collingridge, G. L., Isaac, J. T. R. & Yu, T. W. Receptor trafficking and synaptic plasticity. *Nature Reviews Neuroscience* (2004). doi:10.1038/nrn1556

248. Lee, H. K., Kameyama, K., Huganir, R. L. & Bear, M. F. NMDA induces long-term synaptic depression and dephosphorylation of the GluR1 subunit of AMPA receptors in hippocampus. *Neuron* **21**, 1151–1162 (1998).

249. Benarroch, E. E. Glutamatergic synaptic plasticity and dysfunction in Alzheimer disease: Emerging mechanisms. *Neurology* (2018). doi:10.1212/WNL.0000000000005807

250. Henke, a *et al.* The apoptotic capability of coxsackievirus B3 is influenced by the efficient interaction between the capsid protein VP2 and the proapoptotic host protein Siva. *Virology* **289**, 15–22 (2001).

251. Mulkey, R. M. & Malenka, R. C. Mechanisms underlying induction of homosynaptic long-term depression in area CA1 of the hippocampus. *Neuron* (1992). doi:10.1016/0896-6273(92)90248-C

252. Artola, A. & Singer, W. Long-term depression of excitatory synaptic transmission and its relationship to long-term potentiation. *Trends in Neurosciences* (1993). doi:10.1016/0166-2236(93)90081-V

253. Unsain, N. & Barker, P. A. New Views on the Misconstrued: Executioner Caspases and Their Diverse Non-apoptotic Roles. *Neuron* **88**, 461–474 (2015).

254. Wu, L. J. *et al.* DREAM (Downstream Regulatory Element Antagonist Modulator) contributes to synaptic depression and contextual fear memory. *Mol. Brain* (2010). doi:10.1186/1756-6606-3-3

255. Chen, M. *et al.* Spatially coordinated kinase signaling regulates local axon degeneration. *J. Neurosci.* (2012). doi:10.1523/JNEUROSCI.2039-12.2012

256. Wright, K. M., Linhoff, M. W., Potts, P. R. & Deshmukh, M. Decreased apoptosome activity with neuronal differentiation sets the threshold for strict IAP regulation of apoptosis. *J. Cell Biol.* (2004). doi:10.1083/jcb.200406073

257. Tesco, G. *et al.* Depletion of GGA3 Stabilizes BACE and Enhances β-Secretase Activity. *Neuron* (2007). doi:10.1016/j.neuron.2007.05.012

258. Snigdha, S., Smith, E. D., Prieto, G. A. & Cotman, C. W. Caspase-3 activation as a bifurcation point between plasticity and cell death. *Neurosci. Bull.* **28**, 14–24 (2012).

259. Fasulo, L. *et al.* The neuronal microtubule-associated protein tau is a substrate for caspase-3 and an effector of apoptosis. *J. Neurochem.* (2000). doi:10.1046/j.1471-4159.2000.0750624.x

260. Rissman, R. A. *et al.* Caspase-cleavage of tau is an early event in Alzheimer disease tangle pathology. *J. Clin. Invest.* (2004). doi:10.1172/JCI200420640

261. Gamblin, T. C. *et al.* Caspase cleavage of tau: Linking amyloid and neurofibrillary tangles in Alzheimer's disease. *Proc. Natl. Acad. Sci. U. S. A.* (2003). doi:10.1073/pnas.1630428100

262. Ambros, V. The functions of animal microRNAs. *Nature* (2004). doi:10.1038/nature02871

263. Bartel DP. MicroRNAs: genomics, biogenesis, mechanism, and function. - PubMed - NCBI. *Cell* (2004).

264. Patron, J. P. *et al.* Mir-133b targets antiapoptotic genes and enhances death receptor-induced apoptosis. *PLoS One* **7**, (2012).

ANNEX

8. ANNEX

During the course of my PhD work, I actively participated in several projects, focused in better understanding the role of DR and DR antagonists in cell physiology. Part of this work resulted in publications in international peer-reviewed scientific journals, listed in the second part of the annex (8.2 Publications). Apart from SIVA-1 charachterizarion as a FAIM-L functional antagonist, I have been primarily involved in two projects:

- Description and characterization of two new *FAIM1* isoforms, which findings have been published in 2017 in PLoS ONE.
- Characterization of *FAIM1* isoforms levels regulation by micro RNAs (8.1 microRNAs regulation of FAIM levels).

8.1 microRNAs regulation of FAIM levels

MicroRNAs (miRNAs) are small non-coding RNA molecules that regulate gene expression at the post-transcriptional level via RNA interference pathways[262]. Through complementarity of their seed region miRNAs bind mostly to the 3'untranslated region (UTR) of the target mRNA. As a result mRNA molecules are silenced by either inhibition of translation or degradation[263].

We explored miRNA regulation of FAIM isoforms, as part of our study on their regulation.

8.1.1 Five miRNAs are predicted to target FAIM1 3'UTR

In order to assess which miRNAs target FAIM isoforms we analyzed the 3'UTR sequence of human *FAIM1*, common to all described isoforms, with five prediction algorithms: miRWalk, version 2.0; miRNADA, version 2010; miRDB,

version 4.0; miRMap and TargetScan, version 6.2. *FAIM1* 3'UTR sequence was retrieved from GeneBank. As shown in the diagram in Figure 8.1, five miRNAs were found to target *FAIM1* in all considered analysis: miR-140-3p, miR-206, miR-1-3p, miR-133a and miR-133b. Details of the five miRNAs are reported in Table 8.1 and Figure 8.4. MiR-206 and -1-3p are part of the same miRNA family and share the same seed sequence. MiR-133a and -133b are members of the same miRNA family and extremely similar, differing only in the first nucleotide of their sequence. Given the high similarities of these last two, we decided to consider only one of them to move forward for the study. We selected miR-133b, having it already been reported to target FAIM[264].

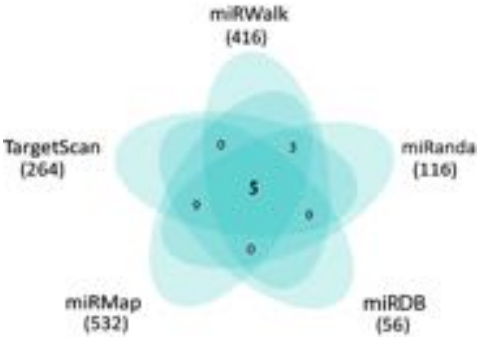

Figure 8.1: Five miRNAs are found to bind to FAIM3'UTR. Venn diagram representing the overlap of predicted miRNAs that can bind to FAIM 3'UTR among five miRNA-target prediction algorithms: miRWalk, miRanda, miRDB, miRMap and Targetscan.

miRNA	miRNA conservation	miRNA target sequence	Site type	MIMAT id	Comment
hsa-miR-140-3p	Broadly conserved	Conserved	8mer	MIMAT0004597	
hsa-miR-206	Broadly conserved	Poorly conserved	8mer	MIMAT0000416	Same miRNA family. Same seed sequence.
hsa-miR-1-3p	Broadly conserved	Poorly conserved	8mer	MIMAT0000462	
hsa-miR-133a	Broadly conserved	Poorly conserved	8mer	MIMAT0000427	Same miRNA family. Difference in the first nucleotide.
hsa-miR-133b	Broadly conserved	Poorly conserved	8mer	MIMAT0000770	

Table 8.1. miRNAs found to target FAIM1 3'UTR. "has" indicates species origin (human miRNA).

8.1.2 miR-206, miR-1-3p and miR-133b, bind to *FAIM1* 3'UTR

miRNAs directly bind to the target region of the mRNA through their seed sequence via base-pairing. To validate the interaction between miRNAs and FAIM 3'UTR we used a luciferase reporter assay. The assay, schematically represented in Figure 8.2, is based on a luciferase encoding gene derived from the sea pansy (*Renilla reniformis*). The 3'UTR fragment of *FAIM1* was cloned downstream of the luciferase gene, and this reporter construct was then co-transfected into HEK293T cells together with mimic-miRNAs. Luciferase signal was then measured.

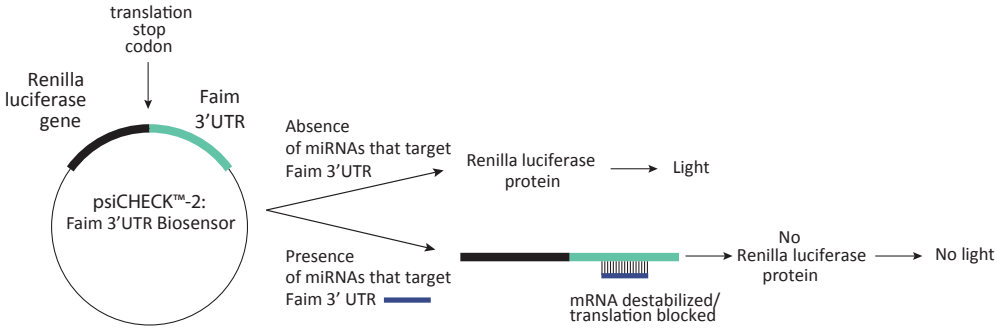

Figure 8.2: psiCHEK-2 vector was used to test miRNA binding to 3'UTR. FAIM 3'UTR was cloned downstream the luciferase genes. Changes in luminescence of Renilla luciferase-3'UTR construct was monitored in presence of miRNAs.

Of the four miRNAs considered, all except miR-140-3p were found to decrease luciferase activity (Figure 8.3).

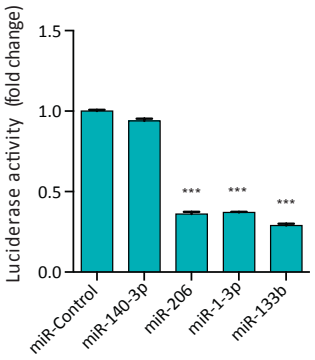

Figure 8.3: miR-206, miR-1-3p and miR-133b, bind to FAIM 3'UTR. Luciferase 3'UTR assays. HEK-293T cells/well were co-transfected with indicated reporter vector and 25nM of miR-140-3p, miR-1-3p, miR-206 or miR-133b. Twenty-four h post-transfection, luciferase assay was performed. Data are represented relative to cells transfected with the miR-Control. One-way ANOVA, ***p<0.001,

Putative binding sites of miRNAs were then mutated in the 3'UTR sequence (Figure 8.4). Wildtype (wt) or mutated 3'UTRs were cloned into psiCHEK-2 plasmid. Luciferase assay was performed by co-transfecting HEK293 cells with psiCHEK-2 constructs and miRNA mimics.

As shown in luciferase assay results of Figure 8.5, miRNAs were able to target wt 3'UTR. Mutation of the sequence targeted by miRNAs seed sequence restored luciferase activity to values comparable to empty psiCHECK2 vector, indicating that the interaction between the binding site in 3'UTR and miRNA is sequence specific.

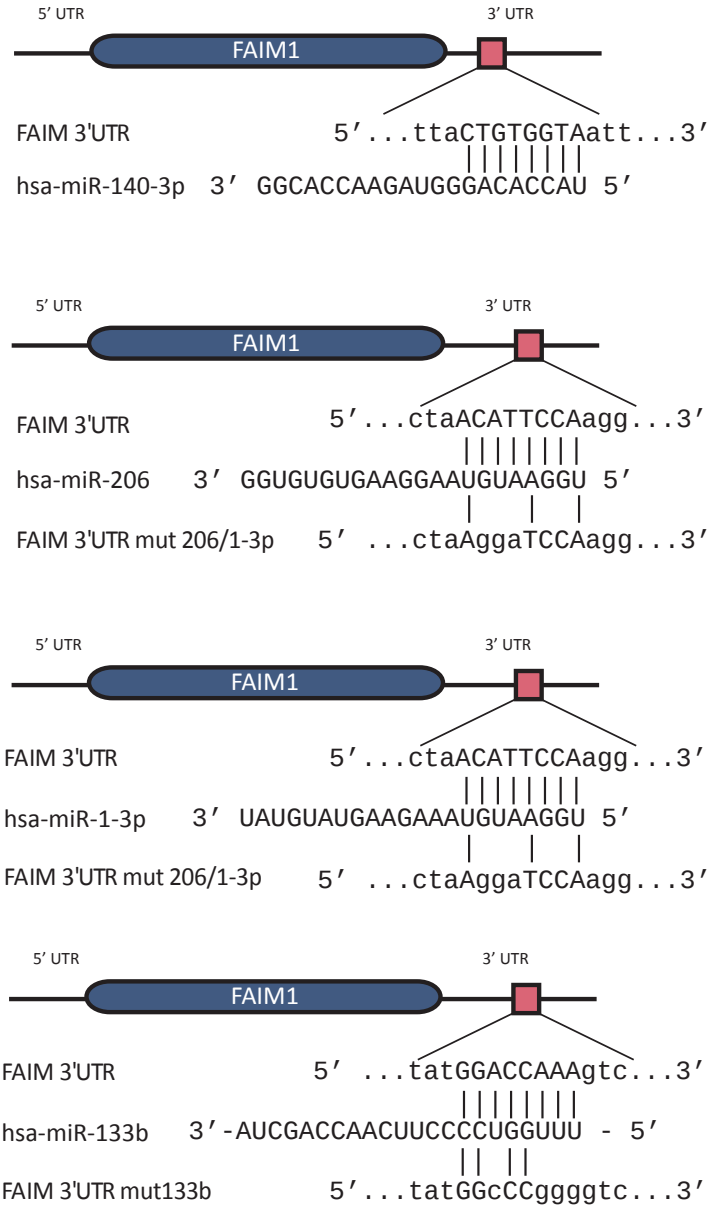

Figure 8.4: Four miRNAs found to target FAIM 3'UTR were considered in our study. Diagram of miRNAs target sites within the 3'UTR of FAIM as predicted by databases. 3'UTR was mutated in putative miRNA binding sites for luciferase assays, FAIM 3'UTR mut 206/1-3p carries mutation of sequence recognized by miR-206 and miR-1-3p seed sequence, FAIM 3'UTR mut133b carries mutation of sequence recognized by miR-133b seed sequence.

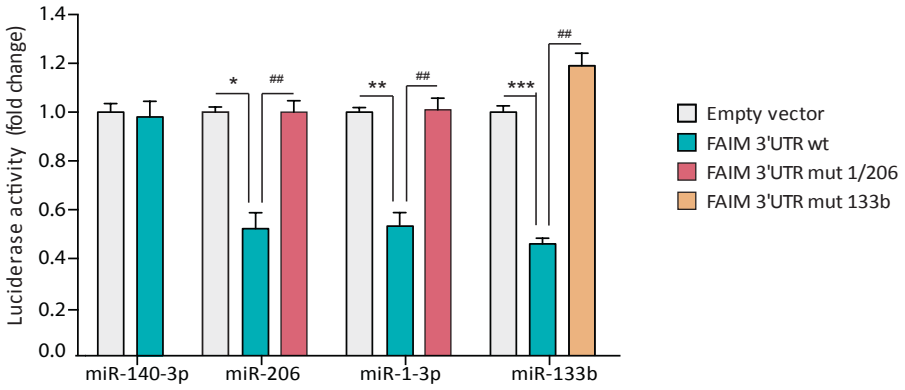

Figure 8.5: Binding site of miRNAs in 3'UTR is sequence specific. Luciferase 3'UTR assays. HEK-293T were co-transfected using indicated reporter vector and 25nM of miR-140-3p, miR-1-3p, miR-206 or miR-133b. Twenty-four h post-transfection, luciferase assay was performed. One-Way ANOVA, * Compares FAIM 3'UTR wt versus empty vector; # compares FAIM 3'UTR versus FAIM 3'UTR mutated. * $p<0.05$, ** $p<0.01$, *** $p<0.001$.

8.1.3 miR-206, miR-1 and miR-133b decrease FAIM isoforms levels in neuroblastoma cell lines

In order to confirm our previous findings, we tested whether the miRNA predicted were able to decrease FAIM in cells. We decided to use two human neuroblastoma derived cell lines, which, due to their origin, express different amounts of FAIM isoforms. In culture, neuroblastoma cells can be divided into neuronal (N), stromal (S) or intermediate (I) phenotype. We chose to use SH-SY5Y (N-type) that express all described isoforms, neuronal form FAIM-L included, and SK-N-AS (S-type), that express only FAIM-S.

SK-N-AS and SH-SY5Y were transfected for 48h with mimic-miRNAs. (RNA molecules designed to mimic endogenous mature miRNAs) We performed qPCR and could corroborate high overexpression of considered microRNAs (Figure 8.6).

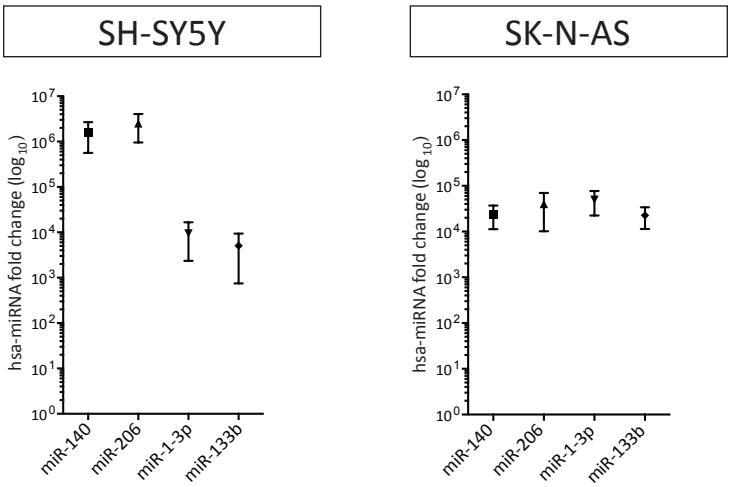

Figure 8.6: overexpression of hsa-miRNAs is efficient. SH-SY5Y and SK-N-AS cells were transfected 48h with hsa-miR mimics. qPCR results of overexpression analysis. Data are represented relative to the levels of miRNA in the miR-control transfected cells.

We then analyzed FAIM isoform levels in miRNA overexpressing cells. We performed qPCR to determine mRNA levels using two qPCR probes, a FAIM1 probe that recognized all isoforms, and a specific FAIM-L probe.

As shown in Figure 8.7 the 3 miRNAs found to bind to FAIM 3'UTR are able to significantly decrease FAIM isoforms in cells, miR-140-3p overexpression did not have any effect.

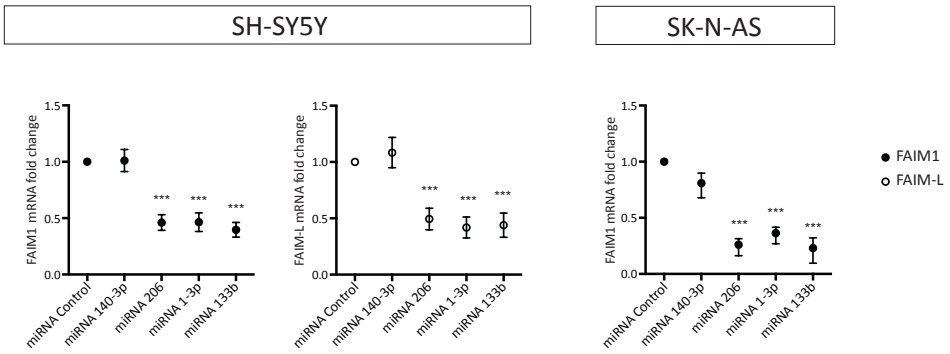

Figure 8.7: miR-206, miR-1-3p and miR-133b decrease FAIM isoforms mRNA levels.

Figure 8.7: qPCR results of FAIM mRNA levels. Two probes were used, a FAIM1 probe that amplifies all isoforms, and a specific FAIM-L probe.

Finally. We confirmed that the decrease found in mRNA is consistent with a decrease of FAIM isoforms protein levels (Figure 8.8).

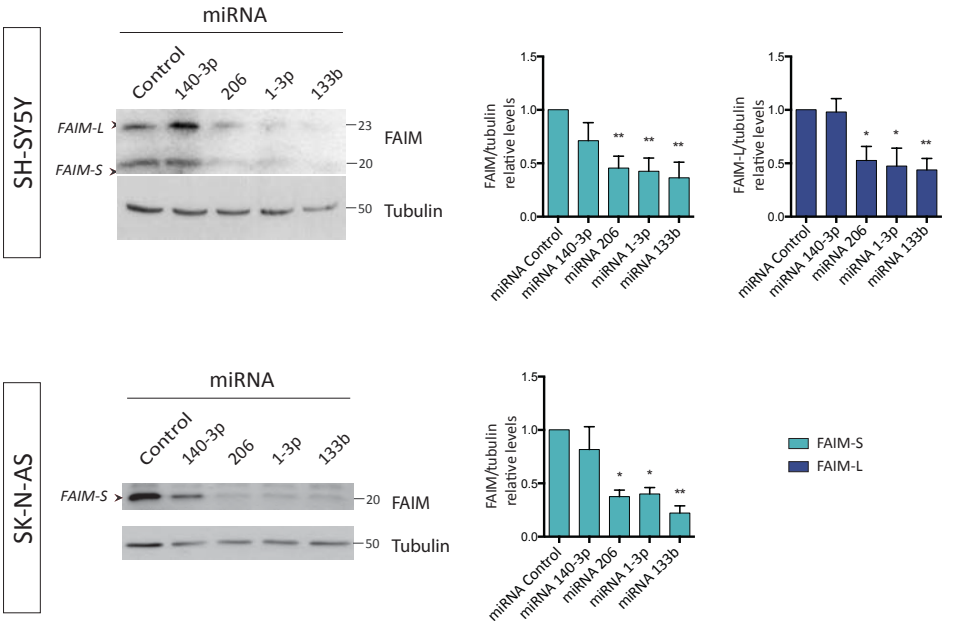

Figure 8.8: miR-206, miR-1-3p and miR-133b decrease FAIM isoforms protein levels. SH-SY5Y and SK-N-AS cells were transfected 48h with hsa-miR mimics. Representative western blot of the two isoforms FAIM-S and FAIML. Tubulin was used as loading control Graphs represent western blot quantification.

Overall, miR-206, miR-1-3p and miR133b are able to target and modulate FAIM isoforms levels.

8.2 Publications

Coccia E., Planells-Ferrer L., Badillos-Rodríguez R., Pascual M, Segura MF., Fernández-hernández R., López-soriano J., Garí E., Soriano E., Barneda-Zahonero B., Moubarak R.S., Pérez-García M.J., Comella J.X. SIVA-1 regulates apoptosis and synaptic function by modulating XIAP interaction with the death receptor antagonist FAIM-L. **Cell Death Dis 2020**
DOI: 10.1038/s41419-020-2282-x.

Coccia E., Calleja-Yagüe, Planells-Ferrer L., Sanuy B., Sanz B., López-SorianoJ., Moubarak R.S., Munell F., Barneda-Zahonero B., Comella J.X., Pérez-García M.J. Identification and characterization of new isoforms of human fas apoptotic inhibitory molecule (FAIM). **PLoS ONE 2017**
DOI:10.1371/journal.pone.0185327

Martínez-Mármol R., Barneda-Zahonero B., Soto D.; Andrés M.R., **Coccia E.**, Gasull X., Planells-Ferrer L., Moubarak R.S., Soriano E., Comella J.X. FAIM-L regulation of XIAP degradation modulates Synaptic Long-Term Depression and Axon Degeneration. **Sci Rep. 2016-10**
DOI:10.1038/srep35775

Planells-Ferrer L., Urresti J., **Coccia E.**, Galenkamp K.M., Calleja-Yagüe I., Carriba P., Lopez-Soriano J. Barneda-Zahonero B., Segura M.F., Comella J.X. FAIMs: more than a death-receptor antagonist in the nervous system. (**Review**) **J Neurochem. 2016-10**
DOI: 10.1111/jnc.13729

Urresti J., Ruiz-Meana M., **Coccia E.**, Arévalo J.C., Castellano J., Fernández-Sanz C, Galenkamp K.M., Planells-Ferrer L., Moubarak R.S., Llecha-Cano N., Reix S., García-Dorado D., Barneda-Zahonero B., Comella J.X. LFG/FAIM2/TMBIM2

inhibits Fas ligand-mediated endoplasmic reticulum-calcium release mandatory for apoptosis in type II cells. **J Cell Biol. 2016-01**
DOI: 10.1074/jbc.m115.677682

Galenkamp K.M., Carriba P., Urresti J., Planells-Ferrer L., **Coccia E.**, Lopez-Soriano J., Barneda-Zahonero B., Moubarak R.S., Segura M.F., Comella J.X..TNFα sensitizes neuroblastoma cells to FasL-, cisplatin- and etoposide-induced cell death by NF-κB-mediated expression of Fas. **Mol Cancer. 2015**
DOI: 10.1186/s12943-015-0329-x

Coccia et al. *Cell Death and Disease* (2020)11:82
https://doi.org/10.1038/s41419-020-2282-x

Cell Death & Disease

ARTICLE Open Access

SIVA-1 regulates apoptosis and synaptic function by modulating XIAP interaction with the death receptor antagonist FAIM-L

Elena Coccia[1,2,3], Laura Planells-Ferrer[1,2,3], Raquel Badillos-Rodríguez[1,2,3], Marta Pascual[2,4,5], Miguel F. Segura[6], Rita Fernández-Hernández[7], Joaquin López-Soriano[1,2,3], Eloi Garí[7], Eduardo Soriano[2,4,5,8], Bruna Barneda-Zahonero[1,2,3], Rana S. Moubarak[1,2,3,9], M. Jose Pérez-García[1,2,3] and Joan X. Comella[1,2,3]

Abstract

The long isoform of Fas apoptosis inhibitory molecule (FAIM-L) is a neuron-specific death receptor antagonist that modulates apoptotic cell death and mechanisms of neuronal plasticity. FAIM-L exerts its antiapoptotic action by binding to X-linked inhibitor of apoptosis protein (XIAP), an inhibitor of caspases, which are the main effectors of apoptosis. XIAP levels are regulated by the ubiquitin-proteasome pathway. FAIM-L interaction with XIAP prevents the ubiquitination and degradation of the latter, thereby allowing it to inhibit caspase activation. This interaction also modulates non-apoptotic functions of caspases, such as the endocytosis of AMPA receptor (AMPAR) in hippocampal long-term depression (LTD). The molecular mechanism of action exerted by FAIM-L is unclear since the consensus binding motifs are still unknown. Here, we performed a two-hybrid screening to discover novel FAIM-L-interacting proteins. We found a functional interaction of SIVA-1 with FAIM-L. SIVA-1 is a proapoptotic protein that has the capacity to interact with XIAP. We describe how SIVA-1 regulates FAIM-L function by disrupting the interaction of FAIM-L with XIAP, thereby promoting XIAP ubiquitination, caspase-3 activation and neuronal death. Furthermore, we report that SIVA-1 plays a role in receptor internalization in synapses. SIVA-1 is upregulated upon chemical LTD induction, and it modulates AMPAR internalization via non-apoptotic activation of caspases. In summary, our findings uncover SIVA-1 as new functional partner of FAIM-L and demonstrate its role as a regulator of caspase activity in synaptic function.

Introduction

Apoptosis plays a crucial role during neural development and adult life[1,2]. The main orchestrators of apoptosis are caspases, effector proteases that mediate the proteolytic cascade that ultimately leads to cell death. Several non-apoptotic functions of caspases have been reported in neurons[2]. Localized activation of caspases has been described as necessary in the physiological context of neuronal pruning, axon guidance, and synaptic plasticity[3]. The activation of caspase-3 via mitochondria is required for AMPA receptor (AMPAR) internalization in NMDA receptor-dependent long-term depression (LTD). Several studies have shown that LTD is abolished in caspase-3 knock-out mice[4], and caspase-3-deficient neurons in culture fail to show spine shrinkage in response to NMDA stimulation (chemical LTD)[5].

FAIM-L is the neuron-specific isoform of FAIM, and it harbors 22 additional amino acids at the N-terminal as compared to FAIM-S. We have previously shown that FAIM-L regulates caspase activation in neurons. Moreover, decreased FAIM-L levels have been associated with the progression of Alzheimer's disease (AD), an irreversible and progressive neurodegenerative disorder that is the most

Correspondence: M. Jose Pérez-García (maria.perez@vhir.org) or Joan X. Comella (joan.comella@vhir.org)
[1]Cell Signaling and Apoptosis Group, Vall d'Hebron Research Institute (VHIR), 08035 Barcelona, Spain
[2]Centro de Investigación Biomédica en Red sobre Enfermedades Neurodegenerativas (CIBERNED), ISCIII, 28031 Madrid, Spain
Full list of author information is available at the end of the article.
Edited by B. Joseph

SPRINGER NATURE CDDpress

common cause of dementia[6]. AD is characterized by neuronal death and the dysregulation of synaptic plasticity[7], mechanisms in which FAIM-L and apoptotic pathways are involved and have been shown to play crucial roles.

FAIM-L modulates death receptor-induced cell death by interacting with death receptors[8] and by interacting and stabilizing the X-linked inhibitor of apoptosis protein (XIAP). XIAP is a key member of the inhibitor of apoptosis protein family that directly binds to and inhibits effector caspases. XIAP levels are regulated by a process of auto-ubiquitination and proteasome degradation. Given its anti-apoptotic role, modification of XIAP levels is a decisive step in cell death induction[9]. FAIM-L confers neurons additional protection against cell death. In fact, FAIM-L interacts with XIAP and inhibits its ubiquitination and degradation by the proteasome, therefore maintaining the role of XIAP in preventing the cleavage and activation of caspases[10]. FAIM-L also participates in processes where caspases play a non-apoptotic role. By stabilizing XIAP levels, FAIM-L prevents AMPAR internalization after chemical induction of LTD (chLTD) in vitro and protects axons from degeneration induced by growth-factor deprivation[11].

Structural prediction algorithms for FAIM-L do not identify any functional domain that could predict potential protein association, and apart from XIAP, no other FAIM-L-interacting protein has been described to date. Here, using a yeast two-hybrid screening approach, we screened for potential FAIM-L partners of relevance for its function. Using either the full-length or the specific N-terminal amino acid sequence of FAIM-L as bait, we identified the proapoptotic SIVA-1 protein as a FAIM-L binding partner. SIVA-1 has been described as a proapoptotic protein, capable of inducing cell death in several cellular models[12]. Moreover, SIVA-1 has been reported to interact with XIAP[13]. Apoptotic induction mediated by SIVA-1 has been proposed to occur through several pathways, and it is essential for p53-induced apoptosis in granular neurons[14]. Here, we studied the contribution of SIVA-1 to the roles of FAIM-L and XIAP in caspase-dependent apoptotic and non-apoptotic functions in neurons. We found that SIVA-1 blocks the antiapoptotic function of FAIM-L by displacing the XIAP/FAIM-L interaction, thereby inducing XIAP degradation, caspase-3 activation and subsequent neuronal death or AMPAR internalization. Our results point to SIVA-1 as one of the proteins of the apoptotic machinery able to modulate caspase-3 activation in response to synaptic plasticity. On the basis of our findings, SIVA-1 emerges as a novel synaptic modulator.

Material and methods

Reagents

Unless otherwise specified, all biochemical reagents were purchased from Sigma-Aldrich.

Yeast two-hybrid screen

The pACT2-mouse cDNA library in *Escherichia coli* (Clontech cat# ML4008AH/cat# 638841) was pre-transformed in the yeast AH109 strain (more than 10^7 independent clones). The full-length FAIM-L and the 22 additional amino acids at the N-terminal FAIM isoform (FAIM-L) bait proteins were subcloned into pGBKT7 vector and transformed in Y187 yeast strain. The two-hybrid selection was performed by mating, following the matchmaker two-hybrid system 3 protocol (cat# K1612-1 Clontech). Positive colonies were selected in drop out medium lacking leucine, tryptophan, and histidine and containing 20 mM aminotriazole. Colonies were analyzed by polymerase chain reaction (PCR). cDNA was sequenced and transformed in *E. coli* (WB Cat# OP50), and interactions of bait and prey were confirmed by back transformation in yeast.

Cell culture

HEK293T cells (ATCC Cat# CRL-3216) were grown in DMEM supplemented with 10% heat-inactivated fetal bovine serum (iFBS) (Invitrogen), 20 U/ml penicillin and 20 µg/ml streptomycin. Rat pheochromocytoma PC12 cells (ATCC Cat# CRL-1721) were grown in DMEM supplemented with 6% iFBS, 6% heat inactivated horse serum (iHS), 10 mM HEPES, 20 U/ml penicillin and 20 µg/ml streptomycin. Cultures were maintained at 37 °C in a 5% CO_2 atmosphere in a humidified incubator.

Primary neuron cultures

Neuron cultures were prepared from wild-type C57BL/6J mice (Envigo, France) at embryonic day 15–16 (E15–16). Cerebral cortices and hippocampi were dissected in phosphate-buffered saline (PBS) pH 7.4. After trypsin and DNase treatment, tissues were mechanically dissociated and filtered through a 40-µm nylon mesh. Cells were resuspended in DMEM supplemented with 5% iFBS, 5% iHBS, 20 U/ml penicillin and 20 µg/ml streptomycin. Cells were then plated in poly-D-lysine-coated plates at a density of 3×10^5 cells/ml or on coverslips at 1.5×10^5 cells/ml for immunocytochemistry experiments. Four hour after seeding, medium was replaced by Neurobasal medium supplemented with B27, glutaMAX (Life Tech), 20 U/ml penicillin and 20 µg/ml streptomycin. Culture medium was partially replaced every 3–4 days with fresh medium. Cultures were kept at 37 °C in a 5% CO_2 atmosphere in a humidified incubator. When pan-caspase inhibitor quinolyl-Val-Asp-OPh (Q-VD) treatment was performed, Q-VD was added directly to culture media at a final concentration of 10 µM. All experimental protocols were approved by the Vall d'Hebron Institutional Review Board.

Plasmids

The constructions used for this study, namely 3xHA-SIVA-1, 3xHA-ΔSIVA-1, 3xFLAG-FAIM-L, 3xHA-FAIM-L, 6xMyc-XIAP and YFP, were expressed under the control of a cytomegalovirus constitutive promoter in the pcDNA3 expression vector (Invitrogen). 3xFLAG-SIVA-1 plasmid was kindly provided by Dr. Ulrike Resch (Medical University of Vienna). Lentiviral plasmids for this study were cloned into pEIGW. Short hairpin RNA (shRNA) targeting SIVA-1 was cloned into the pLVTHM vector, and a scrambled sequence was used as a control.

Lentiviral production

Lentiviruses were produced as described previously by Segura et al.[8]. For infection, lentiviruses were added to the host cell medium. Infection efficiency was monitored by counting green fluorescent protein (GFP)-positive cells.

Cell transfection and infection

HEK293T (ATCC Cat# CRL-3216) or PC12 (ATCC Cat# CRL-1721) cells were transfected with the desired expression plasmid using the calcium phosphate method or Lipofectamine 2000 (Invitrogen), following the manufacturer's instructions. The total amount of transfected DNA was kept constant by adding empty pcDNA3 expression vector. Primary neurons were transfected with Lipofectamine 2000, as described in Dalby et al.[15].

Immunoprecipitation

After 24–48 h of transient transfection for ectopic expression, or after 24 h in culture, HEK293T and PC12 cells were rinsed in PBS 1× and lysed in immunoprecipitation lysis buffer (IP lysis buffer) containing 20 mM Tris/HCl, pH 7.4, 150 mM NaCl, 2 mM EDTA, 10% Glycerol, 1% Triton X-100, and supplemented with a protease inhibitor cocktail (Roche). Samples were lysed for 30 min on ice and centrifuged at 4 °C at 12,000 × *g*. One milligram of total protein was used for immunoprecipitation overnight at 4 °C in an orbital shaker. Specific FLAG M2 Affinity monoclonal agarose beads or anti-ubiquitin-conjugated agarose beads (Santa Cruz Biotechnology Cat# sc-8017 AC) were used for IP:FLAG and IP:Ubiquitin respectively. For IP:Myc, lysates were precleared by 30 min of incubation with 20 µl conjugated protein G suspension and 0.25 µg/µl control mouse IgG. Afterwards, 1 µg Myc antibody (Santa Cruz Biotechnology Cat# sc-40) was added to each sample and incubated for 4 h at 4 °C in an orbital shaker. Finally, 20 µl conjugated protein G suspension was added and incubated overnight on an orbital shaker. After incubation, agarose beads were washed five times with IP lysis buffer and eluted. Elution was performed with a competitor peptide for IP:FLAG and IP:Myc, following the manufacturer's protocol. For IP:Ubiquitin, elution was performed by adding Laemmli buffer (60 mM Tris/HCL 1 M, pH 6.8, 2% sodium dodecyl sulfate (SDS), 10% Glycerol, 0.01% Bromophenol Blue) without dithiothreitol and boiling samples at 95 °C for 5 min. Whole-cell lysate and immunoprecipitated proteins were then analyzed by western blot.

Immunohistochemistry

E16, P0, P5, P15, and adult OF-1 mice (Charles River, Lyon; France) were used for immunohistochemistry experiments. The day the vaginal plug was detected was considered embryonic day 0 (E0), and the day of birth as postnatal day 0 (P0). First, the animals were deeply anesthetized with a Ketolar (Parke-Davies/Pfizer New York, NY; USA)/Rompun (Bayer AG, Leverkusen; Germany) mixture and perfused with 4% paraformaldehyde in 0.1 M phosphate buffer. Brains were dissected, cryoprotected and frozen. Next, 30–50 µm coronal sections were obtained. After blocking, sections were incubated overnight with specific rabbit antibody against SIVA-1 (dilution 1:100, Santa Cruz Biotechnology Cat# sc-48768) or mouse anti-SIVA-1 (dilution 1:100, Sigma-Aldrich Cat#SAB1400393). These primary antibodies were visualized by sequential incubation with biotinylated secondary antibodies (dilution 1:200, Vector Labs Burlingame, CA; USA) and the streptavidin–peroxidase complex (dilution 1:400, Amersham Biosciences Pittsburgh, PA, USA). The peroxidase reaction was developed with diaminobenzidine (DAB) and H_2O_2. The sections were mounted onto gelatinized slides, and then dehydrated and cover-slipped with Eukkit (Panreac).

Sections from E16, P5, P15, and adult mice were used for double immunofluorescence studies. Sections were incubated overnight with the specific antibody detecting SIVA-1 (dilution 1:100, Santa Cruz Biotechnology, Cat# sc-48768) combined with antibodies against neuron-specific nuclear protein (NeuN, dilution 1:100, Millipore Cat# MAB377), PV (dilution 1:3000, Swant Antibodies Cat# PVG-214, RRID:AB_2313848) or GFAP (dilution 1:500, Millipore Cat# AB5804). Primary antibodies were visualized using secondary Alexa Fluor-conjugated antibodies. Sections were mounted with Prolong diamond mounting medium (Thermo Fisher) and viewed under a confocal microscope.

Immunocytochemistry

Hippocampal or cortical primary neurons were cultured on glass coverslips pre-coated with 10 µg/ml poly-D-lysine. After 7–10 days in vitro (DIV), cells were fixed with 4% paraformaldehyde for 30 min at room temperature. Permeabilization and blocking were carried out with a permeabilization solution (PS) containing 5% FBS, 5% bovine serum albumin, and 0.1% Triton-X for 1 h at room temperature, followed by incubation with primary antibodies in PS overnight at 4 °C. The following primary antibodies were used: anti-SIVA-1 (dilution

1:500 Santa Cruz Biotechnology Cat# sc-48768; Sigma-Aldrich Cat# SAB1400393); anti-SIVA-1 (dilution 1:25, Sigma-Aldrich Cat# SAB3500697), anti-XIAP (dilution 1:25, BD Cat# 610762), anti-HA (dilution 1:100, Roche Cat# 1-867-423); anti-Rab5 (dilution 1:500, Cell Signaling Technology Cat# 2143); anti-Calnexin (dilution 1:500, Cell Signaling Technology Cat# 2433S); anti-βIII Tubulin (dilution 1:1000, Covance Research Products Inc Cat# SIG-3840-1000); anti-TrkA (dilution 1:1000, in house); anti-PSD95 (dilution 1:200, Cell Signaling Cat# 3450); anti-Synapsin II (dilution 1:200, Enzo Life Science Cat# ADI-VAS-SV061-E); and anti-GFP (1:2000, Abcam Cat# ab6556). Subsequently, cells were rinsed with PBS and incubated with fluorescent-conjugated secondary antibodies (dilution 1:400–1:1000, Alexa-Fluor Thermo Fisher Scientific Cat# A-11001 Cat# A-11912) diluted in PS for 1 h at room temperature. Prior to the last wash, cells were incubated for 30 min at room temperature with Hoechst 33258 (0.05 µg/ml) to stain nuclear DNA. MitoTracker staining (Invitrogen) was used, following the manufacturer's instructions. Coverslips were finally mounted on slides with Prolong diamond mounting medium (Thermo Fisher).

Cell death quantification

At 4 days post infection, primary neurons were fixed with 2% paraformaldehyde, permeabilized with 0.1% Triton™ X-100 and stained with Hoechst 33342 (0.05 µg/ml). Apoptosis was assessed by counting viable and dead cells, discriminating condensed and fragmented nuclei (apoptotic nuclear morphology type II)[16]. For each experiment quantification was performed in blind testing, and at least 500 cells were counted per condition.

Caspase activity assay

The caspase activity assay was performed as previously described by Galenkamp et al.[17]. Briefly, primary neurons were harvested and lysed in caspase activity buffer (20 mM HEPES-NaOH, pH7.2, 10% sucrose, 150 mM NaCl, 5 mM EDTA, 1% Igepal CA-630, 0.1% CHAPS, and 1× EDTA-free complete protease inhibitor cocktail). Next, 20 µg protein was incubated at 37 °C in caspase activity buffer supplemented with 10 mM DTT and 50 µM of the fluorogenic substrate Ac-DEVD-Afc (Merck Millipore). Plates were read in a fluorometer using excitation and emission wavelengths of 405 and 535 nm, respectively.

Subcellular protein fractionation

Subcellular fractionation was performed as previously described[18]. Adult mouse brains were homogenized in buffer containing 10 mm HEPES, pH 7.4, 2 mm EDTA, 0.32 M sucrose, and protease inhibitor cocktail (Roche). Cell homogenates were centrifuged sequentially at 600 × *g* for 10 min to remove nuclei (N) and unbroken cells, then at 3000 × *g* for 10 min to pellet the plasma membrane (PM) and collect cytosolic fractions (supernatant). Nuclei were extracted from the 600 × *g* pellet with centrifugations at 500 × *g* for 15 min. The supernatants were centrifuged twice at each speed, and pellets were washed twice by resuspension in homogenization buffer and recentrifugation. Pellets were lysed in SET buffer (10 mM Tris-HCl pH7.4, 1 mM EDTA, 150 mM NaCl, 1% SDS). Protein concentration was quantified by a modified Lowry assay (DC protein assay; Bio-Rad, Hercules, CA). Samples were heat-denatured in Laemmli buffer and subjected to SDS polyacrylamide gel electrophoresis.

Western blot

Cells were harvested and lysed in SET buffer. Protein concentration was quantified by a modified Lowry assay (DC protein assay; Bio-Rad, Hercules, CA, USA). Lysates were prepared with Laemmli buffer (60 mM Tris/HCl 1 M pH 6.8, 2% SDS, 100 mM glycerol, 0.01% Bromophenol Blue), resolved in SDS polycramide gels, and transferred onto polyvinylidene fluoride Immobilon-P membranes (Merck Millipore). After blocking with TBS 1× −0.1% Tween-20 containing 5% nonfat dry milk for 1 h at room temperature, membranes were probed with the appropriate primary antibodies, prior to incubation for 1 h with the appropriate specific peroxidase-conjugated secondary antibody. Membranes were developed using the EZ-ECL chemiluminescence detection kit (Biological Industries, Kibbutz Beit Haemek, Israel). The following primary antibodies were used: anti-FAIM-L (dilution 1:2000, in house); anti-caspase-3 (dilution 1:1000, Cell Signaling Technologies Cat# 9662); anti-pan ERK (dilution 1:10000, BD Bioscience Cat# 610123); anti-β-actin (dilution 1:2000, Santa Cruz Biotechnology Cat# sc-47778); anti-alpha-tubulin (dilution 1:50000, Sigma-Aldrich Cat# T5168); anti-XIAP (dilution 1:5000, BD Bioscience Cat# 610762); anti-FLAG (dilution 1:10000, Sigma-Aldrich Cat# F3165); anti-HA (dilution 1:5000, Roche Cat# 11867423001); anti-SIVA-1 (dilution 1:500, Sigma Cat# SAB3500697); anti-GluA2 (1:1000, Millipore Cat# MAB397); anti-cytochromec (1:1000, BDbioscience Cat# 556433); anti-calnexin (1:1000, Abcam Cat# ab31290); anti-histone-3 (1:1000, Cell Signaling Technologies Cat# 9715); and anti-GAPDH (1:2000, Abcan Cat# ab9485).

Chemical LTD induction

Primary neurons were treated at 12–14 DIV with 50 µM N-methyl-D-aspartate (NMDA) for 15 min at 37 °C to induce chLTD as described in Li et al.[4]. Fifty micromolar of BAPTA-AM was used as calcium chelator and 1 µg/ml of cycloheximide (CHX) as an inhibitor of protein translation. Cells were pretreated with BAPTA-AM or CHX during 30 or 60 min, respectively. Treatments were added

to media for the pretreatment and maintained during chLTD induction.

GluA2 internalization assay and surface staining

Internalization assays were performed as described in Martinez-Marmol et al.[11], with minor modifications. Hippocampal neurons at 12–14 DIV were incubated with antibodies against the N-terminus of GluA2 (2 µg/ml, mouse monoclonal, clone 6C4, Millipore Cat# MAB397) for 60 min at 20 °C. They were then either stimulated with medium containing NMDA (50 µM) for 15 min at 37 °C or left unstimulated. Subsequently, they were fixed for 5 min at room temperature in paraformaldehyde:sucrose in PBS. Surface-remaining antibody-labeled receptors were visualized by means of a 1 h incubation with saturated AlexaFluor-647 secondary antibody (15 µg/ml, Abcam Cat# ab150115). Neurons were then permeabilized for 2 min with methanol (−20 °C), and internalized antibody-labeled GluA2 was detected by a 1 h incubation with Alexa 568-conjugated secondary antibody (1 µg/ml; Molecular Probes Cat# A-11004). Simultaneously, infected GFP-positive or HA-positive neurons were stained with antibodies against GFP (5 µg/ml, Abcam; Cat# ab6556) or HA (10 µg/ml Roche Cat# 11867423001), respectively. Thus, the GFP fluorescence of infected neurons was enhanced by a 30 min incubation with Alexa 488-conjugated secondary antibody (4 µg/ml; Thermo Fisher Scientific Cat# A27034). After three washes in PBS 1×, the coverslips were mounted on slides with Prolong diamond mounting medium (Thermo Fisher).

Image acquisition and analysis

Images were acquired with a confocal laser scanning microscope (spectral FV1000; Olympus). The digital images were processed using the FIJI software (Fiji)[19].

Protein co-localization in the dual-color confocal images was measured quantitatively using the JACoP Plug-in (http://fiji.sc/wiki/index.php/Colocalization_Analysis). Co-localization was determined by Pearson's and Manders co-localization coefficients. Briefly, Pearson's coefficient values describe the relationship between two image signals calculated by linear regression. Values can range from 1 to −1, with 1 standing for complete positive correlation and −1 for complete negative correlation. Manders co-localization coefficients (M_1 and M_2) describe the contribution of two selected channels to the pixels of interest, in this case Channel 1 being SIVA-1 and Channel 2 the other markers. Each coefficient represents the fraction of one channel signal that coincides with the signal of the other channel. Manders co-localization coefficients values range from 0 (uncorrelated distributions of two probes with one another) to 1 (perfect co-localization of two images)[20]. At least 15 cells were considered for quantification.

For GluA2 internalization and surface staining, a z-stack of images was obtained through various filter channels (Alexa-488, Alexa-568 and Alexa-674). Typically, 25 serial 2D images were recorded at 45-nm intervals. Image acquisition settings were identical in each experiment. FIJI software was used to make 2D projections from the z-stack of images. We measured the total integrated intensity of internalized GluA2 and surface-remaining GluA2 in the same region of infected (GFP/HA-positive) neurons. For each experiment at least 15–20 cells were counted per condition.

Cell surface biotinylation

Cell surface proteins were biotinylated and isolated using the Pierce® Cell Surface Protein Isolation Kit (Thermo Fisher Scientific), following the manufacturer's instructions. Before immunoprecipitation, the amount and concentration of protein were equalized by Lowry quantification.

RNA extraction and quantitative reverse transcription PCR

Total RNA was isolated from cells using the RNeasy Mini Kit (Qiagen), following the manufacturer's protocol. cDNA was reverse-transcribed using the High-Capacity cDNA Reverse Transcription Kit (Thermo Fisher). SIVA-1 mRNA expression was measured with SYBR green (Applied Biosystems) and normalized against L27 using the following primers: SIVA-1 forward: 5′-GATCACAT ATCGAGCGAAGA-3′, reverse: 5′-GCCTTCCCATCCA CAGATCT-3′; and L27: forward: 5′-AGCTGTCATCG TGAAGAA-3′, reverse: 5′-CTTGGCGATCTTCTTCTT GCC-3′. Analysis was performed using the 7900HT Sequence Detection System 2.3 Software (Applied Biosystems). Relative expression fold change was determined by the comparative $2^{(-\Delta\Delta CT)}$ method[21].

Experimental design and statistical analysis

All results were confirmed in at least three independent experiments. Representative images and western blots are shown in figures, while measurements of all repeated experiments are measured in graphs. Data sets were plotted and analyzed using GraphPad Prism v5 (GraphPad Software; La Jolla, CA, USA). Values were excluded using the analysis to identify outliers included in the software. Values are expressed as mean ± SEM. Statistical significance was set at $p < 0.05$ and was determined by two-tailed unpaired t test for comparisons between two groups, or by two-way ANOVA for multiple groups. Each specific test is indicated in figure legends.

Results

SIVA-1 interacts with FAIM-L

To identify the functional partners of FAIM-L, we performed a yeast-two-hybrid screening using as bait the full-length sequence of FAIM-L or the 22 N-terminal-

Table 1 Yeast two-hybrid analysis. List of protein–protein interactions with full-length FAIM-L and the 22 N-terminal-specific amino acids of the FAIM-L isoform.

Yeast two-hybrid analysis	Bait			Sequence
	pGBKT7 (control)	pGBKT7- full length FAIM-L	pGBKT7-N-term FAIM-L -(MASGDD SPIFEDDESPPYSLEK)	
SIVA-1 (ΔSIVA-1)	−	+	+	MPKRSCPFADAAPLQLKVHVGLKELSHGVFAERYSREV
FERM RhoGEF	−	+	+	HELKKDLIGIDNLVTPGREFIRLGSLSKLSGKGLQQRMFFLFNDVLLYTS RGLTASNQFKVHGQLPLYGMTIEESEEEWGVPHCLTLRGQRQSIIVAA SSRSEMEKWMEDIQMAIDLAEKSNGPTPELLASSPPDNKSPDEA
GAPDH	−	+	+	YSNRMVDLMAYMASKE
COMMD1	−	+	+	EGGKSLSGLLSGLAQNAFHGHSGVTEELLHSQLYPEVPPEEFRPFLA KMRGLLKSIASADMDFNQLEAFLTAQTKKQGGITSEQAAVISKFWKSH KIKIRESLMKQSRWDNGLRGLSWRVDGKSQSRHSTQIHSPVAIIELEFG KNGQESEFLCLEFDEVKVKQILKKLSEVEESINRLMQAA
Calcyclin	−	+	+	DKFVKIYITLTGVHQVPTENVQVHFTERSFDLLVKNLNGKNYSMIVNN LLKPISVESSSKKVKTDTVIILCRKKAENTRWDYLTQVEKECKEKE
AP2m1	−	+	+	PKRACQFNRTQLGDCSGIGDPTHYGYSTGQPCVFIKMNRVINFYAGAN QSMNVTCVGKRDEDAENLGHFVMFPANGSIDLMYFPYYGKKFHVNY TQPLVAVKFLNVTPNVEVNVECRINAANIATDDERDKFAGRVAFKLRINKT

specific amino acids of this isoform. Among the top six hits shown in Table 1, the N-terminal fragment of SIVA-1 was detected (ΔSIVA-1) (Table 1 and Fig. 1a).

We validated this interaction in HEK 293T cells by co-immunoprecipitation experiments using full-length FLAG-tagged FAIM-L, HA-tagged N-terminal SIVA-1 (ΔSIVA-1), or HA-tagged full-length SIVA-1. We confirmed the interactions between FAIM-L and both full-length and ΔSIVA-1 forms (Fig. 1b, lanes 3 and 6). Interaction with the truncated form of SIVA-1 was detected only in the presence of the proteasome inhibitor MG132 (Fig. 1b, lane 6), otherwise it was not stable and was consequently degraded.

Our group reported XIAP as a FAIM-L-interacting partner[10]. XIAP is an inhibitor of caspases and its endogenous levels are crucial for FAIM-L protection against caspase activation and consequent apoptotic or non-apoptotic functions[10,11]. Since Resch and colleagues described an interaction between SIVA-1 and XIAP[13], we performed co-immunoprecipitation experiments and corroborated that XIAP does indeed interact with both FAIM-L and SIVA-1 (Fig. 1c).

To detect the interaction in a semi-endogenous condition, we transfected primary cortical neurons with 3xHA-FAIM-L. We then performed immunocytochemistry against HA, endogenous SIVA-1 and XIAP (Fig. 1d). Co-localization analysis revealed partial correlation of signals of SIVA-1 with both XIAP (Pearson's correlation value $R = 0.412 \pm 0.115$) and HA-FAIM-L (Pearson's correlation $R = 0.607 \pm 0.060$). We could also observe that the interactions between SIVA-1, XIAP and tagged FAIM-L takes place in neuronal cytoplasm.

SIVA-1 is expressed in neurons

FAIM-L expression is restricted to neurons[8]. To understand the biological context in which SIVA-1 may modulate FAIM-L functions, we first examined SIVA-1 expression in mouse brain tissue. Histological analysis showed that SIVA-1 expression occurred in most brain regions throughout development (Fig. 2a–h, stages E16-adult mouse). High levels were detected in the telencephalon (cerebral cortex and hippocampus) and in the cerebellum (Fig. 2e–h). In the embryonic cerebral cortex, labeled cells were located in the cortical plate (CP) and in the subplate (SP), corresponding to postmitotic neurons of these layers (Fig. 2a). At postnatal stages (P0-P15), SIVA-1-positive cells were found throughout the cortical layers, the strongest staining being detected in layers II–III (Fig. 2b, c). At adult stages, the expression of SIVA-1 in the cerebral cortex appeared to be restricted to layer V cortical neurons (Fig. 2d). The cerebellum also showed intense SIVA-1-immunolabeling (Fig. 2e–g). SIVA-1 was expressed in migratory Purkinje cells in the embryonic cerebellum (data not shown). At postnatal P10 and P15 stages, cell bodies and dendrites of Purkinje neurons showed intense SIVA-1-immunostaining (Fig. 2e). These neurons maintained SIVA-1 expression at later stages and also during adulthood (Fig. 2g). At embryonic stages, cells in the hippocampal plate expressed SIVA-1 (data not shown). At postnatal stages, pyramidal neurons in CA1–3 and some

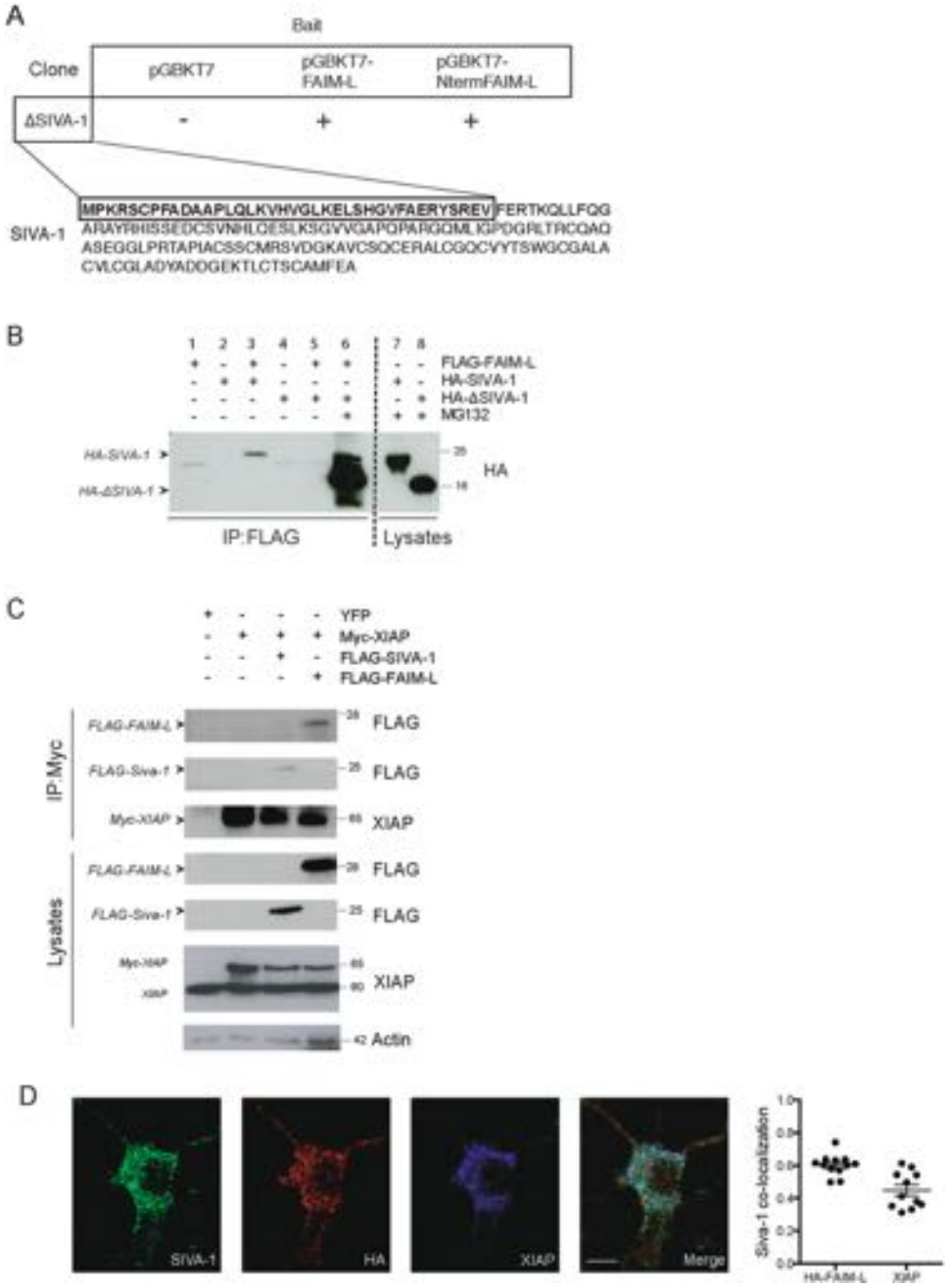

Fig. 1 SIVA-1 interacts with FAIM-L and XIAP. a Schematic representation of the two-hybrid technique results. The N-terminal of SIVA-1(ΔSIVA-1) interacted with both baits, namely full-length FAIM-L and FAIM-L-specific N-terminal 22 amino acids. **b** Immunoprecipitation in HEK 293T cells of FLAG-FAIM-L using M2 Affinity FLAG. FAIM-L was immunoprecipitated and membrane was blotted with anti-HA to detect full-length SIVA-1 and ΔSIVA-1. Ten micromolar of MG132 (proteasome inhibitor) was used to impair the degradation of ΔSIVA-1. **c** Immunoprecipitation of Myc-XIAP using anti-Myc antibody. Cells were transiently transfected with Myc-XIAP, FLAG-FAIM-L, and FLAG-SIVA-1. The membrane was blotted with anti-FLAG to detect both FAIM-L and SIVA-1. XIAP was used as a control of the immunoprecipitation and actin as loading control. **d** Representative confocal images of immunocytochemistry in cortical neurons. Neurons were transfected with HA-tagged FAIM-L at 4 days in vitro. Forty-eight hour after transfection, immunofluorescence was performed staining with anti-SIVA-1 (green), anti-HA (to detect HA-FAIM-L, red), and anti-XIAP (blue). Scale bar 10 μm. Graph reports Pearson's correlation coefficients obtained in co-localization analysis (SIVA-1/HA-FAIM-L $R = 0.607 \pm 0.060$; SIVA-1/XIAP $R = 0.412 \pm 0.115$).

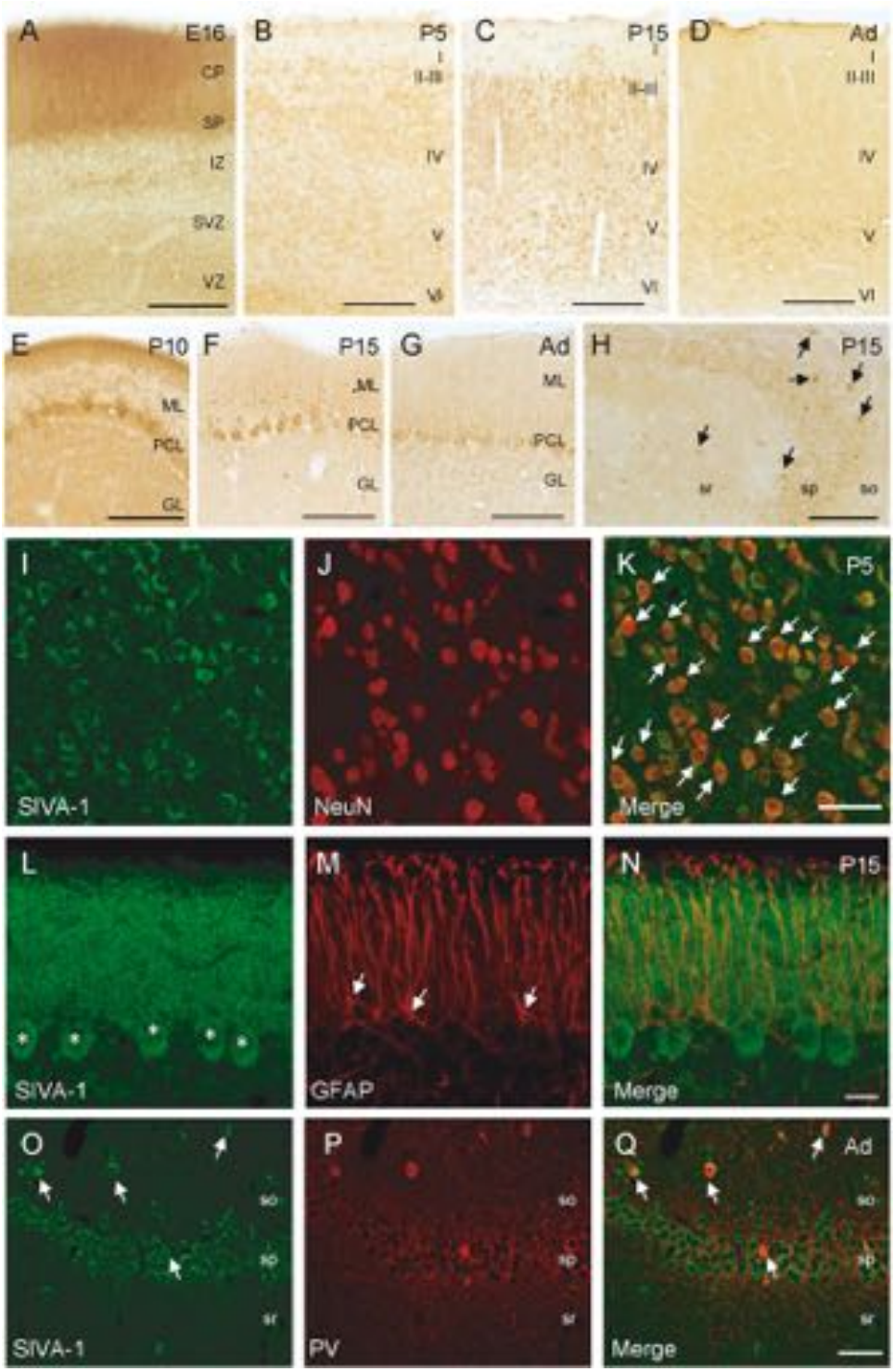

Fig. 2 (See legend on next page.)

(see figure on previous page)
Fig. 2 SIVA-1 is expressed in neurons during the development of the mouse brain. a At embryonic day 16 (E16), neurons in the cortical plate (CP) and subplate (SP) contained SIVA-1. Scale bar 100 µm. **b** At postnatal day 5 (P5), SIVA-1-immunopositive cells were located throughout all cortical layers. Scale bar 200 µm. **c** At postnatal day 15 (P15), SIVA-1-immunoreactive cells were present in all cortical layers. Note that cells located in layers II–III showed intense SIVA-1-immunolabeling. Scale bar 200 µm. **d** In the cerebral cortex of adult mice, expression of SIVA-1 was restricted to cortical cells in layer V. Scale bar 200 µm. **e**–**g** In the cerebellum, the soma and dendrites of Purkinje cells showed SIVA-1 immunostaining at all postnatal stages analyzed. Scale bar 200 µm. **h** In the hippocampus, pyramidal neurons and hippocampal interneurons expressed SIVA-1. Some hippocampal interneurons scattered in all hippocampal layers showed a strong immunostain (arrows in (**h**)). Scale bar 200 µm. **i**–**k** Double immunofluorescence of SIVA-1 and NeuN (arrows) in cortical layer V at P5, showing an almost complete co-localization of the two markers. Scale bar 25 µm. **l**–**n** Immunofluorescence co-localization of SIVA-1 and GFAP in cerebellum at P15 shows SIVA-1 expression in Purkinje cells (asterisks) but not in astrocytes (arrowheads) in the cerebellum. Scale bar 25 µm. **o**–**q** Immunofluorescence co-localization of SIVA-1 and PV shows expression of SIVA-1 in hippocampal interneurons (arrows). MZ marginal zone, IZ intermediate zone, SVZ subventricular zone, VZ ventricular zone, so stratum orines sp stratum pyramidale, sr stratum radiatum, ML molecular layer, PCL Purkinje cell layer, GL granule cell layer.

interneurons throughout the hippocampal layers showed SIVA-1-immunostaining (Fig. 2h, o–q). To confirm the localization of SIVA-1 in neurons, P5 and P15 sections were double immuno-labeled with SIVA-1 and the neuron-specific marker NeuN. This approach revealed an almost complete co-localization of both markers at all the developmental stages analyzed (Fig. 2i–k). Double immunofluorescent studies with the astroglial cell marker Glial fibrillary acidic protein (GFAP) did not show co-localization with SIVA-1 (Fig. 2l–n). Finally, by double immunodetection of SIVA-1 with a specific interneuron subtype marker, parvalbumin (PV), we confirmed the presence of SIVA-1 in hippocampal neurons (Fig. 2o–q). We concluded that SIVA-1 protein is predominantly expressed in developing and adult neurons.

To determine the subcellular localization of SIVA-1, we performed immunocytochemistry in primary cultures of hippocampal neurons. We analyzed SIVA-1 distribution in the cell body, performing co-localization analysis with several organelle markers (i.e., MitoTracker for mitochondria, Rab5 for early endosome, Calnexin for endoplasmic reticulum; Fig. 3a). Manders co-localization coefficients were obtained for each marker (Fig. 3b) and only values higher than 0.5 were considered to indicate co-localization. SIVA-1 showed a mainly cytosolic distribution and co-localized with markers of the cytoplasmic membrane (TrkA; $M1 = 0.68 \pm 0.02$), endocytic vesicles (Rab5; $M1 = 0.66 \pm 0.15$), and cytoskeleton (βIII-tubulin; M1 0.71 ± 0.14). SIVA-1 did not localize to mitochondria (MitoTracker; $M1 = 0.41 \pm 0.04$) or to the endoplasmic reticulum (Calnexin; $M1 = 0.22 \pm 0.15$). SIVA-1 expression was clearly excluded from the nucleus (Hoechst staining; $M1 = 0.06 \pm 0.03$) (Fig. 3a, b). A subcellular protein fractionation assay confirmed the localization of SIVA-1 in cytosolic and light membrane fractions. As expected FAIM-L also was found in cytosolic fraction (Fig. 3c). We also examined SIVA-1 co-localization with synaptic markers in the neurites of 14 DIV hippocampal neurons and found that SIVA-1 can also locate in presynaptic and postsynaptic terminals as indicated by a positive correlation of SIVA-1 immunostaining with both PDS95 and synapsin II (Fig. 3d).

Taken together, our data indicate that SIVA-1 is expressed in the cytoplasm of neurons during development and adult stages. Co-expression of FAIM-L and SIVA-1 in adult neurons in basal conditions suggests that the latter participates in physiological nonlethal processes.

SIVA-1 induces XIAP ubiquitination

XIAP is a potent inhibitor of effector caspases. Its ubiquitination and degradation by the proteasome is crucial for caspase activation and induction of apoptosis[9]. FAIM-L is a XIAP-interacting protein that executes its anti-apoptotic function by inhibiting XIAP ubiquitination, hence stabilizing its levels and inhibition on caspases.

Having reported SIVA-1 interaction with both proteins we proceeded to address whether SIVA-1 interferes with the FAIM-L/XIAP interaction and XIAP ubiquitination.

To this end, we analyzed the FAIM-L/XIAP interaction in the presence of increasing amounts of overexpressed SIVA-1 in PC12 cells (Fig. 4a, lanes 4–6). We performed an immunoprecipitation of Myc-XIAP and found the amount of co-immunoprecipitated FAIM-L to be inversely correlated to SIVA-1 overexpression. Our results thus suggest that SIVA-1 reduces the interaction of FAIM-L with XIAP.

Figure 4b shows ubiquitin immunoprecipitation in HEK293T cells overexpressing HA-tagged SIVA-1, FAIM-L, or a combination of both proteins. XIAP presented basal endogenous ubiquitination, which was enhanced in the presence of SIVA-1 overexpression. FAIM-L overexpression on the other hand reduced XIAP ubiquitination levels, thereby confirming our previous findings[10]. Moreover, overexpression of FAIM-L partially restored SIVA-1-induced XIAP ubiquitination. Overall, our results suggest that SIVA-1 and FAIM-L exert opposite effects on XIAP ubiquitination levels.

SIVA-1 overexpression induces neuronal death by caspase-3 activation

SIVA-1 was first reported as a proapoptotic protein, and its overexpression has been shown to induce apoptosis in various cell lines[12,22–24].

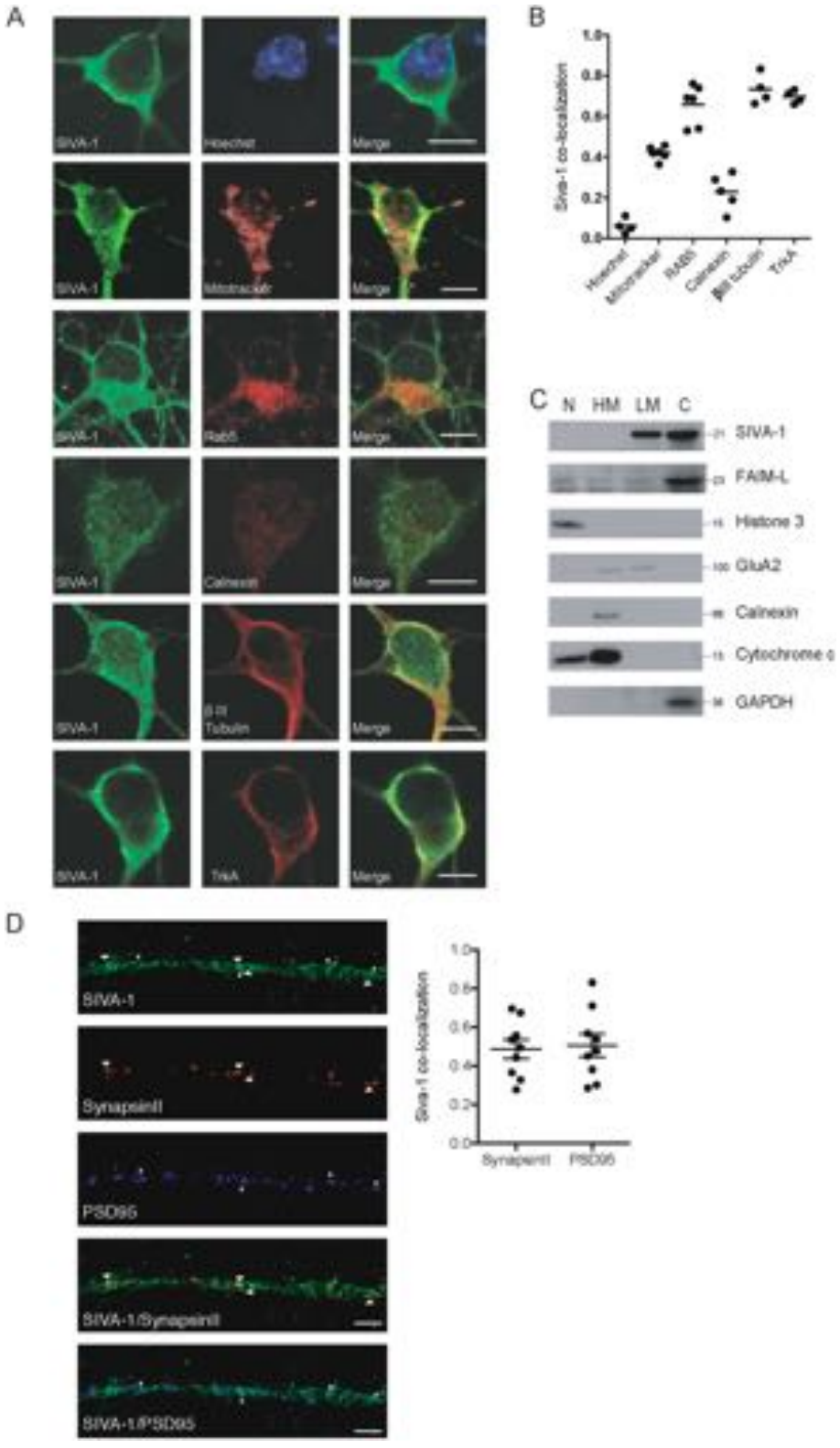

Fig. 3 (See legend on next page.)

(see figure on previous page)

Fig. 3 SIVA-1 has a mainly cytosolic distribution in neurons. a Representative confocal images of hippocampal neurons. At 7 days in vitro, immunofluorescence was performed by staining with anti-SIVA-1 (green), Hoechst (nucleus marker, blue). MitoTracker (mitochondria marker), anti-Rab5 (early endosome marker), anti-calnexin (ER marker), anti-β III Tubulin (cytoskeleton marker), and anti-TrkA (cytosolic membrane marker) were stained in red. Scale bar 10 µm. **b** Graph represents Mander's coefficients M1 corresponding to the channel 1 (SIVA-1) signal that co-located with the channel 2 (cellular markers) signal. Only values higher than 0.5 were considered to indicate co-localization. **c** Subcellular protein fractionation assay of adult mouse brain. Histone 3 antibody was used as a nuclear marker, GluA2 as a plasma membrane marker, anti-calnexin as reticular membrane protein, cytochrome C as a mitochondrial protein, and GAPDH as a cytosolic protein. N nuclear fraction, HM heavy membrane fraction, LM light membrane fraction, C cytosolic fraction. **d** Representative confocal images of hippocampal neurites. At 14 days in vitro, immunofluorescence was performed by staining with anti-SIVA-1 (green), presynaptic markers synapsin II (red) postsynaptic marker PSD95 (blue). The graph represents Mander's coefficient corresponding to co-localization between SIVA-1 and the synaptic markers. SIVA-1 was found to locate in some of the synapses (arrows and asterisks). Scale bar 2 µm.

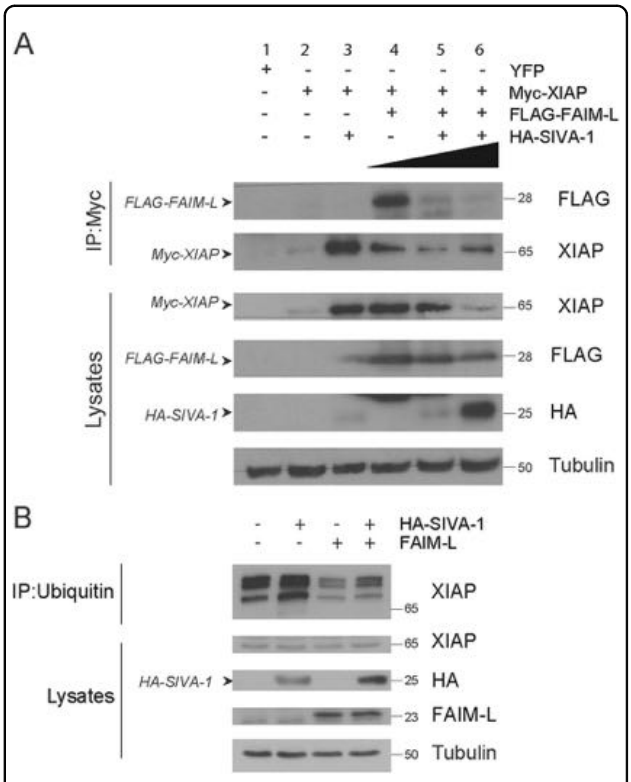

Fig. 4 SIVA-1 promotes XIAP ubiquitination. a PC12 cells were transiently transfected with Myc-XIAP, FLAG-FAIM-L, and two concentrations of HA-SIVA-1. Myc-XIAP was immunoprecipitated using anti-Myc antibody. The membrane was blotted with anti-FLAG to detect FAIM-L and anti-HA to detect SIVA-1. The antibody against XIAP was used as a control of the immunoprecipitation and anti-tubulin as loading control. **b** Cells were transfected with FAIM-L and SIVA-1 (HA-SIVA-1), and endogenous ubiquitin was immunoprecipitated using anti-ubiquitin antibody. The membrane was blotted with FAIM-L, XIAP, and HA to detect SIVA-1, and tubulin was used as a loading control.

Here, we explored the effects of ectopic expression of SIVA-1 in primary hippocampal neurons.

The overexpression of SIVA-1 was sufficient to induce the typical hallmarks of apoptosis, such as chromatin condensation and/or fragmentation, in 10% of the neurons (Fig. 5a, b) respect to the empty vector, strong cleavage of caspase-3 (Fig. 5c), and an evident increase in caspase-3 activity (Fig. 5d). Treating cells with the pan-caspase inhibitor Q-VD consistently abrogated SIVA-1-induced apoptosis (Fig. 5a, b), thereby indicating that SIVA-1 induces caspase-dependent cell death. Western blot analysis of HA-SIVA-1 (Fig. 5e) and immunocytochemistry analysis by counting GFP-positive cells (Fig. 5f) confirmed SIVA-1 overexpression by lentiviral vector in murine hippocampal neurons.

SIVA-1 modulates GluA2 internalization in hippocampal neurons

XIAP and FAIM-L modulate the non-apoptotic function of caspases, such as AMPAR GluA2 subunit internalization, the main mechanism of chLTD[4,11,25]. We found that SIVA-1 interacts with both XIAP and FAIM-L, and is an activator of caspases. We therefore proceeded to analyze whether SIVA-1 also regulates this plasticity process.

We performed a GluA2 internalization assay. Although no change was detected in SIVA-1-overexpressing neurons once NMDA treatment had been applied to induce chLTD, we found that the sole ectopic expression of SIVA-1 was sufficient to induce an increase in the internalization levels of the endogenous AMPAR subunit GluA2 (Fig. 6a–c) in neurons. SIVA-1-induced internalization was blocked by the overexpression of FAIM-L, thereby confirming a functional interaction between these two proteins. As previously described in Martinez-Marmol et al.[11], FAIM-L overexpression abrogated GluA2 internalization induced by chLTD.

Given that caspases are essential for GluA2 internalization, we addressed whether the decrease in GluA2 basal surface level in SIVA-1-overexpressing neurons was caspase-dependent. The presence of the pan-caspase inhibitor Q-VD totally abrogated SIVA-1-induced internalization of GluA2 (Fig. 7a, b), indicating that SIVA-1 modulates postsynaptic receptor levels in a caspase-dependent manner.

To further examine the role of SIVA-1 in the regulation of synaptic receptor internalization, we knocked

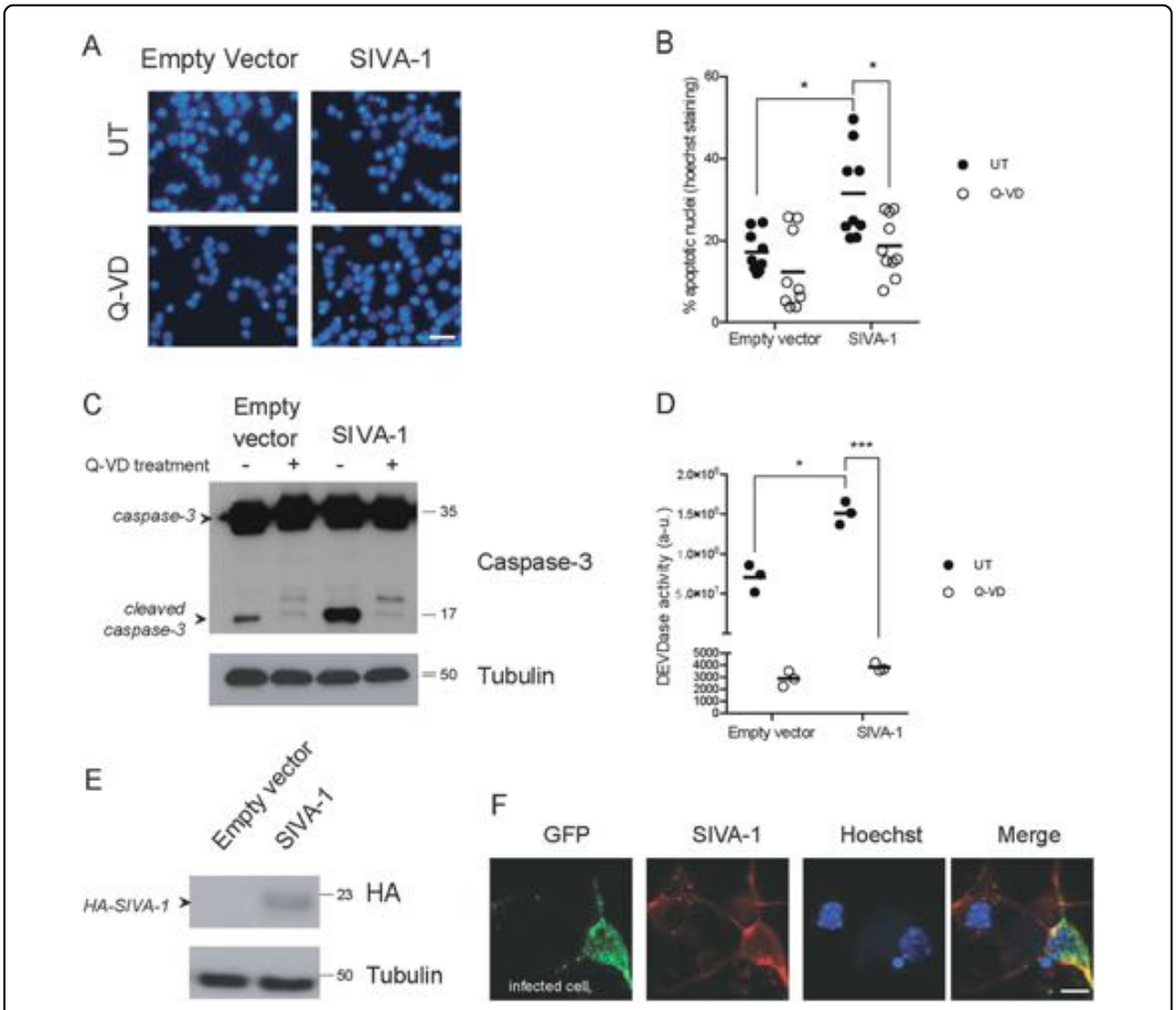

Fig. 5 SIVA-1 induces caspase-3-dependent cell death in neurons. Primary hippocampal neurons were infected for 72 h with lentiviral particles carrying HA-SIVA-1 plasmid. **a** Representative images of Hoechst staining in control and overexpressing cells in the absence or presence of Q-VD, scale bar 20 µm. **b** Quantification of the percentage of nuclei with apoptotic morphology by Hoechst staining. SIVA-1 induced apoptosis, Q-VD treatment rescued cells from SIVA-1-induced cell death. Two-way ANOVA (empty vector vs. SIVA-1, F (1, 36) = 8.537 in untreated condition; F (1, 36) = 7.787 in Q-VD condition) *$p \leq 0.05$. **c** Treatment with 10 µM of pan-caspase inhibitor Q-VD abrogated caspase-3 cleavage. The membrane was immunoblotted with anti-caspase-3 and anti-tubulin as a loading control. **d** DEVDase activity was measured in cells overexpressing SIVA-1 or control empty vector. SIVA-1 induced the activation of caspase-3 (F (1, 8) = 38.69). Q-VD treatment abrogated caspase-3 activity (F (1, 8) = 289.9) UT untreated, Q-VD quinolyl-Val-Asp-OPh. Two-way ANOVA *$p \leq 0.05$; ***$p \leq 0.001$. **e** SIVA-1 expression verified by western blot. HA was used to detect SIVA-1; tubulin was used as a loading control. **f** Immunocytochemistry of SIVA-1 and GFP to confirm lentiviral transfection and overexpression. Hoechst staining was used as a nuclear marker. Scale bar 10 µm.

down SIVA-1 levels and analyzed GluA2 internalization. A decrease in SIVA-1 levels was observed when a shRNA was used (Fig. 7e). Although no change was observed in untreated cells, we did detect a decrease in GluA2 internalization in shSIVA-1-infected neurons after the induction of chLTD. GluA2-induced internalization was marked in shSIVA-1 neurons, but significantly decreased compared to control infected neurons.

SIVA-1 levels are upregulated in chLTD induction

Our findings suggest a role of SIVA-1 in caspase-dependent GluA2 internalization. The expression of several modulators of synaptic plasticity is required for the correct induction and maintenance of plasticity changes[26]. Analysis of SIVA-1 protein levels during chLTD induction showed that they were rapidly induced after 5 min of NMDA treatment (Fig. 8a, b), while SIVA-1 mRNA levels were unaltered (Fig. 8c). The inhibition of protein

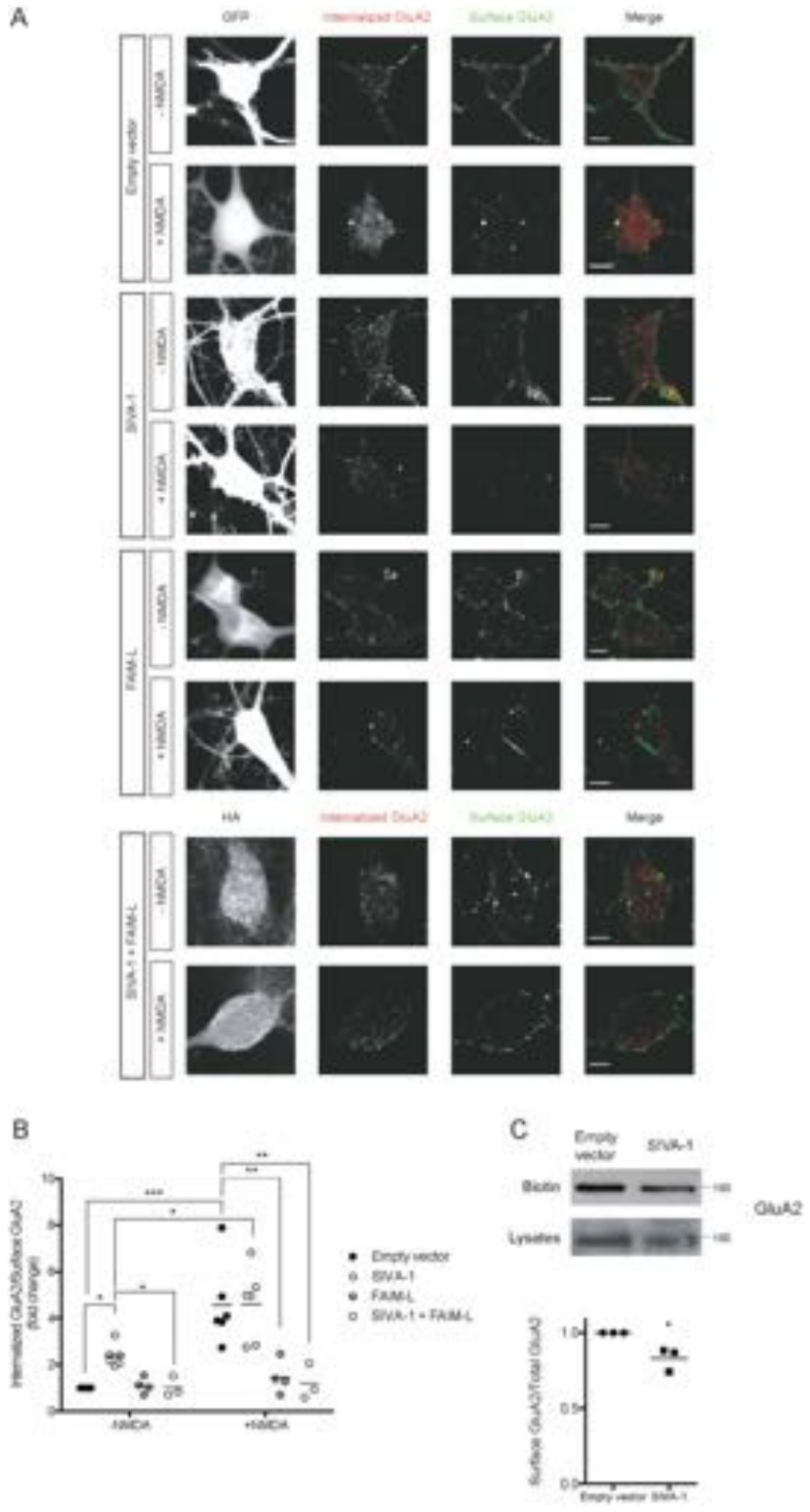

Fig. 6 (See legend on next page.)

(see figure on previous page)
Fig. 6 SIVA-1 promotes GluA2 internalization. a Representative confocal images of neurons transfected with SIVA-1, FAIM-L, or empty vector. GluA2 internalization assay was performed in neurons treated with NMDA to stimulate LTD and in untreated neurons. Only GFP-positive cells (first column) were considered for quantification. Internalized GluA2 (second column, red in merge) and surface GluA2 (third column, green in merge) were measured. Scale bar 10 µm. **b** Results were normalized to empty vector, untreated cells. Induction of chemical LTD induced GluA2 internalization in empty vector condition and SIVA-1 transfected cells (F (1, 632) = 15.85). Non-stimulated cells overexpressing SIVA-1 showed an increase in GluA2 internalization. FAIM-L overexpression blocked LTD induction (F (3, 632) = 15.17), and its overexpression with SIVA-1 in untreated cells restored basal levels of receptor internalization (F (3, 632) = 15.85). Each point represents an independent experimental repeat in which 15–20 cells were analyzed. UT untreated, NMDA N-methyl-D-aspartate. **c** GluA2 surface receptor was isolated with the Biotin surface assay in hippocampal cells transfected with SIVA-1 or empty vector as a control. Lower panel shows quantification of GluA2 surface receptor (t (2) = 3,060). Two-way ANOVA $*p \leq 0.05$; $**p \leq 0.01$; $***p \leq 0.0001$.

translation by cycloheximide blocked the increment of SIVA-1 (Fig. 8d), thereby suggesting posttranscriptional regulation.

Induction of chLTD by NMDA stimulation leads to an increase in Ca^{2+} inflow in neurons, followed by calcineurin and caspase-3 activation, and the internalization of AMPAR. Blockage of calcium by BAPTA-AM treatment inhibited the increase in SIVA-1 expression after chLTD. This observation thus suggests that the first steps of the NMDA stimulation pathways are essential for SIVA-1 induction (Fig. 8d).

In conclusion, we propose SIVA-1 as a new modulator of synaptic plasticity. We demonstrate that SIVA-1 is increased in chLTD, where it activates caspase-3. We propose that SIVA-1, by modulating the FAIM-L/XIAP interaction, induces XIAP degradation and consequent activation of caspases. SIVA-1 therefore emerges as a novel regulator of caspase-dependent apoptotic and non-apoptotic functions in neurons (Fig. 8e).

Discussion

Apoptosis is an essential process for the homeostasis of organisms. It is subjected to multiple and tight mechanisms of regulation, but it can also be unscheduled triggered in pathological processes such as degenerative diseases. In these pathologies, the mechanisms of cellular protection (i.e., antiapoptotic mechanisms) fail. Understanding the underlying components of the dysregulation may provide new opportunities for therapeutic intervention. The disassembly of neuronal integrity during cell death is regulated by cysteine-aspartic acid proteases called caspases. These proteins have been widely characterized for their role in apoptosis[27] and in non-apoptotic functions. In neurons, caspases locate in dendrites, axons, and in presynaptic and postsynaptic terminals. At these sites, they can be locally activated[4] and participate in synaptic plasticity and growth cone motility, among other non-apoptotic functions[28].

FAIM-L is a neuron-specific death receptor antagonist that protects neurons against a variety of neurotoxic insults[6,8,10,29]. We have reported that FAIM-L protects XIAP, an inhibitor of caspases, from ubiquitination and degradation. By stabilizing XIAP levels, FAIM-L regulates caspase-3 activation in apoptosis and exerts non-apoptotic functions[11]. To characterize FAIM-L in depth, we performed a two-hybrid assay to detect interacting proteins.

We identified and confirmed SIVA-1 to be a functional partner of FAIM-L. SIVA-1 was first reported as a CD27-interacting protein[12]. SIVA-1 plays a critical proapoptotic role in several cellular types and is overexpressed in various pathological circumstances, such as ischemic injury and Coxsakie virus B3 infection[14,30–32]. Resch et al.[13] demonstrated that SIVA-1 interacts with XIAP, and suggested that the interaction leads to mutual interference with their action.

Our analysis of SIVA-1 expression and distribution in brain tissues at embryonic and adult stages shows that this protein is expressed in both developing and adult neurons. Nervous system development requires a precise regulation of programmed cell death, and many apoptotic proteins have been found to be crucial. Among these, SIVA-1 appears to play a key role during development, as its deletion has been reported to result in embryonic lethality in mice[33]. The presence of SIVA-1 expression is maintained in adult cortical and hippocampal neurons, thereby suggesting that this protein contributes to neuronal physiological functions.

We examined the subcellular distribution of SIVA-1 in primary hippocampal neurons. Previous studies carried out in various cell types reported controversial findings on the subcellular localization of this protein. Some described that the ectopic expression of SIVA-1 accumulates in the nucleus[24,34,35] and that it can interact with cell surface membrane receptors[12,23,24,34]. Moreover, Jacobs et al.[14] reported membrane localization of SIVA-1 upon DNA-damage induced in the brain. However, most of the functions exerted by SIVA-1 in apoptosis take place in the cytoplasm[36]. Our analysis shows that, in cultured hippocampal neurons, SIVA-1 is located in cellular bodies, neurites and also in synapses, and that it presents a diffuse cytosolic pattern that excludes the nucleus, similar to the localization pattern described for FAIM-L.

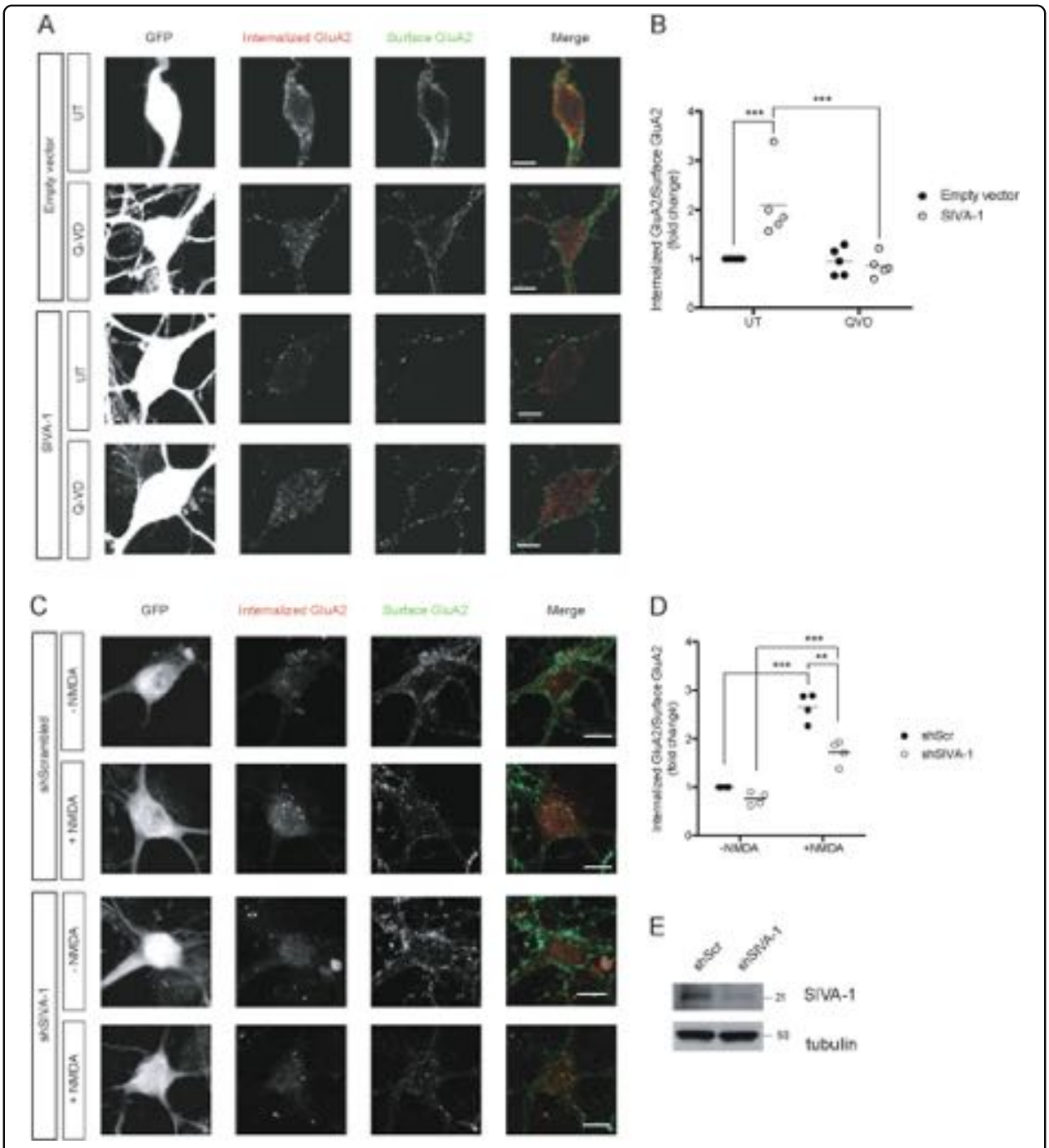

Fig. 7 SIVA-1 modulates AMPAR internalization in a caspase-dependent manner. a Representative confocal images of neurons transfected with SIVA-1 or empty vector and treated with 10 μM of Q-VD (caspase inhibitor). Only GFP-positive cells (first column) were considered for quantification (left panel). Scale bar 10 μm. **b** The results of the quantification of internalized GluA2 vs. surface GluA2 were normalized to empty vector, untreated cells (right panel). Each point represents an independent experimental repeat in which 15–20 cells were analyzed. SIVA-1-transfected cells showed greater internalization of GluA2 receptor (F (1, 97) = 3.840), Q-VD treatment restored internalization to basal levels (F (1, 97) = 7.345). Two-way ANOVA ***$p \leq 0.001$. **c** Representative confocal images of neurons transfected with vectors carrying shSIVA-1 or shScramble as control. The GluA2 internalization assay was performed in neurons treated with NMDA to stimulate LTD and in untreated neurons. Only GFP-positive cells (first column) were considered for quantification. Internalized GluA2 (second column, red in merge) and surface GluA2 (third column, green in merge) were measured. Scale bar 10 μm. **d** The results of the quantification of internalized GluA2 vs. surface GluA2 were normalized to shScrambled, untreated cells. Each point represents an independent experimental repeat in which 15–20 cells were analyzed. NMDA treatment induced GluA2 internalization in both shScrambled and shSIVA-1 cells (F (1, 84) = 167.1). However, shSIVA-1 cells treated with NMDA showed a significant decrease in receptor internalization (F (1, 84) = 33.5). Two-way ANOVA **$p \leq 0.01$; ***$p \leq 0.001$. shScr shScrambled.

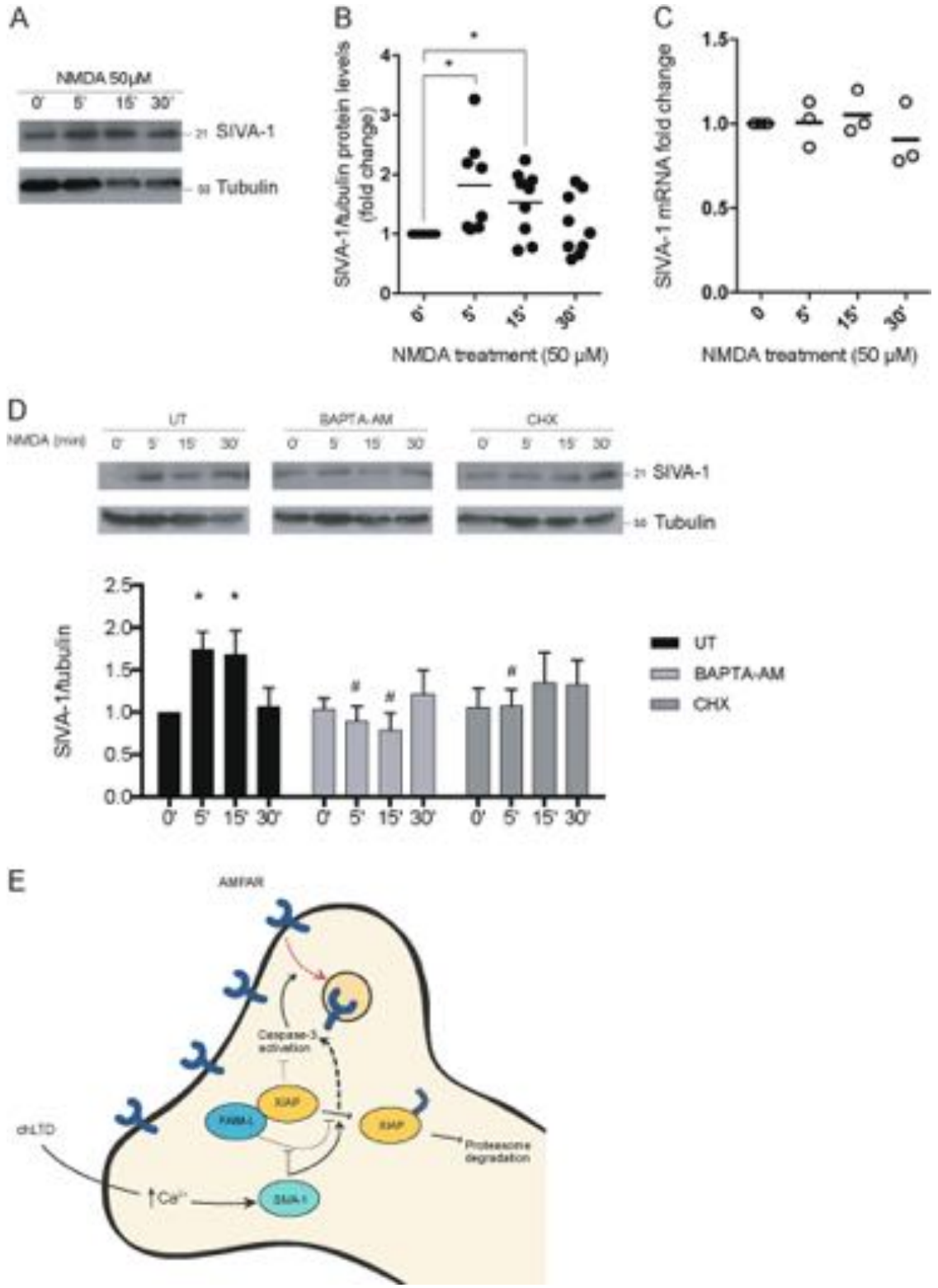

Fig. 8 (See legend on next page.)

(see figure on previous page)

Fig. 8 Levels of SIVA-1 increase after NMDA treatment. a Primary neuronal cells were treated with 50 μM of NMDA at different time points (0–30 min) and protein expression of SIVA-1 was analyzed by SDS-PAGE. Anti-tubulin was used as a loading control. **b** SIVA-1 expression increased with 5 min, and 15 min treatment of NMDA. *t* test (t (15) = 2427; t(15) = 2755). *$p \leq 0.05$. **c** qPCR revealed no change in SIVA-1 mRNA expression after treatment. **d** The increase in SIVA-1 levels (two-way ANOVA $F(2, 6) = 1712$) was blocked by pretreatments with 50 μM of BAPTA-AM for 30 min or 1 μg/ml of cycloheximide for 1 h (two-way ANOVA (F (3, 9) = 1326)). *$p \leq 0.05$ for comparison between time points in the same treatment, $^{\#}p \leq 0.05$ for comparison between treatments. **e** Schematic representation of SIVA-1 function. In neurons, SIVA-1 was increased after chemical LTD induction. SIVA-1 destabilized XIAP by increasing its ubiquitination and impairing its interaction with FAIM-L. We propose that this is one of the mechanisms through which SIVA-1 triggers caspase-3 activation in neurons and consequent apoptosis and caspase-3-dependent GluA2 internalization. CHX cycloheximide, BAPTA-AM 1,2-Bis(2-aminophenoxy)ethane-N,N,N′,N′-tetraacetic acid tetrakis(acetoxymethyl ester), chLTD chemical long-term depression.

We then analyzed the possible functions of SIVA-1 in relation to the previously described FAIM-L function on XIAP modulation[10,11]. Our data show that SIVA-1 overexpression displaces the FAIM-L/XIAP interaction. Loss of interaction with FAIM-L can be sufficient to promote XIAP instability, thereby inducing ubiquitination-mediated proteasomal degradation. We reveal that SIVA-1 overexpression also has a direct effect on promoting XIAP ubiquitination. Given that SIVA-1 is a XIAP-interacting protein, it might confer structural changes to XIAP that permit auto-ubiquitination, or it may serve as an ubiquitin ligase on XIAP. In fact, SIVA-1 has been described to have E3 ubiquitin ligase activity and to direct E3 ubiquitin ligases to promote the ubiquitination of other proteins and consequent changes in their function or stability[37,38]. In a complex process such as apoptosis, which involves hundreds of molecules, the regulation between proapoptotic and antiapoptotic proteins is common and can often be mediated by ubiquitination[39].

Here, we report the proapoptotic activity of SIVA-1 in primary cultures of hippocampal neurons. SIVA-1 overexpression is sufficient to induce apoptosis through effector caspase activation. We propose that the promotion of cell death induced by SIVA-1 overexpression occurs through XIAP destabilization and consequent inhibition of XIAP action on effector caspases. Here we provide evidence that SIVA-1 participates in XIAP modulation and apoptosis and that it exerts the opposite function to FAIM-L.

We addressed whether SIVA-1 has a neuron-specific non-apoptotic role. We demonstrate that SIVA-1 is expressed in cultured hippocampal neurons in the absence of proapoptotic stimuli. This finding points to a non-apoptotic role of the protein. We studied LTD, a well characterized caspase-dependent mechanism, which requires a controlled activation of the same mitochondrial pathway and that involves the same proteins that can lead to apoptotic cell death. Many apoptotic regulatory proteins modulate caspase activation in synaptic depression, and among these we find both FAIM-L and XIAP as inhibitors of the process. We used as a model for our study the extensively described chLTD. After NMDA stimulation, chLTD is induced. A rapid increase in calcium levels is triggered by NMDA receptor activation, followed by an involvement of calcineurin and caspase-3. The activation culminates in AMPAR internalization and therefore synaptic weakening[40]. When measuring surface AMPAR levels in our cellular primary cultures, we observed that SIVA-1 induces an increase in GluA2 internalization in non-stimulated neurons in a caspase-dependent manner. Moreover, SIVA-1 knockdown significantly decreases receptor internalization following chLTD. Therefore SIVA-1 emerges as another regulator of apoptosis that is also required for functions not related to cell death. FAIM-L overexpression abrogates GluA2 internalization following chLTD and also restores SIVA-1 induction of GluA2 internalization in hippocampal neurons.

Protein composition at synapses is modulated in response to neuronal activity, through new synthesis and removal[41,42]. We show an increase in SIVA-1 protein levels in primary cultures after a few minutes of NMDA treatment. The increase is blocked by cycloheximide and does not affect SIVA-1 mRNA levels, thereby indicating specific translational regulation. The increase in SIVA-1 could be directly associated with NMDA receptor stimulation after treatment, since a calcium chelating agent, BAPTA-AM, blocks this increase. BAPTA-AM pretreatment has been reported to block LTD induction, thus eliminating available calcium ions to start a stimulation response after NMDA or electrical application[43,44]. The enhanced SIVA-1 expression in chLTD supports the relevance of this protein in the modulation of this synaptic plasticity mechanism.

In summary, our results reveal novel key roles of SIVA-1 in neurons. We show that SIVA-1 interacts with both FAIM-L and XIAP and that it is also a caspase activator. We associate SIVA-1-induced caspase activation with neural apoptosis, which is consistent with its previously described functions. Moreover, we demonstrate a novel function of SIVA-1 as regulator of synaptic function.

Acknowledgements
This work was funded by grants awarded by the Spanish "Ministerio de Economía y Competitividad" (SAF2013-47989-R, SAF2016-80236-R, CIBERNED CB06/05/1104 and PIE13/00027), the Generalitat de Catalunya (2014SGR1609), and the Fundació La Marató de TV3 (201414-30) to J.X.C. E.C. is supported by a

predoctoral fellowship from the Vall d´Hebron Research Institute (VHIR). R.B. is supported by a predoctoral fellowship from the Spanish "Ministerio de Economía y Competitividad" (BES-2018-080846).

Author details
[1]Cell Signaling and Apoptosis Group, Vall d'Hebron Research Institute (VHIR), 08035 Barcelona, Spain. [2]Centro de Investigación Biomédica en Red sobre Enfermedades Neurodegenerativas (CIBERNED), ISCIII, 28031 Madrid, Spain. [3]Institut de Neurociències, Departament de Bioquímica i Biologia Molecular, Facultat de Medicina, Universitat Autònoma de Barcelona, 08031 Bellaterra, Spain. [4]Institut de Neurociències, Universitat de Barcelona, Bellaterra, Spain. [5]Department of Cell Biology, Physiology and Immunology, Institut de Neurociències, Universitat de Barcelona, 08031 Barcelona, Spain. [6]Group of Translational Research in Child and Adolescent Cancer, Vall d'Hebron Research Institute (VHIR)-UAB, 08035 Barcelona, Spain. [7]Cell Cycle Laboratory, Institut de Recerca Biomèdica de Lleida (IRBLleida), and Departament de Ciències Mèdiques Bàsiques; Facultat de Medicina, Universitat de Lleida, 25198 Lleida, Catalonia, Spain. [8]ICREA Academia, Barcelona, Spain. [9]Present address: Department of Pathology, NYU Langone Health, New York 10016 NY, USA

Author contributions
E.C., L.P.-F., B.B.-Z., E.S., R.S.M., J.X.C., and M.J.P.-G. designed the research; E.C., L. P.-F., R.B.-R., M.P., M.F.S., R.F.-H., E.G., and R.S.M. performed the research; E.C., M. P., L.P.-F., and E.G. analyzed the data; and E.C., J.X.C, and M.J.P.-G. wrote the paper.

Conflict of interest
The authors declare that they have no conflict of interest.

Publisher's note
Springer Nature remains neutral with regard to jurisdictional claims in published maps and institutional affiliations.

Received: 7 June 2019 Revised: 8 January 2020 Accepted: 9 January 2020
Published online: 03 February 2020

References

1. Fuchs, Y. & Steller, H. Live to die another way: modes of programmed cell death and the signals emanating from dying cells. *Nat. Rev. Mol. Cell Biol.* **16**, 329–344 (2015).
2. Hyman, B. T. & Yuan, J. Apoptotic and non-apoptotic roles of caspases in neuronal physiology and pathophysiology. *Nat. Rev. Neurosci.* **13**, 395–406 (2012).
3. Hollville, E. & Deshmukh, M. Physiological functions of non-apoptotic caspase activity in the nervous system. *Semin Cell Dev. Biol.* **82**, 127–136 (2018).
4. Li, Z. et al. Caspase-3 activation via mitochondria is required for long-term depression and AMPA receptor internalization. *Cell* **141**, 859–871 (2010).
5. Erturk, A., Wang, Y. & Sheng, M. Local pruning of dendrites and spines by caspase-3-dependent and proteasome-limited mechanisms. *J. Neurosci.* **34**, 1672–1688 (2014).
6. Carriba, P. et al. Amyloid-beta reduces the expression of neuronal FAIM-L, thereby shifting the inflammatory response mediated by TNFalpha from neuronal protection to death. *Cell Death Dis.* **6**, e1639 (2015).
7. Tu, S., Okamoto, S., Lipton, S. A. & Xu, H. Oligomeric Abeta-induced synaptic dysfunction in Alzheimer's disease. *Mol. Neurodegener.* **9**, 48 (2014).
8. Segura, M. F. et al. The long form of Fas apoptotic inhibitory molecule is expressed specifically in neurons and protects them against death receptor-triggered apoptosis. *J. Neurosci.* **27**, 11228–11241 (2007).
9. Scott, F. L. et al. XIAP inhibits caspase-3 and -7 using two binding sites: evolutionarily conserved mechanism of IAPs. *EMBO J.* **24**, 645–655 (2005).
10. Moubarak, R. S. et al. FAIM-L is an IAP-binding protein that inhibits XIAP ubiquitinylation and protects from Fas-induced apoptosis. *J. Neurosci.* **33**, 19262–19275 (2013).
11. Martinez-Marmol, R. et al. FAIM-L regulation of XIAP degradation modulates synaptic long-term depression and axon degeneration. *Sci. Rep.* **6**, 35775 (2016).
12. Prasad, K. V. et al. CD27, a member of the tumor necrosis factor receptor family, induces apoptosis and binds to Siva, a proapoptotic protein. *Proc. Natl Acad. Sci. USA* **94**, 6346–6351 (1997).
13. Resch, U. et al. Siva1 is a XIAP-interacting protein that balances NFkappaB and JNK signalling to promote apoptosis. *J. Cell Sci.* **122**, 2651–2661 (2009).
14. Jacobs, S. B., Basak, S., Murray, J. I., Pathak, N. & Attardi, L. D. Siva is an apoptosis-selective p53 target gene important for neuronal cell death. *Cell Death Differ.* **14**, 1374–1385 (2007).
15. Dalby, B. et al. Advanced transfection with Lipofectamine 2000 reagent: primary neurons, siRNA, and high-throughput applications. *Methods* **33**, 95–103 (2004).
16. Susin, S. A. et al. Two distinct pathways leading to nuclear apoptosis. *J. Exp. Med.* **192**, 571–580 (2000).
17. Galenkamp, K. M. et al. TNFalpha sensitizes neuroblastoma cells to FasL-, cisplatin- and etoposide-induced cell death by NF-kappaB-mediated expression of Fas. *Mol. Cancer* **14**, 62 (2015).
18. Urresti, J. et al. Lifeguard inhibits Fas ligand-mediated endoplasmic reticulum-calcium release mandatory for apoptosis in type II apoptotic cells. *J. Biol. Chem.* **291**, 1221–1234 (2016).
19. Schindelin, J. et al. Fiji: an open-source platform for biological-image analysis. *Nat. Methods* **9**, 676–682 (2012).
20. Dunn, K. W., Kamocka, M. M. & McDonald, J. H. A practical guide to evaluating colocalization in biological microscopy. *Am. J. Physiol. Cell Physiol.* **300**, C723–C742 (2011).
21. Livak, K. J. & Schmittgen, T. D. Analysis of relative gene expression data using real-time quantitative PCR and the 2(-Delta Delta C(T)) Method. *Methods* **25**, 402–408 (2001).
22. Yoon, Y., Ao, Z., Cheng, Y., Schlossman, S. F. & Prasad, K. V. Murine Siva-1 and Siva-2, alternate splice forms of the mouse Siva gene, both bind to CD27 but differentially transduce apoptosis. *Oncogene* **18**, 7174–7179 (1999).
23. Spinicelli, S. et al. GITR interacts with the pro-apoptotic protein Siva and induces apoptosis. *Cell Death Differ.* **9**, 1382–1384 (2002).
24. Py, B., Slomianny, C., Auberger, P., Petit, P. X. & Benichou, S. Siva-1 and an alternative splice form lacking the death domain, Siva-2, similarly induce apoptosis in T lymphocytes via a caspase-dependent mitochondrial pathway. *J. Immunol.* **172**, 4008–4017 (2004).
25. Li, Z., Okamoto, K., Hayashi, Y. & Sheng, M. The importance of dendritic mitochondria in the morphogenesis and plasticity of spines and synapses. *Cell* **119**, 873–887 (2004).
26. Klann, E. & Dever, T. E. Biochemical mechanisms for translational regulation in synaptic plasticity. *Nat. Rev. Neurosci.* **5**, 931–942 (2004).
27. Riedl, S. J. & Shi, Y. Molecular mechanisms of caspase regulation during apoptosis. *Nat. Rev. Mol. Cell Biol.* **5**, 897–907 (2004).
28. Gilman, C. P. & Mattson, M. P. Do apoptotic mechanisms regulate synaptic plasticity and growth-cone motility? *Neuromol. Med.* **2**, 197–214 (2002).
29. Liu, X. et al. SRT1720 promotes survival of aged human mesenchymal stem cells via FAIM: a pharmacological strategy to improve stem cell-based therapy for rat myocardial infarction. *Cell Death Dis.* **8**, e2731 (2017).
30. Singaravelu, K. & Padanilam, B. J. p53 target Siva regulates apoptosis in ischemic kidneys. *Am. J. Physiol. Ren. Physiol.* **300**, F1130–F1141 (2011).
31. Padanilam, B. J. & Lewington, A. J. & Hammerman, M. R. Expression of CD27 and ischemia/reperfusion-induced expression of its ligand Siva in rat kidneys. *Kidney Int.* **54**, 1967–1975 (1998).
32. Henke, A. et al. Apoptosis in coxsackievirus B3-caused diseases: interaction between the capsid protein VP2 and the proapoptotic protein siva. *J. Virol.* **74**, 4284–4290 (2000).
33. Van Nostrand, J. L. et al. The p53 target gene SIVA enables non-small cell lung cancer development. *Cancer Discov.* **5**, 622–635 (2015).
34. Lin, F. T., Lai, Y. J., Makarova, N., Tigyi, G. & Lin, W. C. The lysophosphatidic acid 2 receptor mediates down-regulation of Siva-1 to promote cell survival. *J. Biol. Chem.* **282**, 37759–37769 (2007).
35. Balci-Peynircioglu, B. et al. Pyrin, product of the MEFV locus, interacts with the proapoptotic protein, Siva. *J. Cell Physiol.* **216**, 595–602 (2008).
36. Chu, F. et al. The Siva-1 putative amphipathic helical region (SAH) is sufficient to bind to BCL-XL and sensitize cells to UV radiation induced apoptosis. *Apoptosis* **9**, 83–95 (2004).
37. Wang, X. et al. Siva1 inhibits p53 function by acting as an ARF E3 ubiquitin ligase. *Nat. Commun.* **4**, 1551 (2013).
38. Han, J. et al. SIVA1 directs the E3 ubiquitin ligase RAD18 for PCNA mono-ubiquitination. *J. Cell Biol.* **205**, 811–827 (2014).
39. Lee, J. C. & Peter, M. E. Regulation of apoptosis by ubiquitination. *Immunol. Rev.* **193**, 39–47 (2003).

40. Benarroch, E. E. Glutamatergic synaptic plasticity and dysfunction in Alzheimer disease: Emerging mechanisms. *Neurology* **91**, 125–132 (2018).
41. Sajikumar, S. & Frey, J. U. Anisomycin inhibits the late maintenance of long-term depression in rat hippocampal slices in vitro. *Neurosci. Lett.* **338**, 147–150 (2003).
42. Kauderer, B. S. & Kandel, E. R. Capture of a protein synthesis-dependent component of long-term depression. *Proc. Natl Acad. Sci. USA* **97**, 13342–13347 (2000).
43. Mulkey, R. M. & Malenka, R. C. Mechanisms underlying induction of homosynaptic long-term depression in area CA1 of the hippocampus. *Neuron* **9**, 967–975 (1992).
44. Artola, A. & Singer, W. Long-term depression of excitatory synaptic transmission and its relationship to long-term potentiation. *Trends Neurosci.* **16**, 480–487 (1993).

PLOS ONE

RESEARCH ARTICLE

Identification and characterization of new isoforms of human fas apoptotic inhibitory molecule (FAIM)

Elena Coccia[1,2,3☯], Isabel Calleja-Yagüe[1,2,3☯], Laura Planells-Ferrer[1,2,3], Blanca Sanuy[1,2,3], Belen Sanz[1,2,3¤a], Joaquin López-Soriano[1,2,3], Rana S. Moubarak[1,2,3¤b], Francina Munell[4], Bruna Barneda-Zahonero[1,2,3], Joan X. Comella[1,2,3]*, M. Jose Pérez-García[1,2,3]*

1 Cell Signaling and Apoptosis Group, Vall d´Hebron Institute of Research (VHIR), Barcelona, Spain, **2** Centro de Investigación Biomédica en Red sobre Enfermedades Neurodegenerativas (CIBERNED), ISCIII, Madrid, Spain, **3** Institut de Neurociències, Departament de Bioquímica i Biologia Molecular, Facultat de Medicina, Universitat Autònoma de Barcelona, Bellaterra, Spain, **4** Pediatric Neurology Group, Vall d´Hebron Institute of Research (VHIR), Barcelona, Spain

☯ These authors contributed equally to this work.
¤a Current address: Cell Division and Cancer Group, Spanish National Cancer Research Centre (CNIO), Madrid, Spain
¤b Current address: Department of Pathology, NYU Langone Medical Center, New York, United States of America
* maria.perez@vhir.org (MJPG); joan.comella@vhir.org (JXC)

Citation: Coccia E, Calleja-Yagüe I, Planells-Ferrer L, Sanuy B, Sanz B, López-Soriano J, et al. (2017) Identification and characterization of new isoforms of human fas apoptotic inhibitory molecule (FAIM). PLoS ONE 12(10): e0185327. https://doi.org/10.1371/journal.pone.0185327

Editor: Valentin Ceña, Universidad de Castilla-La Mancha, SPAIN

Received: April 27, 2017

Accepted: September 11, 2017

Published: October 5, 2017

Data Availability Statement: All relevant data are within the paper and its Supporting Information files.

Funding: This work was funded by the Spanish Government "Ministerio de Economía y Competitividad" (SAF2013-47989-R, SAF2016-80236-R, CIBERNED CB06/05/1104 and PIE13/00027), Generalitat de Catalunya (2014SGR1609), and Fundació La Marató de TV3 (201414-30) to JXC. Fellowship BES-2014-069550 to IC-Y.

Abstract

Fas Apoptosis Inhibitory Molecule (*FAIM*) is an evolutionarily highly conserved death receptor antagonist, widely expressed and known to participate in physiological and pathological processes. Two *FAIM transcript* variants have been characterized to date, namely FAIM short (FAIM-S) and FAIM long (FAIM-L). FAIM-S is ubiquitously expressed and serves as an anti-apoptotic protein in the immune system. Furthermore, in neurons, this isoform promotes NGF-induced neurite outgrowth through NF-κB and ERK signaling. In contrast FAIM-L is found only in neurons, where it exerts anti-apoptotic activity against several stimuli. In addition to these two variants, *in silico* studies point to the existence of two additional isoforms, neither of which have been characterized to date. In this regard, here we confirm the presence of these two additional FAIM isoforms in human fetal brain, fetal and adult testes, and placenta tissues. We named them FAIM-S_2a and FAIM-L_2a since they have the same sequence as FAIM-S and FAIM-L, but include exon 2a. PCR and western blot revealed that FAIM-S_2a shows ubiquitous expression in all the tissues and cellular models tested, while FAIM-L_2a is expressed exclusively in tissues of the nervous system. In addition, we found that, when overexpressed in non-neuronal cells, the splicing factor nSR100 induces the expression of the neuronal isoforms, thus identifying it as responsible for the generation of FAIM-L and FAIM-L_2a. Functionally, FAIM-S_2a and FAIM-L_2a increased neurite outgrowth in response to NGF stimulation in a neuronal model. This observation thus, supports the notion that these two isoforms are involved in neuronal differentiation. Furthermore, subcellular fractionation experiments revealed that, in contrast to FAIM-S and FAIM-L, FAIM-S_2a and FAIM-L_2a are able to localize to the nucleus, where they may

Competing interests: The authors have declared that no competing interests exist.

have additional functions. In summary, here we report on two novel FAIM isoforms that may have relevant roles in the physiology and pathology of the nervous system.

Introduction

The homeostasis of tissues, organs, and the whole organism is maintained by a fine and continuous balance between cell growth, differentiation, and death. Cell death is, therefore, a fundamental process of life. In this regard, genomes contain several sophisticated cell death-inducing machineries. The regulation of cell death and survival is critical for controlling the number of cells in an organism. Deregulation of these processes can result in pathologies such as neurodegeneration and cancer, conditions characterized by excess of cell death or proliferation, respectively. During development, the removal of excess cells through programmed cell death (PCD) is essential for the establishment and maintenance of the nervous system. Similar regulatory mechanisms that control PCD during development also appear to control PCD in the adult brain[1]. Various proteins regulate these processes and they are organized into two main pathways. The intrinsic pathway is activated by intrinsic signals, such as DNA damage and growth factor starvation. These signals induce the permeabilization of the mitochondrial outer membrane by activating Bcl-2 homology domain 3 (BH3)-only proteins, thus triggering the caspase-9-dependent cascade[2]. In contrast, the extrinsic pathway is activated by death ligands, which bind and activate Death Receptors (DRs) on the cytoplasmic membrane, thereby inducing the recruitment of caspase-8 and/or -10. These initiator caspases trigger apoptosis by activating effector caspases[3]. Various endogenous proteins such as c-FLIP, cIAPs, XIAP, Lifeguard and FAIM are able to inhibit DR-induced apoptosis[4–7].

FAIM molecules are a recently discovered family of evolutionarily conserved proteins structurally unrelated to other DR-induced apoptosis inhibitors[8]. Human *FAIM1* is located in the long arm of chromosome 3 (3q22.3), and it contains six exons and three putative translational start sites in exon 3. To date, two protein products namely FAIM-L and FAIM-S, generated by alternative splicing (AS) have been described[9].

In 1999, FAIM-S was isolated from Fas-resistant B lymphocytes and described as a 20 kDa soluble protein that is ubiquitously expressed and capable of inhibiting Fas-induced cell death [10]. Later, FAIM-S was reported to promote neuronal differentiation and branching through activation of the ERK and NF-kB pathways upon stimulation of nerve growth factor (NGF)[5]. Studies using mouse knock-out of FAIM-L and FAIM-S revealed a phenotype of spontaneous non-hyperphagic obesity accompanied by hepatosteatosis, adipocyte hypertrophy, dyslipidaemia, hyperglycaemia and hyperinsulinaemia[11].

With 66 more nucleotides than FAIM-S, FAIM-L is generated by the inclusion of exon 2b and is expressed exclusively in neurons[9]. Also, FAIM-L has a cytosolic distribution and exerts protection against TNFα- and Fas-induced apoptosis, thereby preventing the activation of caspase 8[12], and/or by interacting with and stabilizing the anti-apoptotic protein XIAP [13]. FAIM-L also acts as a regulator in two neuronal processes that require caspase-3 activation, namely: axon-selective pruning and long-term depression. By stabilizing of XIAP levels and consequent caspase-3 inhibition, FAIM-L prevents these two processes in models of neuronal cells *in vitro*[14]. It has been proposed that loss of FAIM-L function is involved in neurodegenerative diseases such as Alzheimer's disease (AD). In this regard, FAIM-L levels are reduced in the hippocampus of mouse models of AD (APP/PS1; APP) and in post-mortem human tissue samples and they play a key role in determining the fate of neurons when these cells are exposed to molecules with pro- and anti-inflammatory effects[15].

In silico gene expression analysis of human *FAIM1* pointed to the existence of two transcript splice variants of FAIM-S and FAIM-L that include an additional exon. To address this question, here we validate the existence of two new isoforms at the mRNA (both) and protein level (FAIM-S_2a) and show their capacity to modulate neurite outgrowth. Our findings thus, support the notion that these two new variants participate in neuronal differentiation. They also show that FAIM-L and FAIM-L_2a are expressed exclusively in tissues of the nervous system and are regulated by the splicing factor nSR100.

Materials and methods

Reagents

Recombinant human sFasL (superFasL, Enzo Life Sciences) and NGF (Sigma-Aldrich, Saint Louis; MO, USA) were used at a concentration of 100 ng/ml. All biochemical reagents were purchased from ThermoFisher Scientific™ (Waltham, MA, USA).

Human tissue samples

Frozen human samples of fetal brain, fetal and adult testes and placenta were obtained from aborted fetuses at the Pediatric Neurology Unit of the *Hospital Universitari Vall d´Hebron*.

Ethics statement

The use of tissues from aborted fetuses was approved by the Ethics Committee of the *Hospital Universitari Vall d'Hebron*.

Cell culture

All cell lines were obtained from the American Type Culture Collection (ATCC, Rockville, MD). Rat pheochromocytoma PC12 cells were grown on collagen-coated 100-mm tissue culture plates (Falcon Discovery Labware; BD Bioscience) in DMEM supplemented with 6% heat-inactivated fetal bovine serum (iFBS) and 6% heat-inactivated horse serum (iHS), 10mM HEPES, 20U/ml penicillin, and 20μg/ml streptomycin. Human embryonic kidney cells (HEK293T), human neuroblastoma cells (SK-N-AS) and kidney epithelial Vero cells (kindly provided by Dr. Albert Pol; IDIBAPS, Hospital Clinic, Barcelona, Spain) were maintained in DMEM supplemented with 10% iFBS, 20U/ml penicillin, and 20μg/ml streptomycin. Human neuroblastoma (SH-SY5Y) cells were grown in DMEM supplemented with 15% iFBS, 20U/ml penicillin, and 20μg/ml streptomycin. Cultures were maintained at 37˚C in a humidified atmosphere of 95% air and 5% CO_2.

Generation of plasmid constructs

pLDPuro-hsnSR100N lentiviral vector was obtained from Addgene (plasmid #35172) [16]. FAIM-S_2a and FAIM-L_2a expressing vectors were constructed using the coding sequence of human FAIM-S_2a (GenBank™ accession NM_001033030.1) and FAIM-L_2a (GenBank™ accession XM_011512950.2). These sequences were flanked by BamHI/XhoI restriction sites. They were synthesized using the GeneArt system (Thermo Fisher Scientific™), cloned into the pMT4 vector, and subcloned into pcDNA3 containing 3x-FLAG or GFP.

Cell transfection

HEK293T, PC12, Vero, and SK-N-AS cells at 80% confluence were transfected with the desired expression plasmids using Lipofectamine 2000® (Thermo Fisher Scientific™) in Opti-MEM (Gibco), following the manufacturer's instructions.

SH-SY5Y cells were transfected using the Amaxa™ 4D-Nucleofector™ (Lonza, Basilea, Switzerland) system. Cell lines were transfected with FAIM isoforms subcloned into pcDNA3-containing 3x-FLAG or GFP.

RNA extraction and RT-PCR

Total RNA was isolated from human cell lines and tissues using the RNeasy Mini Kit (Qiagen) and following the manufacturer´s instructions. Equal amounts of RNA (1 μg) were converted to single-stranded cDNA using the High Capacity RNA-to-cDNA Kit (Applied Biosystems), following the manufacturer's instructions.

One μl of the resulting cDNA was amplified by PCR using the primers described in Table 1 (Sigma Aldrich).The following PCR conditions were used: 94˚C for 3 min, 40 cycles of 94˚C for 45 s, 58˚C or 55˚C for 30 s, 72˚C for 1 min and 72˚C for 10 min. The ribosomal protein L27 was used as internal control. Experiments were repeated at least three times with independent samples.

Western blot analysis

Total protein from the human cell lines was lysed using SET buffer (10 mM Tris-HCl pH 7.4, 150 mM NaCl, 1 mM EDTA and 1% SDS) supplemented with EDTA-free complete protease inhibitor mixture (Roche). Protein from the human tissues was extracted with RIPA buffer (50 mM Tris-HCl pH 7.4–8, 150 mM NaCl, 0.1% SDS, 1% Nonidet P-40 and 0.25% deoxycholic acid), plus 1x complete EDTA-free protease inhibitor (Roche). The suspension was then centrifuged at 16,000 x *g* at 4˚C for 30 min, and the supernatants were collected. Protein concentration was quantified by a modified Lowry assay (DC protein assay; Bio- Rad, Hercules, CA). Samples were heat-denatured in loading buffer, resolved by SDS-PAGE and transferred onto polyvinylidene difluoride (PDVF) Immobilon-P membranes (Millipore, Bedford, MA). After blocking with Tris-buffered saline with 0.1% Tween-20 containing 5% non-fat dry milk for 1 h at room temperature, membranes were incubated overnight at 4˚C with the following primary antibodies: anti-FAIM (in house antibody [5];1:2000); anti-2b FAIM (in house antibody [5] 1:2000); anti-FLAG (Sigma,1:20000); anti-α-tubulin (Sigma; 1:20000) and anti-nSR100 (kindly provided by Benjamin Blencowe (Donnelly Centre, University of Toronto, Toronto, ON M5S 3E1, Canada[17]), 1:5000). Horseradish peroxidase-labeled goat anti-rabbit (Sigma, 1:20000) and rabbit anti- mouse IgG (Sigma, 1:20000) were used as secondary antibodies. The following primary antibodies were used for subcellular fractionation: anti-FLAG (Sigma; 1:20000); anti-calnexin (Cell Signaling; 1:1000); anti-actin-HRP (Santa Cruz Biotechnology; 1:1000) and anti-tri-methyl-H3 (Cell Signaling; 1:1000).

Afterwards the membranes were incubated with the chemiluminescent substrate EZ-ECL (Biological Industries, Kibbutz Beit Haemek, Israel). Experiments were repeated three times with independent samples.

Protein stability assay

PC12 cells were transfected with pcDNA3-FLAG (empty vector), pcDNA3-FLAG-FAIM-L, pcDNA3-FLAG-FAIM-S, pcDNA3-FLAG-FAIM-L-2a or pcDNA3-FLAG-FAIM-S-2a. Four hours after transfection cells were treated with MG-132 (2.5 μM) for 48 h. Cell extracts were

Table 1. List of specific primers for each exon used for RT-PCR.

Primer Name	Region Amplified	Direction	Sequence 5 -> 3
1aF	*Faim* exon 1a	F	CTTCGGCTAAGGCAGAGGA
1bF1	*Faim* exon 1b	F	GACTACGTCGTGGGATCG
1bF2	*Faim* exon 1b	F	TGGTGAAACCTACCCCAGAG
2aF	*Faim* exon 2a	F	TGGCCCATTCTATCCTATGC
2bF	*Faim* exon 2b	F	GCATCTGGAGATGACAGTCC
2aR	*Faim* exon 2a	R	GCAGAGTCCGGAGATACCAA
2a3R	*Faim* 2a – 3junction	R	TAGGCTGTAAGGAGGGCTCA
2bR	*Faim* exon 2b	R	CCATGGTTGGCAAAAACAGTCTCA
3R	*Faim* exon 3	R	TGCCTGATGTAGTCCCATGT
6R	*Faim* exon 6	R	TTCCGCTTCCCACTACTGAC
nSR100F	*NSR100*	F	ATTGTCGCCAGTATCACGGC
nSR100R	*NSR100*	R	TTTCTTGTGCCTCTTCTCATCTC
L27F	*RPL27*	F	AGCTGTCATCGTGAAGAA
L27R	*RPL27*	R	CTTGGCGATCTTCTTCTTGCC

F: Forward; R: Reverse.

https://doi.org/10.1371/journal.pone.0185327.t001

lysed using SET buffer and then analyzed by western blot using an anti-FLAG antibody (dilution 1:20000). Anti-tubulin was used as a loading control.

Subcellular protein fractionation

Subcellular fractionation was performed as previously described[18] with minor modifications. Vero cells were plated at a density of 30,000 cells/cm^2 and transfected with pcDNA3-FLAG (empty vector), pcDNA3-FLAG-FAIM-L, pcDNA3-FLAG-FAIM-S, pcDNA3-FLAG-FAIM-L-2a or pcDNA3-FLAG-FAIM-S-2a. Cells were homogenized in 10mM HEPES, pH 7.4, 2mM EDTA, 0.32M sucrose and EDTA-free complete protease inhibitor (Roche). Cell homogenates were centrifuged at 600 x *g* for 10 min to remove nuclei (n), then at 3000 x *g* for 10 min to pellet the plasma membrane and heavy intracellular membranes (HM), and finally at 15,000 x *g* for 15 min to yield the light membranes (LM) in the pellet and the microsomal and cytosolic (Cyt) fractions in the supernatant. Supernatants were centrifuged twice at each speed, and pellets were washed twice by resuspension in homogenization buffer and then centrifuged. Pellets were lysed in SET buffer. Protein concentration was quantified by a modified Lowry assay (DC protein assay; Bio- Rad, Hercules, CA). Samples were heat-denatured in Laemmli buffer and subjected to SDS-PAGE. The experiment was repeated twice.

Immunofluorescence

Vero cells were plated on tissue culture plates (15,000 cells/cm^2) and transfected with pcDNA3-FAIM-L-2a-GFP or pcDNA3-FAIM-S-2a-GFP. Twenty-four hours later, they were rinsed with PBS 1x at room temperature and fixed with paraformaldehyde 4% for 30 min at room temperature. They were washed then twice with PBS 1x and blocked using 5% bovine serum albumin (Sigma) in PBS1x- 0.1% Triton X-100 for 90 min at room temperature. Cells were incubated overnight at 4˚C with anti-calnexin (Abcam; 1:50). Alexa Fluor 594 (ThermoFisher Scientific™; 1:300) was used as a secondary antibody. Mitotracker (ThermoFisher Scientific™; 100nM) was used following the manufacturer's instructions. Cells were rinsed three times with PBS 1x and incubated with the secondary antibody 1h at room temperature, protected from light. An

incubation of 1h at room temperature with a PBS solution containing Hoechst 33258 (Sigma; 0.05 μg/ml) was used for nucleic acid stain. Confocal micrographs were obtained using a FluoView1000 spectral confocal microscope (Olympus). The observations were made in two independent experiments and at least 10 cells per condition were analyzed.

mRNA stability and real time PCR

SH-SY5Y cells were treated with Actinomycin D (5 μg/ml) for various times (3, 6, 9 and 12 h), to block mRNA synthesis. Total RNA was isolated using the RNeasy Mini Kit (Qiagen) and RT-PCR was performed. Real time PCR (qPCR) amplifications were performed using Sybr-Green PCR Master Mix (Applied Biosystems). Samples were run in an ABI Prism 7900HT sequence detector (Applied Biosystems) under the conditions indicated by the manufacturer. Triplicate determinations were averaged at each data-point. 18S amplification was used as an internal control.

Cell death assays

SK-N-AS cells were plated in 24-well tissue culture plates and transfected with pcDNA3-FLAG (empty vector), pcDNA3-FLAG-FAIM-L, pcDNA3-FLAG-FAIM-S, pcDNA3-FLAG-FAIM-L-2a or pcDNA3-FLAG-FAIM-S-2a. Twenty hours later, they were treated with super-FasL. Apoptotic cell death was measured 24 h after treatment. Apoptotic nuclei (condensed or fragmented) were counted after Hoechst 33258 (0.05 μg/ml) staining (1h at room temperature). Experiments were repeated at least three times, and minimum of 500 cells were counted per condition.

Measurement of neurite outgrowth

PC12 cells were plated in poly-D-Lysine coated tissue culture plates and transfected with pcDNA3-FLAG, pcDNA3-FLAG-FAIM-L, pcDNA3-FLAG-FAIM-S pcDNA3-FLAG-FAIM-L-2a or pcDNA3-FLAG-FAIM-S-2a. Twenty-four hours later, they were treated with NGF (100 ng/ml) for 24h. They were then fixed with 4% paraformaldehyde and photographs of random fields were taken using an inverted microscope (Olympus). Neurite outgrowth was assessed by measuring neurite pixels using the Adobe Photoshop 6.0 software (Adobe Systems, San Jose, CA). Three independent experiments were performed, considering 100 cells per condition.

In silico analyses

GenBank was used to identify the transcripts produced by human *FAIM1*. To predict the secondary structure of FAIM mRNA, we used the Mfold program (version 3.2) http://www.bioinfo.rpi.edu/applications/mfold/ [19] and RNAStructure [20]. Optimal secondary structures for both sequences were obtained in dot-bracket notation with minimum free energy.

Statistical analysis

Data were analyzed with GraphPad Prism 5 software (GraphPad Software, Inc., La Jolla, CA, USA). Differences in distribution were tested using the t-test or one-way ANOVA. A p value less than 0.05 was considered significant.

Results

FAIM-S_2a and FAIM-L_2a are novel human FAIM isoforms that include exon 2a

I*n silico* analysis pointed to the existence of alternative and uncharacterized FAIM isoforms (GenBank™ accession numbers: NM_001033030.1 and XM_0111512950.2). These isoforms would be generated by the inclusion of exon 2a in the previously described FAIM-S and FAIM-L isoforms (Fig 1).

We sought to first confirm the existence of these additional transcripts at the mRNA level. To this end, we designed specific primers for each *FAIM1* exon using the sequences reported in GenBank (Fig 2A) in order to perform RT-PCR using cDNA isolated from human neuronal and non-neuronal cells (SH-SY5Y, SK-N-AS, and HEK293T) and human tissue samples. While FAIM-S_2a was detected in all the human cell lines, FAIM-L_2a was detected only in the neuronal cell line SH-SY5Y (Fig 2B). The SK-N-AS cell line was included as a control of neuronal-lineage but with no detectable expression of FAIM-L. Moreover, tissue samples analyses showed that FAIM-L_2a mRNA was present only in the fetal cortex, while FAIM-S_2a was detected in all the tissues tested (Fig 2C).

Both exon 1a and 1b are present in FAIM isoforms. The GenBank sequences of the four isoforms (NM_001033032.1, NM_001033031.1, NM_001033030 and XM_0011512950.2) shared exon 1b. However *in silico* tools, predicted the FAIM-L_2a sequence to contain 91 additional nucleotides at the 5'UTR (exon 1a, light gray square in FAIM-L_2a in Fig 1). To ascertain the structure of exon 1 in the isoforms, we mapped it by RT-PCR. We used specific primers to amplify exon 1a and exon 1b (Fig 2A and Table 1) in human cell lines. Exon 1b was detected in the four isoforms (Fig 2D). FAIM-S and FAIM-S_2a were amplified in all the cell lines with products of 277 bp for FAIM-S and 470 bp for FAIM-S-2a. FAIM-L (337 bps) and

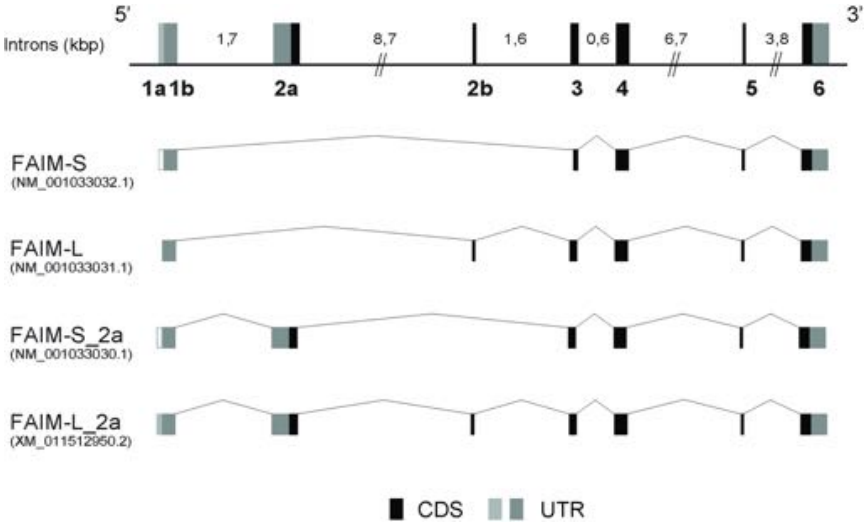

Fig 1. Schematic representation of FAIM isoforms. The genomic structure of *FAIM1* gene is shown. Coding sequences are shown in black boxes (CDS), and non-coding alternative exons in dark gray boxes (UTR), and alternative exons not described in NCBI in white boxes. Intron length is indicated above (kilobase). The new exons described are named following the HUGO nomenclature. The figure shows all transcripts of *FAIM1*. The following four transcripts are represented: FAIM-S (GenBank accession number NM_001033032.1), FAIM-L (GenBank accession number NM_001033031.1), FAIM-S_2a (GenBank accession number NM_001033030.1) and FAIM-L_2a (GenBank accession number XM_011512950.2). CDS: coding sequence; UTR: untranslated region.

https://doi.org/10.1371/journal.pone.0185327.g001

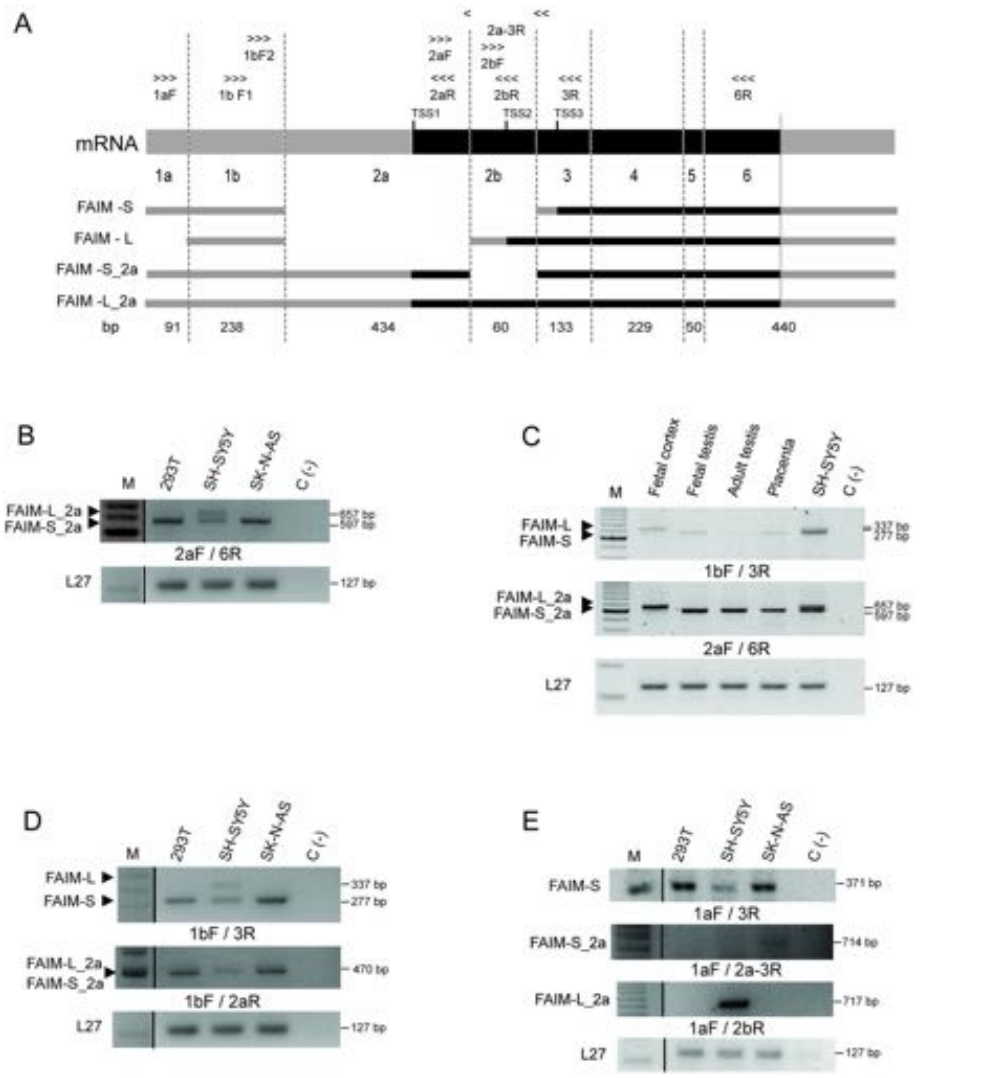

Fig 2. FAIM-S_2a and FAIM-L_2a are expressed in human cell lines and human tissues. A: Schematic representation of the primers used for RT-PCR and the localization in each exon. The 5´ and 3´UTRs are represented in gray, and CDS regions in black. Length of exons is indicated in base pairs (bp). TSS: Transcriptional start site, TSS1: TSS of FAIM-S_2a and FAIM-L_2a; TSS2: TSS of FAIM-L; TSS3: TSS of FAIM-S. **B:** RT-PCR analysis of exon 2a in human cell lines using a 2aF/6R primer combination (the 2aF primer is common to exon 2a in FAIM-L_2a and FAIM-S_2a). Bands of 657 and 597 bp were detected in the neuroblastoma cell line (SH-SY5Y) corresponding to the predicted size of FAIM-L_2a and FAIM-S_2a, respectively. In non-neuronal derived cell lines, namely HEK293T and SK-N-AS, only one band of FAIM-S_2a was detected. **C:** RT-PCR analysis of all the four isoforms in the fetal cortex, fetal and adult testes and placenta using specific primers for exon 2a (2aF/6R) and 1b (1bF/3R). **D:** RT-PCR analysis of exon 1b in HEK293T, SH-SY5Y and SK-N-AS cell lines. Primers used: 1bF/3R or 1bF/2aR. Only one band was observed in SH-SY5Y cells, but FAIM-L_2a and FAIM-S_2a were estimated to have a band of 470 bp. **E:** mRNA amplification of FAIM-S, FAIM-S_2a and FAIM-L_2a using a primer in the region of exon 1a (1aF/3R; 1aF/2a-3R; 1aF/2bR). Negative control (C(-)) was performed with water instead of cDNA. 100 bp DNA Ladder Plus was used to determine the size of each DNA band. L27 was used as an internal control. The primers used are indicated below the agarose gel.

https://doi.org/10.1371/journal.pone.0185327.g002

FAIM-L_2a (470 bps) were amplified only in SH-SY5Y cells. Primers used in the exon 1b region were unable to distinguish between FAIM-S_2a and FAIM-L_2a since they showed the

same sequence length. The inclusion of exon 1b in the two isoforms was confirmed by product size using another primer combination. These results suggest that the 5´UTR of all the isoforms contain exon 1b thereby confirming what is reported in GenBank (Fig 2A and 2D).

We then performed RT-PCR analysis using specific primers for exon 1a in order to determine the presence of this region in the sequences of the isoforms (Table 1). Three of the four transcripts were amplified using a forward primer in exon 1a (1aF). We found that FAIM-S (expressed in all cell lines) with the expected size 371 bp, FAIM-S_2a (only detected in SK-N-AS) with the expected size 714 bp, and FAIM-L_2a (expressed in SH-SY5Y) with the expected size 717 bp contained exon 1a in the 5´UTR (Fig 2E).

Similar mRNA stability in FAIM isoforms

To better understand the mRNA structure of these isoforms, we studied mRNA stability. SH-SY5Y cells were treated with the inhibitor of transcription Actinomycin D (5 μg/ml) for 3, 6, 9 and 12h. At different time points, RNA was isolated and qPCR was performed. mRNA half-life was calculated as the time needed to reduce transcript levels to half (50%, discontinuous line) of their initial abundance at time 0. The half-life of all the isoforms was around 165–180 min (Fig 3A). Following the study, differences in the abundance of mRNA transcripts in SH-SY5Y cells were found. The number of cycles to amplify (similar in size product) FAIM-S, FAIM-L, FAIM-S_2a and FAIM-L_2a by qPCR was different for each isoform, thereby indicating differences in its abundance in SH-SY5Y cells. FAIM isoforms were detected at 24 cycles for FAIM-S, 25 cycles for FAIM-L, 27 and 31 cycles for FAIM-S_2 and FAIM-L_2a respectively. These findings reveal a higher presence of FAIM-S mRNA and lower levels of FAIM-L_2a (Fig 3B).

FAIM-S_2a is consistently translated to protein

We next examined whether FAIM-S_2a and FAIM-L_2a are expressed at the protein level in human cell lines and human tissues. Using the ProtParam tool available at expasy.org, we predicted the molecular weight of each isoform, indicated in Fig 4A. Western blot analysis of HEK293T, SH-SY5Y and SK-N-AS cell lines showed a band of 20 kDa corresponding to FAIM-S and a band of 24 kDa compatible with the apparent and predicted molecular weight of FAIM-S_2a in all cell lines. This finding suggested that FAIM-S_2a is expressed ubiquitously, similarly to FAIM-S. A band of 23 kDa compatible with the predicted molecular weight of FAIM-L was detected only in the neuronal SH-SY5Y cell line, but FAIM-L_2a expression was not detected. When the analysis was performed in human tissues, only FAIM-S_2a was detected in fetal cortex, fetal and adult testes and placenta (Fig 4C). FAIM-L_2a was not detected in any sample, suggesting that this isoform was either below detectable levels or not translated to protein.

Furthermore, we observed that FAIM-L_2a and FAIM-S_2a showed only slight overexpression in comparison with overexpression of the shorter isoforms (i.e. FAIM-L and FAIM-S). Given the lack of detectable endogenous FAIM-L_2a protein and the low levels of endogenous FAIM-S_2a, we sought to characterize the two proteins in transient transfection conditions, in order to have a consistent amount of both proteins. After transfection, the expression of the extra-long isoforms dropped drastically compared to the transfected forms of FAIM-L and FAIM-S, which both maintained their expression over several days in cell culture (Fig 5A). Experiments using the proteasome inhibitor MG-132 (Fig 5B) showed accumulation of FAIM-L_2a and FAIM-S_2a after 48h of culture, thereby suggesting that these proteins were partially and rapidly degraded via the proteasome. When FAIM-L_2a and FAIM-S_2a were overexpressed, we also observed an increase in the shorter corresponding isoforms of FAIM-L

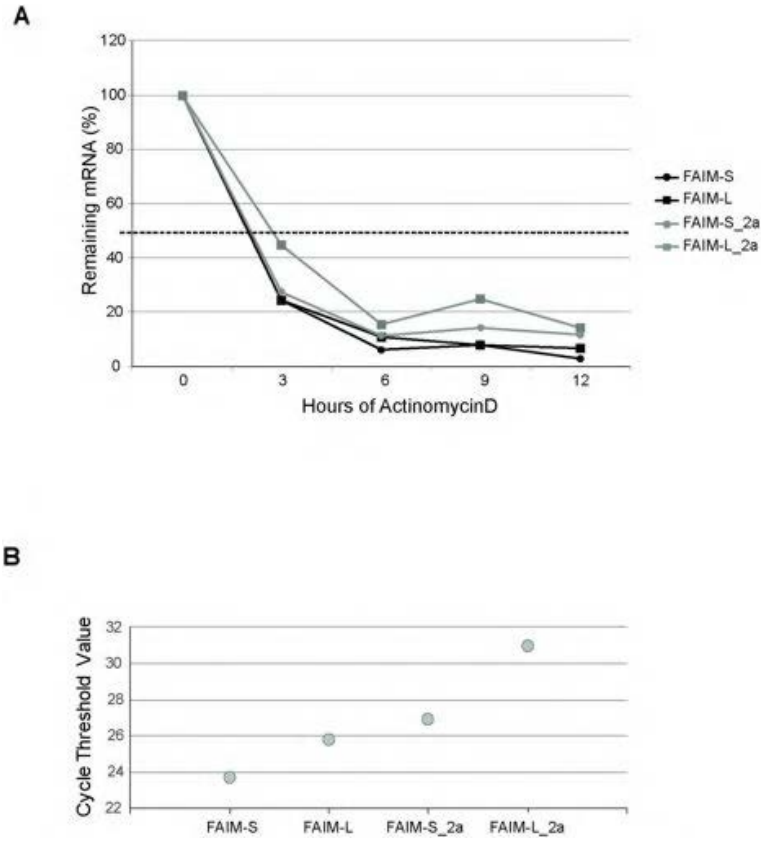

Fig 3. Treatment with Actinomycin D (ActD). SH-SY5Y cells were treated with ActD for a range of times (3, 6, 9 and 12 h). **A:** The half-life of mRNA was measured by treating cells with ActD (5 μg/ml) and collecting total RNA at the times shown, whereupon the levels of *FAIM* mRNA and *18S mRNA* (a stable, housekeeping control mRNA) were measured by RT–qPCR analysis. mRNA half-life was calculated as the time needed to reduce transcript levels to half (50%, discontinuous line) of their initial abundance at time 0. **B:** Number of cycles needed to detect similar size product of FAIM-S, FAIM-L, FAIM-S_2a and FAIM-L_2a by qPCR (SybrGreen) using the following pairs of primers: (1bF2/3R for FAIM-S; 2bF/3R for FAIM-L; 2aF/2a3R for FAIM-S_2a and 2aF/2bR for FAIM-L_2a).

https://doi.org/10.1371/journal.pone.0185327.g003

and FAIM-S, respectively. Using an antibody specific for the neuronal exon 2b, we found that FAIM-L was detectable in HEK293T cells when FAIM-L_2a was overexpressed (Fig 5C). This result suggests that the translational start site of FAIM-S and FAIM-L is preferential or that the longer forms give rise to the shorter ones through proteolysis. Using a dot blot technique, we discarded the proteolytic hypothesis, since the FLAG at the N-terminal of FAIM-L_2a was not present in the lysate. (S1 Fig).

FAIM-S_2a and FAIM-L_2a mRNA secondary structures have lower levels of thermodynamic stability

To better understand the absence of FAIM-L_2a protein expression, we analyzed the 5´UTR in *FAIM1*. It is known that a widespread mechanism modulating mRNA translational efficiency depends on short upstream open reading frames (uORFs) encoded in sequence of this region[21]. uORFs tend to reduce the translation efficiency of downstream protein-coding ORFs[22–24]. uORFs are found in up to 50% of mammalian genes and their utilization is frequently regulated by alternative splicing[25,26].

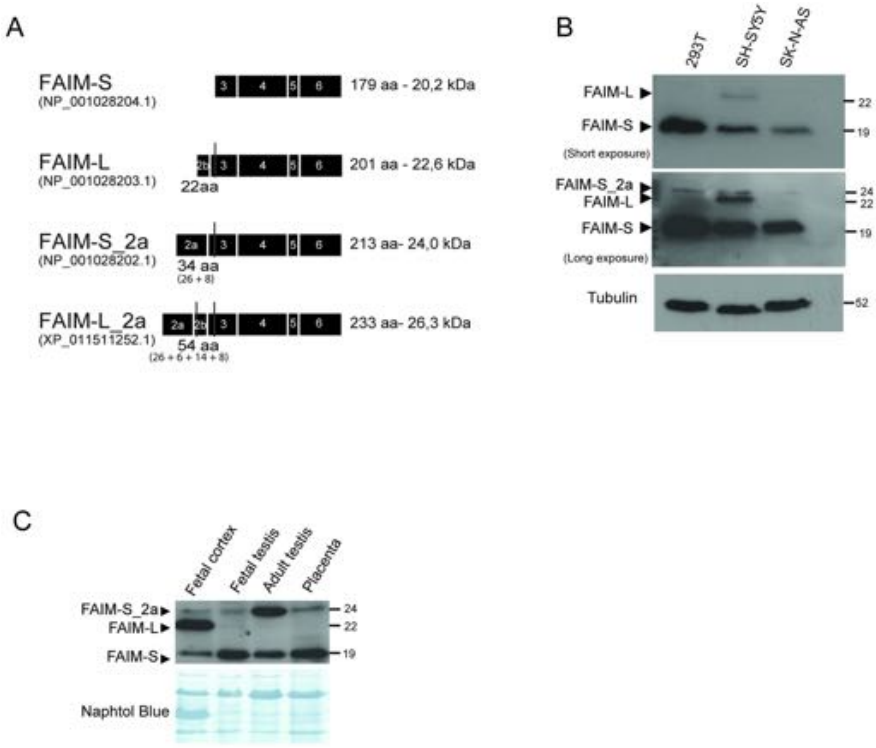

Fig 4. The protein FAIM-S_2a is expressed in all the human cell lines and tissues analyzed. A: Schematic representation of predicted protein structure of each isoform. FAIM-S (GenBank: NP_001028204.1) has a predicted molecular weight of 20.2 kDa and 179 amino acids (aa). FAIM-L (GenBank: NP_001028203.1) has an apparent molecular weight of 22.6 KDa with 22 additional residues at the N-terminus compared to FAIM-S. FAIM-S_2a (GenBank: NP_001028202.1) has an extra 34 aa in the N-terminus and FAIM-L_2a contains an extra 22 aa of FAIM-L plus 32 aa (GenBank: XP_011511252.1). **B:** Western blot analysis of the human cell lines (HEK293T, SH-SY5Y and SK-N-AS) using anti-FAIM antibody (dilution 1:2000). Two different exposures of the film are shown in order to facilitate observation of the bands of all isoforms. Anti-tubulin was used as a loading control. **C:** Western blot analysis of fetal cortex, fetal and adult testes, and placenta. An anti-FAIM antibody was used to detect FAIM expression in human tissues. Naphtol blue staining was used as a loading control.

https://doi.org/10.1371/journal.pone.0185327.g004

The transcriptional start site (TSS) for FAIM-L_2a and FAIM-S_2a is located in exon 2a, for FAIM-L in the exon 2b and for FAIM-S in the exon 3. To study the differential regulation of translation, we used bioinformatics tools to study the sequence of the 5' UTRs of these isoforms to identify potential regulatory elements, such as uAUGs, mRNA secondary structures and G/C rich sequences that may impede translation. The 5'UTR sequences of FAIM-S_2a and FAIM-L_2a included exons 1a, 1b and the sequence of exon 2a that precedes the TSS. The two extra-long isoforms therefore share the same 5'UTR sequence of 683 nucleotides. On the other hand, FAIM-S and FAIM-L have shorter 5'UTR sequences, with 329 nucleotides (FAIM-S 5'UTR includes exon 1a, 1b and the exon 3 sequence that precedes its TSS) and 238 nucleotides (FAIM-L 5'UTR includes exon 1b and the exon 2b sequence that precedes the TSS), respectively. Using ORFfinder (www.ncbi.nlm.nih.gov/orffinder/), we observed that FAIM-S_2a and FAIM-L_2a contain 3 uAUGs in the sequence of exon 2a included in the 5'UTR, thereby pointing to a more complex regulation of these longer isoforms.

Another decisive element in the regulation of mRNA translation is the secondary structure of the 5´UTR[19]. We used the MFold and RNAStructure web servers to predict and analyze 5'UTR structure of the four isoforms. A higher level of thermodynamic stability and a higher

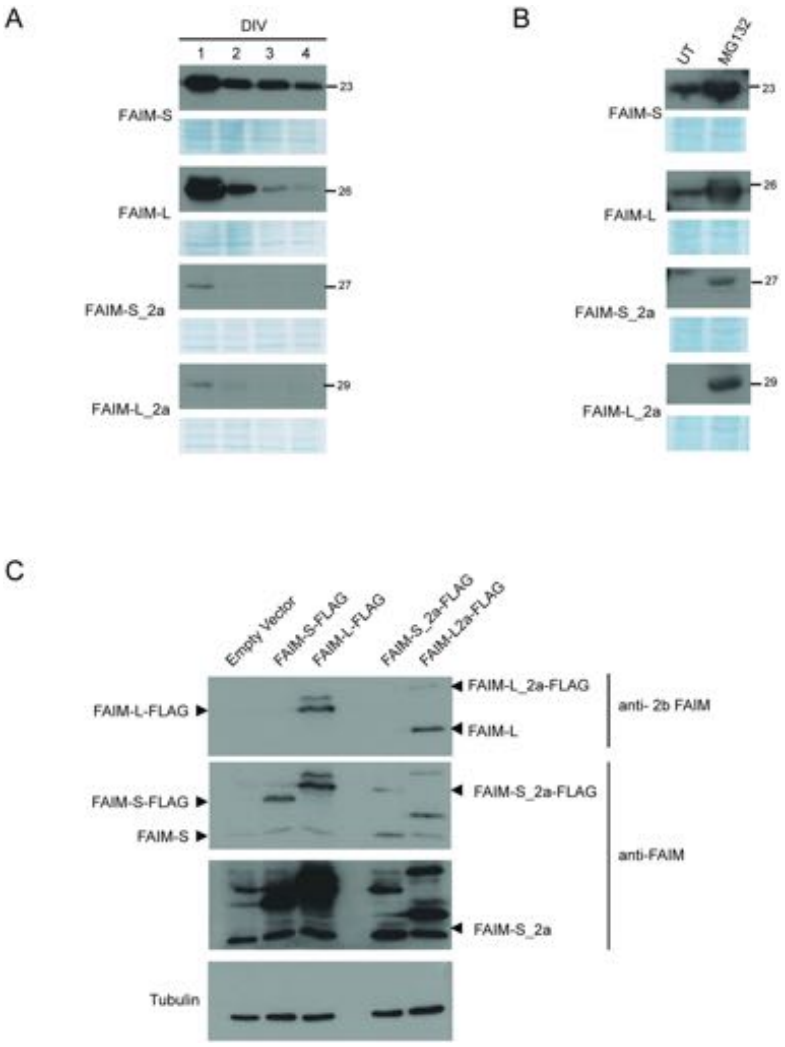

Fig 5. Isoforms expression in cell lines. A: SH-SY5Y cells were transfected with the pCDNA3-FLAG-FAIM-S, pCDNA3-FLAG-FAIM-S_2a, pCDNA3-FLAG-FAIM-L or pCDNA3-FLAG-FAIM-L_2a vector. At a range of time points, cells were harvested and protein expression was assessed by western blot using an anti-FLAG antibody (dilution 1:20000). **B**: PC12 cells were transfected with the isoform vectors (above mentioned) and treated with MG-132 (2.5 μM). Cell extracts were then resolved by western blot analysis, and FAIM expression was measured using an anti-FLAG antibody (dilution 1:20000). **C:** HEK293T cells transfected with pcDNA3-FLAG-FAIM-L, pcDNA3-FLAG-FAIM-S, pcDNA3-FLAG-FAIM-L-2a or pcDNA3-FLAG-FAIM-S-2a vector were lysed, and protein extracts were analyzed by western blot. An anti-FAIM-L (anti-2b FAIM, specific for neuronal exon 2b) and anti-FAIM (that recognizes the common part of the isoforms) were used. Anti-tubulin was used as a loading control. Two different exposures of the film are shown in order to facilitate observation of the bands of all isoforms. DIV: days *in vitro* (n = 3).

https://doi.org/10.1371/journal.pone.0185327.g005

presence of Guanine/Cytosine-rich sequences (G/C) for the secondary structure of FAIM-S_2a (dG = -279.4 Kcal/mol, with 45.9% G/C) and FAIM-L_2a (dG = -279.4 Kcal/mol, with 45.8% G/C) was detected compared to FAIM-S (dG = -156.9 Kcal/mol, with 43.7% G/C) or FAIM-L (dG = -110.9 Kcal/mol, with 41.8% G/C) respectively (Table 2) (Fig 6). A lower Gibb's free energy (dG) indicates stronger secondary RNA structure formation and a lower probability of translation. Therefore, the difference in dG values may explain the increased complexity of the translation of these two extra-long isoforms and their lower expression levels.

Table 2. Thermodynamic stability of the secondary structure of the 5´UTR.

Gene	Region	dG (Kcal/mol)	5´UTR Length	% G/C
FAIM-S_2a	5' UTR	-279.4	683 nt	45,9
FAIM-L_2a	5' UTR	-279.4	683 nt	45,8
FAIM-L	5' UTR	-110.9	238 nt	41,8
FAIM-S	5' UTR	-156.9	329 nt	43,7

https://doi.org/10.1371/journal.pone.0185327.t002

Undetectable levels of FAIM-L_2a in human tissues may also be due to a different temporal regulation. Here we analyzed the expression of FAIM-L_2a protein only in the fetal cortex and therefore we cannot rule out the possibility that this isoform is expressed in adult brain or under pathological conditions.

Alternative splicing of exon 2b is regulated by nSR100 in FAIM-L and FAIM-L_2a

The reason why FAIM-L isoforms are restricted to neuronal tissues is unknown. A recent study reported that neuron-specific splicing isoforms are regulated by the 100-kDa Neural-Specific Serine/Arginine Repetitive Splicing Factor (nSR100)[27,28]. To confirm the role of nSR100 in the expression of FAIM-L isoforms, we examined its expression in various cell lines (HEK293T, SH-SY5Y and SK-N-AS). nSR100 was expressed only in the human neuronal SH-SY5Y cell line, where it showed the same expression pattern as that of FAIM-L (Fig 7A). To confirm the regulation of FAIM-L and FAIM-L_2a by nSR100, we ectopically expressed nSR100 in the non-neuronal HEK293T cell line and analyzed FAIM-L isoforms expression by RT-PCR. nSR100 overexpression in HEK293T cells induced mRNA expression of FAIM-L and FAIM-L_2a (Fig 7B). When protein levels were analyzed in the same conditions, only a band of 23 kDa, corresponding to FAIM-L, was detected (Fig 7C). Expression of FAIM-L_2a remained below detection levels. These results indicate that nSR100 promotes the expression of the two FAIM-L isoforms through the inclusion of exon 2b.

FAIM-S_2a and FAIM-L_2a have a cytosolic and nuclear distribution pattern

FAIM-L and FAIM-S are reported to be cytosolic soluble proteins showing a diffuse cytosolic pattern that excluded the nucleus[10,12]. To study the localization of the new isoforms, we performed subcellular protein fractionation in cells ectopically expressing FAIM-S_2a and FAIM-L_2a. Unexpectedly, these two isoforms were detected in the nuclear and cytosolic fractions (Fig 8A), thereby suggesting that they serve a potential role in the nucleus. Immunocytochemical analysis confirmed the presence of FAIM-S_2a and FAIM-L_2a in the nucleus and in the cytosol (Fig 8B).

FAIM-S_2a and FAIM-L_2a increase neurite length in NGF-stimulated PC12 cells

To assess an initial functional role of these new isoforms, we compared the function of FAIM-L_2a and FAIM-S_2a in cell differentiation and resistance to DR-induced cell death, properties previously attributed to FAIM-S and FAIM-L respectively (reviewed in[8]). We transfected the FLAG-tagged forms of FAIM-L, FAIM-S, FAIM-L-2a, and FAIM-S-2a into neuroblastoma derived cells and stimulated these cells with soluble Fas Ligand (sFasL).

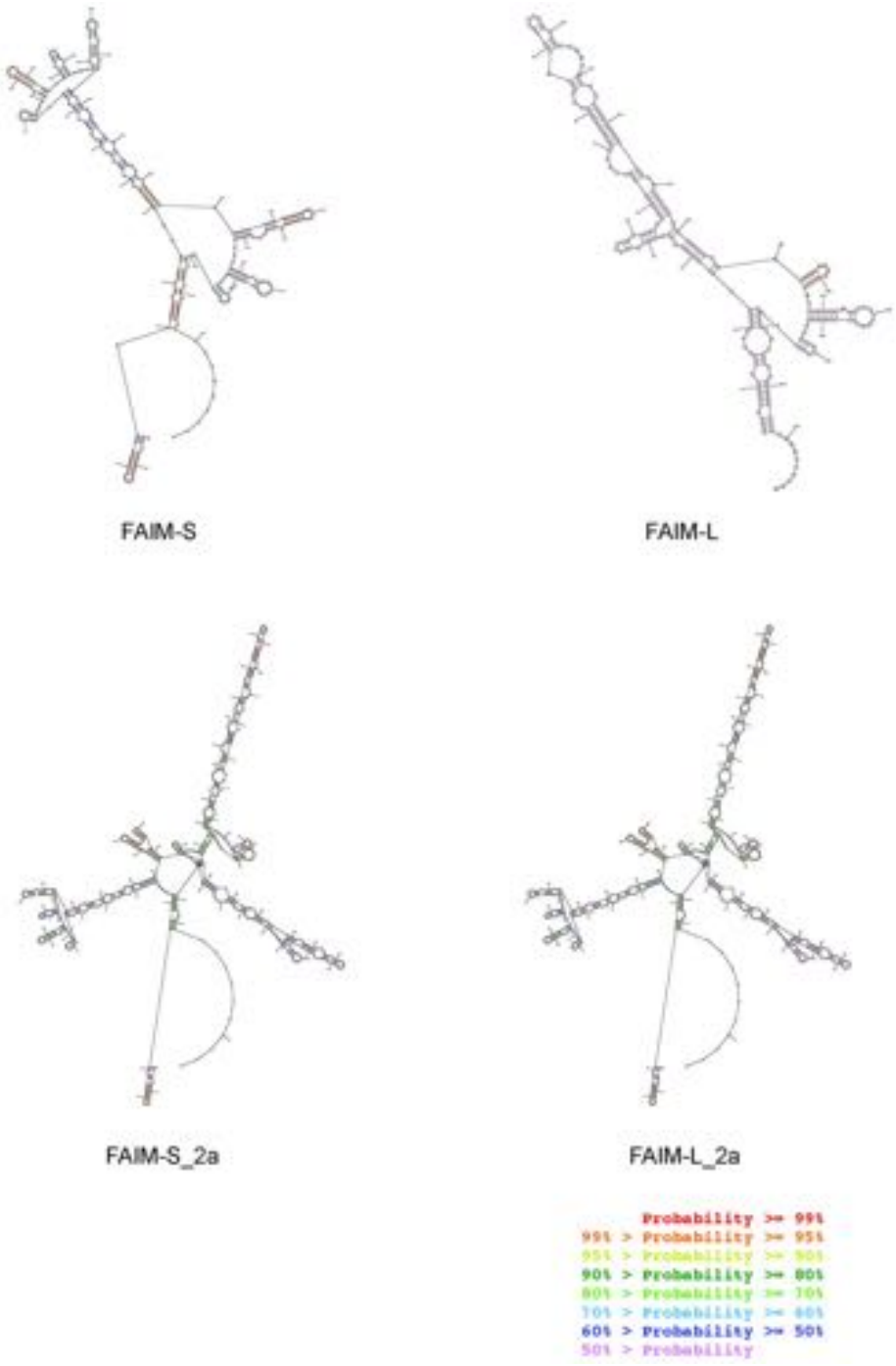

Fig 6. mRNA secondary structure. 5´UTR sequences of FAIM isoforms structures as shown by the output of the RNAStructure web server (http://rna.urmc.rochester.edu/RNAstructureWeb/Servers/Predict1/Predict1.html). The optimal secondary prediction for all the sequences was obtained in dot-bracket notation with the lowest free energy structure for the input sequence. Colour annotation of the structures provides information about the confidence in the prediction of a specific pair (base paired or unpaired nucleotides). The highest probabilities are red and the lowest are purple.

https://doi.org/10.1371/journal.pone.0185327.g006

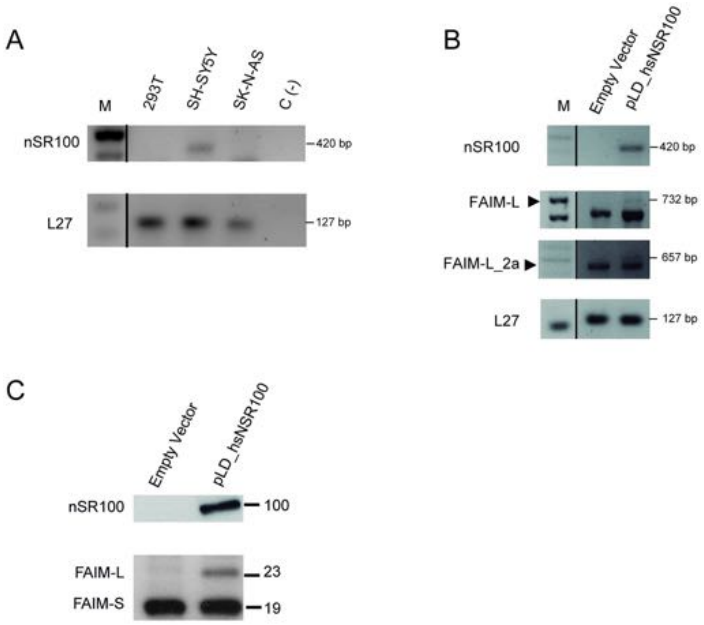

Fig 7. Overexpression of nSR100 induce FAIM-L_2a and FAIM-L in HEK293T cells. A: nSR100 transcript was amplified by RT-PCR. In SH-SY5Y cells, a band of 420 bp was detected. **B:** RT-PCR in HEK293T cells after transient transfection with nSR100 using Lipofectamine 2000®. Transcripts of FAIM-L and FAIM-L_2a were observed at 732 bp and 657 bp bands. L27 was used as an internal control in all PCRs. **C:** Western blot analysis using anti-FAIM in HEK293T cells after transfection with nSR100 vector (pLD_hsnSR100). A band of 23 kDa (FAIM-L) was detected in nSR100 transfection conditions. As a negative control, we used an empty vector (n = 3).

https://doi.org/10.1371/journal.pone.0185327.g007

FAIM-L was the only protein that reduced FasL-induced apoptosis (Fig 9A). Next, we studied the modulation of neurite outgrowth after NGF stimulation. All isoforms, except FAIM-L, increased the neurite length of neuronal cells stimulated with NGF (Fig 9B). This result suggests that FAIM-S-2a and FAIM-L_2a participate in neurite outgrowth rather than in the prevention of DR-induced cell death.

Discussion

In recent years, the application of genome-wide profiling technologies, coupled to bioinformatics approaches has revealed that more than 90% of human genes undergo alternative splicing[29,30]. This process is crucial for regulating the levels and tissue specificity of gene expression, and any disruption of this mechanism can lead to disease[30,31]. Eukaryotic gene expression is regulated at the level of mRNA translation and stability, in which regulation of the 5´UTR plays a fundamental role[32]. In the present study, we focused on the characterization of splicing products of the human *FAIM1*, a death receptor antagonist known to participate in neuronal differentiation, DR-induced apoptosis, obesity and hyperinsulinaemia[11]. The two isoforms of *FAIM1* first described were FAIM-S and FAIM-L. In this regard, FAIM-S was first reported in 1999 as an antagonist of Fas in lymphocytes[10]. It promotes neuronal differentiation by NGF activating ERK and NF-κB pathways[5]. FAIM-L, a longer splice variant that contains 22 additional amino acids at the N-terminal end of the protein was identified in 2001[9]. This isoform protects neurons from DR-induced cell death by either binding to the Fas receptor and preventing the activation of caspase-8, thereby inhibiting the apoptotic cascade at initiator caspase level[12], or by stabilizing the antiapoptotic protein XIAP[13]. In

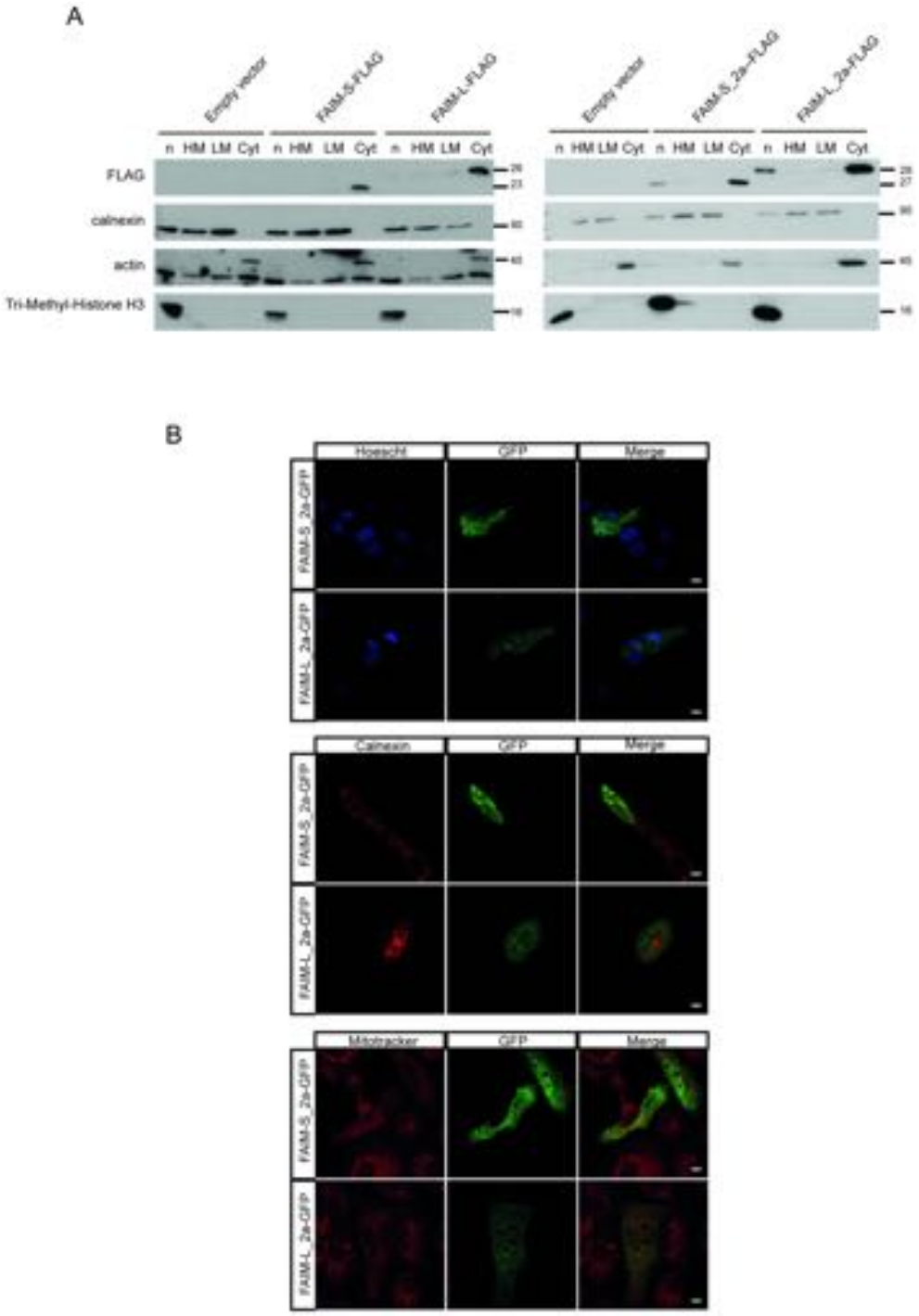

Fig 8. FAIM-S_2a and FAIM-L_2a are localized in the cytoplasm and nucleus. A: Western blot analysis using anti-FLAG to detect the presence of FAIM-S, FAIM-L, FAIM-S_2a and FAIM-L_2a in the distinct cellular compartments. Anti-calnexin was used as a marker for the membrane fraction, anti-actin as a marker of the cytosolic fraction, and anti-Tri-Methyl-Histone H3 as a marker of the nucleus. **B:** Immunofluorescence in Vero cells 24 h after transfection with pcDNA3-GFP containing the extra-long isoforms. Anti-calnexin (reticular protein), Mitotracker (mitochondrial marker) and Hoechst (nuclei staining) were used to examine the co-localization of FAIM isoforms. Scale bars 10 **μ**m.

https://doi.org/10.1371/journal.pone.0185327.g008

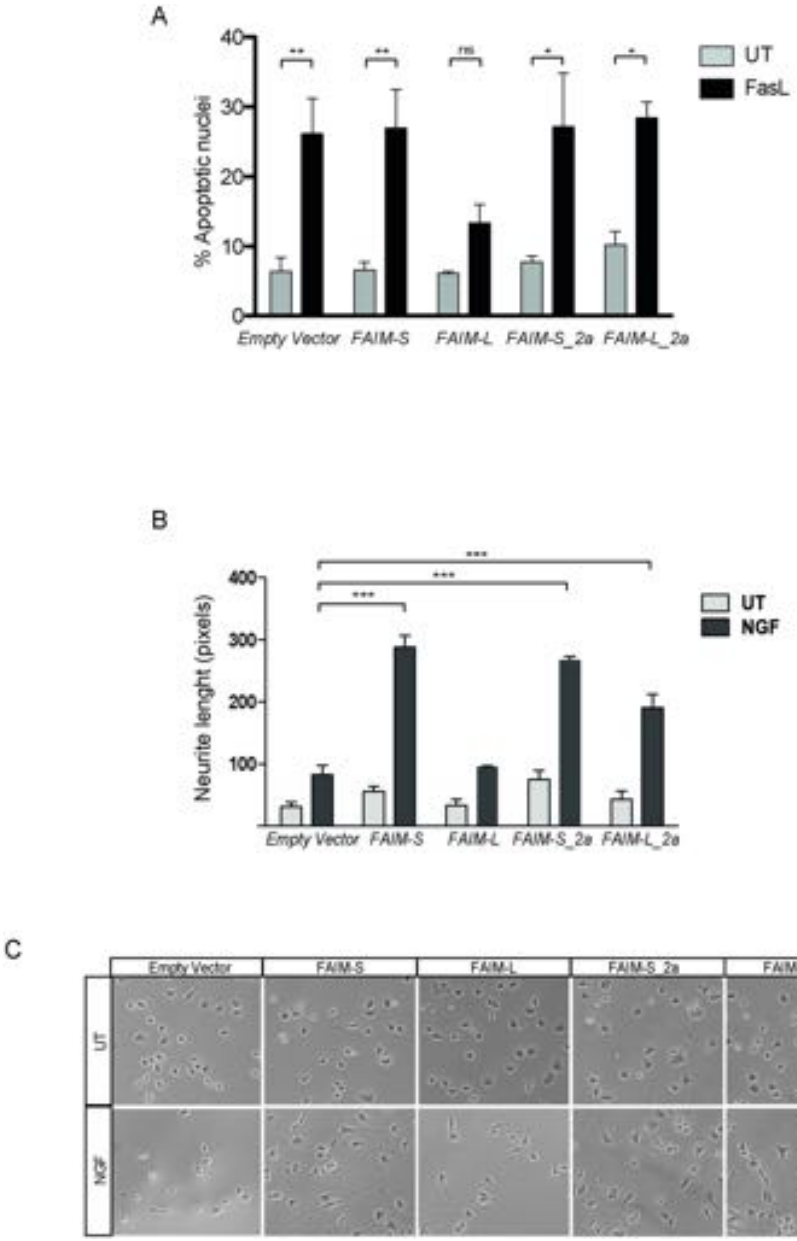

Fig 9. FAIM-S_2a and FAIM-L_2a increase NGF induced neurite outgrowth in PC12 cells. A: Cell death was measured in SK-N-AS cells by counting condensed nuclei after Hoechst 33258 (0.05 μg/ml) staining. Cells were transfected with empty vector (pcDNA3-FLAG) or pcDNA3-FLAG-containing all the isoforms and then treated or not with FasL (100 ng/ml). Graph represents the percentage of apoptotic nuclei of a minimum of 500 cells per condition. Experiments were repeated at least three times. Statistical significance was determined by one-way ANOVA. *ns*: no significant and *p<0.05;**p<0.01. **B:** Neurite length was measured in PC12 cells treated with NGF (100ng/ml) or left untreated after transfection of the isoform vectors. At least three independent experiments were performed. Statistical significance was determined by one-way ANOVA, ***p<0.001. **C:** Representative images of neurite outgrowth in the different conditions. UT: untreated; NGF: nerve growth factor (100 ng/ml) (n = 3 per experiment).

https://doi.org/10.1371/journal.pone.0185327.g009

addition to these two previously known isoforms, two longer splicing isoforms (FAIM-S_2a and FAIM-L_2a) are reported in databases; however, this is the first study to provide details of

their expression and function. Here we characterized FAIM-S_2a and FAIM-L_2a and the role of these isoforms in neurite outgrowth and cell death.

Studies by Zhong and col. suggested that FAIM-S and FAIM-L isoforms are generated by AS[9].This process is crucial in the evolution of increased proteomic and functional complexity and is especially relevant in the nervous system[33]. FAIM-L mRNA expression increases during development, while that of FAIM-S remains unaltered[12].

AS has played a major role in the evolutionary expansion of the proteomic and functional complexity underlying many cellular processes and is especially prevalent in the vertebrate nervous system[34,35]. The mechanisms that control neural-specific AS are poorly understood. AS is regulated by a member of a large class of proteins harboring Ser/Arg (SR)-repetitive regions[36]. The vertebrate- and neural-specific SR-related protein of 100 kDa (nSR100/SRRM4) regulates a network of brain-specific alternative exons concentrated in genes involved in various aspects of neurogenesis[16,27]. nSR100 is required for neural cell differentiation *in vivo*. Knockdown of nSR100 disrupts the inclusion of a large set of nervous system specific alternative exons[27]. In fact, our results show that the ectopic expression of nSR100 in non-neuronal cells (i.e. HEK293T) induced the formation of the neuronal-specific splice variants FAIM-L and FAIM-L_2a. Concurring with our observation, FAIM-L also appeared in a list of genes modulated by nSR100 in HEK293T cells[28]. The expression of this protein may be the factor that regulates the inclusion of exon 2b, and therefore the nervous system specific expression pattern of FAIM-L and FAIM-L_2a. In fact, there is a putative nSR100 binding site before the start of exon 2b (-41 GCTGC/GCTGCT -13).

All the isoforms examined contained exon 1b (238 nucleotides). In this study, we confirm that exon 1a (91 nucleotides) is also present in FAIM-L_2a, FAIM-S_2a and FAIM-S, thereby indicating that the previous annotated sequences for FAIM-S (NM_001033032.1) and FAIM-S_2a (NM_001033030.1) are not accurate. In summary, all the FAIM isoforms examined except FAIM-L included exon 1a.

While we detected FAIM-L_2a mRNA in human cell lines and tissues, we were unable to detect its protein expression. Fig 5C and S1 Fig show that, in presence of FAIM-L_2a overexpression, most overexpressed mRNA is translated to FAIM-L, as reflected by an induction in FAIM-L expression. Since the TSS of FAIM-L and FAIM-S are conserved in the mRNA sequences of the longer isoforms (Fig 2A), we hypothesise that the increase in FAIM-L expression is attributable to the TSS of FAIM-L being preferential.

Moreover, as we show in Fig 6 and Table 2, the thermodynamic stability of the 5'UTR secondary structure of FAIM-L_2a is lower than that of FAIM-L, thereby indicating differences in mRNA stability. The secondary structure complexity of FAIM-L_2a mRNA may hinder the binding of the ribosomal complex and therefore its translation into protein.

FAIM-S_2a was less expressed in fetal tissues and placenta; we should therefore consider that the low levels of the isoforms may be due to differential temporal expression. The presence of CpG islets in the 5´UTR of *FAIM1* may point out to a role in the adult, since it has been demonstrated that such regions can define differential pre- or postnatal expression.

The analysis of protein localization shows that FAIM-L_2a and FAIM-S_2a overexpression localized in the cytoplasm and nucleus. In contrast, FAIM-L and FAIM-S were located only in the cytoplasm. Supporting the localization of both isoforms (FAIM-L_2a and FAIM-S_2a) in the nucleus, we found the presence of a nuclear export signal (NES), in the amino acid sequence encoded by exon 2a. NESs are usually found in proteins with nuclear functions and they facilitate active transport through the nuclear membrane[37]. The role of these isoforms in the nucleus is unclear and further experiments are required to elucidate this question.

While FAIM-S_2a has similar functions to FAIM-S in promoting neurite outgrowth, FAIM-L_2a was not capable of recapitulating FAIM-L function in preventing DR-induced cell

death. One possible explanation may be that the first 22 amino acids of FAIM-L are essential for interaction with XIAP[13]. Since the FAIM-L_2a sequence has 26 additional amino acids at the N-terminal of the protein, the known interactions with FAIM-L partners could be lost.

In summary, here we provide the first evidence of FAIM-S_2a and FAIM-L_2a expression in human cell lines and tissues suggesting that these two isoforms could play a significant role in the nervous system.

Supporting information

S1 Fig. FAIM-S_2a and FAIM-L_2a mRNA can be processed to FAIM-S and FAIM-L. HEK293T cells were transiently transfected with the four FLAG-tagged isoforms (Fig 5C). 2.5μg of lysate was spotted on a Nitrocellulose membrane (LifeScience). The membrane was blocked with 5% BSA in TBS-T for 1h at room temperature, and in order to evaluate a possible processing at the protein level, it was incubated with FLAG antibody (1:20000) 1h at room temperature. After incubation with Horseradish peroxidase conjugated anti-Mouse IgG, membrane was developed using the EZ-ECL chemiluminescence detection kit. Naphtol blue staining was used to verify equal loading.
(TIF)

Acknowledgments

This work was funded by grants awarded to JXC from the Spanish "Ministerio de Economía y Competitividad" (SAF2013-47989-R, SAF2016-80236-R, CIBERNED CB06/05/1104 and PIE13/00027), the "Generalitat de Catalunya" (2014SGR1609), and the "Fundació La Marató de TV3" (201414–30). IC-Y is a recipient of fellowship BES-2014-069550

Author Contributions

Funding acquisition: Joan X. Comella.

Investigation: Elena Coccia, Isabel Calleja-Yagüe, Rana S. Moubarak, Francina Munell.

Methodology: Elena Coccia, Isabel Calleja-Yagüe, Laura Planells-Ferrer, Blanca Sanuy, Belen Sanz, Bruna Barneda-Zahonero.

Project administration: Joaquin López-Soriano.

Supervision: Bruna Barneda-Zahonero, Joan X. Comella, M. Jose Pérez-García.

Writing – original draft: M. Jose Pérez-García.

Writing – review & editing: Rana S. Moubarak, Joan X. Comella, M. Jose Pérez-García.

References

1. Kim WR, Sun W. Programmed cell death during postnatal development of the rodent nervous system. Dev Growth Differ. 2011; 53: 225–235. https://doi.org/10.1111/j.1440-169X.2010.01226.x PMID: 21338348
2. Cheng EH, Wei MC, Weiler S, Flavell RA, Mak TW, Lindsten T, et al. BCL-2, BCL-X(L) sequester BH3 domain-only molecules preventing BAX- and BAK-mediated mitochondrial apoptosis. Mol Cell. 2001; 8: 705–11. PMID: 11583631
3. Evin G. Future Therapeutics in Alzheimer's Disease: Development Status of BACE Inhibitors. BioDrugs. 2016; 30: 173–94. https://doi.org/10.1007/s40259-016-0168-3 PMID: 27023706
4. Irmler M, Thome M, Hahne M, Schneider P, Hofmann K, Steiner V, et al. Inhibition of death receptor signals by cellular FLIP. Nature. 1997; 388: 190–5. https://doi.org/10.1038/40657 PMID: 9217161

5. Sole C, Dolcet X, Segura MF, Gutierrez H, Diaz-Meco M-T, Gozzelino R, et al. The death receptor antagonist FAIM promotes neurite outgrowth by a mechanism that depends on ERK and NF-kapp B signaling. J Cell Biol. 2004; 167: 479–92. https://doi.org/10.1083/jcb.200403093 PMID: 15520226
6. Urresti J, Ruiz-Meana M, Coccia E, Arévalo JC, Castellano J, Fernández-Sanz C, et al. Lifeguard Inhibits Fas Ligand-mediated Endoplasmic Reticulum-Calcium Release Mandatory for Apoptosis in Type II Apoptotic Cells. J Biol Chem. 2016; 291: 1221–1234. https://doi.org/10.1074/jbc.M115.677682 PMID: 26582200
7. Hu L, Smith TF, Goldberger G. LFG: a candidate apoptosis regulatory gene family. Apoptosis. 2009; 14: 1255–65. https://doi.org/10.1007/s10495-009-0402-2 PMID: 19784873
8. Planells-Ferrer L, Urresti J, Coccia E, Galenkamp KMO, Calleja-Yagüe I, López-Soriano J, et al. Fas apoptosis inhibitory molecules: more than death-receptor antagonists in the nervous system. J Neurochem. 2016; 139: 11–21. https://doi.org/10.1111/jnc.13729 PMID: 27385439
9. Zhong X, Schneider TJ, Cabral DS, Donohoe TJ, Rothstein TL. An alternatively spliced long form of Fas apoptosis inhibitory molecule (FAIM) with tissue-specific expression in the brain. Mol Immunol. 2001; 38: 65–72. PMID: 11483211
10. Schneider TJ, Fischer GM, Donohoe TJ, Colarusso TP, Rothstein TL. A novel gene coding for a Fas apoptosis inhibitory molecule (FAIM) isolated from inducibly Fas-resistant B lymphocytes. J Exp Med. 1999; 189: 949–56. PMID: 10075978
11. Huo J, Ma Y, Liu J-J, Ho YS, Liu S, Soh LY, et al. Loss of Fas apoptosis inhibitory molecule leads to spontaneous obesity and hepatosteatosis. Cell Death Dis. 2016; 7: e2091. https://doi.org/10.1038/cddis.2016.12 PMID: 26866272
12. Segura MF, Sole C, Pascual M, Moubarak RS, Perez-Garcia MJ, Gozzelino R, et al. The long form of Fas apoptotic inhibitory molecule is expressed specifically in neurons and protects them against death receptor-triggered apoptosis. J Neurosci. 2007; 27: 11228–41. https://doi.org/10.1523/JNEUROSCI.3462-07.2007 PMID: 17942717
13. Moubarak RS, Planells-Ferrer L, Urresti J, Reix S, Segura MF, Carriba P, et al. FAIM-L is an IAP-binding protein that inhibits XIAP ubiquitinylation and protects from Fas-induced apoptosis. J Neurosci. 2013; 33: 19262–75. https://doi.org/10.1523/JNEUROSCI.2479-13.2013 PMID: 24305822
14. Martínez-Mármol R, Barneda-Zahonero B, Soto D, Andrés RM, Coccia E, Gasull X, et al. FAIM-L regulation of XIAP degradation modulates Synaptic Long-Term Depression and Axon Degeneration. Sci Rep. Nature Publishing Group; 2016; 6: 35775. https://doi.org/10.1038/srep35775 PMID: 27767058
15. Carriba P, Jimenez S, Navarro V, Moreno-Gonzalez I, Barneda-Zahonero B, Moubarak RS, et al. Amyloid-β reduces the expression of neuronal FAIM-L, thereby shifting the inflammatory response mediated by TNFα from neuronal protection to death. Cell Death Dis. Nature Publishing Group; 2015; 6: e1639. https://doi.org/10.1038/cddis.2015.6 PMID: 25675299
16. Raj B, O'Hanlon D, Vessey JP, Pan Q, Ray D, Buckley NJ, et al. Cross-Regulation between an Alternative Splicing Activator and a Transcription Repressor Controls Neurogenesis. Mol Cell. 2011; 43: 843–850. https://doi.org/10.1016/j.molcel.2011.08.014 PMID: 21884984
17. Raj B, Blencowe BJ. Alternative Splicing in the Mammalian Nervous System: Recent Insights into Mechanisms and Functional Roles. Neuron. Elsevier Inc.; 2015; 87: 14–27. https://doi.org/10.1016/j.neuron.2015.05.004 PMID: 26139367
18. Jacobs SBR, Basak S, Murray JI, Pathak N, Attardi LD. Siva is an apoptosis-selective p53 target gene important for neuronal cell death. Cell Death Differ. 2007; 14: 1374–85. https://doi.org/10.1038/sj.cdd.4402128 PMID: 17464332
19. Zuker M. Mfold web server for nucleic acid folding and hybridization prediction. Nucleic Acids Res. 2003; 31: 3406–15. PMID: 12824337
20. Gruber AR, Bernhart SH, Hofacker IL, Washietl S. Strategies for measuring evolutionary conservation of RNA secondary structures. BMC Bioinformatics. 2008; 9: 122. https://doi.org/10.1186/1471-2105-9-122 PMID: 18302738
21. Wethmar K. The regulatory potential of upstream open reading frames in eukaryotic gene expression. Wiley Interdiscip Rev RNA. 2014; 5: 765–78. https://doi.org/10.1002/wrna.1245 PMID: 24995549
22. Barbosa C, Peixeiro I, Romão L. Gene expression regulation by upstream open reading frames and human disease. Fisher EMC, editor. PLoS Genet. 2013; 9: e1003529. https://doi.org/10.1371/journal.pgen.1003529 PMID: 23950723
23. Wethmar K, Barbosa-Silva A, Andrade-Navarro MA, Leutz A. uORFdb—a comprehensive literature database on eukaryotic uORF biology. Nucleic Acids Res. 2014; 42: D60–7. https://doi.org/10.1093/nar/gkt952 PMID: 24163100
24. Somers J, Pöyry T, Willis AE. A perspective on mammalian upstream open reading frame function. Int J Biochem Cell Biol. 2013; 45: 1690–700. https://doi.org/10.1016/j.biocel.2013.04.020 PMID: 23624144

25. Lee S, Liu B, Lee S, Huang S- X, Shen B, Qian S- B. Global mapping of translation initiation sites in mammalian cells at single-nucleotide resolution. Proc Natl Acad Sci U S A. 2012; 109: E2424–32. https://doi.org/10.1073/pnas.1207846109 PMID: 22927429

26. Calvo SE, Pagliarini DJ, Mootha VK. Upstream open reading frames cause widespread reduction of protein expression and are polymorphic among humans. Proc Natl Acad Sci U S A. 2009; 106: 7507–12. https://doi.org/10.1073/pnas.0810916106 PMID: 19372376

27. Calarco JA, Superina S, O'Hanlon D, Gabut M, Raj B, Pan Q, et al. Regulation of vertebrate nervous system alternative splicing and development by an SR-related protein. Cell. 2009; 138: 898–910. https://doi.org/10.1016/j.cell.2009.06.012 PMID: 19737518

28. Raj B, Irimia M, Braunschweig U, Sterne-Weiler T, O'Hanlon D, Lin Z-Y, et al. A Global Regulatory Mechanism for Activating an Exon Network Required for Neurogenesis. Mol Cell. 2014; 56: 90–103. https://doi.org/10.1016/j.molcel.2014.08.011 PMID: 25219497

29. Wang ET, Sandberg R, Luo S, Khrebtukova I, Zhang L, Mayr C, et al. Alternative isoform regulation in human tissue transcriptomes. Nature. 2008; 456: 470–6. https://doi.org/10.1038/nature07509 PMID: 18978772

30. Keren H, Lev-Maor G, Ast G. Alternative splicing and evolution: diversification, exon definition and function. Nat Rev Genet. 2010; 11: 345–55. https://doi.org/10.1038/nrg2776 PMID: 20376054

31. Wang G-S, Cooper TA. Splicing in disease: disruption of the splicing code and the decoding machinery. Nat Rev Genet. 2007; 8: 749–61. https://doi.org/10.1038/nrg2164 PMID: 17726481

32. Guigó R, Valcárcel J. Unweaving the Meanings of Messenger RNA Sequences. Mol Cell. 2006; 23: 150–151. https://doi.org/10.1016/j.molcel.2006.07.003 PMID: 16857580

33. Li Q, Lee J-A, Black DL. Neuronal regulation of alternative pre-mRNA splicing. Nat Rev Neurosci. 2007; 8: 819–31. https://doi.org/10.1038/nrn2237 PMID: 17895907

34. Ule J, Darnell RB. RNA binding proteins and the regulation of neuronal synaptic plasticity. Curr Opin Neurobiol. 2006; 16: 102–10. https://doi.org/10.1016/j.conb.2006.01.003 PMID: 16418001

35. Li Q, Zheng S, Han A, Lin C-H, Stoilov P, Fu X-D, et al. The splicing regulator PTBP2 controls a program of embryonic splicing required for neuronal maturation. Elife. 2014; 3: e01201. https://doi.org/10.7554/eLife.01201 PMID: 24448406

36. Änkö M-L. Regulation of gene expression programmes by serine-arginine rich splicing factors. Semin Cell Dev Biol. 2014; 32: 11–21. https://doi.org/10.1016/j.semcdb.2014.03.011 PMID: 24657192

37. La Cour T, Kiemer L, Mølgaard A, Gupta R, Skriver K, Brunak S. Analysis and prediction of leucine-rich nuclear export signals. Protein Eng Des Sel. 2004; 17: 527–536. https://doi.org/10.1093/protein/gzh062 PMID: 15314210